AD-775 229

INFLUENCE OF PORE WATER PRESSURE ON THE ENGINEERING PROPERTIES OF ROCK

Kekuichiro Adachi, et al

Illinois University

Prepared for:

Advanced Research Projects Agency
Bureau of Mines

September 1973

Unclassified

3200.8 (Att 1 to Encl 1)
Mar 7, 66

Security Classification

DOCUMENT CONTROL DATA - R & D AD775229

(Security classification of title, body of abstract and indexing annotation must be entered when the overall report is classified)

1. ORIGINATING ACTIVITY (Corporate author)

Department of Civil Engineering
University of Illinois at Urbana-Champaign
Urbana, Illinois 61801

2a. REPORT SECURITY CLASSIFICATION
Unclassified

2b. GROUP

3. REPORT TITLE

INFLUENCE OF PORE WATER PRESSURE ON THE ENGINEERING PROPERTIES OF ROCK

4. DESCRIPTIVE NOTES (Type of report and inclusive dates)
Final Technical Report, June 1972-Sept. 1973

5. AUTHOR(S) (First name, middle initial, last name)

Kakuichiro Adachi
Gholamreza Mesri

6. REPORT DATE	7a. TOTAL NO. OF PAGES	7b. NO. OF REFS
September 1973	~~238~~ 243	49

8a. CONTRACT OR GRANT NO.	9a. ORIGINATOR'S REPORT NUMBER(S)
H0220069	6
b. PROJECT NO. ARPA Order No. 1579, Amend. No. 3	
c. Program Code 2F10	9b. OTHER REPORT NO(S) (Any other numbers that may be assigned this report)
d.	

10. DISTRIBUTION STATEMENT

Distribution of this document is unlimited

11. SUPPLEMENTARY NOTES	12. SPONSORING MILITARY ACTIVITY
	Advanced Research Project Agency, ARPA

13. ABSTRACT

A 2,000 psi-capacity triaxial compression cell was designed and constructed for the present study. The special design provisions allowed saturation of low porosity rock specimens (2 1/8"D x 4 1/4" L) and accurate control or measurement of volume changes and pore water pressures.

Isotropic and triaxial compression tests under drained and undrained conditions were performed on Berea sandstone, Salem limestone, Vermont marble, and Barre granite. Pore water pressure responses in undrained tests were analyzed in terms of pore pressure parameters B, A and $\bar{A}$.

The value of B-coefficient was a function of the effective confining pressure. At small effective confining pressures, B-values were in the range of 0.85 to 1.0; they decreased continuously with effective confining pressure to a range of 0.3 to 0.6 at 1500 psi. The $\bar{A}$-coefficient maximized at the early stage of loading and then decreased continously. The maximum $\bar{A}$-coefficient for the rocks tested ranged between 0.2 and 0.4. The equations for B- and $\bar{A}$-coefficient were summarized and also a new equation for the $\bar{A}$-coefficient was proposed. The proposed equation agreed with reasonable accuracy with the measured $\bar{A}$-values.

The stress-strain, volume change, shear-induced pore water pressure and strength data indicate that the principle of effective stress holds for the rocks tested. The drained and undrained tests resulted in a single Mohr-Coulomb, and a single modified Mohr-Coulomb failure envelope in terms of effective stress for each rock type.

DD FORM 1473

Unclassified
Security Classification

Unclassified

KEY WORDS	LINK A		LINK B		LINK C	
	ROLE	WT	ROLE	WT	ROLE	WT
pore water pressure						
rock						
engineering properties						
triaxial cell						
triaxial compression test						
B-coefficient						
$\underline{A}$-coefficient						
$\overline{A}$-coefficient						
effective stress						

Final Technical Report

on

INFLUENCE OF PORE WATER PRESSURE ON THE ENGINEERING PROPERTIES OF ROCK

Sponsored by
Advanced Research Projects Agency
ARPA Order No. 1579, Amend. No. 3
Program Code 2F10

Monitored by

Bureau of Mines, Department of Interior
under Contract No. H0220069
Program Code Number 62701D

Effective Date of Contract	May 31, 1972
Contract Expiration Date	July 31, 1973
Amount of Contract	$ 34,000

Report Submitted by
Department of Civil Engineering
University of Illinois at Urbana-Champaign
Urbana, Illinois

Principal Investigator	G. Mesri, Ext. 217-333-6934
Project Scientist	G. Mesri, Ext. 217-333-6934

September 1973

TECHNICAL REPORT SUMMARY

The objective of this investigation is to determine the influence of pore water pressure on the engineering properties of rock. Under a previous contract, H0110085, pore water pressure effects were investigated by means of unconfined compression tests on dry and saturated rock specimens and using various rates of loading. A permeameter was also designed and built during the first year. The research program for the second year of investigation consists of studying the pore pressure effects by means of confined compression tests under controlled drainage or pore pressure conditions.

Two types of triaxial cell tops were designed and constructed at the early stage of the second year research program. The addition of the triaxial cell top to the previous permeameter resulted in a triaxial cell. The cell has a confining pressure capacity of 2000 psi with a factor of safety of 4.0. Special design provisions allowed saturation of low porosity rock specimens under pressure gradient and back pressure, and accurate control or measurement of volume changes and pore water pressures. The cell was used successfully to study the stress-strain, pore pressure, and volume change characteristics of cylindrical rock specimens (2 1/8-inch diameter, 4 1/4-inch long) in response to increasing all-around pressure or increasing axial load under drained and undrained conditions.

A series of drained triaxial compression tests were performed on Vermont marble in order to study strain rate effects. Six specimens were tested at an effective confining pressure of 500 psi and using rates

of axial strain ranging from 9.5×10^{-6} in/in/min to 5.9×10^{-3} in/in/min. For rates of axial strain less than about 3×10^{-4} in/in/min, peak deviator stress remained practically constant while at higher rates it decreased. Based on these results and consideration of the limitations of time and equipment, all of the triaxial compression tests were performed at a rate of strain of 3×10^{-4} in/in/min.

Isotropic compression and triaxial compression tests under drained and undrained conditions were performed on Berea sandstone, Salem limestone, Vermont marble, and Barre granite.

From the results of Isotropic compression tests, Skempton's B-coefficients were calculated. For all four rock types, the value of B-coefficient is found to be a function of the effective confining pressure. At small effective pressures, the values of B-coefficient were in the range of 0.85 to 1.0; they decreased continuously as a function of effective confining pressure to a range of 0.3 to 0.6 at 1500 psi. The B-coefficients were also computed using theoretical equations. The theoretical B-coefficients were higher than the experimental values for all rock types. All of the parameters used in the computations were either directly measured or could be estimated fairly accurately, with the exception of the compressibility of pore water. It is suggested that the compressibility of pore water is different than the compressibility of free, pure, deaired water.

Drained triaxial compression tests were performed at confining pressures of 400 psi, 1000 psi, and 2000 psi. Undrained tests were performed using confining pressures of 800 psi, 1400 psi, and 2000 psi and an initial back pressure of 400 psi (initial effective confining

pressures; 400 psi, 1000 psi and 1600 psi). All of the rock specimens tested herein exhibited volume decreases in drained tests and developed positive shear-induced pore water pressures in undrained tests at the initial stage of loading. The volume decreases and pore pressure increases leveled off at about one third of the axial strain corresponding to the maximum principal stress difference. Upon further loading the specimens started to dilate, leading to volumetric expansions in drained tests and pore pressure decreases in undrained tests.

Skempton's $\bar{A}$-coefficients were calculated with the results of undrained tests. The $\bar{A}$-coefficient maximized at the early stage of loading (at axial strains of less than 0.1%) and then decreased continuously, becoming negative at or near rupture for all rock types. The maximum $\bar{A}$-coefficient for the rocks tested in the present study ranged between 0.2 and 0.4. The equations for A- or $\bar{A}$-coefficient were summarized. A new equation for the $\bar{A}$-coefficient was proposed in terms of the compressibility coefficients from drained isotropic compression tests and drained triaxial compression tests. The new equation was compared with $\bar{A}$-values from undrained tests. The proposed equation agreed with reasonable accuracy with the directly measured $\bar{A}$-values for Berea sandstone and Salem limestone. However the $\bar{A}$-measurements on Vermont marble and Barre granite did not agree with the values given by the equations. It is suggested that drained tests on these rocks were performed too rapidly.

The stress-strain, volume change, shear-induced pore water pressure and strength data indicate that the principle of effective stress holds for

the rocks tested in this investigation. That is, the changes in effective normal stress, defined as total normal stress minus the pore water pressure, control deformation and strength of these rocks (within the range of variation in effective stress used in the present study).

The drained and undrained tests resulted in a single Mohr-Coulomb failure envelope in terms of effective stress for each rock type. In all cases the failure envelope was concave to the normal stress axis. The modified Mohr-Coulomb failure envelope plotted as a straight line for each rock type.

Rock is a porous material and under natural conditions its pores are saturated with water. The effective normal stresses rather than total normal stresses are expected to control deformation and strength characteristics of rock. Therefore a knowledge of pore water pressures in rock in conjunction with a suitable effective stress equation will be of value in design of deep underground structures.

ACKNOWLEDGMENT

This research was supported by the Advanced Research Projects Agency of the Department of Defense and was monitored by the Bureau of Mines under contract No. 0220069. Mr. Peter G. Chamberlain, Twin Cities Mining Research Center, U. S. Bureau of Mines, has served as the technical project officer. Mr. Chamberlain's cooperation throughout the research program is sincerely appreciated.

TABLE OF CONTENTS

LIST OF TABLES

LIST OF FIGURES

Figure | Page

SYMBOLS

A	Pore pressure coefficient
$\bar{A}$	Pore pressure coefficient, $A \cdot B$
B	Pore pressure coefficient
C_c^I	Volume compressibility of a cylindrical specimen measured in a drained triaxial compression test with constant lateral stress
C_s^{II}	Volume compressibility of a cylindrical specimen measured in a drained triaxial lateral extension test with constant axial stress
C_c^{III}	Volume compressibility of rock skeleton measured under an all-around stress increase under drained condition ($= C_{sk}$)
C_s^{III}	Volume compressibility of rock skeleton measured under an all-around stress decrease under drained condition
C_L	Compressibility of pore water lines (change in internal volume of lines per unit change in pressure)
C_M	Compressibility of pore-pressure measuring device (change in volume of the device per unit change in pressure)
C_{min}	Volume compressibility of mineral particles due to the change in spherical component of stress
$\bar{C}_{min}$	Volume compressibility of mineral particles due to the change in intergranular stress
C_{sk}	Bulk (volume) compressibility of rock skeleton (measured by external strain gages)
C'_{sk}	Bulk (volume) compressibility of rock skeleton (measured by the volume of pore water drained out of specimen)
C_w	Compressibility of water
$\bar{c}$	Cohesion intercept
D	Scott's dilatancy coefficient
$\bar{d}$	Value of q at $\bar{p} = 0$
E	Modulus of elasticity (Young's modulus)
E_{50}	Tangent modulus at 50% peak principal stress difference
K	Bulk modulus
k	Coefficient of permeability
n	Porosity

$\bar{p}$	$\frac{\bar{\sigma}_1+\bar{\sigma}_3}{2}$
q	$\frac{\sigma_1-\sigma_3}{2}$
S_r	Degree of saturation
t	Time
u	Pore water pressure
Δu	Change in pore water pressure; Shear-induced pore water pressure
u_o	Initial pore water pressure; Back pressure
V	Volume
V_L	Volume of water in pore-pressure measuring system
V_v	Volume of voids
V_w	Volume of water
V_{sk}	Volume of rock skeleton
ΔV_{sk}	Volume change of rock skeleton
ε_z	Axial strain
ν	Poisson's ratio
ν^I	Volumetric strain of a rock specimen measured in a drained triaxial compression test with constant lateral stress
ν^{III}	Volumetric strain of a rock specimen measured under an all-around stress increase in drained condition
$\sigma_1,\sigma_2,\sigma_3$	Major, intermediate, and minor principal stresses
$\bar{\sigma}$	Effective stress
σ_o	Initial stress
σ_c,σ_3	Confining pressure; All-around pressure
σ_{oct}	Octahedral normal stress
τ	Shear stress
τ_{oct}	Octahedral shear stress
$\bar{\phi}$	Angle of internal friction
$\bar{\psi}$	Slope of q versus $\bar{p}$

SECTION 1

INTRODUCTION

1.1 Statement of Problem

In intact rock, resistance to deformation and rupture is developed by the intrinsic shear strength of minerals and shearing resistance at mineral contacts. The shearing resistance at mineral contacts is controlled by the frictional characteristics of mineral surfaces and intergranular contact stresses as well as by the cohesive bonds at the contacts. Pore water as a component of rock could alter the shearing resistance at mineral contacts in two distinct ways. The pressure in pore water can either decrease or increase intergranular contact stress (Terzaghi, 1945; Skempton, 1961). Pore water could interact with mineral surfaces and could alter their surface properties as well as the nature of bonding.

The pore water pressure in rock could develop either due to a static water head, or due to steady state seepage, or it could be generated by a permanent or transient change in the state of stress. Skempton (1954) proposed the use of pore water pressure coefficients A, $\bar{A}$, and B for soils. The A-coefficient is a measure of the pore pressures generated by the changes in the deviatoric (shear) component of stress, the B-coefficient is a measure of the pore pressures generated by changes in the spherical (hydrostatic) component of total stress, and $\bar{A} = B \cdot A$.

The magnitude of A-, $\bar{A}$-, and B-coefficients for rock could depend on such variables as:

1) degree of saturation of rock
2) porosity and permeability of rock

3) relative bulk compressibility of pore fluid, the minerals of which the grains are composed, and the rock skeleton
4) rate of change of the external stress state
5) boundary drainage conditions
6) stress history of the rock.

The purpose of this study is to determine the influence of pore water pressure on the engineering properties of intact rock.

1.2 Research Program

Under the previous contract, H0110085, pore water pressure effects were investigated by means of unconfined compression tests on dry and saturated rock specimens and using various rates of loading. A special permeameter was also designed and constructed in the first year. The permeameter was used to saturate rock specimens, measure rock permeabilities, and measure rock pore water pressures under changes in all-around confining pressures. A comprehensive literature survey was also made in order to review and summarize published theoretical and experimental studies of pore pressure effects in rock and other porous materials.

The research program for the second year of investigation consisted of studying the pore pressure effects on rock by means of triaxial compression tests under controlled drainage or pore water pressure conditions.

A triaxial cell top and a new loading cap were designed and constructed at the early stage of the second year research program. The addition of the triaxial cell top to the previous permeameter resulted in a triaxial cell.

A series of drained triaxial compression tests on Vermont marble was performed at various loading rates to determine an axial loading rate to be used in the main test series.

Drained triaxial compression tests and undrained triaxial compression tests with pore water pressure measurements were performed on four types of rock, namely: Berea sandstone, Salem limestone, Vermont marble, and Barre granite. Three different confining pressures ranging from 400 psi to 2,000 psi were used for each rock. Skempton's A- and B-coefficients were calculated and the influence of pore water pressure on the engineering properties of rock was studied.

1.3 Review of the First Year Research Accomplishments

A comprehensive literature survey was made in order to review and summarize published theoretical and experimental studies of pore pressure and effective stress in rock and other similar porous materials. There have been extensive studies dealing with the application of the effective stress equation to rock. The conclusion appears to be that the Terzaghi effective stress equation will hold true for rocks, except for those of very low porosity in which the pores are disconnected. Also as the effective confining pressure increases beyond the yield strength of the rock grains, the individual grains of rock undergo plastic deformation, thus reducing boundary porosity. For this condition, the effective stress equation is less applicable. The literature survey also indicated that pore fluids which have a high dielectric constant and are strongly adsorbed to the mineral surfaces, such as water,

can influence the surface properties of rock grains and the shear resistance at contacts. The nature of the interactions and the magnitude of these effects are mainly determined by the mineralogy of the rock.

Five series of unconfined compression tests were performed on Barre granite, Berea sandstone, Clinch sandstone, Nevada tuff, and Vermont marble. In all, a total of 112 unconfined compression tests were performed with rates of strain varying from 0.0001 in/in/min to 10.0 in/in/min. Tests were performed using 2 1/8-inch diameter and 4 1/2-inch long rock specimens under dry and saturated conditions.

Pore water had some influence on the strength of all rock types tested. For Berea sandstone and Clinch sandstone, the strengths of the saturated samples were less than the strengths of the samples which were tested dry. But as the rate of strain was decreased, the difference in the strength of dry and saturated specimens decreased. This behavior seems to suggest that the decrease in the strength of saturated specimens would be explained by positive pore pressure effects (positive A-coefficients). In the case of Vermont marble, both the deleterious effects of water and pore pressure effects were apparent. The saturated specimens were weaker than the dry specimens at slow rates of loading, but as the rate of strain was increased, the saturated specimens increased in strength, while the strength of dry specimens remained practically constant. The increase in the strength of the saturated specimens of Vermont marble with increase in strain rate is attributed to dilation of the rock during compression, producing negative pore water pressures (negative A-coefficients). For Barre granite and Nevada tuff, the

saturated specimens were weaker than the dry specimens and the difference in the strength of the dry and saturated specimens remained constant at all strain rates. In the case of Nevada tuff the strength reduction could be due to deleterious effects of water, whereas for Barre granite the reduction in the strength of saturated specimens is more likely due to positive pore pressure effects which were not appreciably influenced by the rate of strain.

A permeameter was designed and constructed. The permeameter was successfully used to saturate rock specimens and measure permeabilities and B-coefficients of the rock specimens.

Skempton's B-coefficient was measured for Barre granite, Clinch sandstone, Vermont marble and Berea sandstone. Skempton's equation for B-coefficient includes the compressibilities of the pore fluid and the rock skeleton and is based on the assumption that solids are relatively incompressible and Terzaghi's effective stress equation is applicable. According to Skempton's equation, the value of B-coefficient will be close to unity whenever the compressibility of the rock skeleton is much higher than the compressibility of the pore water. In cases where the compressibility of the rock skeleton is close to the compressibility of rock solids, Skempton's equation for B-coefficient does not apply and in this case the compressibility of rock solids has to be included in any equation for prediction of B-coefficients.

Rather interesting and, in some respects, surprising results were obtained in the B-coefficient measurements. At a back pressure of about 100 psi, and a cell pressure of about 140 psi, Berea sandstone and

Vermont marble gave B-coefficients of unity. Under the same conditions, Barre granite and Clinch sandstone gave a B-value of approximately 0.85. In all rocks, B-coefficients were low under small back pressures and continuously increased as back pressure increased.

SECTION 2

EXPERIMENTAL PROCEDURE

2.1 Description of Rocks Tested

2.1.1 Barre Granite

Barre granite is a uniform, gray, black, and white, medium-grained, dense rock with an interlocking, crystalline texture. The specimens were obtained from a quarry in Barre, Vermont. The petrographic description (Deere and Miller, 1966), based on thin-section micrographs, is as follows: "The sections show the typical bypidiomorphic granular texture of granite. Brown biotite (7%), altering in places to penninite, contains small crystals of zircon. Quartz (29%) exhibits undulatory extinction and is interstitial to the subhedral grains of plagioclase (An_7, 15%), orthoclase, and microcline (35% combined). Perthitic intergrowths of microcline and plagioclase make up 9% of the rock. Muscovite (4%) has developed in cleavage planes, or as irregular masses on the orthoclase. Accessory apatite, zircon, and magnetite make up less than 1% of the total." Barre granite has a dry unit weight of 165 pcf, a porosity of 2.7%, a specific gravity of solids of 2.70, and an unconfined compressive strength of 16,300 to 29,000 psi.

2.1.2 Berea Sandstone

Berea sandstone is a light gray, fine-grained, massive, porous rock with a cemented, partially interlocking texture of subangular grains.

The rock samples came from Amherst, Ohio. The petrographic description (Deere and Miller, 1966), based on thin-section micrographs, is as follows: "This rock consists of tightly packed subangular grains of quartz, and small amounts of plagioclase and microcline, all having a well sorted average grain size of 0.15 to 0.20 mm. Secondary quartz growth serves as the predominant cementing material; however, in places, a fine-grained calcite cement holds the detrital quartz grains in place." Berea sandstone has a dry unit weight of 138 pcf, a porosity of 20.3%, a specific gravity of solids of 2.66, and an unconfined compressive strength of 6,000 to 10,500 psi.

2.1.3 Vermont Marble (Taconic White)

Vermont marble is a very pure white, uniform, fine-grained, massive, saccharsidal marble with tightly interlocking, crystalline texture. The samples were supplied by Vermont Marble Company and obtained from West Rutland, Vermont. The petrographic description (Deere and Miller, 1966), based on thin-section micrographs, is as follows: "A coarse-grained calcite marble with interlocking calcite grains (2 mm.), some containing round quartz crystals." The marble has a dry unit weight of 169 pcf, a porosity of 2.1%, a specific gravity of solids of 2.75, and an unconfined compressive strength of 7,000 to 14,000 psi.

2.1.4 Salem Limestone

Salem limestone is a light-tan to brown, massive, porous rock. It is also called Spergen, Indiana, or Bedford limestone. The rock samples were supplied by Bureau of Mines and came from Bedford, Indiana. The geologic occurrence (Krech, 1973) is as follows: "Salem is a flat lying Mississippian age limestone which underlines the St. Louis limestone and in Indiana overlies the Harrodsburg limestone. In Indiana, Salem limestone is typically massive and lenticular, attaining thicknesses of 50 to 60 ft but locally pinching out.

Salem limestone is a distinctive rock type which may be called a micro-coquina and has even been referred to as a spergenite because of the abundance of fossils and fossil fragments. As the fossil shells accumulated, they were washed back and forth by waves, swept along by currents and finally deposited as bars and shoals along a shoreline, grading seaward into a normally bedded limestone. Megascopically the fossil remains resemble clean winnowed sand. After its burial, the calcareous sand was cemented by crystalline calcite."

The petrographic description (Krech, 1973) is as follows:

"Texture: Bioclastic.
Shells of gastropods, crinoid stems and calices are cemented together by crystalline calcite.

Phasis: Fossiliferous calcite - 69%, calcite cement - 31%.

Classification: Brecciated limestone or coquina."

Salem limestone has a dry unit weight of 146 pcf, a porosity of 12.6%, a specific gravity of solids of 2.66, and an unconfined compressive strength of 7,300 psi (0.02% strain/min load rate).

2.2 Specimen Preparation

Rock specimens were obtained by coring 6-inch thick quarry blocks. All of the specimens were cored with their longitudinal axes perpendicular to the bedding planes. The blocks were drilled with a 2 1/8-inch diameter, water-cooled, diamond-bit core barrel. The samples were then cut to a length which gave a height-diameter ratio of two, using a water-cooled diamond saw. Next the sample ends were polished using a Crane Lapmaster until the variation in height was less than 0.005 inches. After lapping, the samples were cleaned with benzene to remove the lapping fluid and any particles of rock or lapping abrasive which might have accumulated on the ends of the samples. The samples were then scrubbed with soap and water and rinsed thoroughly.

During the saturation and permeability measurements it was discovered that the Crane Lapmaster method of end preparation resulted in low permeability end surfaces (fine particles plugged the voids of the rock at the end surfaces). In order to avoid this problem the method of end preparation was modified for Berea sandstone and Salem limestone which were of relatively high permeability. The modified method of end preparation consisted of machining the ends using a lathe and a diamond bit. This procedure worked very satisfactorily for these samples.

2.3 Apparatus

2.3.1 Triaxial Compression Cell

A 2,000 psi capacity triaxial cell was designed and constructed for this study, Figures 2.1 and 2.2. The triaxial cell was designed for 2 1/8-inch diameter (NX core) and 4 1/4-inch long specimens. The cell can be used for: (1) saturation of rock specimens, (2) measurement of permeability, B-coefficient, and volumetric strain, and (3) drained or undrained triaxial compression tests with pore water pressure control. In the design and construction of the cell, special attention was paid to provisions for accurate measurement and control of pore water pressure.

There are two drainage connections in the base pedestal and two drainage connections in the loading cap. The drainage connections can be used to saturate the rock specimens, and to measure volume changes or pore water pressures under hydrostatic and deviatoric stress conditions. The drainage lines are made of continuous stainless steel tubing (O.D. = 0.125-inch, I.D. = 0.073-inch) with no sharp bends or any intermediate connections. This important feature substantially reduces the compressibility of the pore-pressure measuring system and practically eliminates the possibility of trapping air bubbles in the pore pressure lines. The drainage tubings are connected to the drainage fittings using Eccobond 51 epoxy adhesive supplied by Emerson and Cuming Inc., Canton, Massachusetts. In the pore water pressure measuring system all of the connections are made with cone fittings, and as much as possible valves are eliminated from the pore pressure connections. This feature further reduces the compressibility of the system.

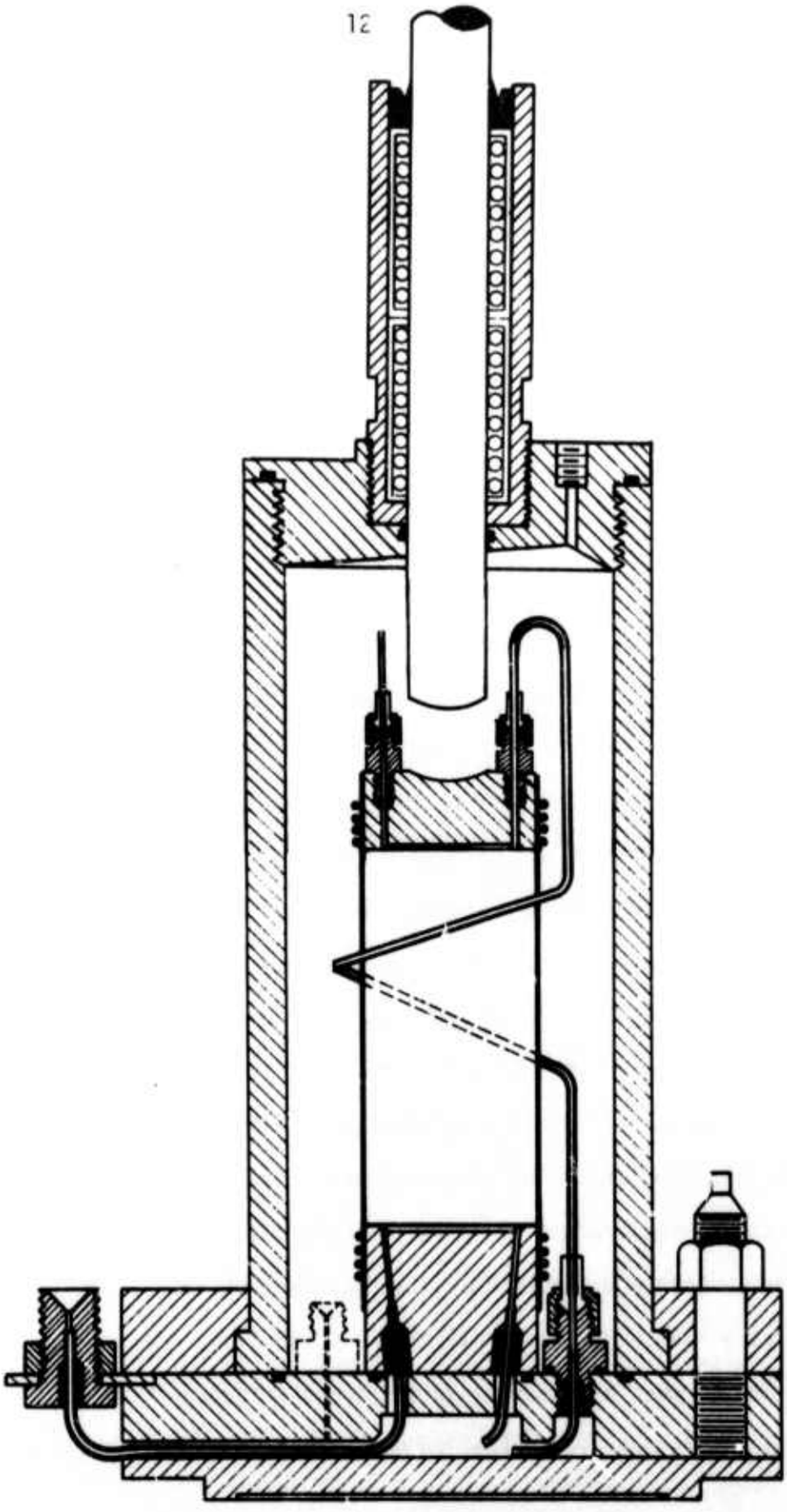

Fig. 2.1 Triaxial Compression Cell, Cross Section A-A

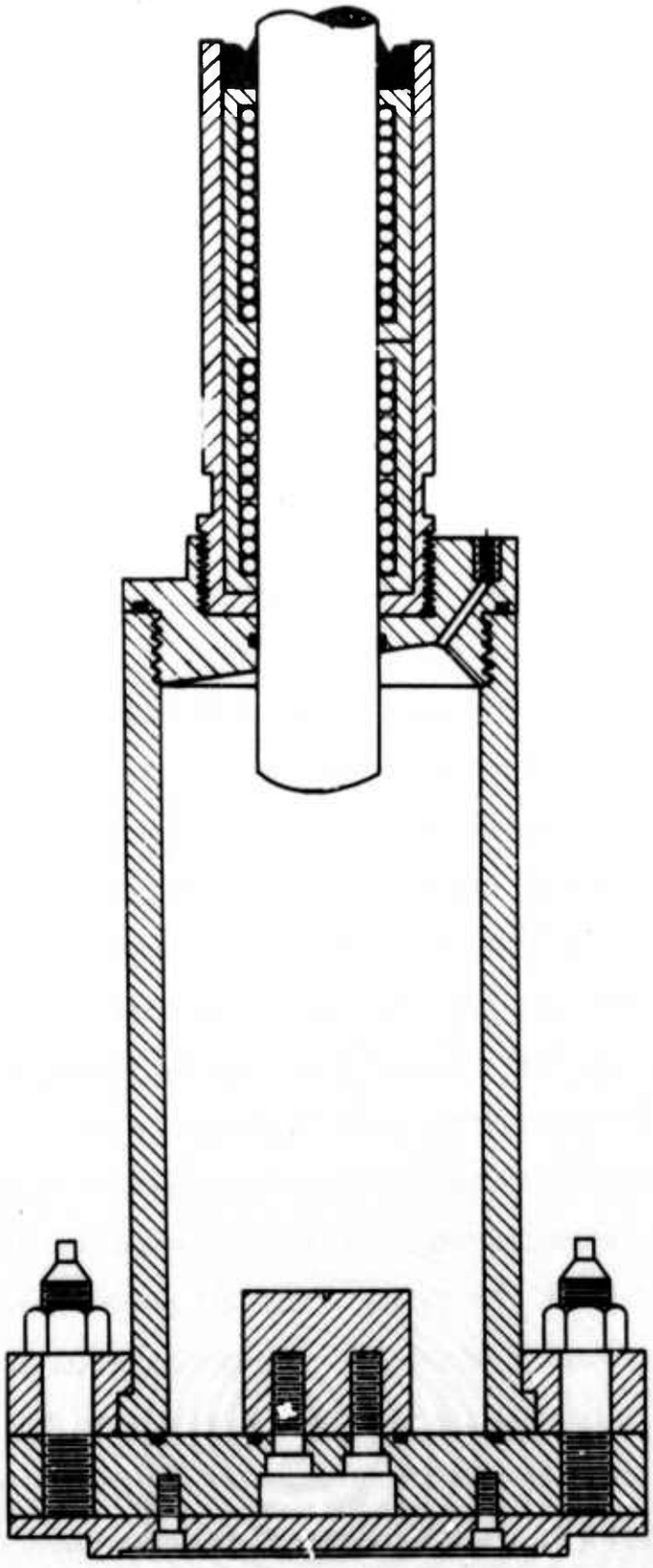

Fig. 2.2 Triaxial Compression Cell, Cross Section B-B

There is only one 2000 psi-capacity Circle Seal valve in each pore pressure line, and this valve is absolutely necessary for back pressure control.

The triaxial cell is constructed of stainless steel. All of the O-ring grooves have been designed for minimum volume change during cell pressure change, and all of the stainless steel surfaces which act as seals are highly polished. These provisions reduce the compressibility of the cell and practically eliminate leakage of the cell fluid. This feature allows accurate control and measurement of the total volume of the rock samples under various loading conditions.

The triaxial cell top consists of a highly polished and hardened, 1-inch diameter, type 440 C stainless steel loading piston supplied by Thomson Industries Inc., and has an axial loading capacity of 60 kips, Figure 2.3. Also a modified higher capacity triaxial cell top was constructed. It consists of a highly polished and hardened, 1 1/2-inch diameter stainless steel loading piston and has an axial loading capacity of 135 kips, Figure 2.4. The stainless steel loading piston is guided into the cell by two Thomson Series-A ball bushings. A wiper seal at the top helps to keep dust out of the bushing assembly, and an X-ring pressure seal manufactured by Minnesota Rubber Co. is used between the lower ball bushing and the cell fluid. The X-ring is made of Buna-N rubber with a Shore A durameter hardness of 70 degrees. Photographs of the triaxial cell top and the triaxial cell are shown in Figures 2.5 and 2.6. The detailed design drawings of the modified higher capacity triaxial cell top are included in Appendix A. Design drawings of the other parts are included in the previous reports (Mesri et al, 1972; Mesri and Adachi, 1972).

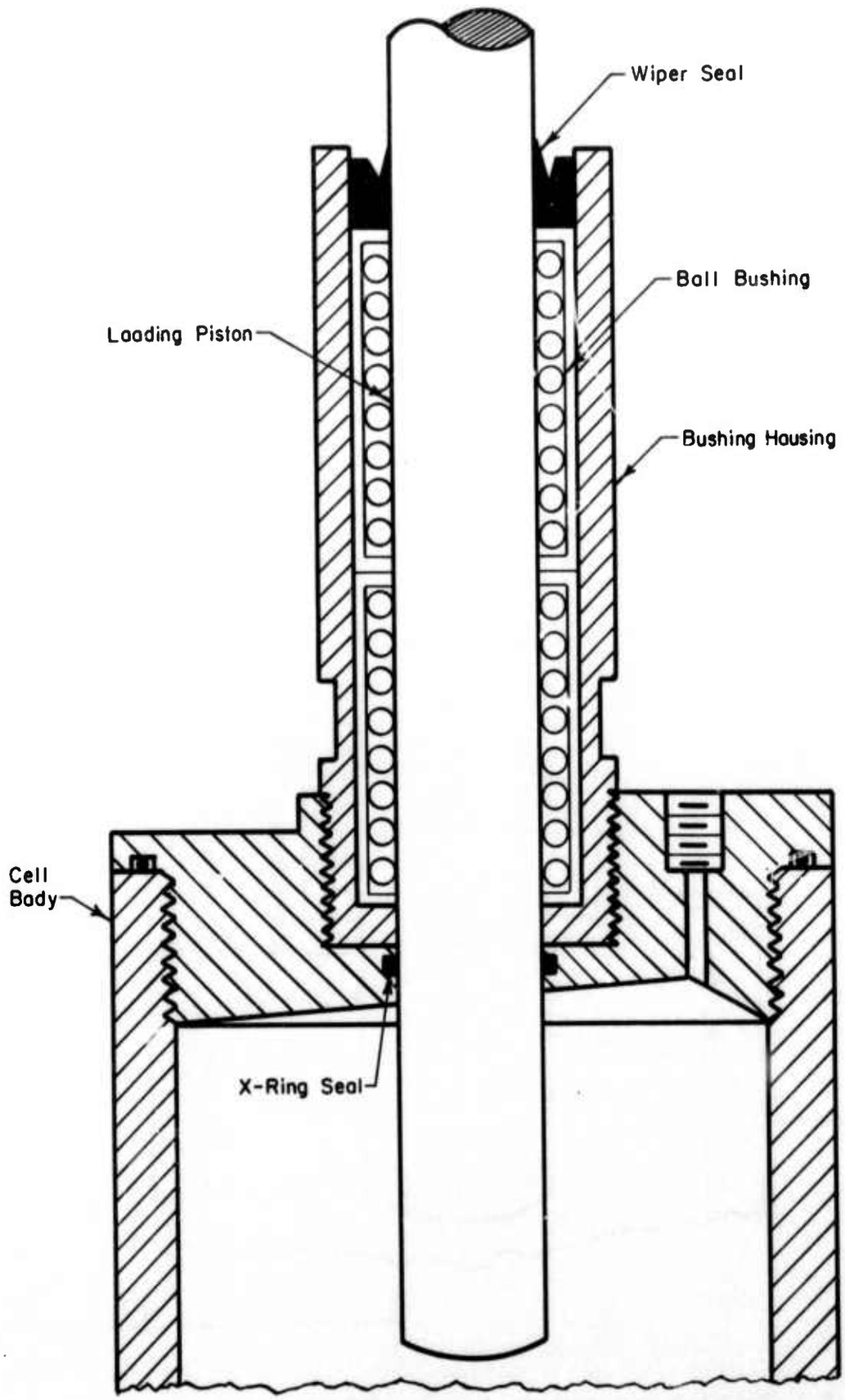

Fig. 2.3 Triaxial Cell Top, Cross Section

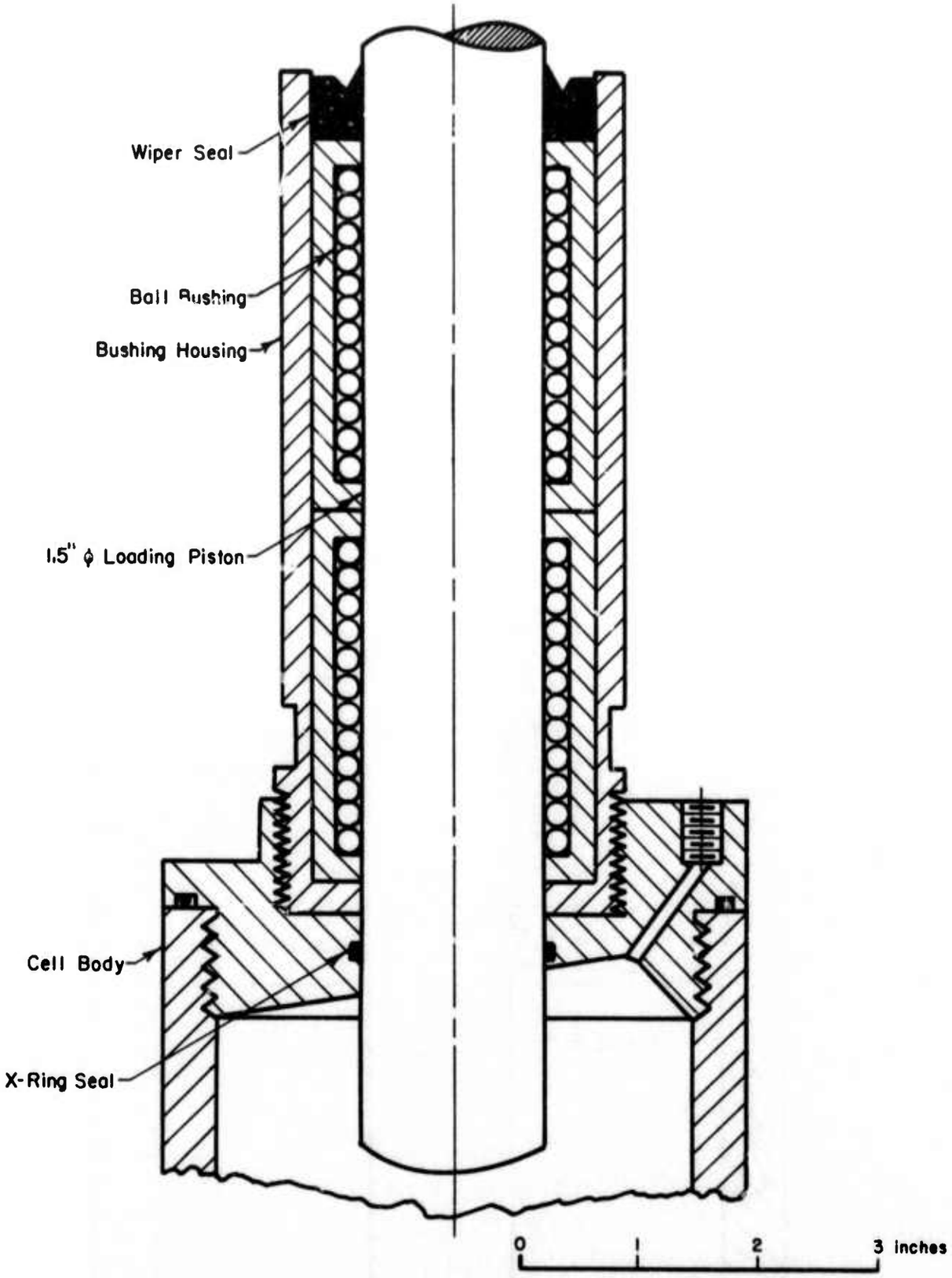

Fig. 2.4 Modified High Capacity Triaxial Cell Top, Cross Section

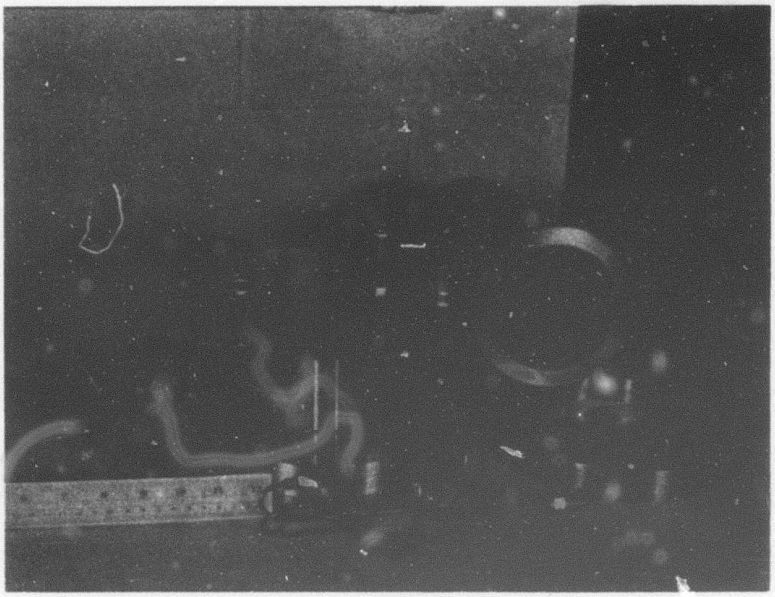

Fig. 2.5 Triaxial Compression Cell, Unassembled

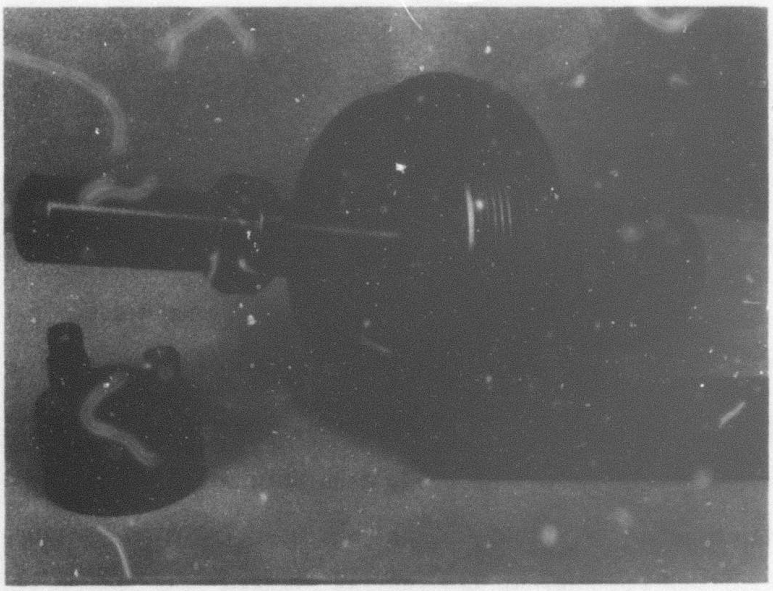

Fig. 2.6 Triaxial Cell Top

2.3.2 Pressure Control and Loading System

Compressed notrogen gas and air regulator valves were used to apply and control confining pressure and back pressure to the rock specimens, Figure 2.7. A specially designed gas-mercury-water transfer unit was used in order to eliminate the possibility of gas diffusion into the cell and rock specimens. A pressure control panel with various regulators and pressure gages was used to monitor cell and back pressures.

Drained or undrained triaxial compression tests were performed using an "L"-type Tinius-Olsen testing machine manufactured by Tinius-Olsen Testing Machine Co., Willow Grove, Pennsylvania. The machine has a selecto-range indicator which provides rates of deformation from 2.0×10^{-5} inch per minute to 1.0 inch per minute. The maximum load at full range can be selected from 16 kips, 80 kips, and 400 kips. The displacement of the loading ram was measured by a 0.0001-inch dial gage which was used to calculate the axial deformation or axial strain of the rock specimen. Figure 2.8 shows the "L"-type Tinius-Olsen testing machine.

2.3.3 Pore-Water-Pressure Measuring Equipment

Two types of pore-water pressure transducers were used in this study. A Dynisco, Model PT25 electrical pressure transducer with a range of 0 to 1000 psi was used in low pressure tests, and a thin film strain-gauge pressure transducer Model PG856-5M, manufactured by Statham Instruments, Inc. with a range of 0 to 5,000 psi was used for high pressure tests. These transducers are temperature compensated, having less than 0.5%

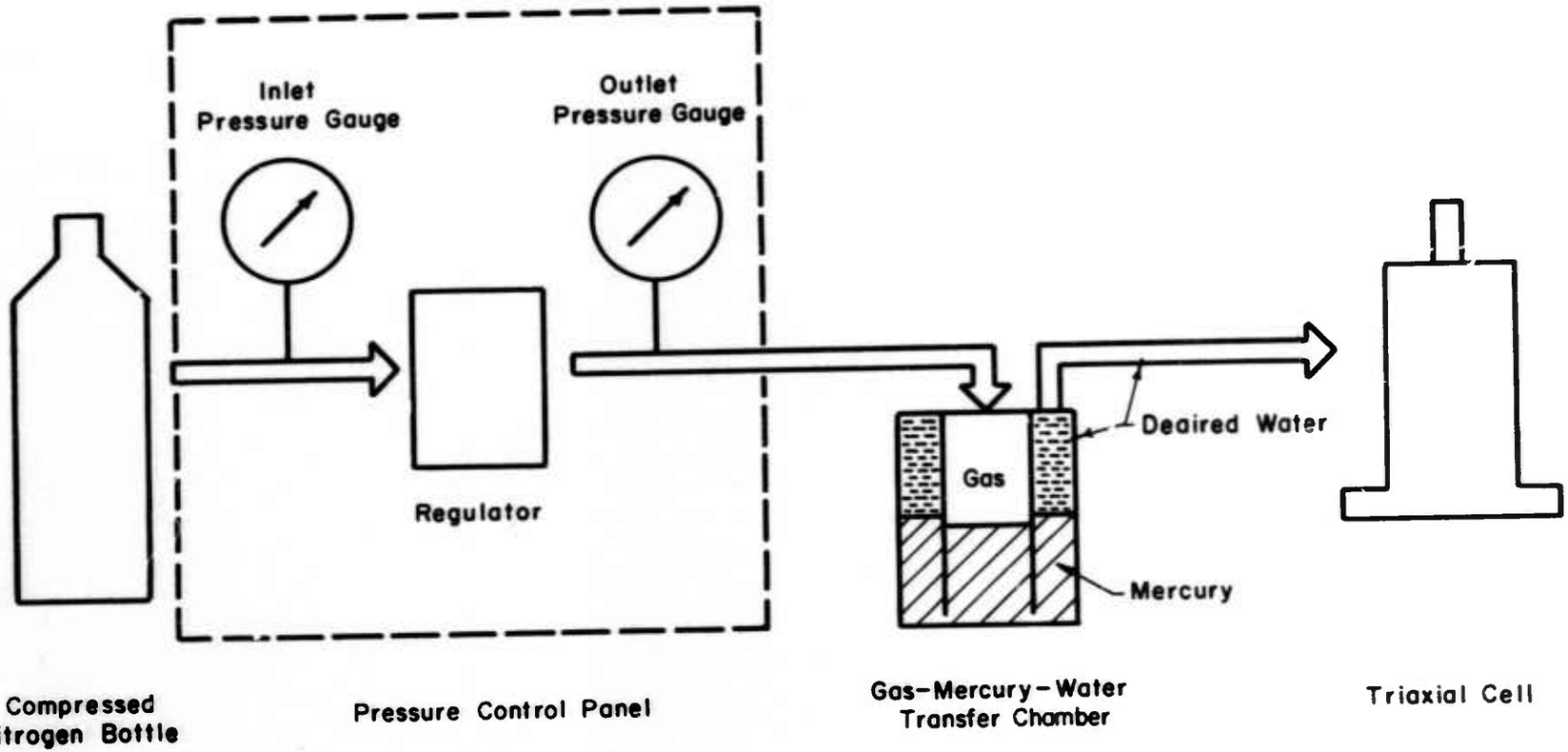

Fig. 2.7 Pressure Control System

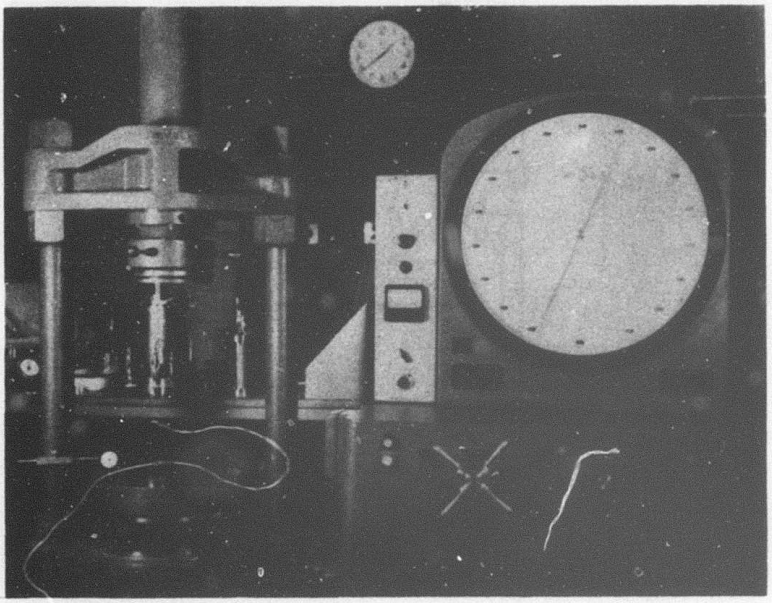

Fig. 2.8 "L"-type Tinius-Olsen Testing Machine

non-linearity and hysteresis, and exhibit very small volume changes during pore pressure measurements. The output of the transducers were measured by a Type N SR-4 strain indicator manufactured by Baldwin-Lima-Hamilton Company. Detailed descriptions of the pore pressure transducers are included in Appendix B.

2.4 Testing Procedure

The triaxial testing procedure consists of six major steps: (1) preparation of rock specimens, (2) setting up of rock specimens in the triaxial cell, (3) saturation of the system and rock specimens and measurement of rock permeability, (4) measurement of Skempton's B-coefficient, (5) measurement of volumetric strain, and (6) axial loading of the rock specimen under drained or undrained conditions. In drained tests volume changes are measured and in undrained tests pore pressure transduers are used to monitor excess pore water pressures. In some control drained tests pore pressure was measured at the base while drainage was allowed at the top of the specimen.

2.4.1 Specimen Setup

The rock specimens were oven-dried for at least 48 hours under a temperature of 110°C before being set up in the triaxial cell, in order to remove hygroscopic moisture which could block pores during the saturation stage. Then the specimens were cooled in a vacuum-desiccator and were set up in the triaxial cell.

All of the drainage lines were saturated prior to specimen setup with distilled, deaired water. The rock specimen was placed on the base pedestal and the loading cap was placed on it. The contacts between the rock specimen and the base pedestal or the loading cap represent discontinuities into which rubber membranes may protrude and rupture under high confining pressures. To prevent the above occurrence, three layers of thin aluminum foil were placed around the contacts. Then the specimen was encased in three 0.012-inch thick rubber membranes. The membranes were sealed at both ends by means of four No. 222 rubber O-rings, Figure 2.9. Before placing the first rubber membrane on the sample, a thin layer of high-vacuum silicon grease was placed on the base pedestal and the loading cap. Silicon grease was placed also on the membrane-to-membrane contacts under the O-ring seals. For the porous rock specimens such as Berea sandstone or Salem limestone, the rubber membranes were protected against protrusion and rupture by a layer of thin aluminum foil which was placed around the rock specimen. Figure 2.9 shows a specimen after setup on the triaxial base. The cell then was assembled and filled with cell fluid. Distilled, deaired water was used as the cell fluid in this study.

2.4.2 Saturation of Rock Specimens and Permeability Measurements

A cell-fluid pressure was applied, which sealed the membranes against the sample surface, and then distilled, deaired water was forced to flow from the bottom up through the specimen under a constant pressure difference. A pressure difference in the range of 20 to 800 psi was used

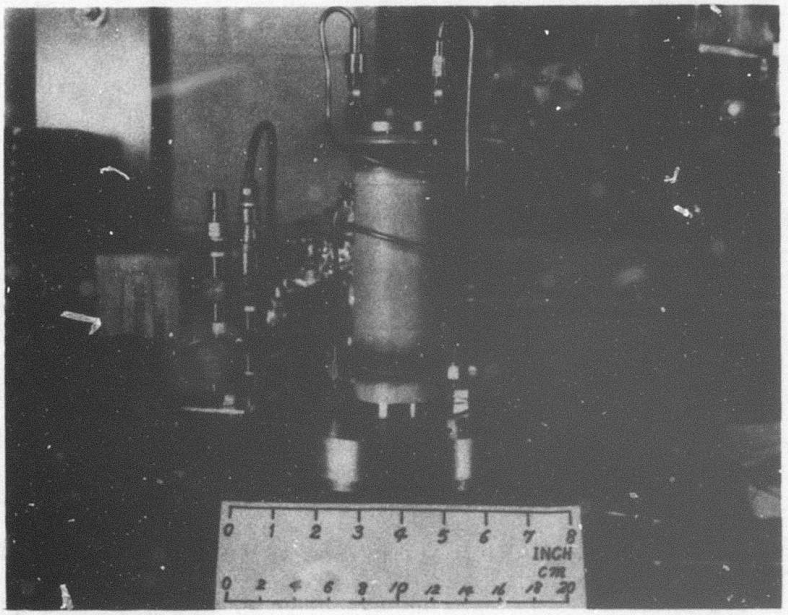

Fig. 2.9 Specimen Setup

depending on the estimated permeability of the rock specimen. The cell fluid pressure was selected to be higher than the back pressure by about 150 psi, which was enough to seal the contact between the membrane and the specimen. A vacuum was applied to the top drainage connection to further promote specimen saturation. When a constant rate of flow was established, permeability of the specimen was calculated.

2.4.3 B-Coefficient Measurements

After the rock specimen was saturated with the drainage line to the top of the specimen open, a confining pressure was applied and the specimen was allowed to come to equilibrium under the pressure. At the end of this period all of the drainage lines were reflushed by distilled, deaired water to insure complete saturation of the drainage lines. Next, a 1000-psi or 5000-psi capacity pore-water pressure transducer was connected to one of the drainage lines. With all of the valves to the other drainage lines closed, the cell pressure was increased by an increment and the change in pore water pressure was observed with time. When the pore pressure became constant with time, a back pressure equal to the cell pressure increment was applied in order to pressure saturate the specimen and maintain a constant effective confining pressure. This procedure was repeated until a constant B-coefficient was observed under the given effective confining pressure.

The whole process was continued under a different effective confining pressure. Finally a relationship between B-coefficient and effective

confining pressure was obtained for each type of rock. Typical B-coefficient measurement results are shown in Figure 2.10, which illustrate the above-mentioned testing sequence.

2.4.4 Volumetric Strain Measurements

One of the drainage lines from the saturated rock specimen was connected to a pipette to measure volume changes of the specimen under a change in all-around confining pressure. An all-around confining pressure was applied to the specimen and the corresponding volume changes were observed with time until the specimen came into equilibrium under the pressure. Then a different confining pressure was applied and volume changes were observed. By continuing the process, a relation between volumetric strain and confining pressure was obtained for each type of rock.

2.4.5 Drained Triaxial Compression Tests

Drained triaxial compression tests were performed using an "L"-type Tinius-Olsen testing machine. Tests were all performed at constant rates of deformation of 0.001-inch per minute (3.0×10^{-4} in/in/min). The rate was selected after a strain rate study (see Section 3.1).

The triaxial cell with a saturated rock specimen was placed in the loading frame, and a confining pressure was applied through the pressure control system to the cell. In drained tests, three different confining pressures of 400 psi, 1000 psi and 2000 psi were used for each type of rock. One of the drainage lines from the specimen was connected to a pipette and

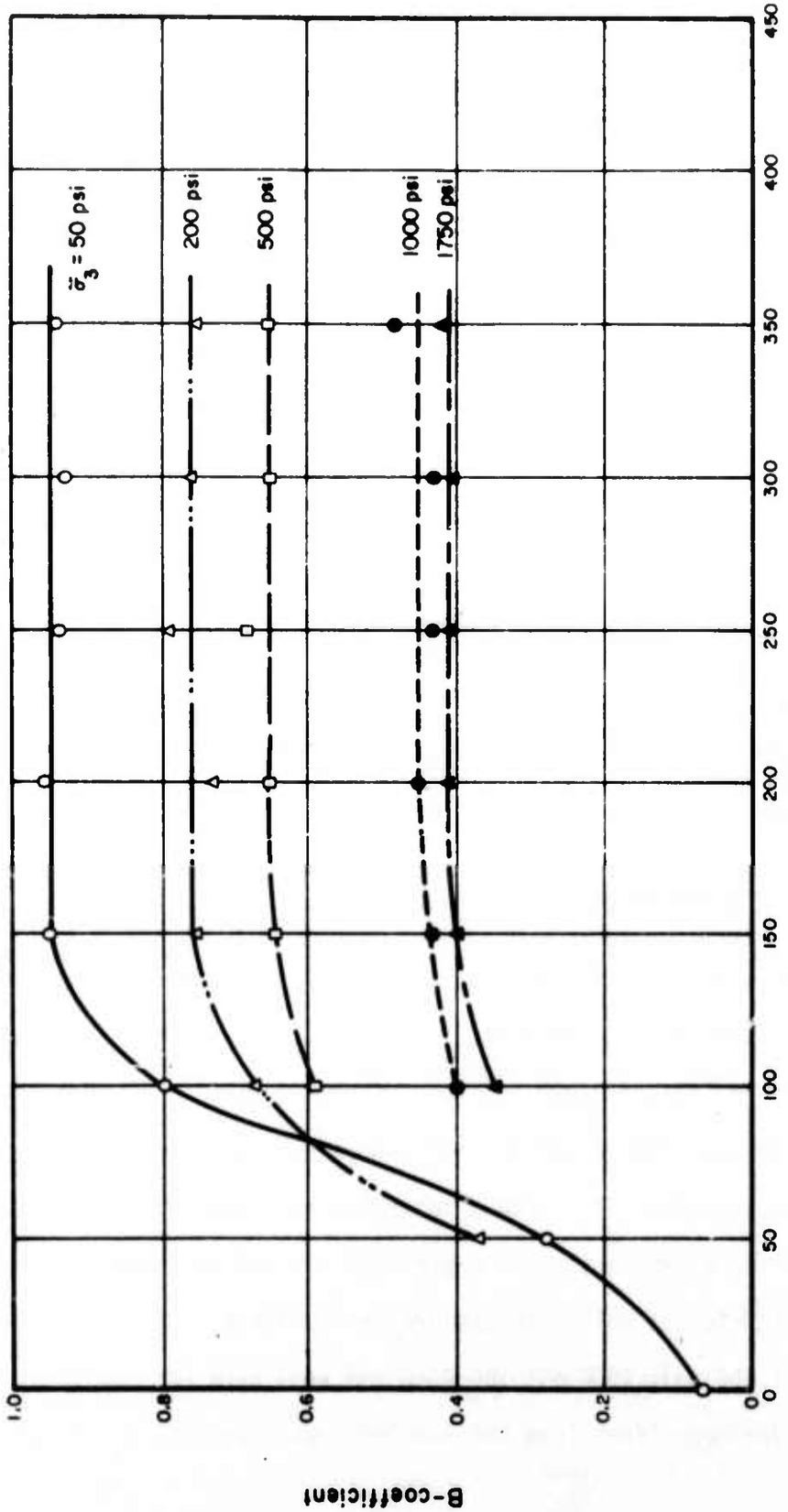

Fig. 2.10 B-Coefficient Measurements, Vermont Marble

volume changes were measured until equilibrium was established under the applied confining pressure. Then the axial load was applied with a selected rate of deformation, leaving the top drainage line open (In a number of control tests pore pressure was observed through the base drainage connection.). The test was continued until the failure of the rock specimen took place. During the testing, applied loads, loading ram displacements, volume changes, and time were recorded, Figure 2.11.

After the testing, the specimen was carefully dismantled and its total weight measured in order to calculate the degree of saturation. Finally the failed specimen was put into a plastic bag and stored for future reference.

2.4.6 Undrained Triaxial Compression Tests

Except for the drainage conditions, undrained triaxial compression tests were performed in the same manner as drained triaxial compression tests. In undrained triaxial compression tests, one of the drainage lines was connected to a pore water pressure transducer and changes in pore water pressure were measured, while all the drainage lines were kept closed. In undrained tests, the pore water pressure at the beginning of the tests was equal to 400 psi for all of the specimens and three different confining pressures of 800 psi, 1400 psi, and 2000 psi were used for each type of rock. After the testing, $\bar{A}$-coefficients were calculated from the measured pore water pressure changes.

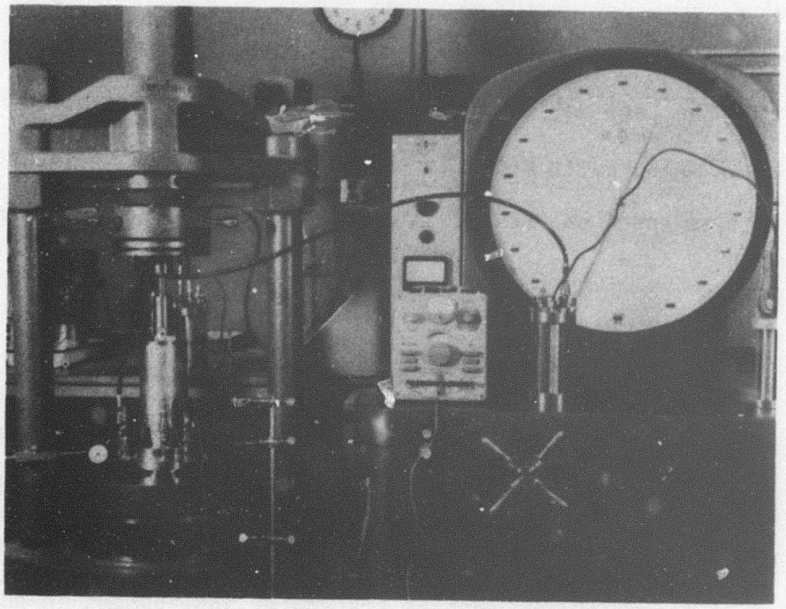

Fig. 2.11 Overall Setup of Triaxial Compression Tests

SECTION 3

EXPERIMENTAL RESULTS

3.1 Strain Rate Study

A series of drained triaxial compression tests were performed on Vermont marble specimens in order to determine the axial strain rate to be used in the rest of the research program. Vermont marble was selected for the strain rate study because it has the lowest permeability among the rock types which have been tested.

Six Vermont marble specimens were tested at rates of axial deformation ranging from 9.6×10^{-6} in/in/min to 5.9×10^{-3} in/in/min under the confining pressure of 500 psi. The test results are summarized in Table 3.1. The average porosity of all the specimens is about 2%, the average degree of saturation is about 95% (ranging from 80% to 100%) and there is a general tendency toward volume decrease during shear.

The test results are shown in Figures 3.1 to 3.6 in terms of principal stress difference and volumetric strain versus axial strain. The deformation of the system was calibrated and axial strains were adjusted to exclude system deformations.

The results are summarized in Figure 3.7 in which maximum principal stress difference at failure and maximum volumetric strain are plotted versus strain rate. The observed volume decreases ranging from 0.05% to 0.1% appear to indicate that positive pore water pressures were

Table 3.1 Summary of Strain Rate Tests, Vermont Marble

Sample No.	Porosity n(%)	Degree of Saturation S_r(%)	Confining Pressure σ_3(psi)	Loading Rate in/in/min	At $(\sigma_1-\sigma_3)_{max}$ Axial Strain ε_z(%)	$\sigma_1-\sigma_3$ (psi)	Max. Volumetric Strain ν^I_{max}(%)
101	1.9	100	500	5.88×10^{-3}	0.728	10,360	-0.043
102	2.1	100	500	4.71×10^{-5}	0.665	11,700	-0.118
103	2.2	80	500	1.18×10^{-3}	0.591	8,850	-0.080
104	2.0	92	500	9.41×10^{-6}	0.590	11,400	-0.110
105	1.9	100	500	2.35×10^{-4}	0.691	11,910	-0.090
106	4.3	81	500	1.18×10^{-3}	0.495	10,360	-0.060

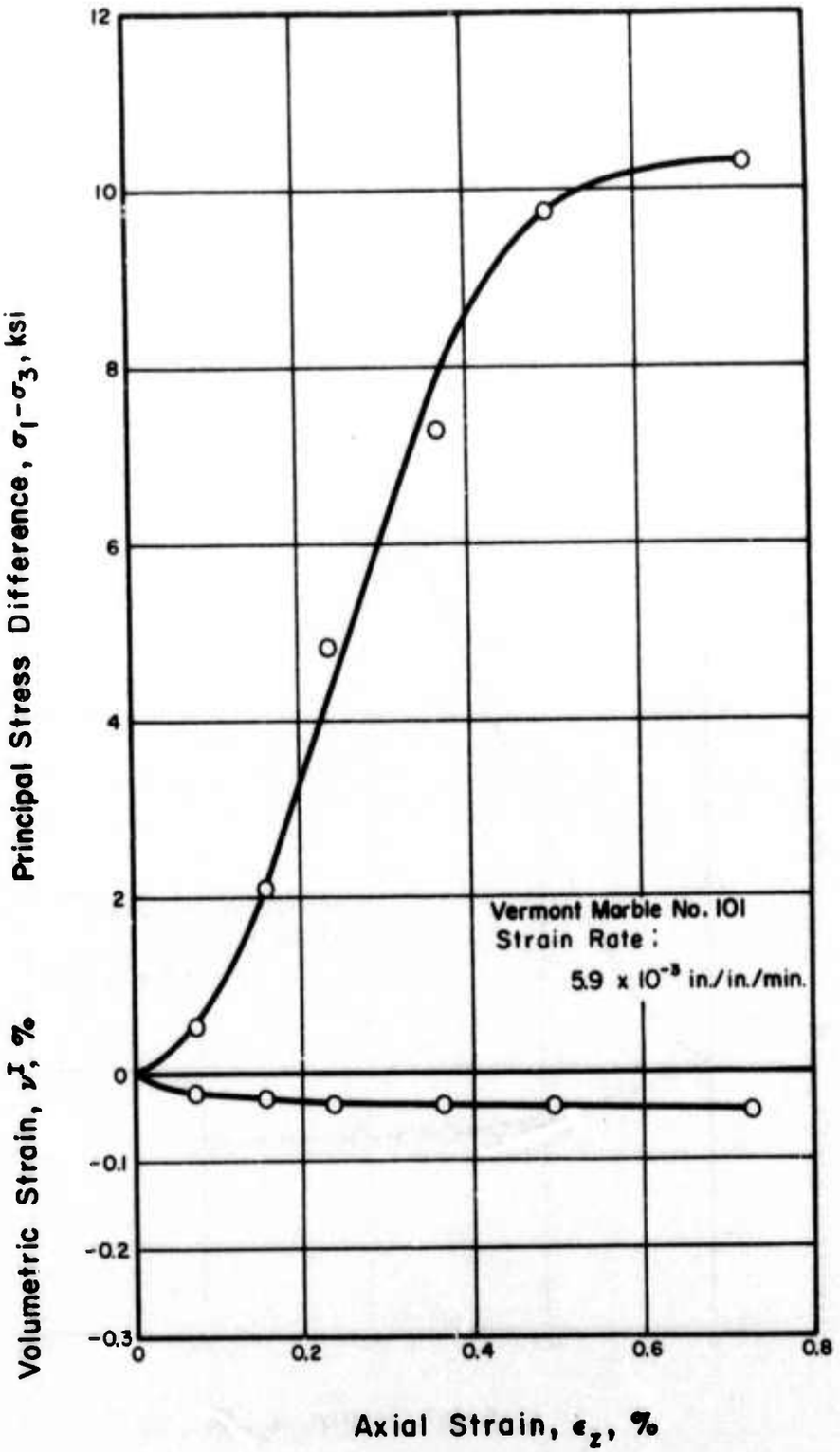

Fig. 3.1 Principal Stress Difference and Volumetric Strain Versus Axial Strain, Vermont Marble, No. 101

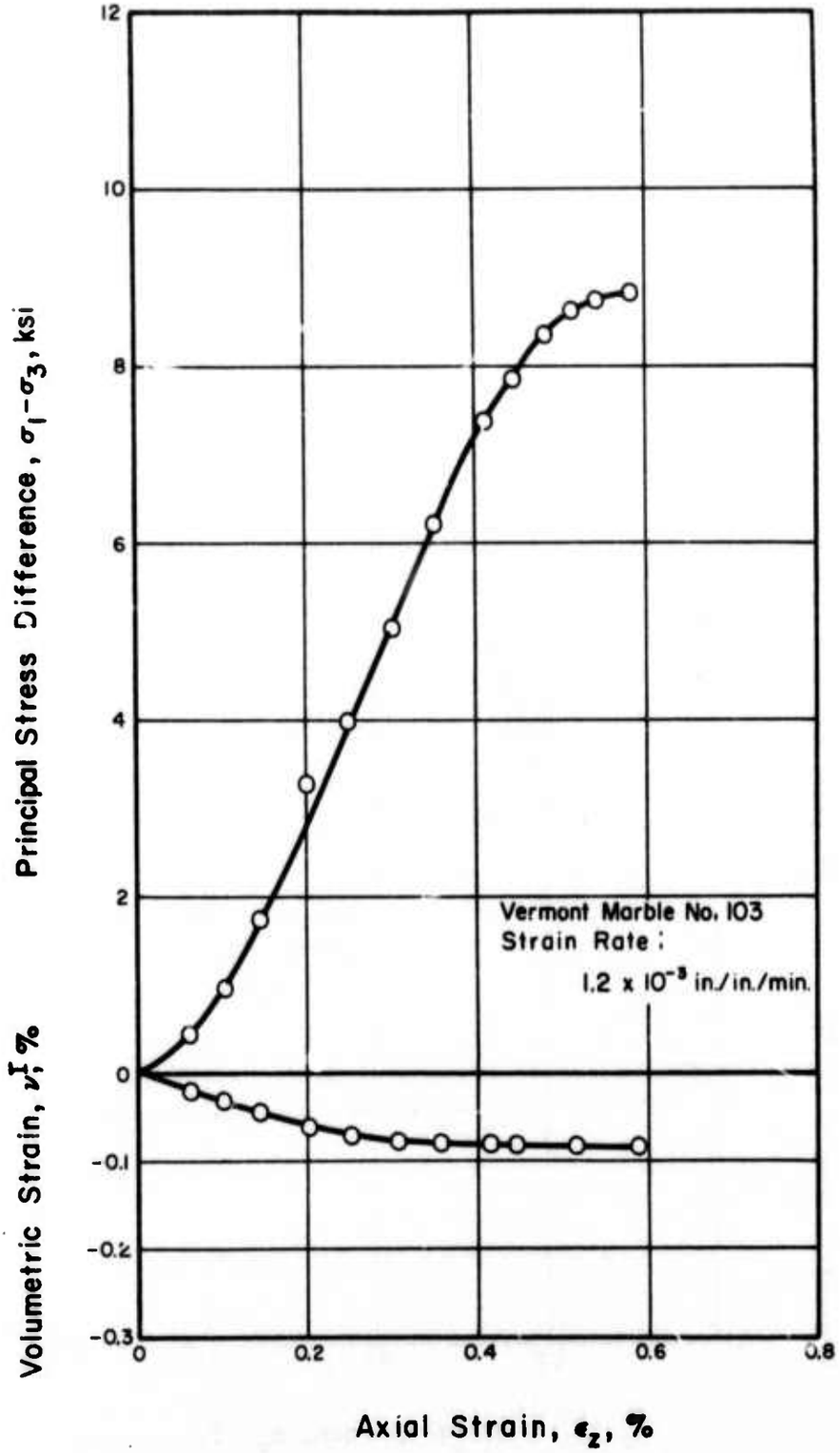

Fig. 3.2 Principal Stress Difference and Volumetric Strain Versus Axial Strain, Vermont Marble, No. 103

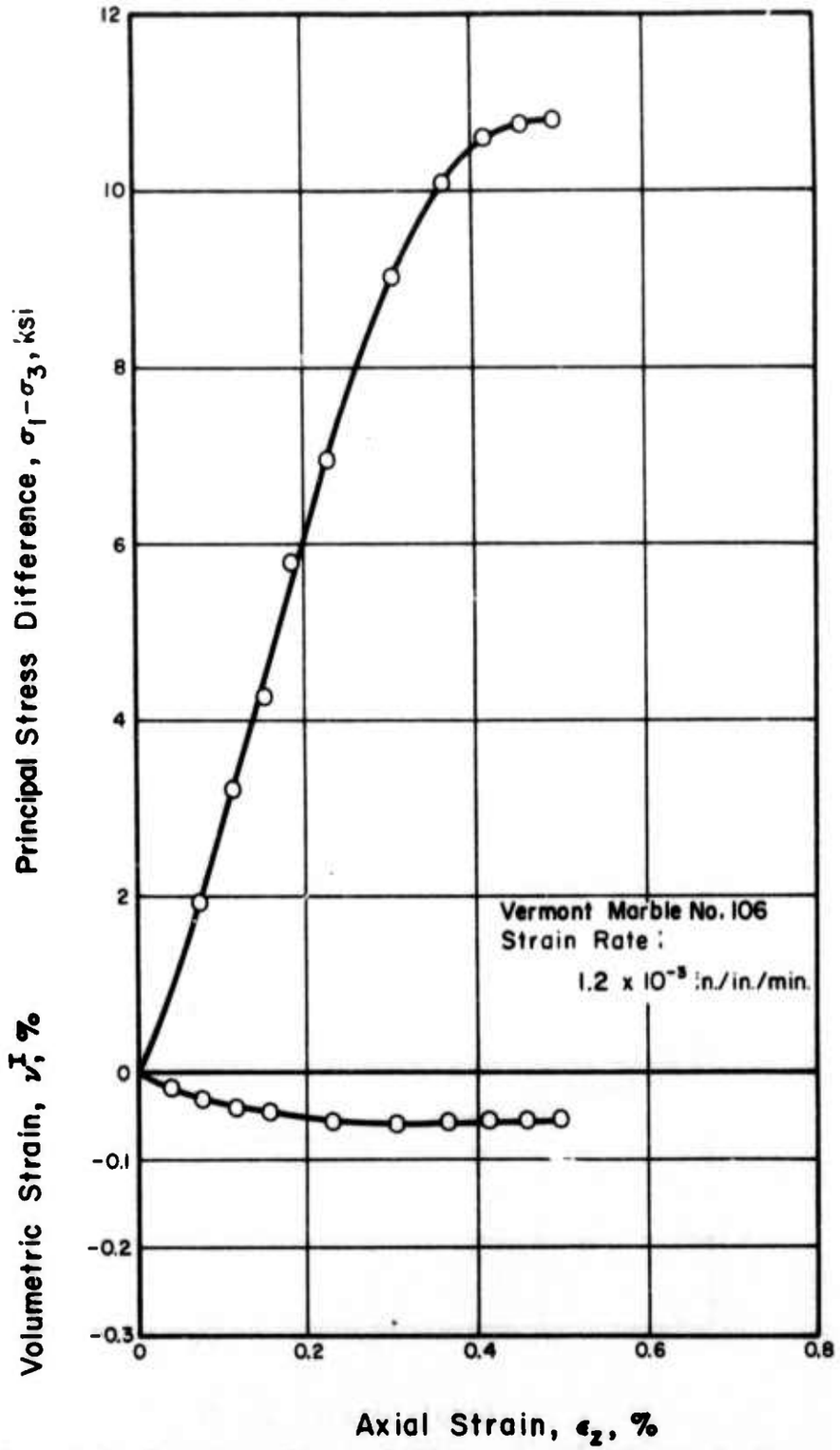

Fig. 3.3 Principal Stress Difference and Volumetric Strain Versus Axial Strain, Vermont Marble, No. 106

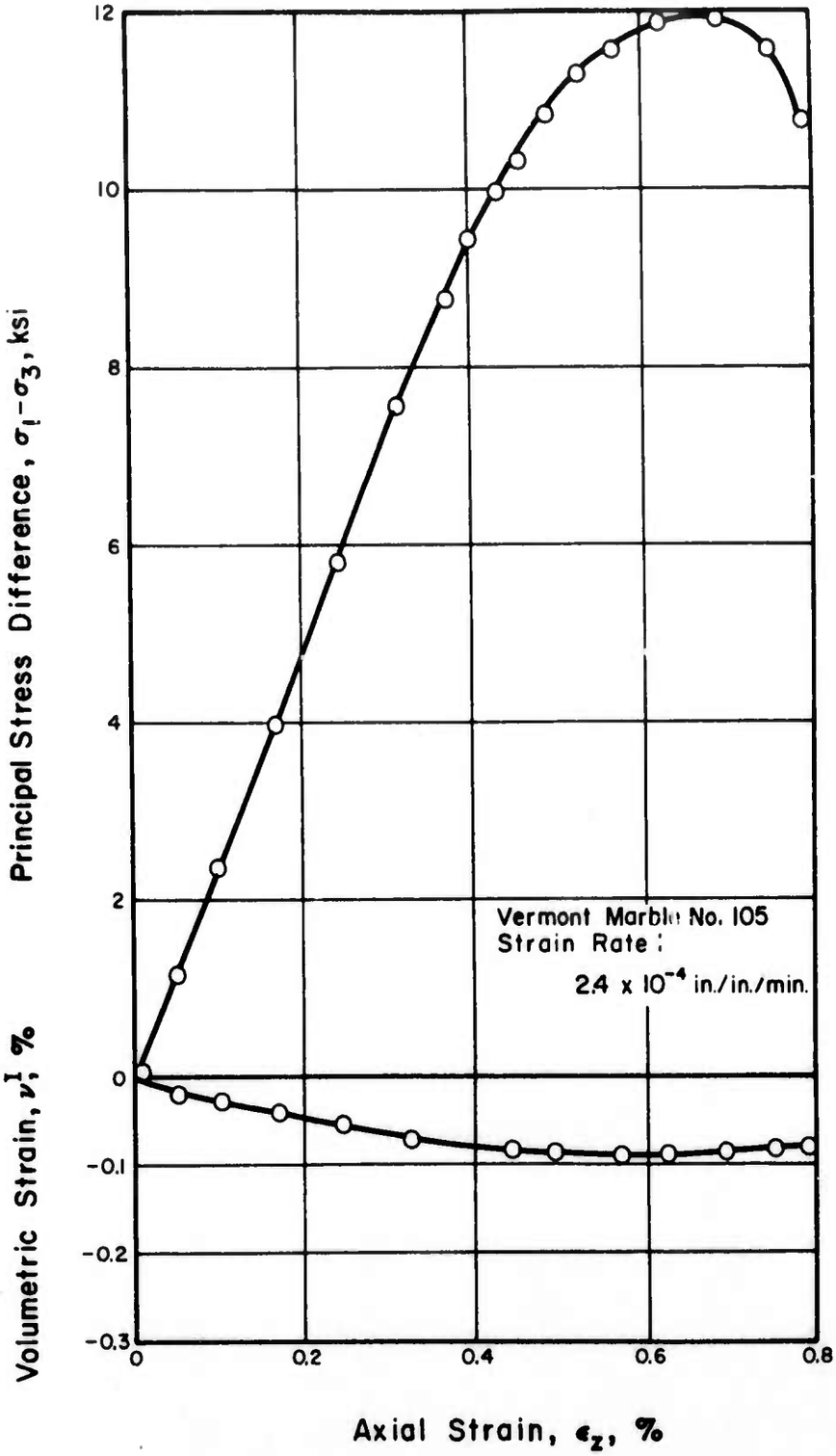

Fig. 3.4 Principal Stress Difference and Volumetric Strain Versus Axial Strain, Vermont Marble, No. 105

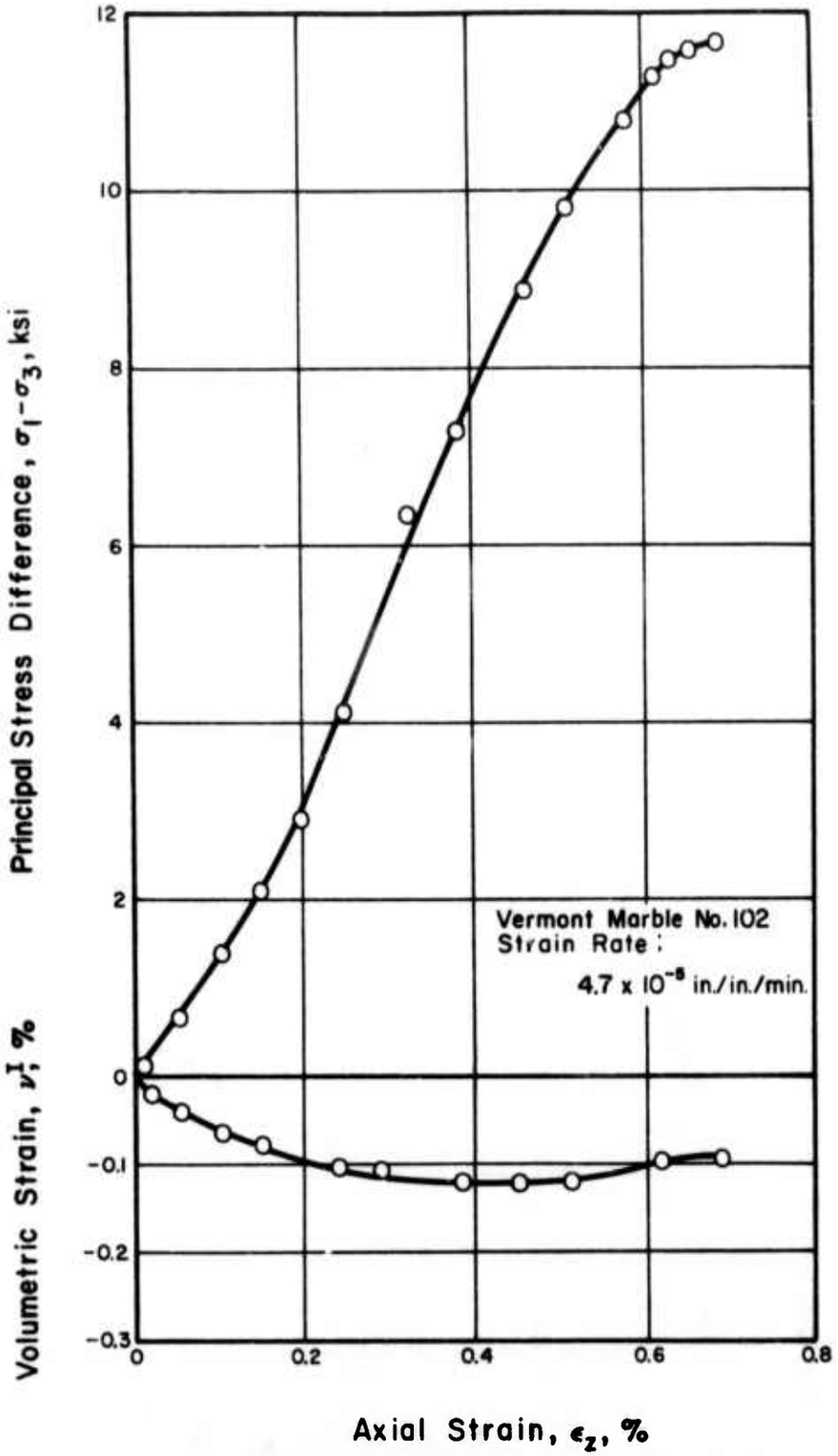

Fig. 3.5 Principal Stress Difference and Volumetric Strain Versus Axial Strain, Vermont Marble, No. 102

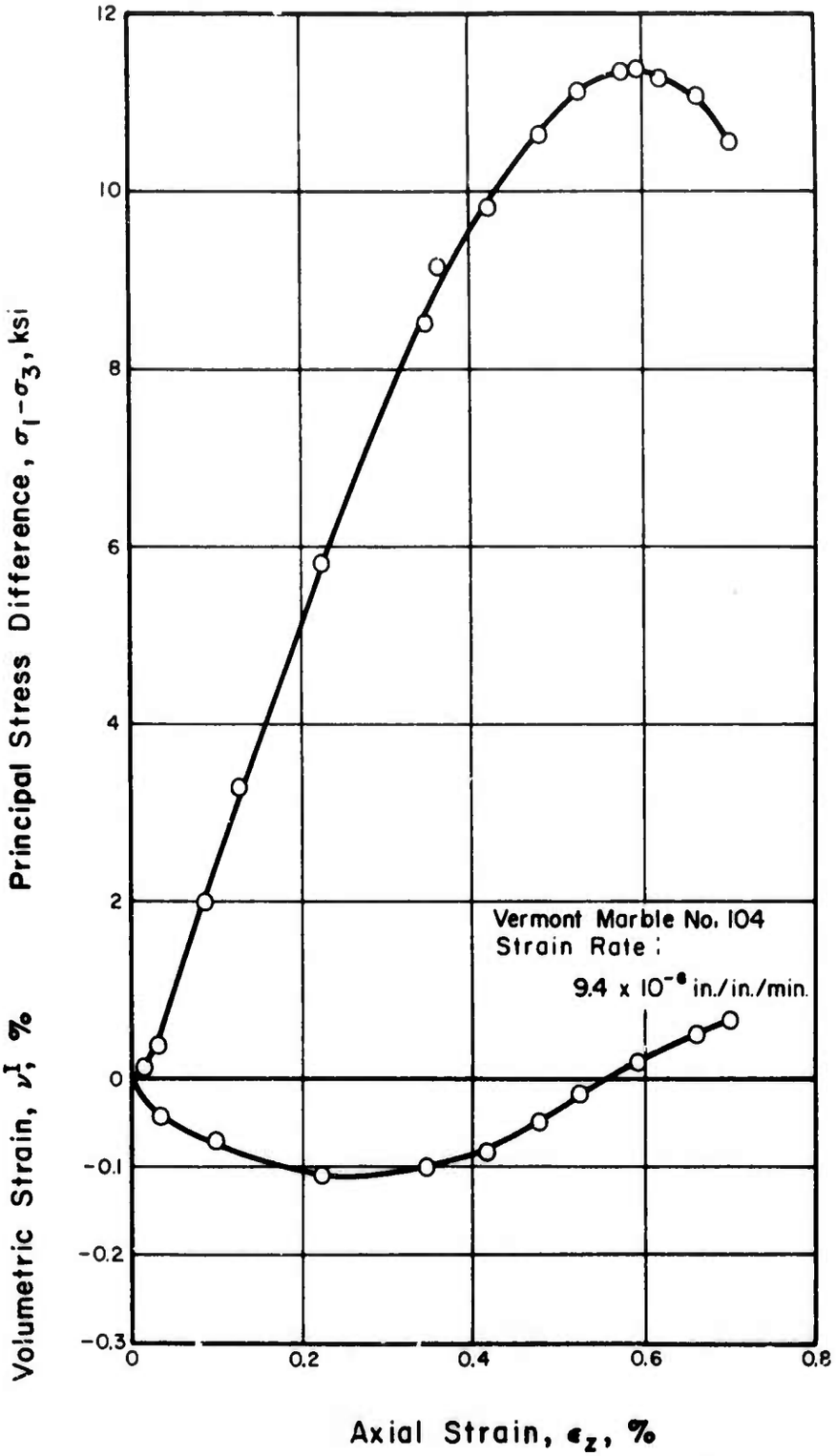

Fig. 3.6 Principal Stress Difference and Volumetric Strain Versus Axial Strain, Vermont Marble, No. 104

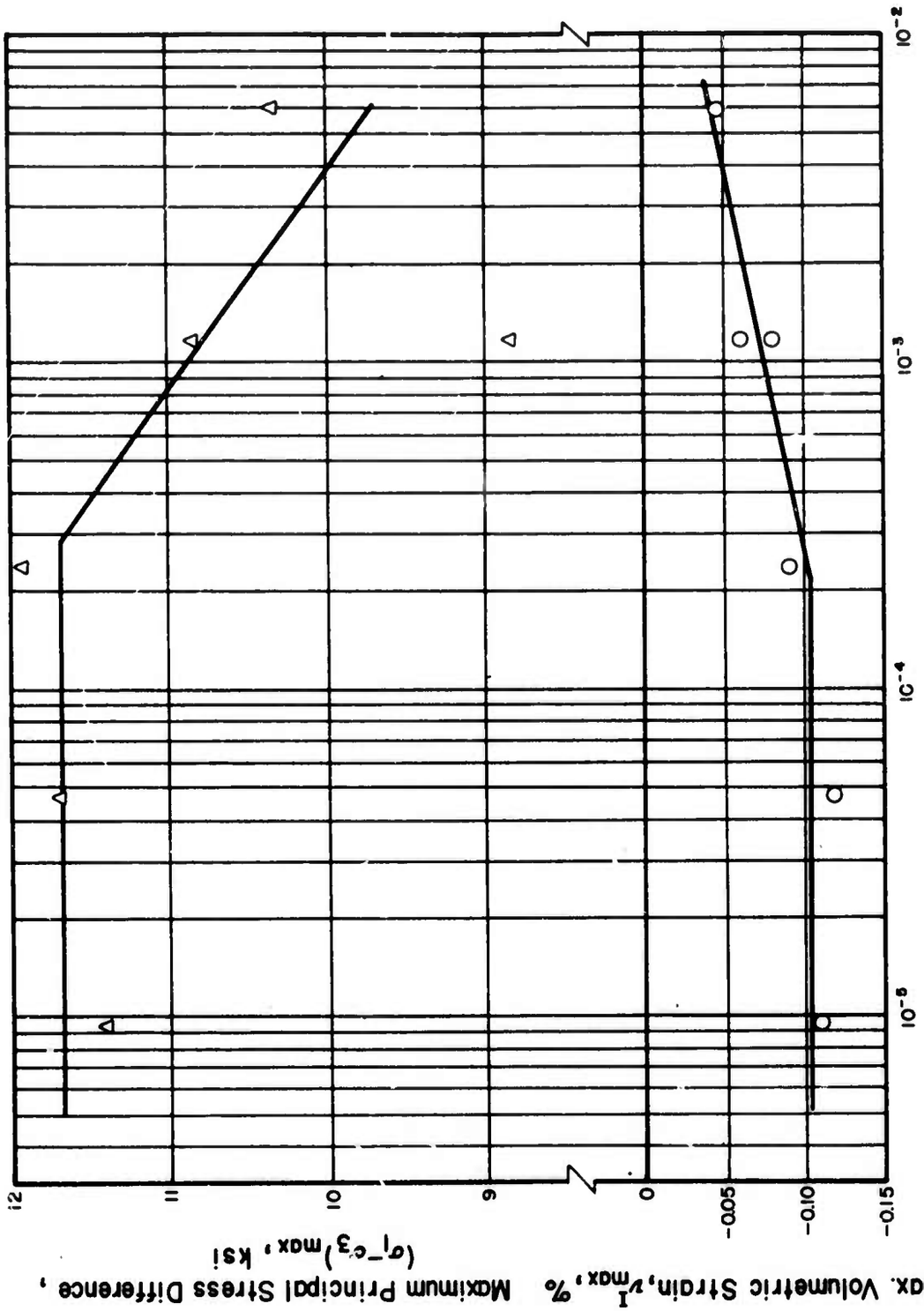

Fig. 3.7 Results of Strain Rate Study, Vermont Marble

generated during shear and caused the strength decrease when higher strain rates were used. As the strain rate was increased the volume changes at failure decreased (for all the specimens except VM No. 104) indicating that in fast tests the excess pore water pressure did not have sufficient time to dissipate.

Assuming the scatter in the test results to be mainly due to inherent differences in the rock specimens (macroscopic structural discontinuities, etc.) it was decided that rates of deformation less than 3.0×10^{-4} in/in/min could be used for the rest of the tests.

3.2 B-Coefficients, Volumetric Strains, and Permeabilities

B-coefficients, volumetric strains, and permeabilities were measured on Berea sandstone, Salem limestone, Vermont marble, and Barre granite. The results are presented and discussed in the remainder of this section.

3.2.1 B-Coefficients

The B-coefficient is defined as the ratio of the pressure generated in the pore water of a saturated compressible porous medium to the increment of total isotropic stress applied to that medium; that is $B = \Delta u/\Delta\sigma_3$ (Skempton,1954). In soil mechanics, it is generally found that a B-coefficient of unity is obtained for saturated soils. But the results of B-coefficient measurements on rocks show a notable difference as compared to the results

for soils. The results of B-coefficient measurements on four types of rock are presented here.

Effects of the initial degree of saturation on B-coefficients are shown in Figure 3.8. The back pressure applied to a specimen prior to B-coefficient measurement is taken as the abscissa and the measured B-coefficient is taken as the ordinate. Test results on three Salem limestone specimens are presented. All of the results shown here were measured under an effective confining pressure of 50 psi. Specimen SL No. 105 was subjected to a 60-psi pressure difference during its saturation operation and showed a low value of B-coefficient as compared to other specimens, apparently indicating that this specimen was not completely saturated. It is also seen that SL No. 105 did not reach a constant value of B-coefficient even with a back pressure of 300 psi. Specimens SL No. 103 and SL No. 104 were subjected to an 800 psi pressure difference during saturation operation. These specimens showed higher values of B-coefficient under a small value of back pressure and also exhibited constant B-values for back pressures greater than 100 to 200 psi. These results indicate the following:

1) When a specimen is saturated, it exhibits a constant value of B-coefficient under a given effective confining pressure.
2) The back pressuring technique worked well to saturate rock specimens.

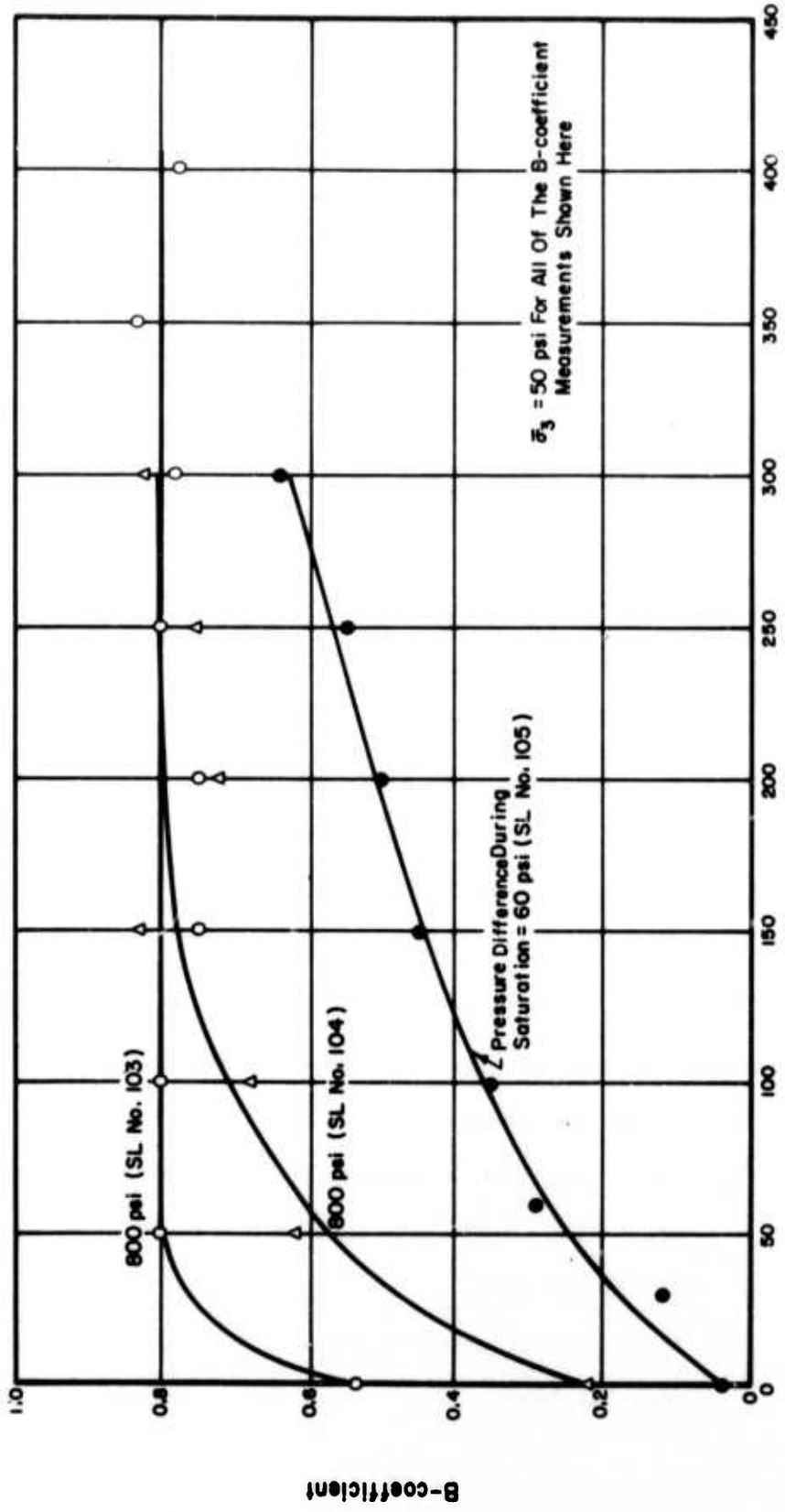

Fig. 3.8 Effects of Initial Degree of Saturation on B-Coefficient, Salem Limestone

3) It is generally necessary to repeat B-coefficient measurements several times with different back pressures under a constant effective confining pressure in order to find the correct value of B-coefficient for that particular effective confining pressure.

The above findings are applicable to all of the rocks tested.

Figures 3.9 to 3.12 show B-coefficient versus back pressure relations for all rock types for different effective confining pressures. These results show that the value of B-coefficient is not a constant for a given rock specimen but is a function of effective confining pressure. Generally as the effective confining pressure increases, the measured B-coefficient decreases, indicating that under higher confining pressure, the bulk compressibility of the rock skeleton becomes small and produces a small value of B-coefficient. These results could be explained by the equation: $B = \frac{1}{1+n\frac{C_w}{C_{sk}}}$ (Skempton, 1954), where n is the porosity of rock specimen, C_w the compressibility of pore fluid, and C_{sk} the bulk compressibility of the rock skeleton. The results shown in Figures 3.9 to 3.12 are plotted in terms of B-coefficient versus effective confining pressure in Figures 3.13 to 3.16. For all rock types which were tested, it is generally observed that relatively high values of B-coefficient (0.8 to 1.0) were obtained under small effective confining pressures, i.e. on the order of 100 psi or less. However as the effective confining pressure

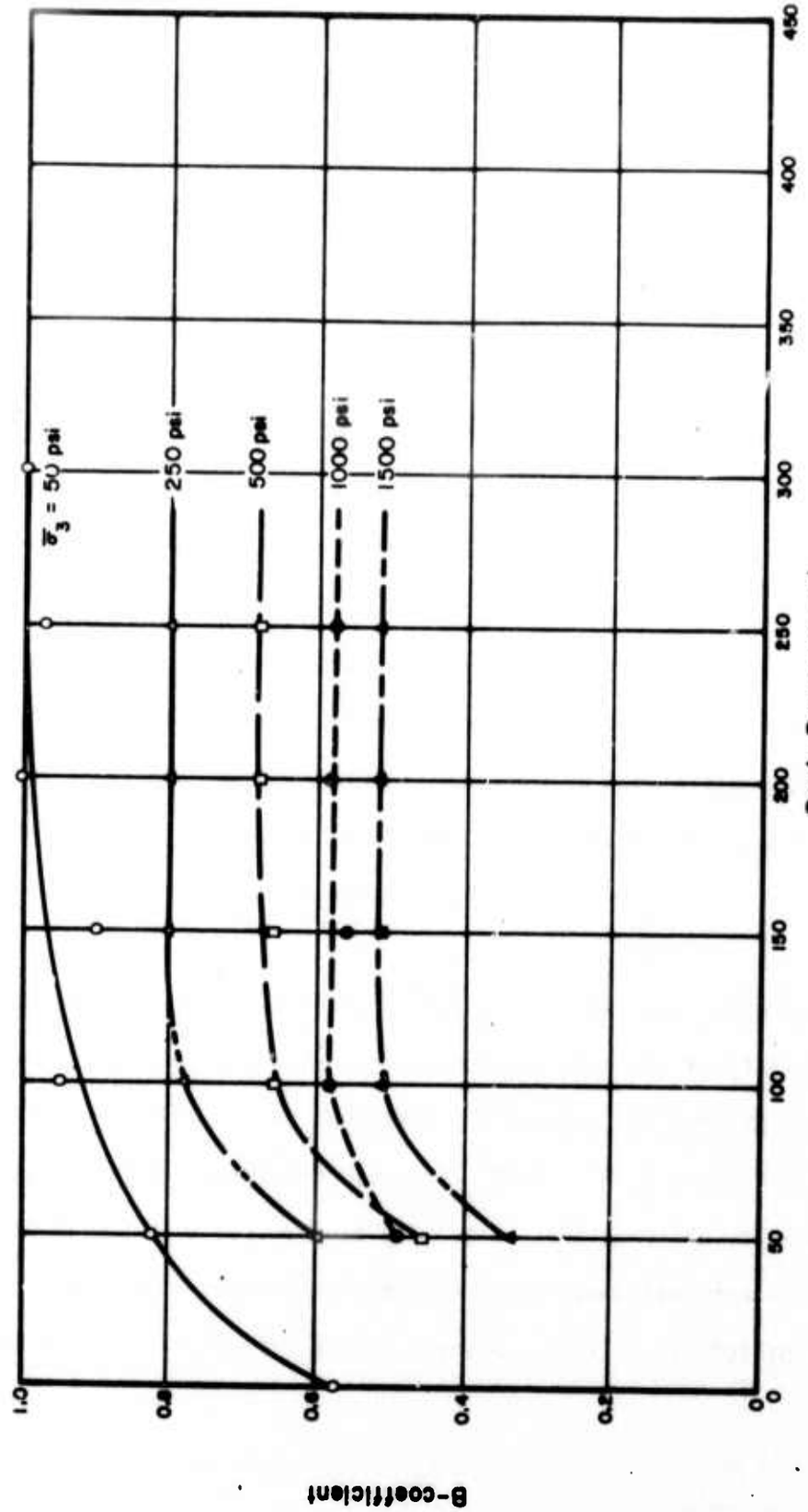

Fig. 3.9 Effects of Effective Confining Pressure on B-Coefficient, Berea Sandstone, No. 108

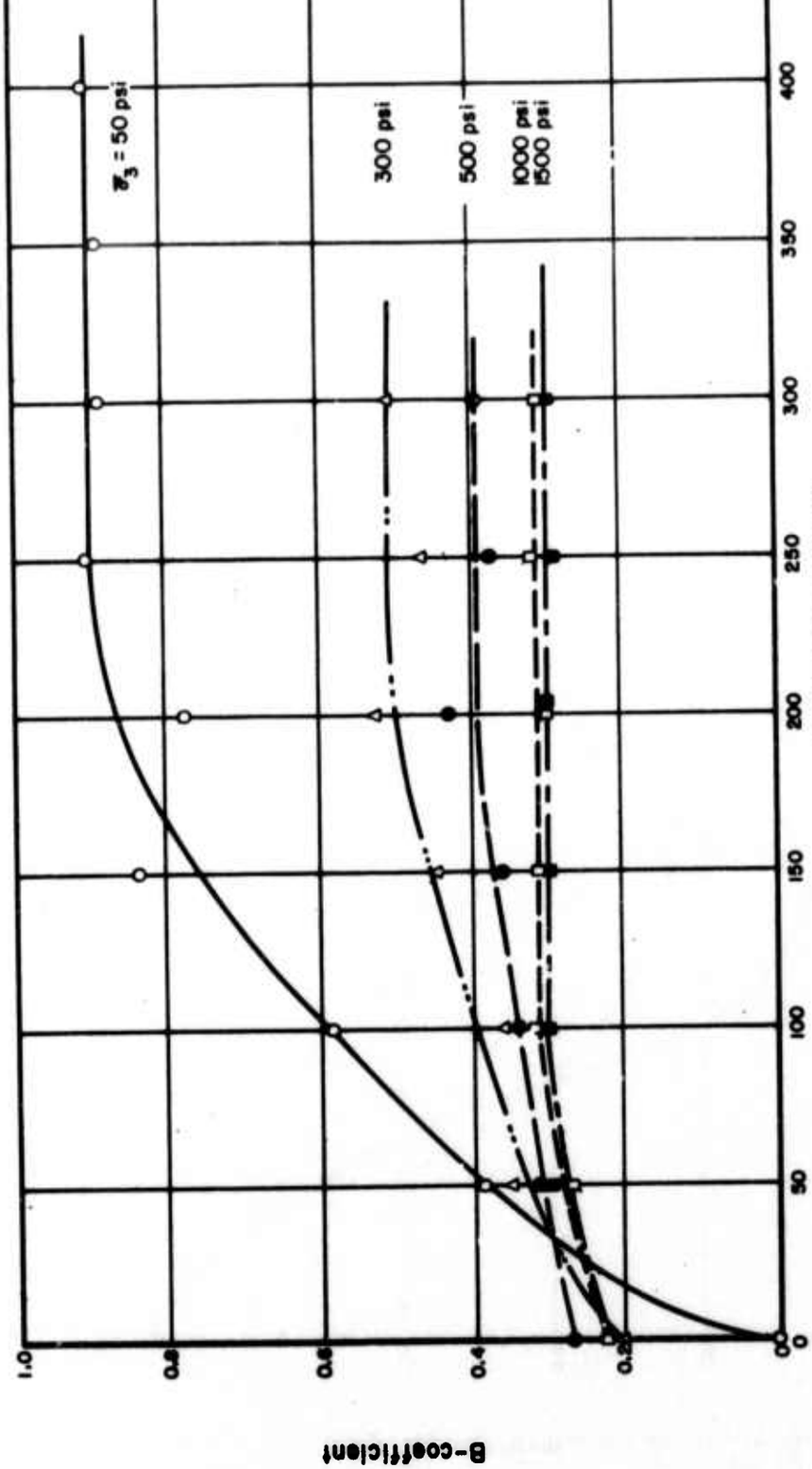

Fig. 3.10 Effects of Effective Confining Pressure on B-Coefficient , Salem Limestone, No. 106

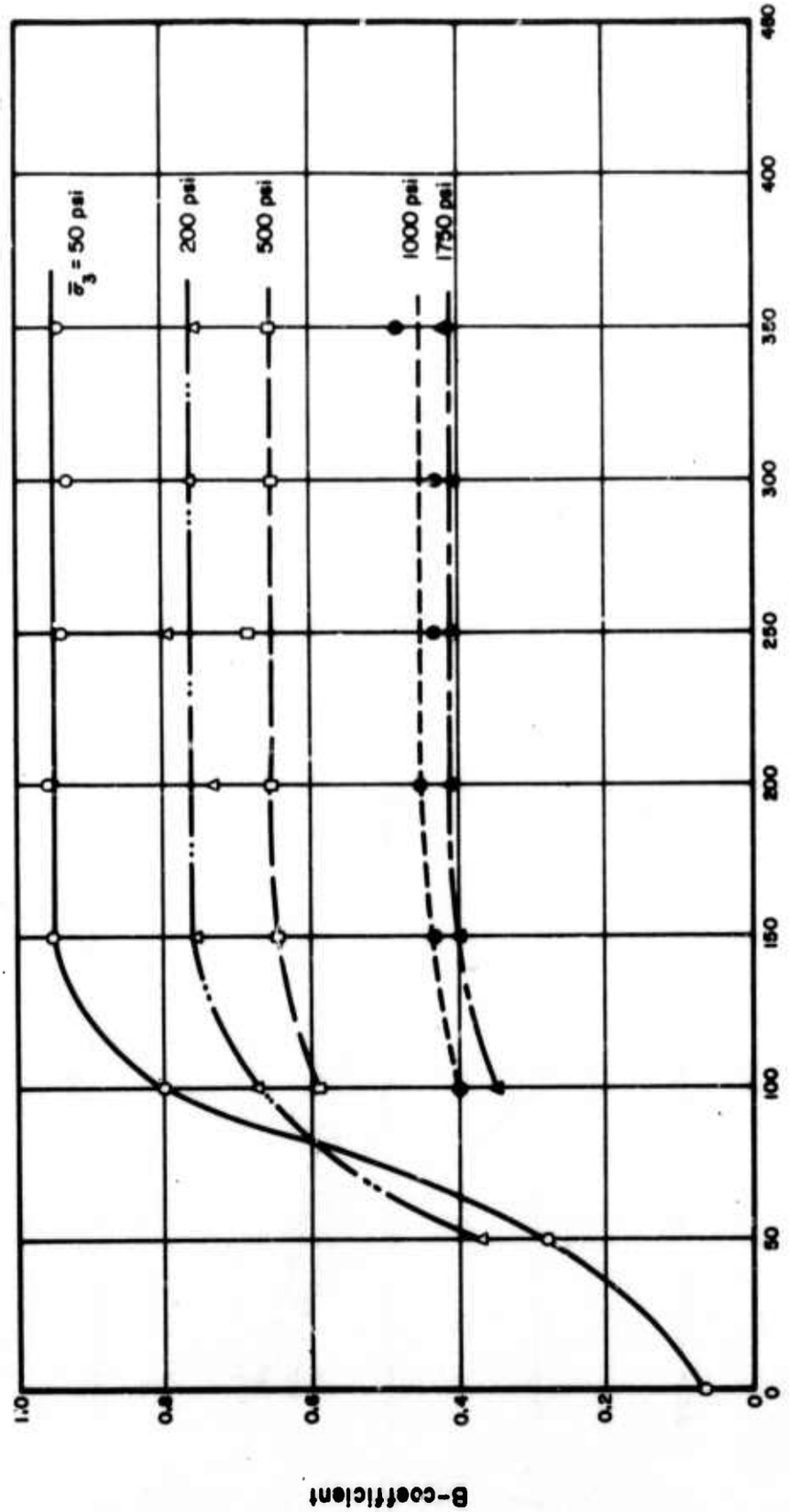

Fig. 3.11 Effects of Effective Confining Pressure on B-Coefficient , Vermont Marble, No. 112

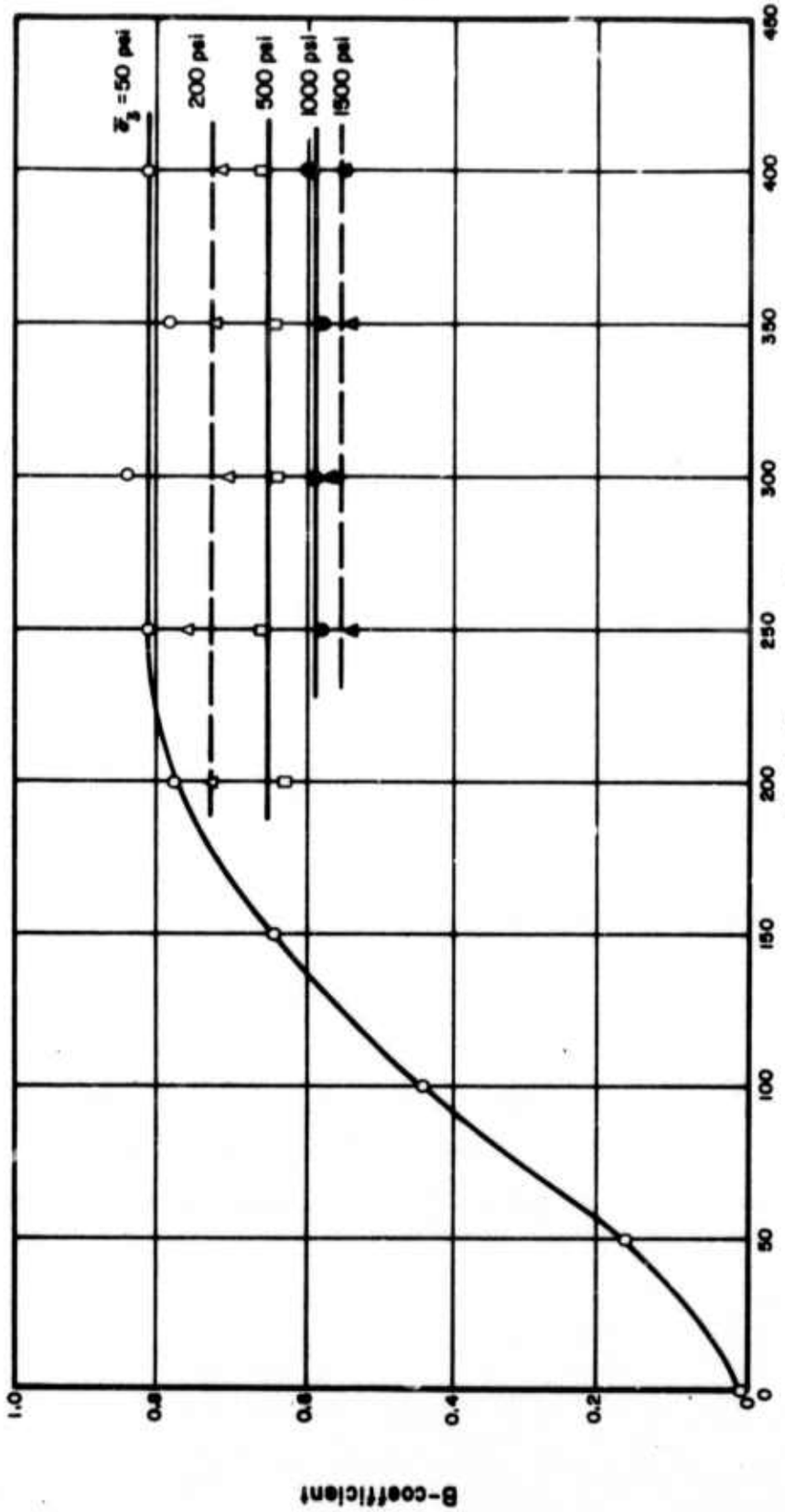

Fig. 3.12 Effects of Effective Confining Pressure on B-Coefficient, Barre Granite, No. 105

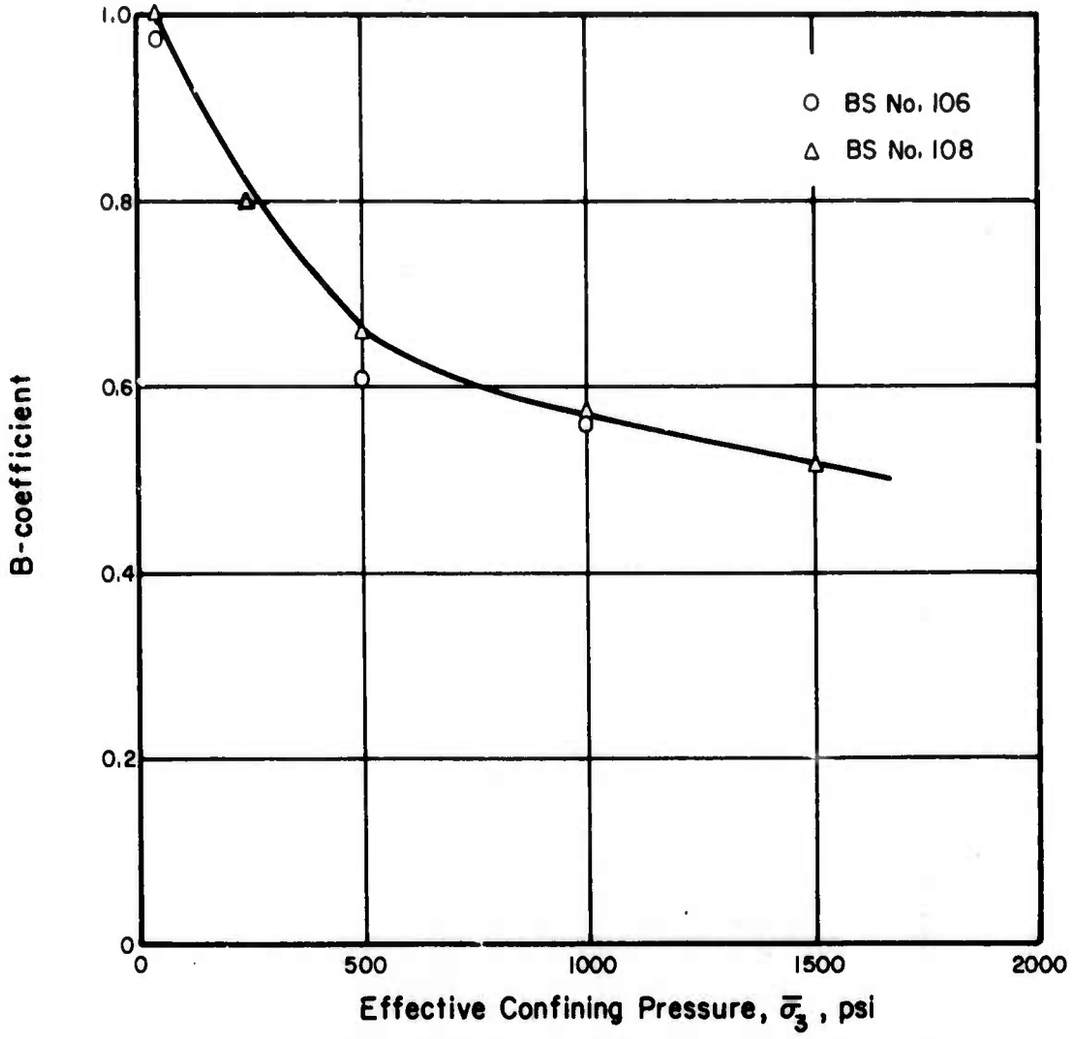

Fig. 3.13 B-Coefficient Versus Effective Confining Pressure, Berea Sandstone

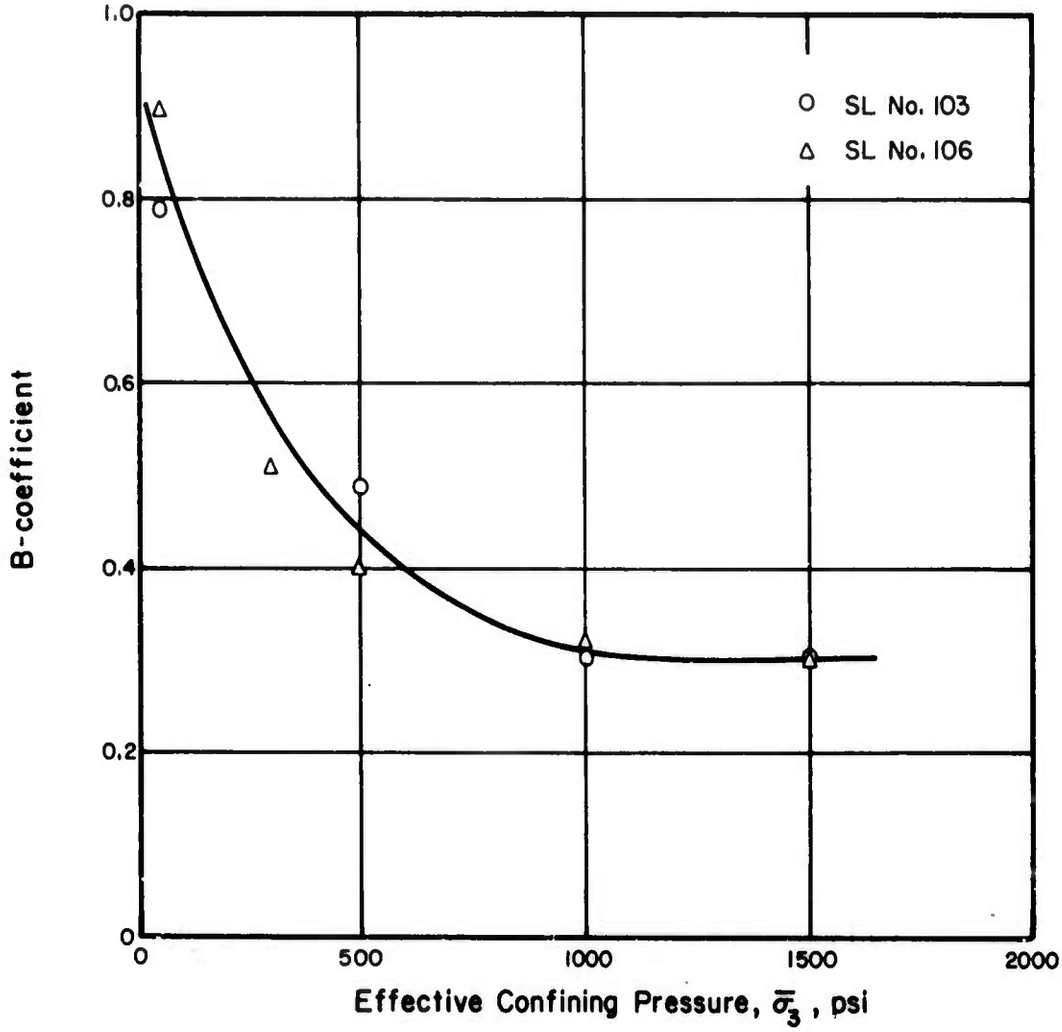

Fig. 3.14 B-Coefficient Versus Effective Confining Pressure, Salem Limestone

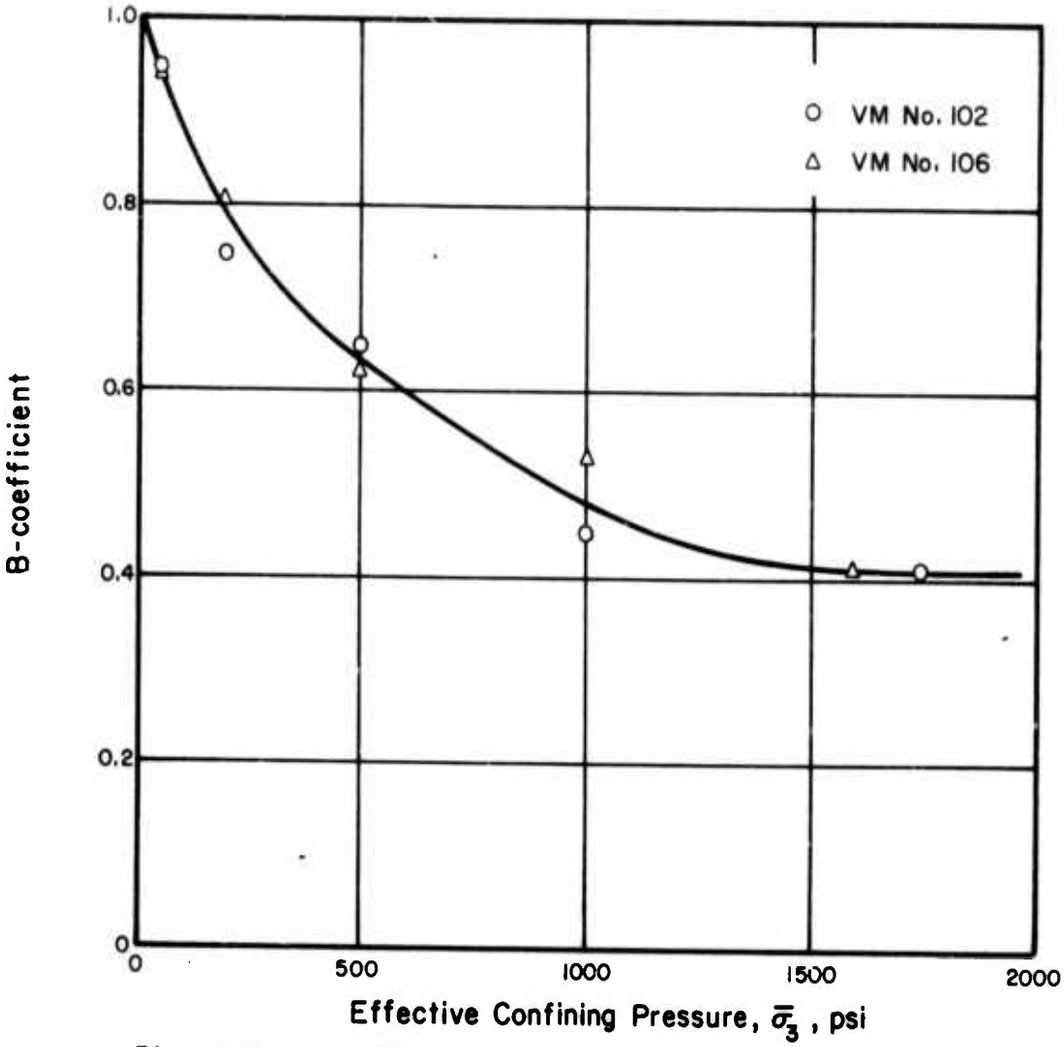

Fig. 3.15 B-Coefficient Versus Effective Confining Pressure, Vermont Marble

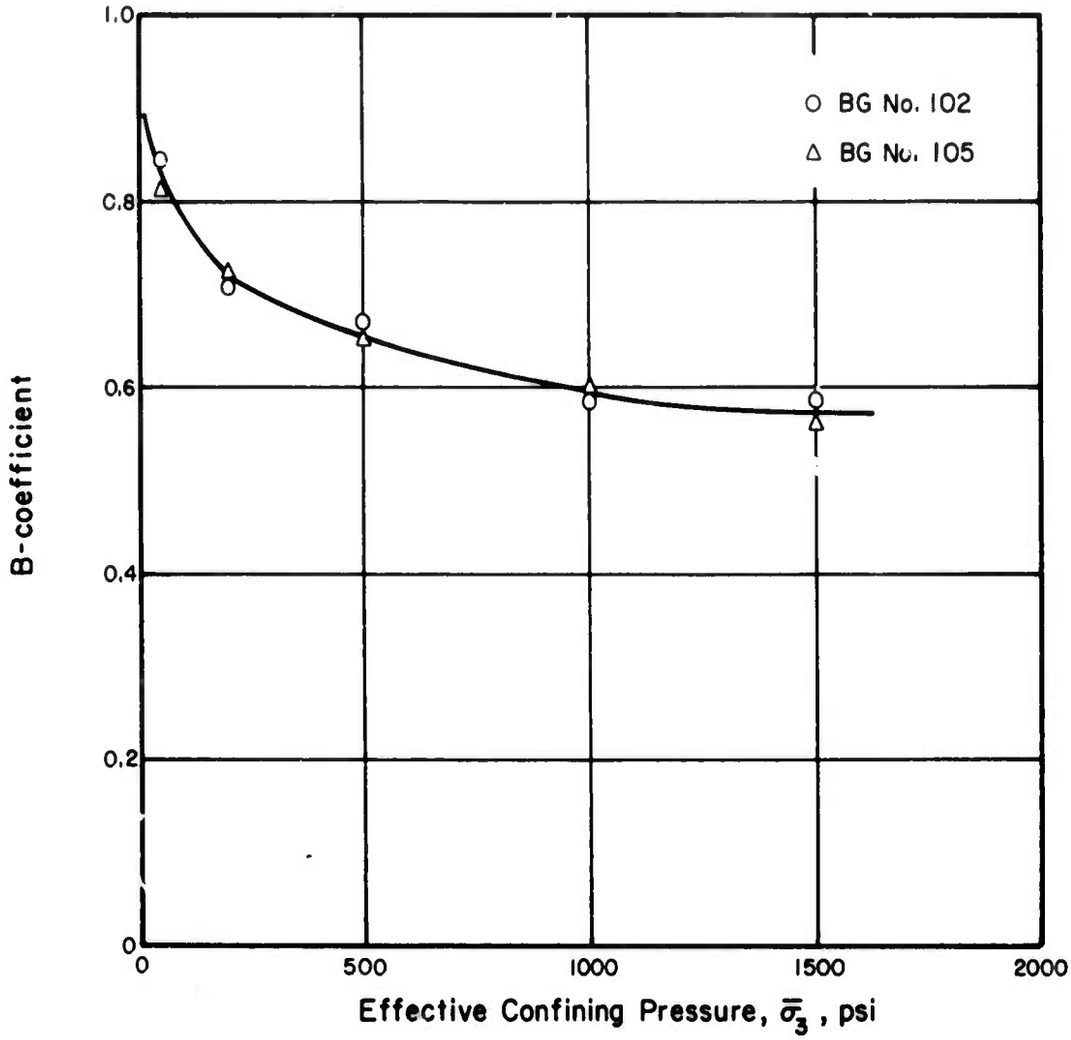

Fig. 3.16 B-Coefficient Versus Effective Confining Pressure, Barre Granite

increases, the value of the B-coefficient decreases substantially and it seems to reach a particular, constant value for each type of rock under an effective confining pressure of about 2,000 psi.

3.2.2 Volumetric Strains

Volumetric strains, $v^{III} = \Delta V/V$, are plotted versus confining pressure in Figure 3.17 for four types of rock. Volumetric strains are measured on saturated rock specimens by subjecting the rock specimen to a confining pressure under drained condition and measuring the volume of drained pore water (see Section 2). Berea sandstone gave the highest value of volumetric strain, Salem limestone was intermediate, and Vermont marble and Barre granite exhibited the smallest values of volumetric strain. Tangents to these curves, $\frac{\Delta v^{III}}{\Delta \sigma_3}$, are the bulk compressibilities of the rock skeleton. These bulk compressibilities of the rock skeleton versus confining pressure are shown in Figure 3.18. Under small confining pressures, higher bulk compressibilities, on the order of 1.0×10^{-5} per psi, were obtained which decreased with increasing confining pressure, ending in values of 1.0×10^{-6} per psi or less under the confining pressure of 2,000 psi. Note that the compressibility of water is 48×10^{-6} per kg/cm^2 or 3.2×10^{-6} per psi at the pressure of 1.0 kg/cm^2 or 15 psi (Skempton, 1961). Relations among bulk compressibilities, Young's modulus, and $\bar{A}$- and B- coefficients will be discussed in Section 4.

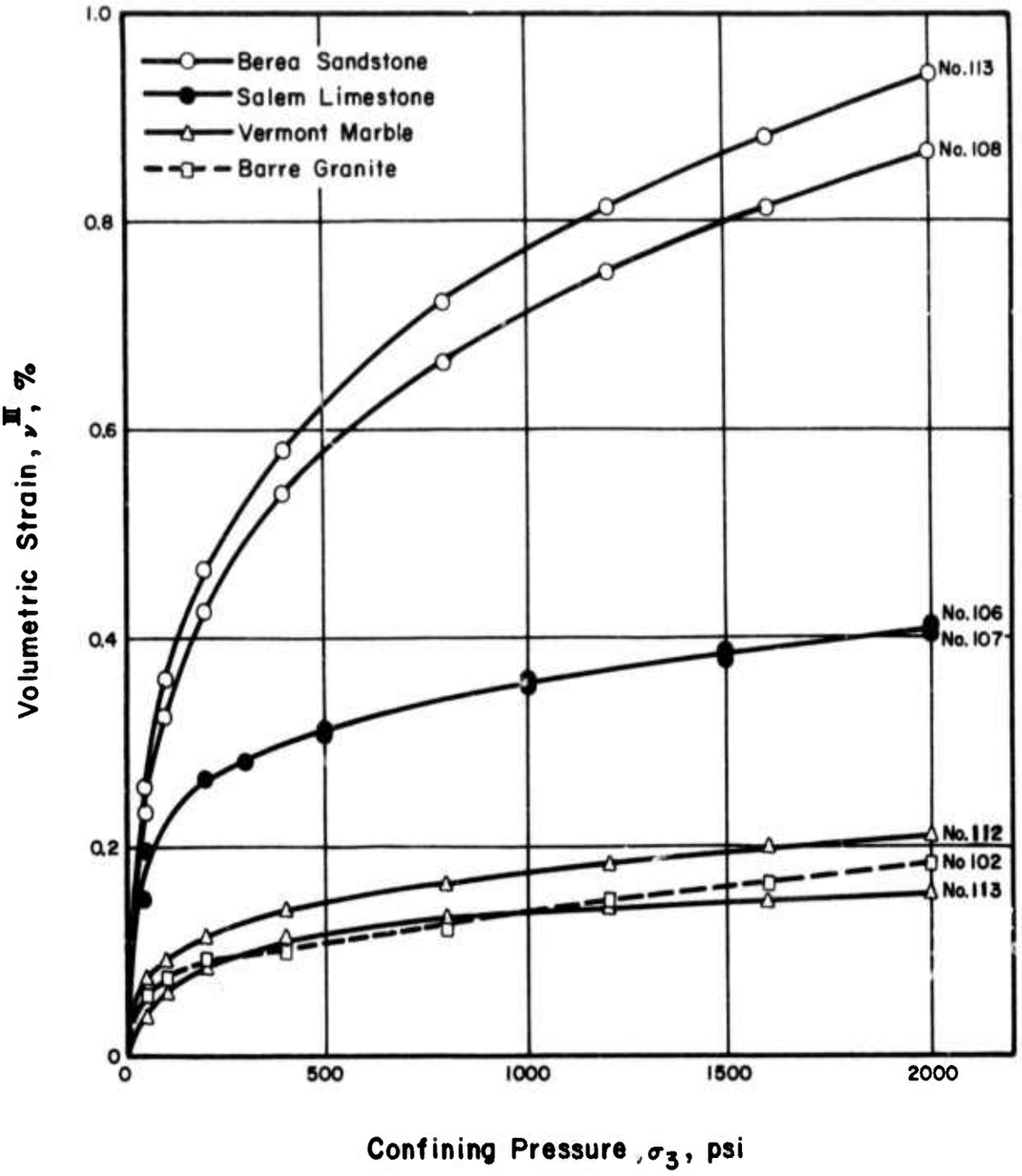

Fig. 3.17 Volumetric Strain Versus Confining Pressure, Drained Test

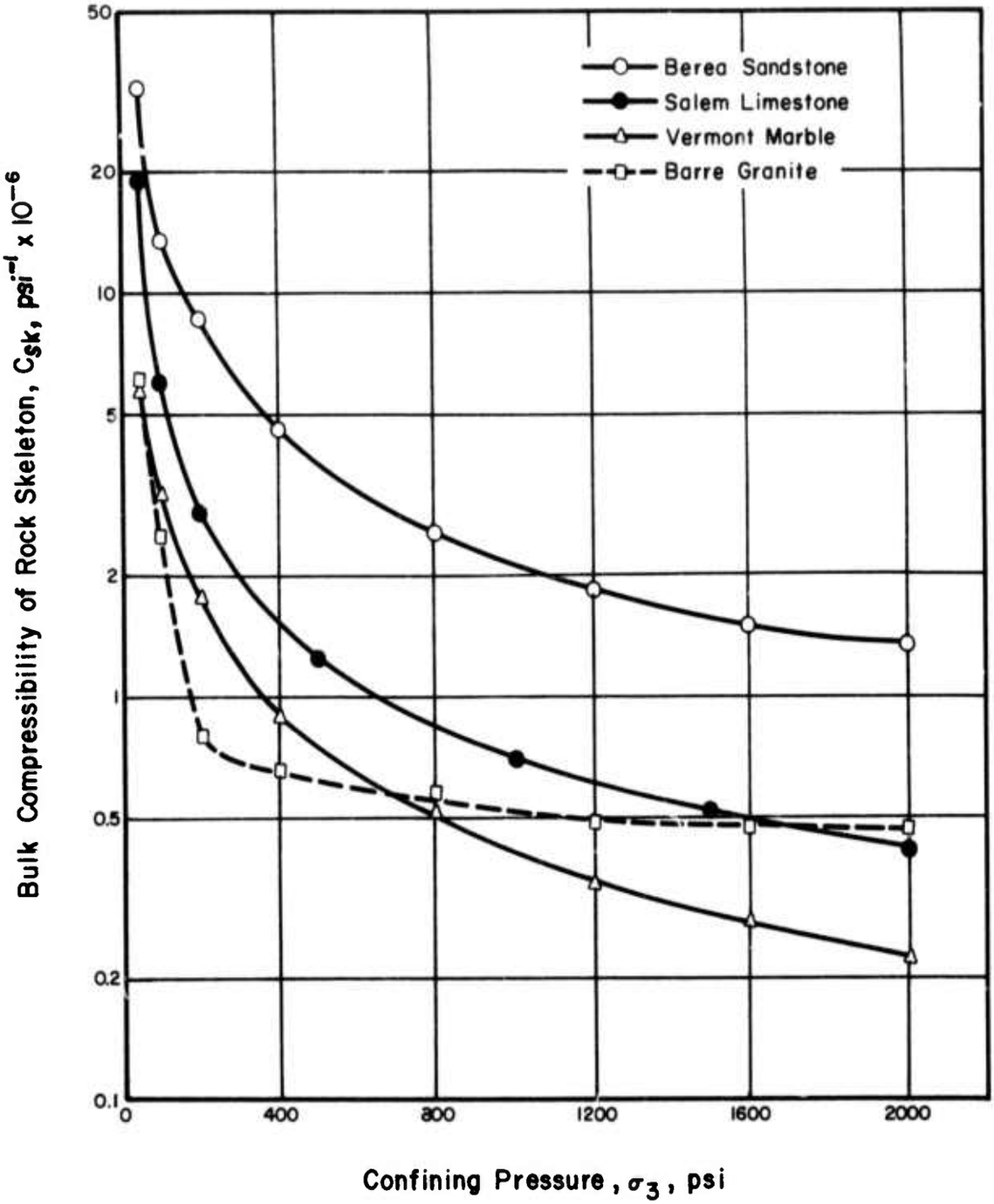

Fig. 3.18 Bulk Compressibility of Rock Skeleton Versus Confining Pressure, Drained Test

3.2.3 Permeabilities

Permeabilities, porosities, and degrees of saturation were calculated for each rock specimen tested and are reported in Tables 3.3 to 3.13 in the next section. The average values for each type of rock are summarized in Table 3.2.

The degree of saturation for each rock specimen was calculated using the total weight of the sheared specimen at the completion of the test. The volume of the sheared specimen could not be measured accurately since the specimen in general was broken up into fragments.

Table 3.2 Permeabilities, Porosities, and Degrees of Saturation

Rock Type	Permeability k(cm/sec)	Porosity n(%)	Degree of Saturation S_r(%)
Berea Sandstone	2.8×10^{-4}	20.3	98
Salem Limestone	2.7×10^{-7}	12.6	100
Vermont Marble	5.2×10^{-10}	2.1	97
Barre Granite	7.9×10^{-10}	2.7	99

Therefore the initial pre-test volume of the rock specimen which was determined from the measured dimensions of the specimen was used in the computation of the degree of saturation. Thus the computed degrees of saturation for the

sheared specimens represent only an estimate of the true values. However these values are in agreement with the results of previous tests which employed similar methods of saturation and were used specifically to study the saturation techniques (Mesri, Jones and Adachi, 1972). Also the pre-shear B-coefficient measurements seem to indicate satisfactory degrees of saturation.

3.3 Triaxial Compression Tests

A series of drained and a series of undrained triaxial compression tests were performed on each type of rock. In undrained tests pore water pressure measurements were made and in drained tests volume changes were measured. The confining pressures in drained tests were 400 psi, 1000 psi, and 2000 psi. In undrained tests the confining pressures were either 800 psi, 1400 psi or 2000 psi. In undrained tests, the pore water pressure at the beginning of the tests was equal to 400 psi. Hence the initial effective confining pressures were 400 psi, 1000 psi, and 1600 psi. A constant axial strain rate of 2.35×10^{-4} in/in/min was used for all triaxial compression tests.

3.3.1 Failure Modes

Terzaghi (1945) classified types of failure for axially-loaded cylindrical rock or concrete specimens into three types. They include splitting failure, shear failure, and pseudo-shear failure, Fig. 3.19. The modes of failure exhibited by the rock specimens in triaxial compression tests were failures of pseudo-shear or shear type.

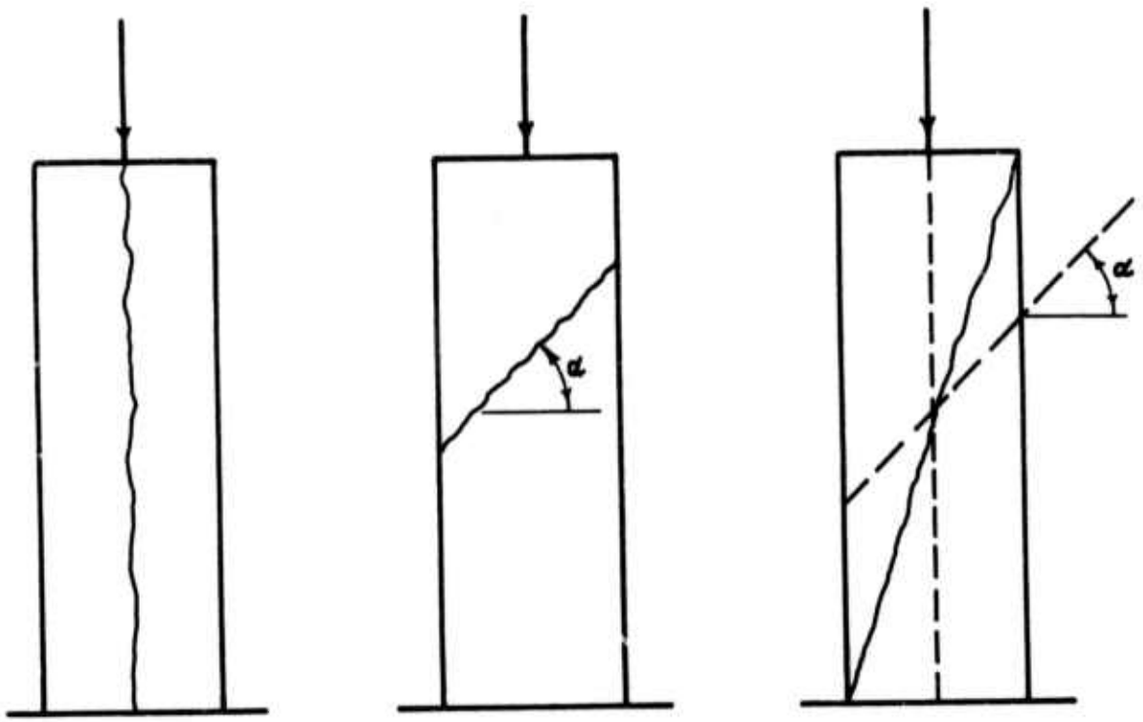

(a) Splitting (b) Shear Failure (c) Pseudo-Shear

Fig. 3.19 Types of Failure (After Terzaghi, 1945)

Most of the Berea sandstone specimens failed through one or two major shear planes. Figure 3.20 shows photographs of triaxially sheared Berea sandstone specimens. Some specimens exhibited conical rupture surfaces after failure. The angles between the shear planes and the vertical axes of specimens varied between 20° and 30°, Figure 3.20 (a). These failure modes can be classified as failures of pseudo-shear type. The sheared surfaces were gouged and rock flour was found on these surfaces. In some specimens, horizontal splitting through bedding planes was also found, Figure 3.20 (b). All of the Berea sandstone specimens exhibited brittle fracture by violent rupture, accompanied by an audible noise.

Salem limestone specimens failed through a single major shear plane. The angles between the shear planes and the vertical axes of specimens varied between 35° and 40°. The failure mode of Salem limestone can be classified as a shear type failure. Most of the Salem limestone specimens showed considerable ductility after the peak stress was reached and for complete rupture required an additional strain equal to 10 to 100% of the strain corresponding to peak axial stress. Higher confining pressure notably increased ductility in Salem limestone specimens. The sheared planes were gouged and appeared to have slickensided surfaces. Rock flour was found on these surfaces. Figure 3.21 shows photographs of triaxially sheared Salem limestone specimens.

Vermont marble specimens exhibited multiple shear planes consisting of two groups of parallel planes, which crossed each other and

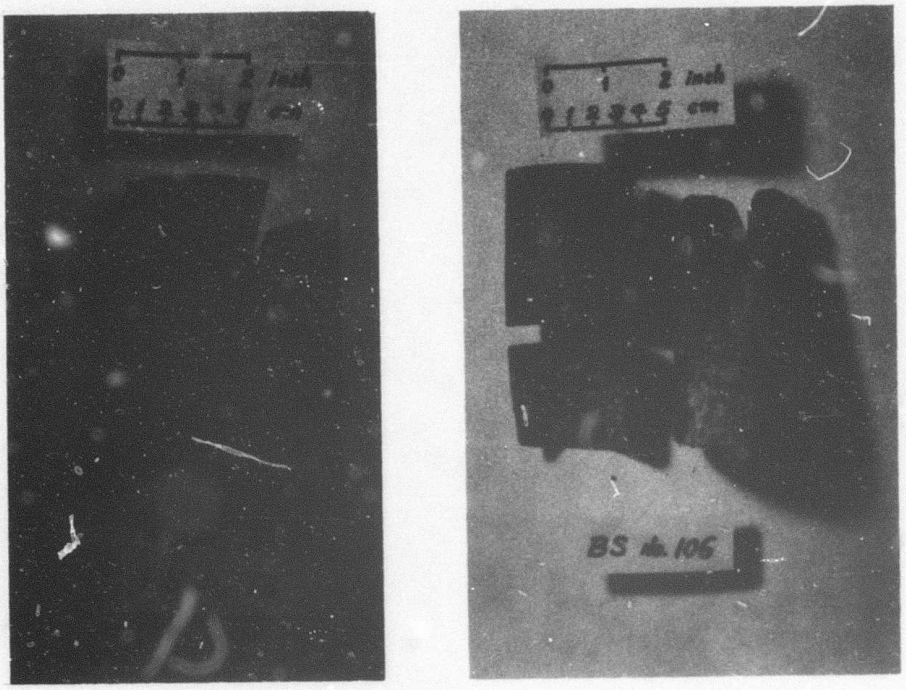

(a) (b)

Fig. 3.20 Triaxially Sheared Specimens, Berea Sandstone

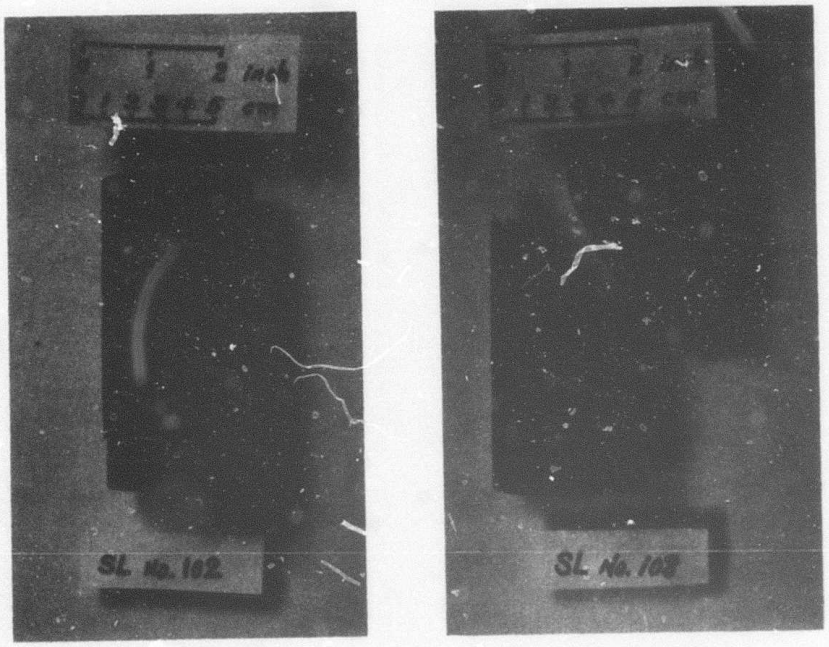

(a) (b)

Fig. 3.21. Triaxially Sheared Specimens, Salem Limestone

made an angle of 30° to the vertical axis. All of the Vermont marble specimens underwent ductile strains before complete rupture. Most of the specimens required an additional strain equal to 50% to 60% of the peak strain for a single plane rupture. Figure 3.22 shows photographs of triaxially sheared Vermont marble specimens.

Barre granite specimens failed through one major shear plane. In addition, some specimens exhibited several minor shear planes, Fig. 3.23. The major shear planes were about 25° to the vertical axis. All of the specimens exhibited brittle fractures accompanied by a highly audible noise. The sheared surfaces were gouged and rock flour was found on these surfaces.

3.3.2 Test Results on Berea Sandstone

The results of drained triaxial compression tests on Berea sandstone are shown in Figures 3.24 to 3.28 in terms of principal stress difference and volumetric strain versus axial strain. The results are also summarized in Table 3.3. Berea sandstone specimens exhibited maximum principal stress difference, $(\sigma_1 - \sigma_3)_{max}$, at axial strains of 0.8% to 1.2%. The axial strain corresponding to the maximum principal stress difference increased as confining pressure increased. All of the specimens underwent volume decreases at the initial stage of loading and reached their maximum negative volumetric strains of 0.25% to 0.50% at axial strains of about 0.6%. Upon further loading, the specimens started to dilate. Most of the specimens failed at the instant when the volumetric strains were approaching zero.

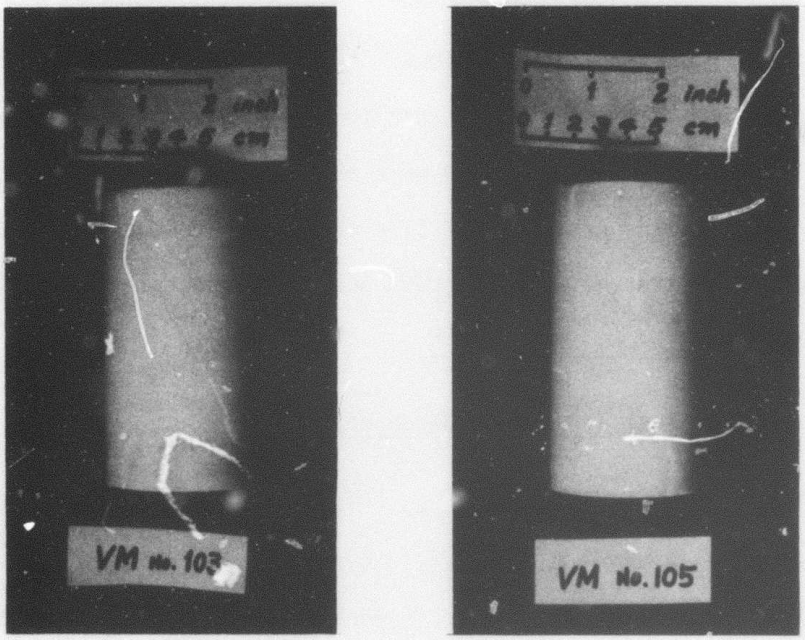

(a) (b)

Fig. 3.22 Triaxially Sheared Specimens, Vermont Marble

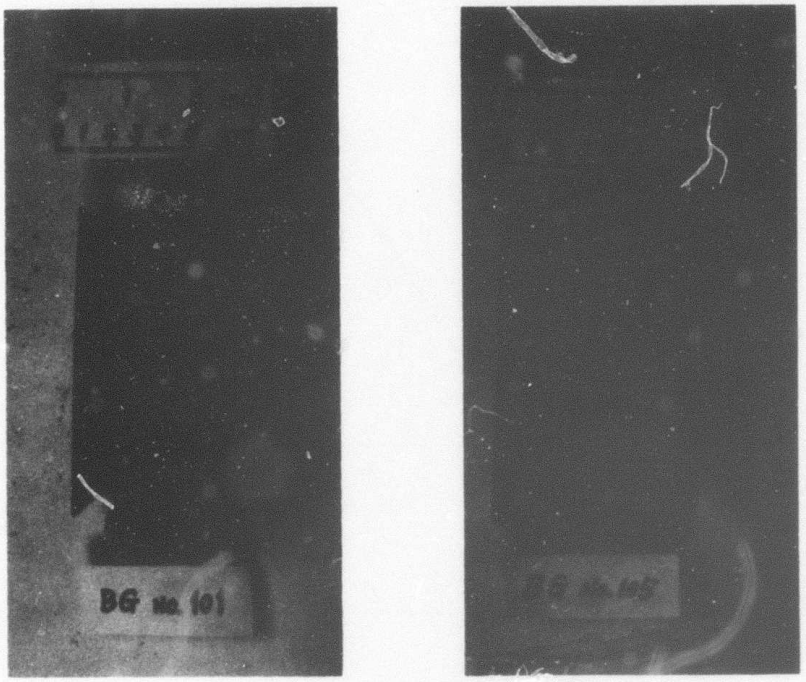

(a) (b)

Fig. 3.23 Triaxially Sheared Specimens, Barre Granite

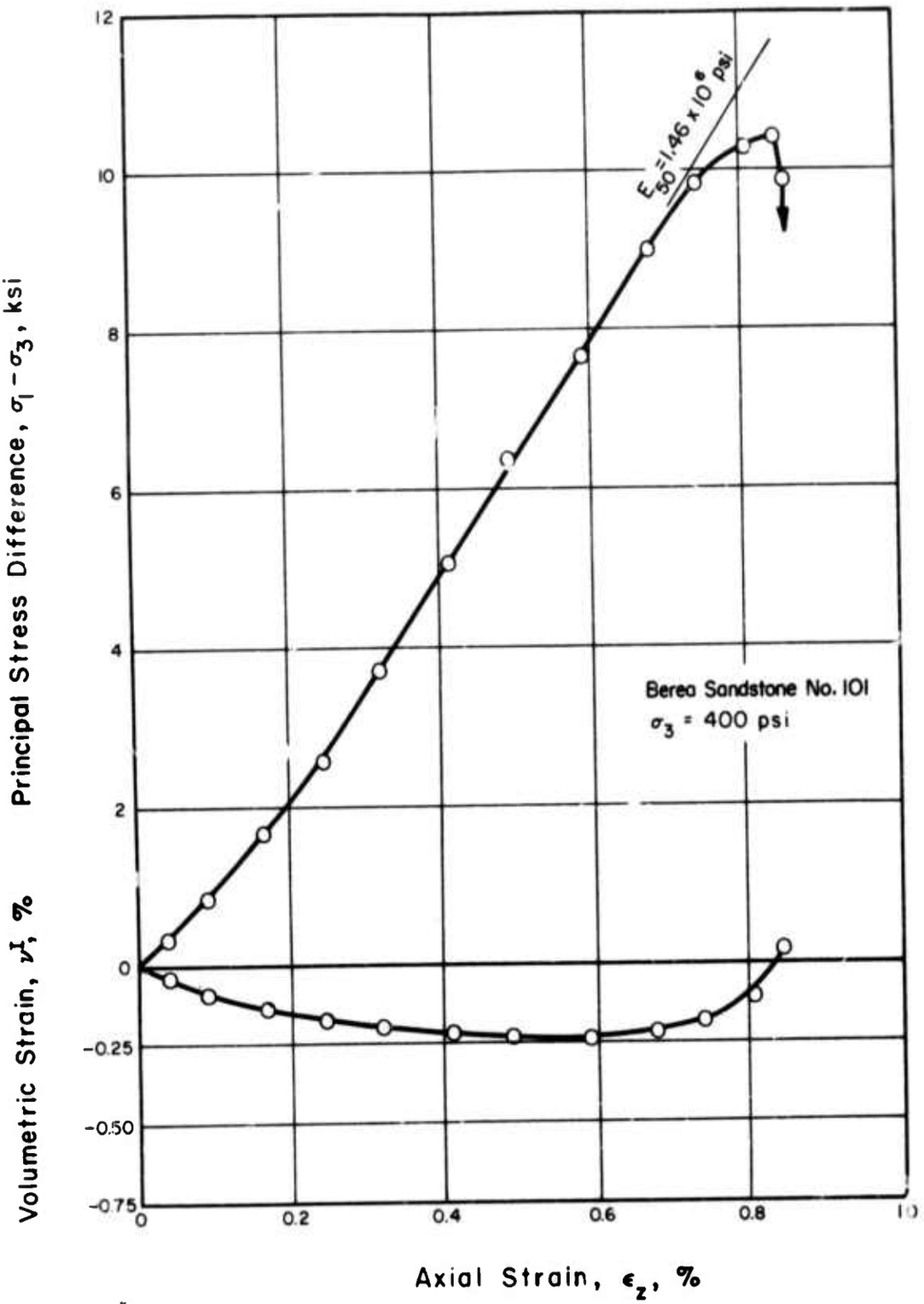

Fig. 3.24 Principal Stress Difference and Volumetric Strain Versus Axial Strain, Berea Sandstone, No. 101

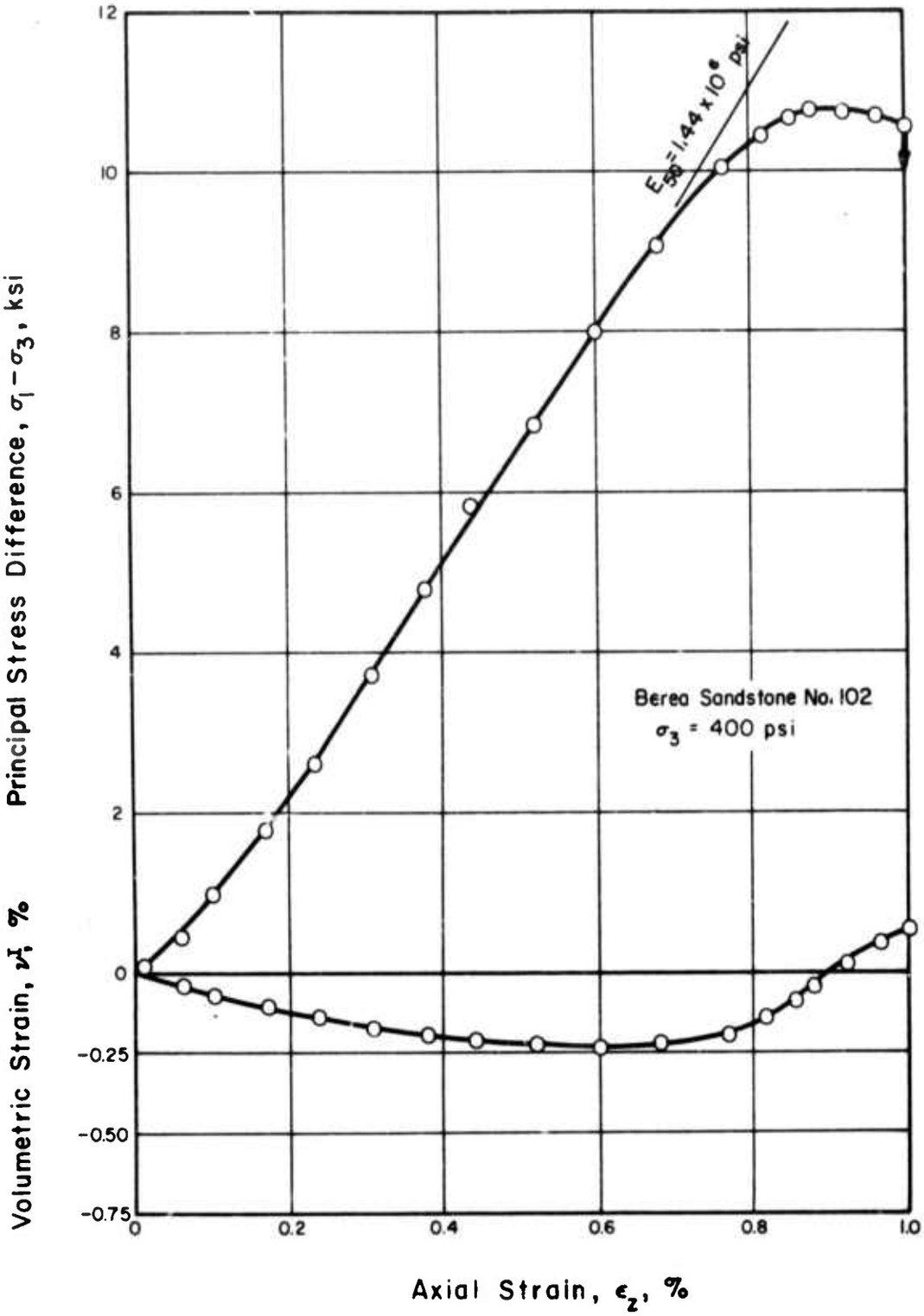

Fig. 3.25 Principal Stress Difference and Volumetric Strain Versus Axial Strain, Berea Sandstone, No. 102

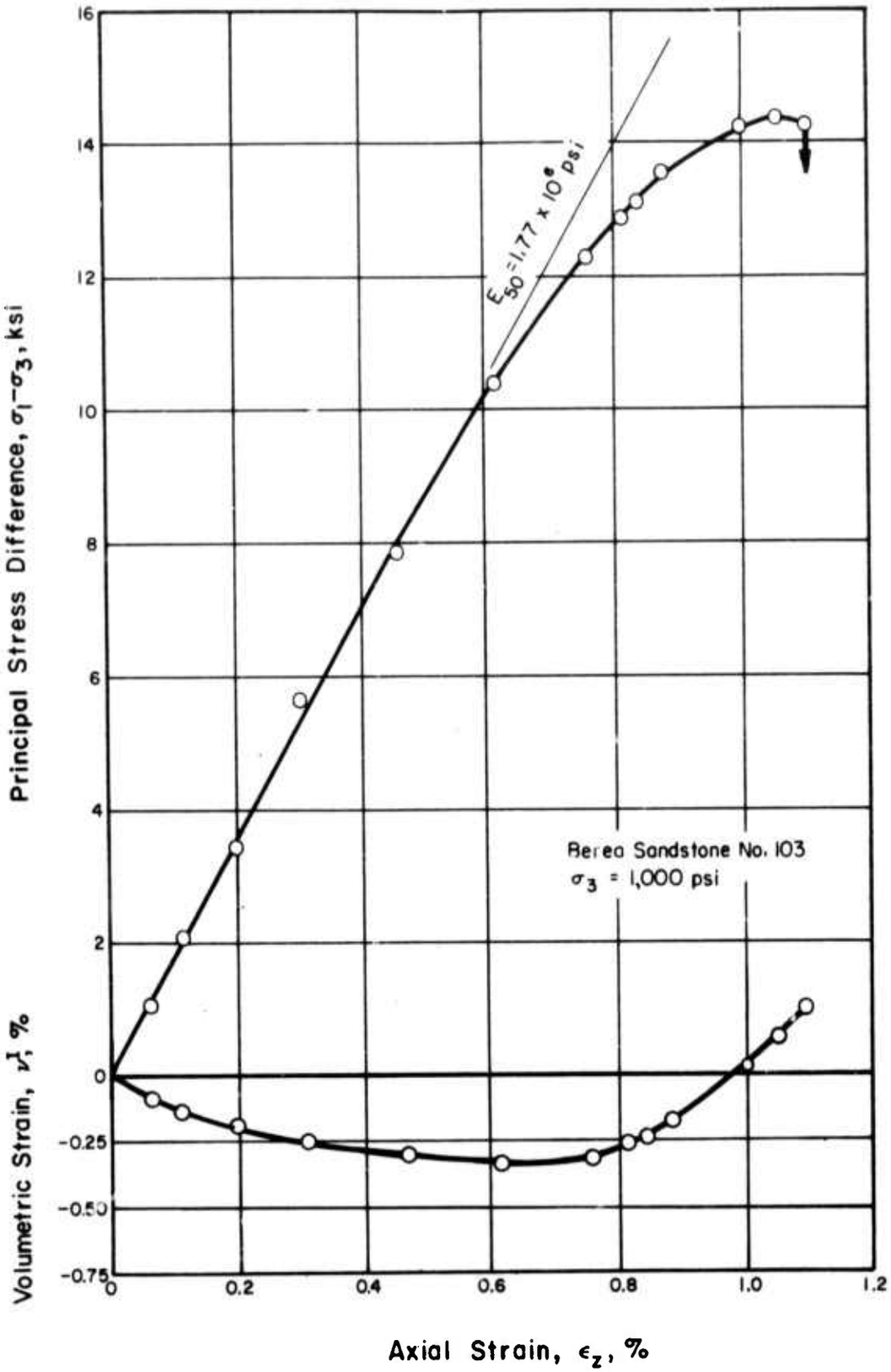

Fig. 3.26 Principal Stress Difference and Volumetric Strain Versus Axial Strain, Berea Sandstone, No. 103

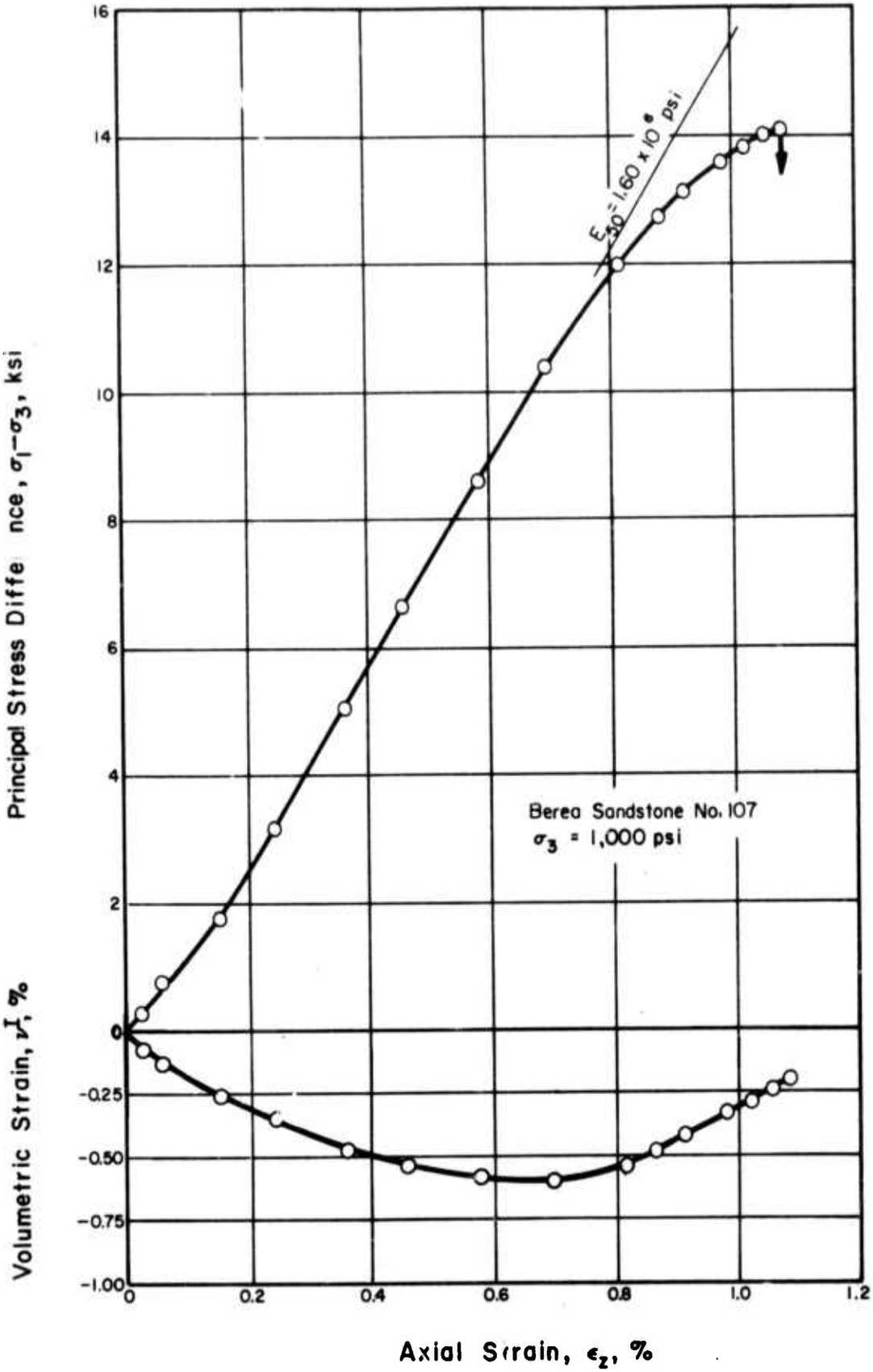

Fig. 3.27 Principal Stress Difference and Volumetric Strain Versus Axial Strain, Berea Sandstone, No. 107

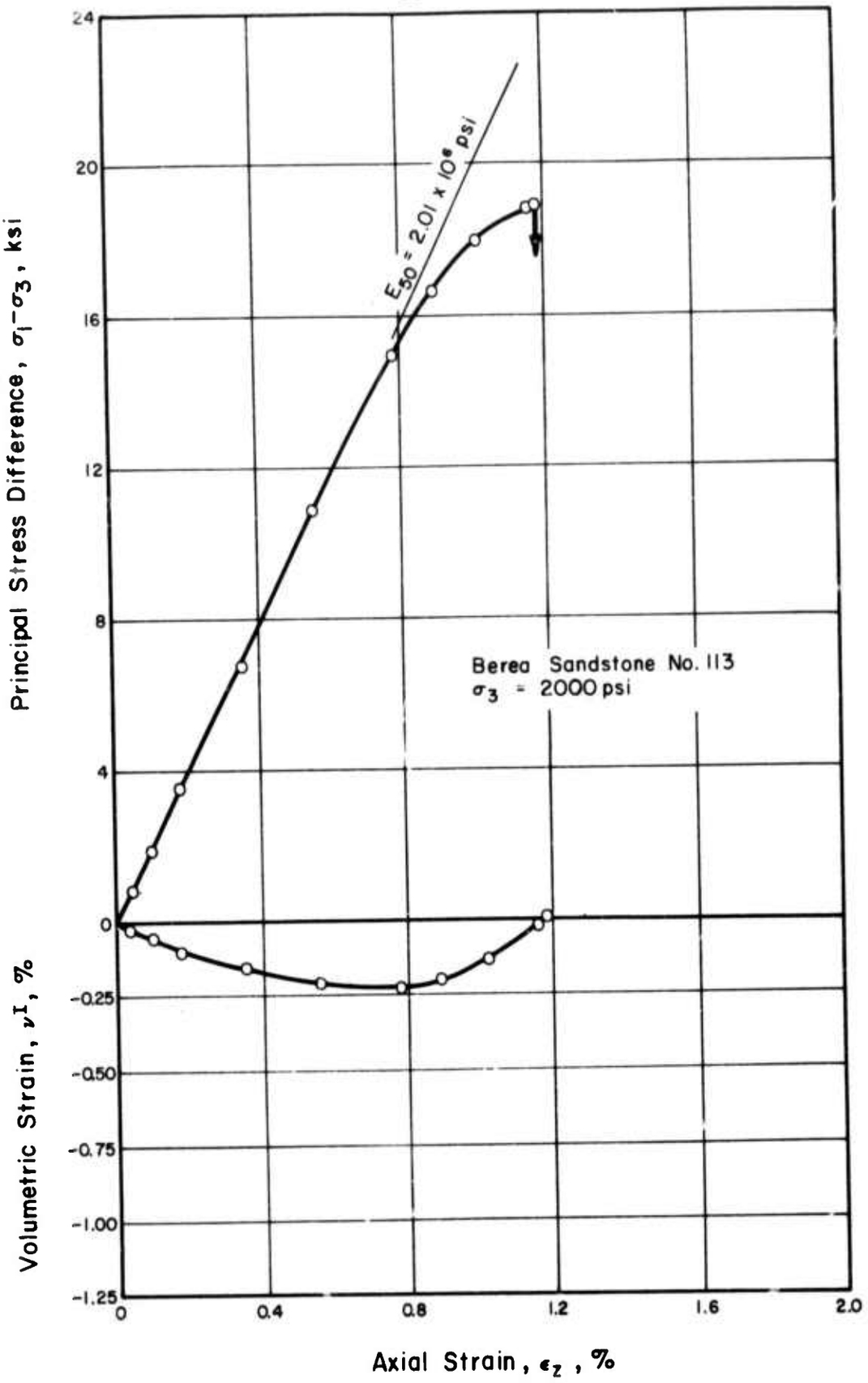

Fig. 3.28 Principal Stress Difference and Volumetric Strain Versus Axial Strain, Berea Sandstone, No. 113

Table 3.3 Summary of Drained Triaxial Compression Tests, Berea Sandstone

Sample No.	Porosity n (%)	Permeability k (cm/sec)	Degree of Saturation S_r (%)	Confining Pressure σ_3 (psi)	At $(\sigma_1 - \sigma_3)_{max}$			Max. Volumetric Strain v^I_{max} (%)
					Axial Strain ε_z (%)	$\sigma_1 - \sigma_3$ (psi)	Volumetric Strain v^I (%)	
101	20.4	3.3×10^{-4} ~ 3.2×10^{-5}	100	400	0.845	10,410	+0.04	-0.24
102	20.2	3.3×10^{-4} ~ 3.2×10^{-5}	99	400	0.880	10,770	-0.04	-0.23
103	20.2	8.2×10^{-4} ~ 3.2×10^{-5}	95	1,000	1.050	14,380	-0.26	-0.51
107	20.3	5.0×10^{-4} ~ 3.5×10^{-5}	96	1,000	1.080	14,060	--	--
113	20.1	7.3×10^{-4}	98	2,000	1.157	18,920	+0.008	-0.23
1	18.3	--	98	0	0.572	6,700	--	--
2	18.0	--	100	0	0.592	6,640	--	--

Notes: No. 101 ~ 113: Triaxial Tests, Strain Rate = 2.35×10^{-4} in/in/min
No. 1 2: Uniaxial Tests, Strain Rate = 1.4×10^{-4} in/in/min

Results of undrained triaxial compression tests with pore water pressure measurements are presented in Figures 3.29 to 3.31 where principal stress difference, shear-induced pore water pressure, effective principal stress ratio, and $\bar{A}$-coefficient are plotted versus axial strain. The undrained test results are also summarized in Table 3.4.

The A- and the $\bar{A}$- coefficients are defined by Skempton (1954) using the following equations:

$$\Delta u = B[\Delta\sigma_3 + A\ (\Delta\sigma_1 - \Delta\sigma_3)],$$

$$\Delta u = B\cdot\Delta\sigma_3 + \bar{A}\ (\Delta\sigma_1 - \Delta\sigma_3),$$

where Δu is the change in pore water pressure, B is the B-coefficient, $\Delta\sigma_3$ is the change in minor principal stress, and $\Delta\sigma_1$ is the change in major principal stress. In case of undrained triaxial compression tests the confining pressure, σ_3, is kept constant, i.e. $\Delta\sigma_3 = 0$. Hence the $\bar{A}$- coefficient is the ratio of the change in the pore water pressure to the increment of axial stress; that is $\bar{A} = \frac{\Delta u}{\Delta\sigma_1}$.

Berea sandstone specimens exhibited maximum principal stress difference, $(\sigma_1 - \sigma_3)_{max}$, at axial strains of 0.9% to 1.4% in undrained tests. These strains at $(\sigma_1 - \sigma_3)_{max}$ are slightly higher than the corresponding strains in drained tests. The magnitude of the axial strain at maximum principal stress difference increased with confining pressure. Positive shear-induced pore water pressures were observed at the initial stage of loading for all of the specimens. As the loading continued, the pore pressures began to decrease and became negative for all specimens.

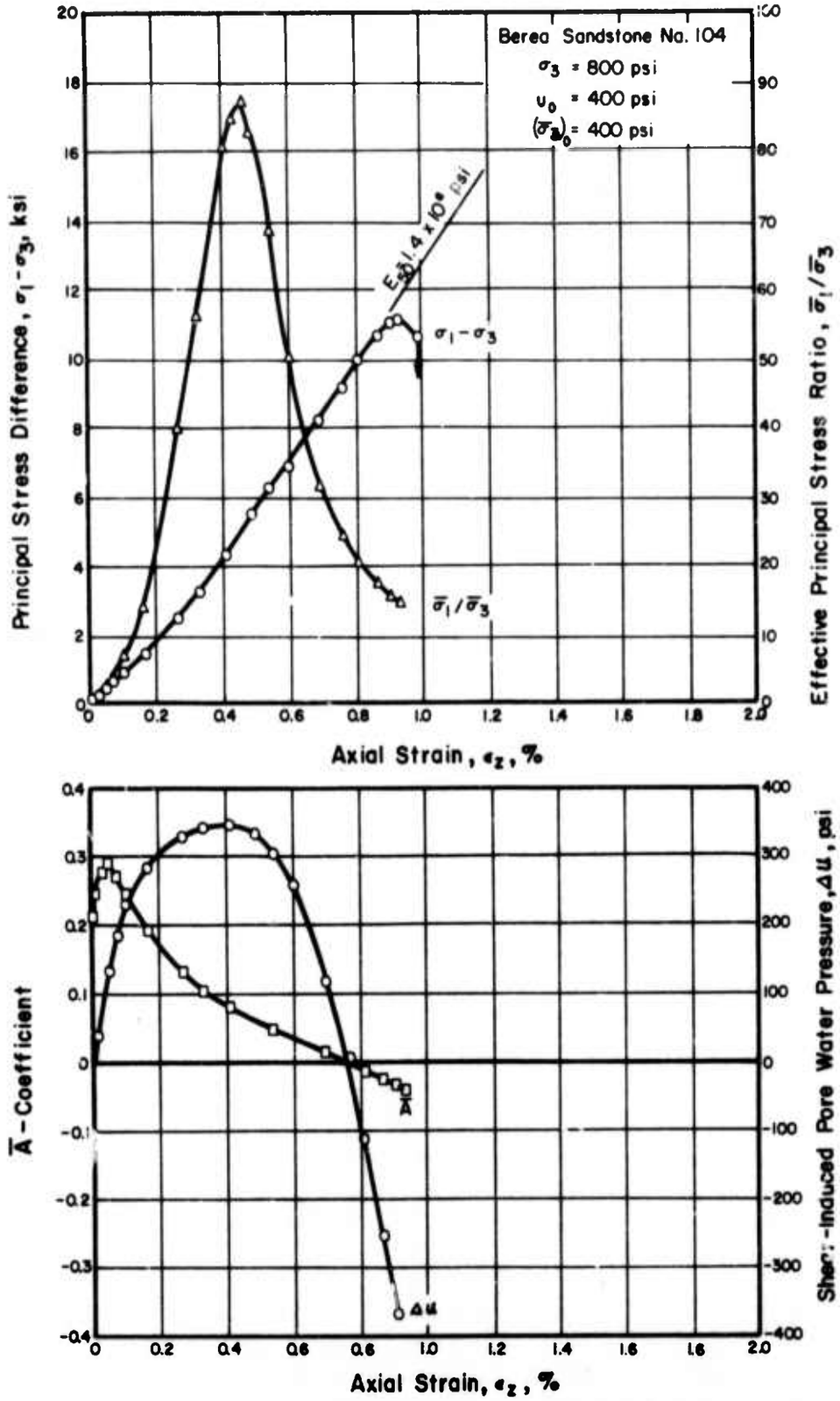

Fig. 3.29 Principal Stress Difference, Shear-Induced Pore Water Pressure, Effective Principal Stress Ratio, and $\bar{A}$-Coefficient Versus Axial Strain, Berea Sandstone, No. 104

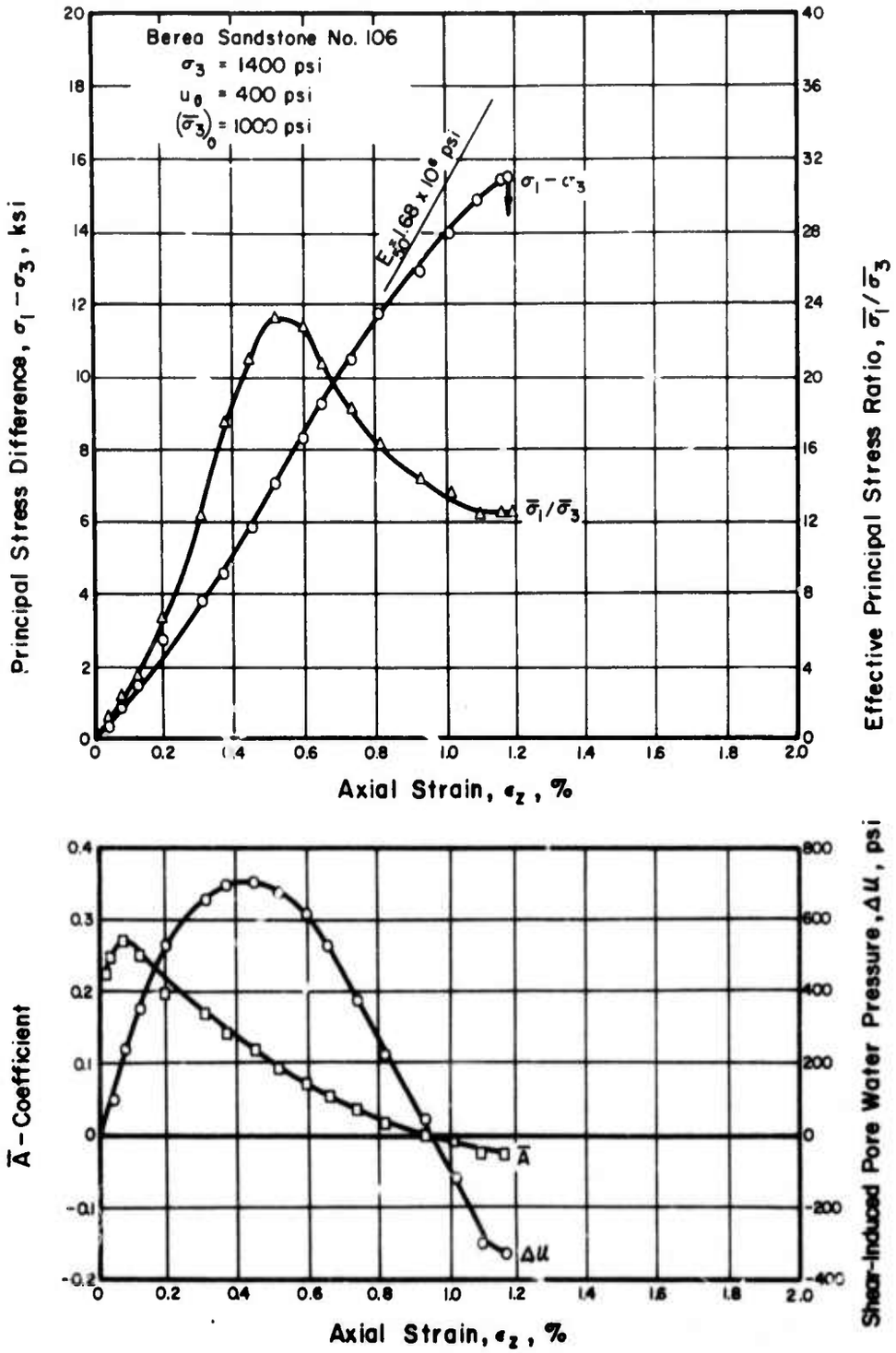

Fig. 3.30 Principal Stress Difference, Shear-Induced Pore Water Pressure, Effective Principal Stress Ratio, and $\bar{A}$-Coefficient Versus Axial Strain, Berea Sandstone, No. 106

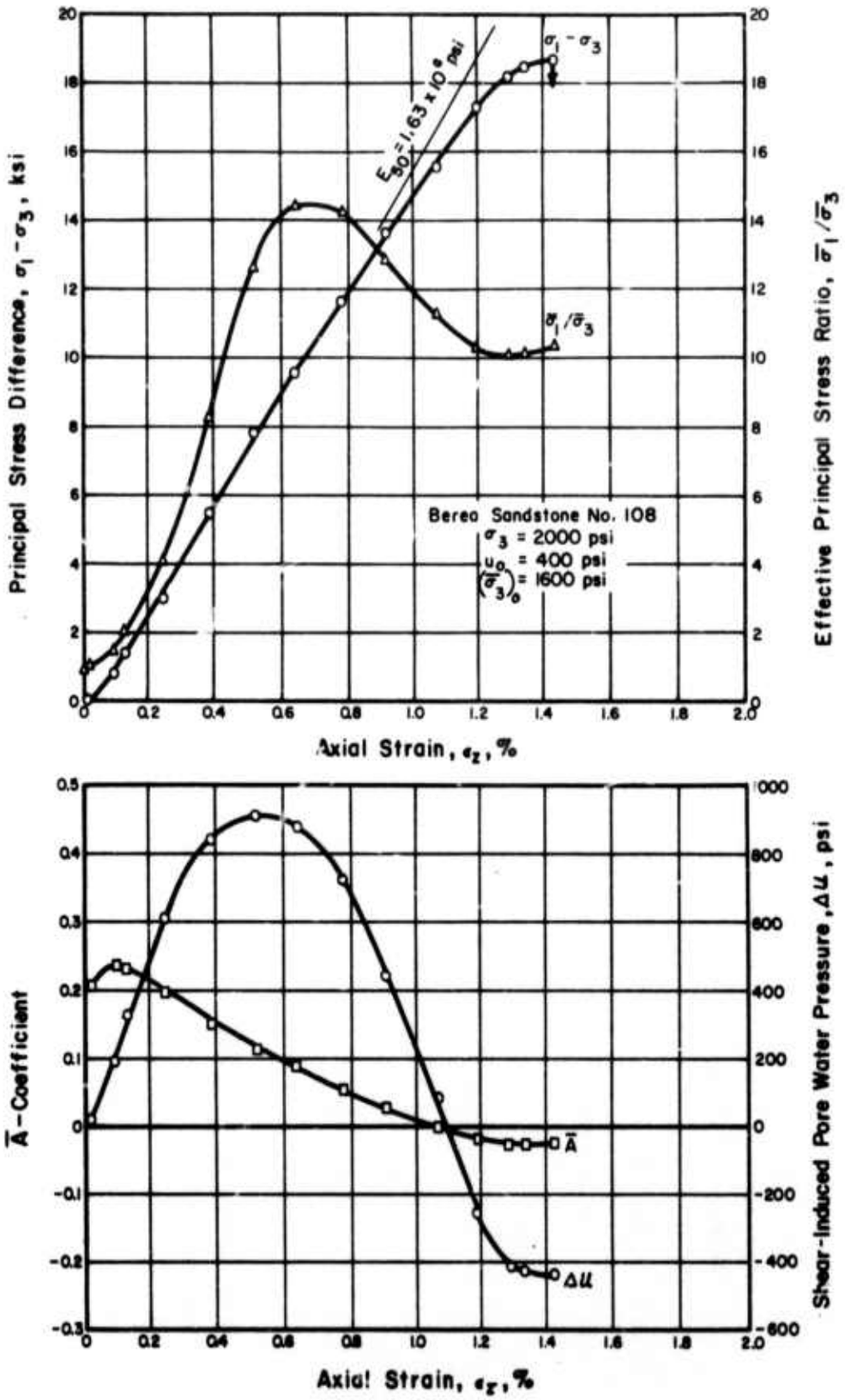

Fig. 3.31 Principal Stress Difference, Shear-Induced Pore Water Pressure, Effective Principal Stress Ratio, and $\bar{A}$-Coefficient Versus Axial Strain, Berea Sandstone, No. 108

Table 3.4 Summary of Undrained Triaxial Compression Tests, Berea Sandstone

Sample No.	Porosity n(%)	Permeability k(cm/sec)	Degree of Saturation S_r(%)	Confining Pressure σ_3(psi)	$(\bar{\sigma}_3)_o^{(3)}$ (psi)	At $(\sigma_1-\sigma_3)_{max}$			Maximum Value of		
						ϵ_z (%)	$\sigma_1-\sigma_3$ (psi)	$\Delta u^{(4)}$ (psi)	$\Delta u^{(4)}$ (psi)	$\bar{A}$	$\bar{\sigma}_1/\bar{\sigma}_3$
104	20.5	4.0×10^{-4} ~ 2.7×10^{-5}	97	800	400	0.93	11,160	- 426	346	0.288	86.9
106	20.2	5.2×10^{-5} ~ 2.8×10^{-5}	99	1400	1000	1.18	15,650	- 328	705	0.270	23.2
108	20.3	4.6×10^{-4} ~ 4.2×10^{-4}	100	2000	1600	1.43	18,740	- 432	922	0.244	14.5

Notes: (1) Axial Strain Rate = 2.35×10^{-4} in/in/min

(2) Pore Water Pressure at the Beginning of Tests = 400 psi

(3) $(\bar{\sigma}_3)_o$: Initial Effective Confining Pressure

(4) Δu : Shear-Induced Pore Water Pressure

The $\bar{A}$-coefficient maximized at the early stage of loading (at axial strains less than 0.1%) and then decreased continuously until it became negative at or near rupture. The maximum observed $\bar{A}$-coefficient was 0.29 for the test with an initial effective confining pressure of 400 psi. The maximum $\bar{A}$-value that was obtained for any test decreased with increasing initial effective confining pressure. An $\bar{A}$-coefficient of 0.24 was observed for the test with 1600 psi initial effective confining pressure.

The stress conditions corresponding to the $(\sigma_1 - \sigma_3)_{max}$ for drained and undrained tests on Berea sandstone are shown in a Mohr-Coulomb diagram in terms of effective stresses in Figure 3.32. A modified Mohr-Coulomb diagram is also plotted in Figure 3.32. In the modified Mohr-Coulomb diagram, the maximum shear stress and its corresponding effective normal stress (the top point of the Mohr circle) is plotted. The results plot almost as a straight line according to the following equation:

$$q_f = \bar{d} + \bar{p}_f \cdot \tan \bar{\psi}$$

where

$$\bar{d} = 0.9 \text{ ksi and } \bar{\psi} = 37°.$$

From $\bar{d}$ and $\bar{\psi}$, $\bar{c}$ and $\bar{\phi}$ are calculated to be 1.5 ksi and 49° respectively, where $\sin \bar{\phi} = \tan \bar{\psi}$ and $\bar{c} = \dfrac{\bar{d}}{\cos \bar{\phi}}$. It should be noted that drained and undrained triaxial compression tests plot on the same failure envelope

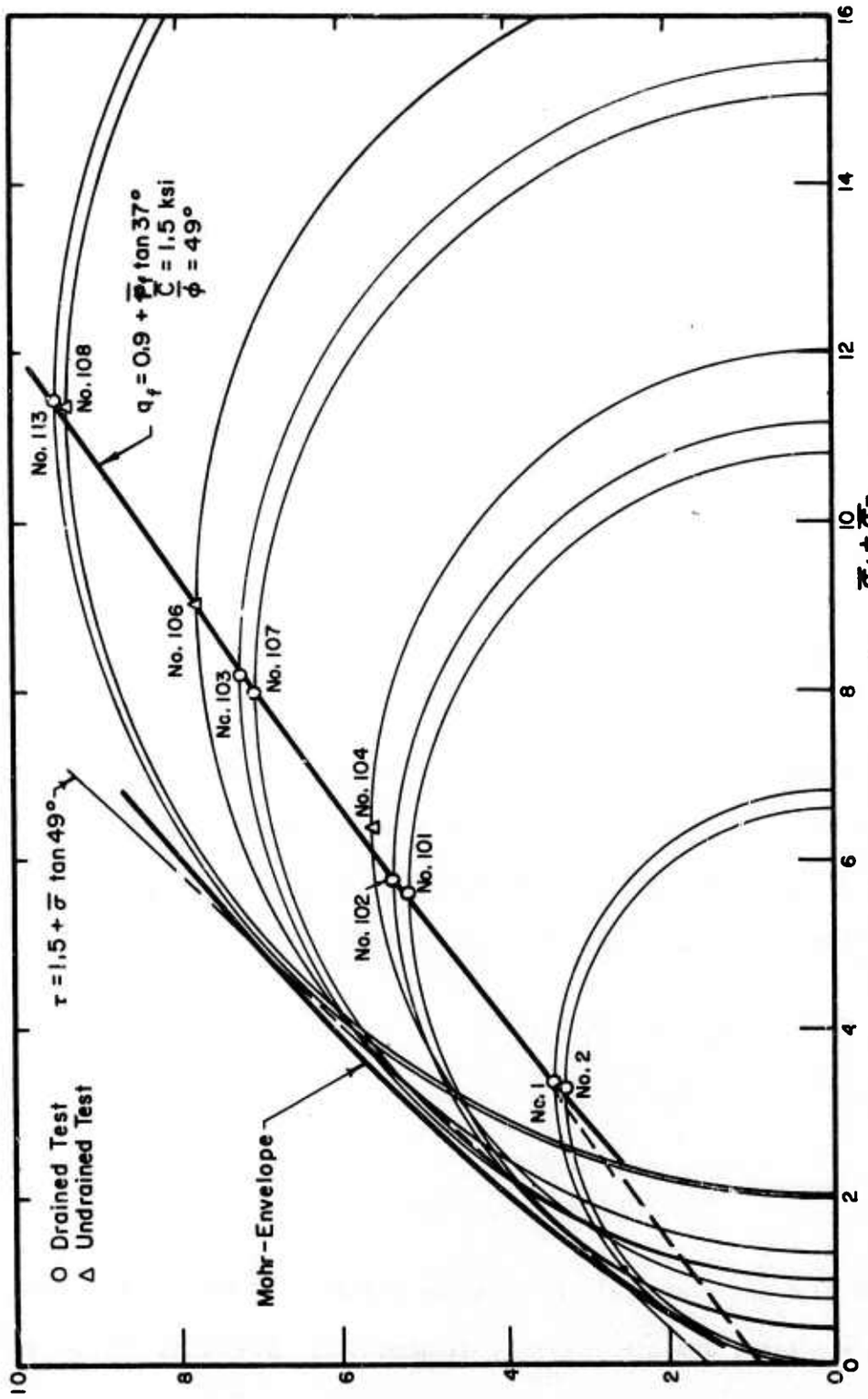

Fig. 3.32 Mohr-Coulomb Diagram, Berea Sandstone

in terms of effective stresses. It should also be noted that the Mohr failure envelope is not a straight line and is concave to the normal stress axis.

Relations between principal stress difference and axial strain for drained and undrained tests are summarized in Figures 3.33 and 3.34, respectively. The tangent moduli for Berea sandstone at 50% of maximum strength were calculated and are shown in Table 3.5. An increase in confining pressure resulted in a higher Young's modulus under both drained and undrained conditions. Also for specimens with the same initial effective confining pressure, drained tests gave higher values of Young's modulus than undrained tests.

3.3.3 Test Results on Salem Limestone

The results of drained triaxial compression tests on Salem limestone are shown in Figures 3.35 to 3.38 in terms of principal stress difference and volumetric strain versus axial strain. The results are also summarized in Table 3.6. Salem limestone specimens exhibited the maximum principal stress difference, $(\sigma_1 - \sigma_3)_{max}$, at axial strains of 0.65% to 0.84% All of the specimens underwent volume decrease at the initial stage of loading and reached their maximum negative volumetric strains of 0.03% to 0.30% at an axial strain of about 0.6%. Specimen SL No. 101, which was tested under a confining pressure of 400 psi, showed a maximum volumetric strain at the peak of principal stress difference

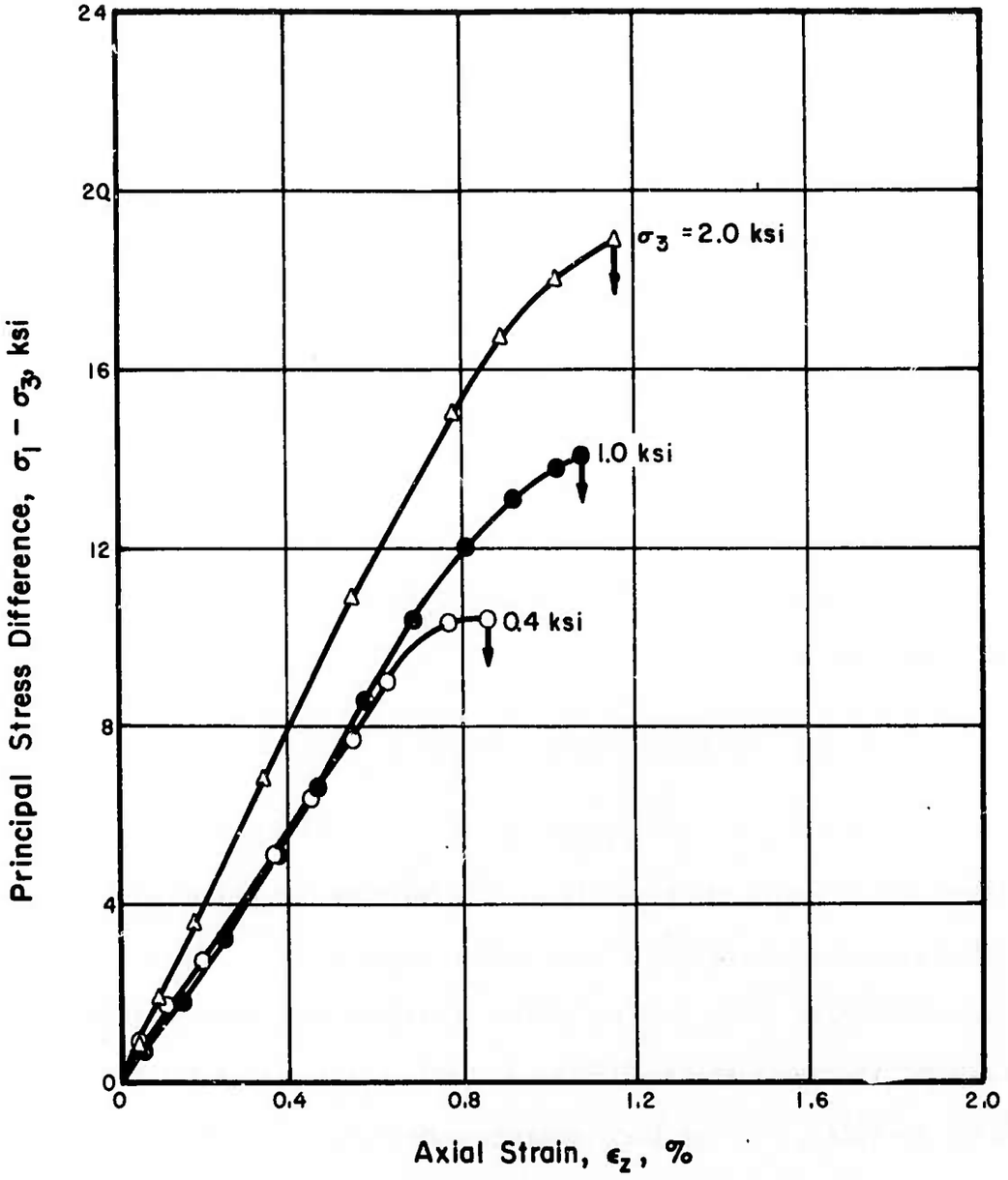

Fig. 3.33 Principal Stress Difference Versus Axial Strain, Drained Tests, Berea Sandstone

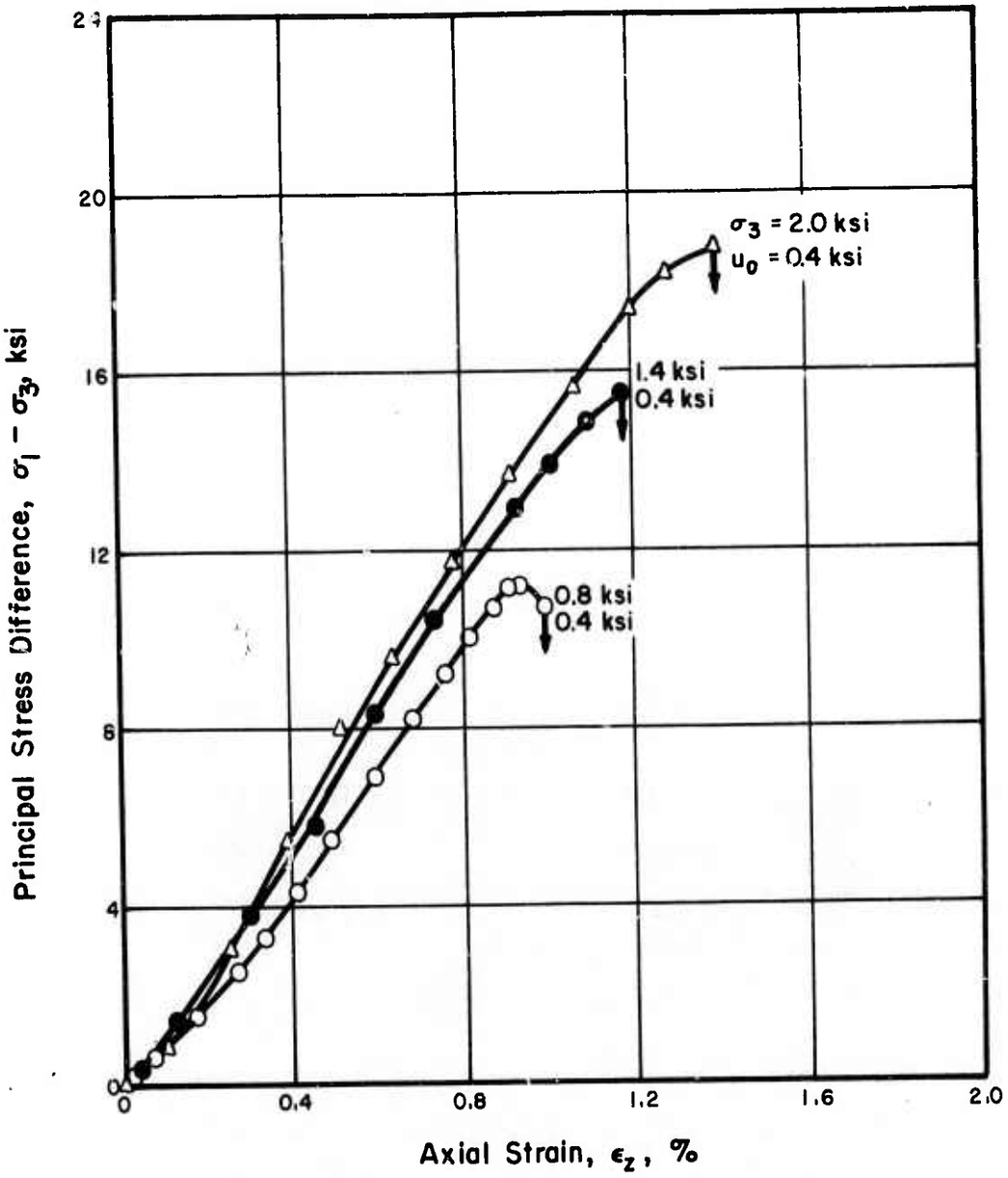

Fig. 3.34 Principal Stress Difference Versus Axial Strain, Undrained Tests, Berea Sandstone

Table 3.5 Tangent Modulus at 50% of Maximum Strength, Berea Sandstone

	Initial Effective Confining Pressure $(\bar{\sigma}_3)_o$ (psi)	Tangent Modulus at 50% of Maximum Strength E_{50} (psi)
Drained Tests	400	1.44×10^6
		1.46×10^6
	1000	1.60×10^6
		1.77×10^6
	2000	2.01×10^6
Undrained Tests	400	1.41×10^6
	1000	1.62×10^6
	1600	1.63×10^6

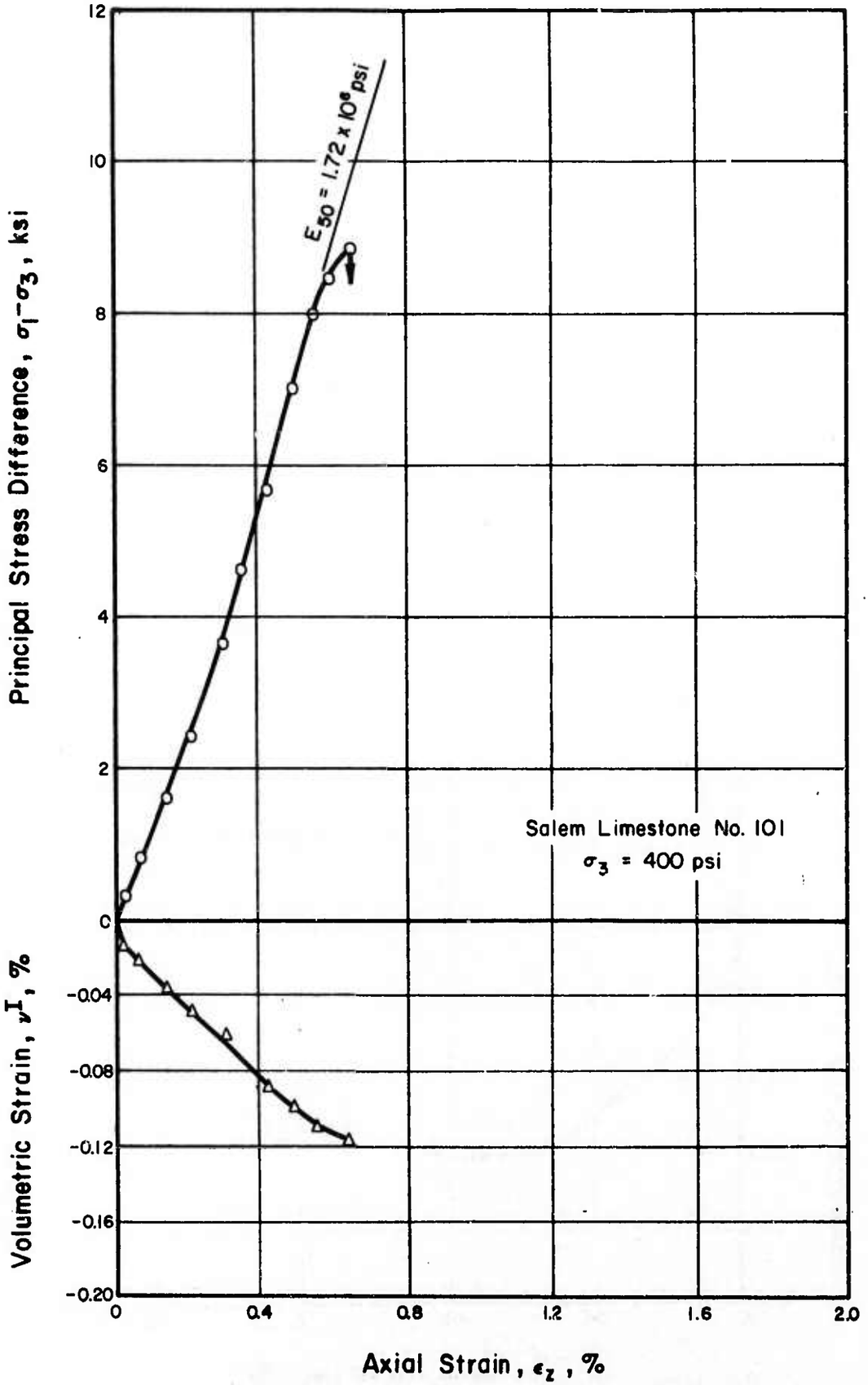

Fig. 3.35 Principal Stress Difference and Volumetric Strain Versus Axial Strain, Salem Limestone, No. 101

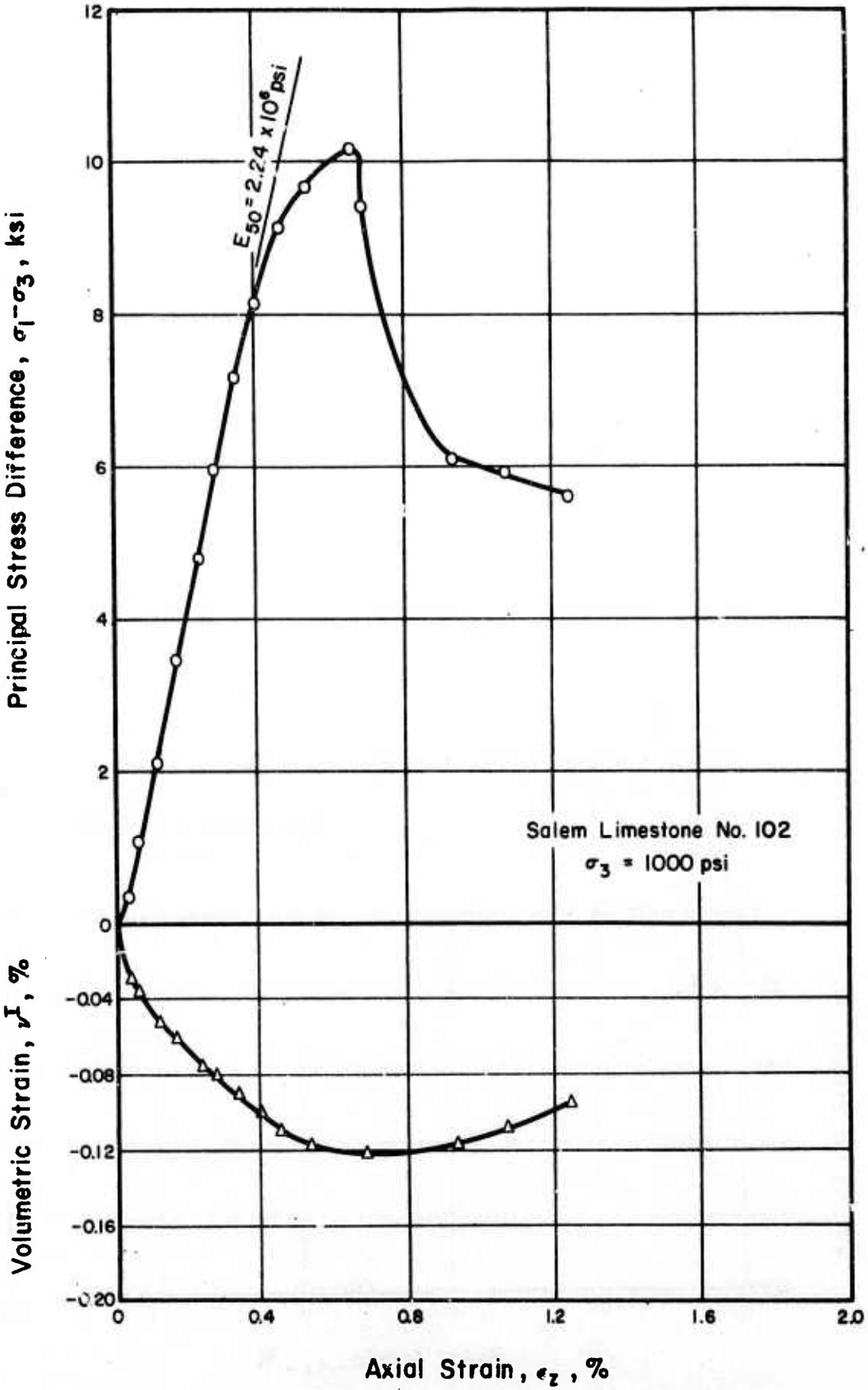

Fig. 3.36 Principal Stress Difference and Volumetric Strain Versus Axial Strain, Salem Limestone, No. 102

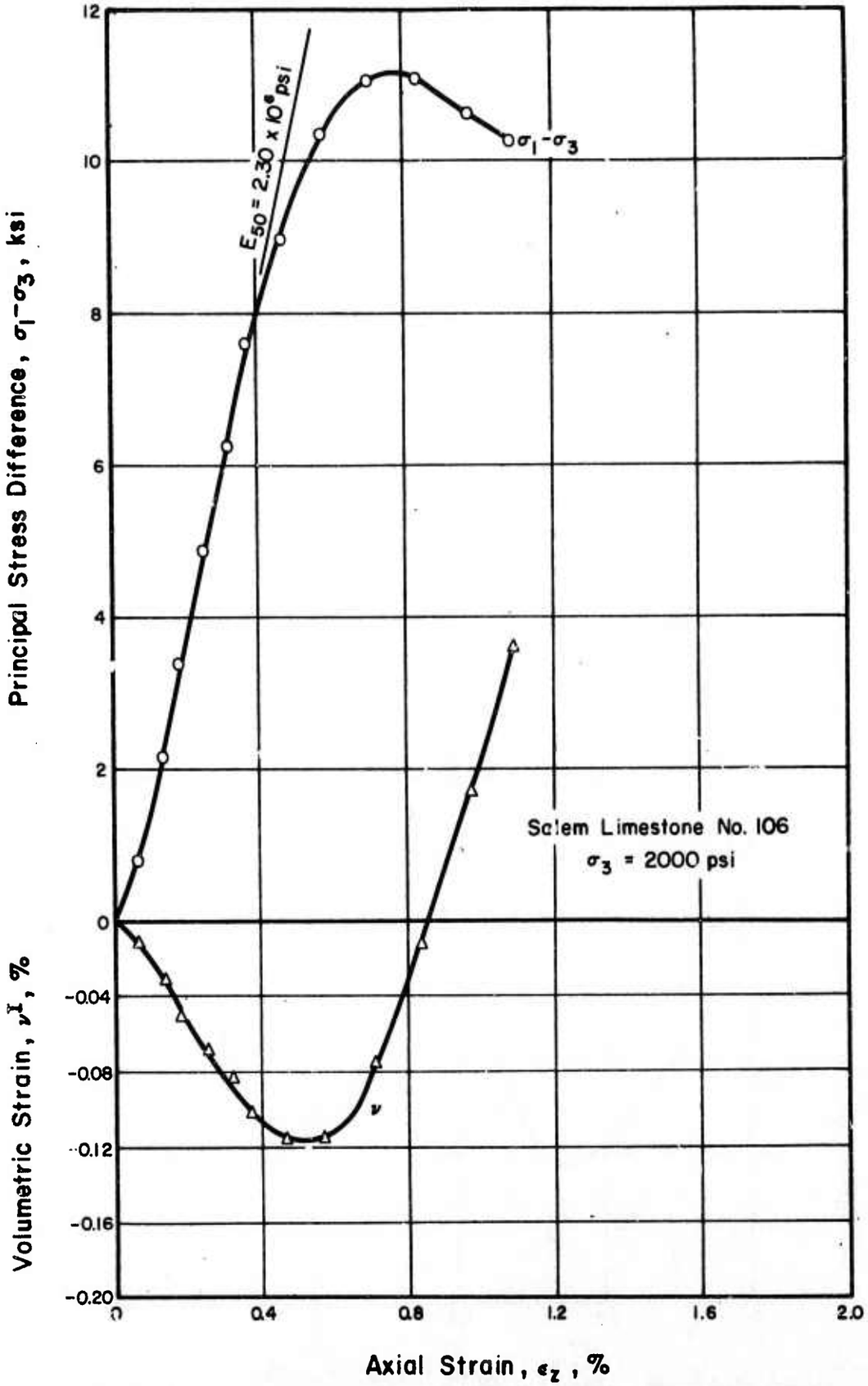

Fig. 3.37 Principal Stress Difference and Volumetric Strain Versus Axial Strain, Salem Limestone, No. 106

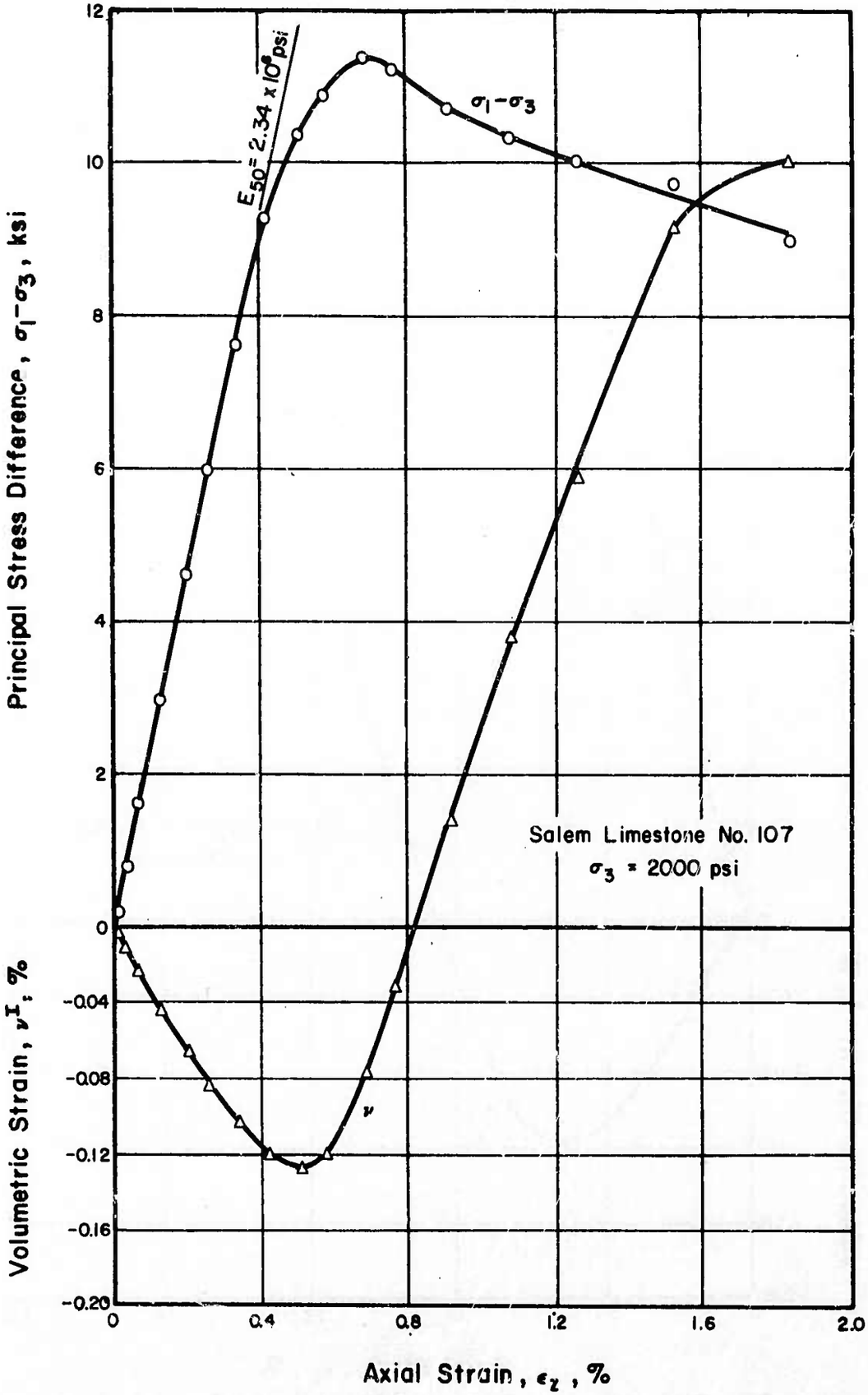

Fig. 3.38 Principal Stress Difference and Volumetric Strain Versus Axial Strain, Salem Limestone, No. 107

Table 3.6 Summary of Drained Triaxial Compression Tests, Salem Limestone

Sample No.	Porosity n (%)	Permeability k (cm/sec) x 10^{-7}	Degree of Saturation S_r (%)	Confining Pressure σ_3 (psi)	At $(\sigma_1 - \sigma_3)_{max}$			Max. Volumetric Strain ν^I_{max} (%)
					Axial Strain ε_z (%)	$\sigma_1 - \sigma_3$ (psi)	Volumetric Strain ν^I (%)	
103	12.7	3.48 ~ 2.23	100	0	0.390	7,290	--	--
101	12.7	0.80 ~ 0.42	94	400	0.664	8,850	-0.119	-0.119
102	12.7	1.18 ~ 0.24	100	1000	0.660	10,200	-0.120	-0.122
106	12.5	5.01 ~ 3.56	100	2000	0.840	11,140	-0.030	-0.300 (+0.380)
107	12.7	6.21 ~ 3.28	100	2000	0.690	11,400	-0.200	-0.332 (+1.096)

Notes: No. 101, 102, 106, 107: Triaxial Tests, Strain Rate = 2.35×10^{-4} in/in/min

No. 103 : Uniaxial Tests, Strain Rate = 2.35×10^{-4} in/in/min

and instantaneously ruptured without any ductile deformation. Specimen SL No. 102, which was tested under a confining pressure of 1000 psi, also showed a maximum volumetric strain at the peak principal stress difference, but then exhibited a ductile deformation. Volume increase was observed during this ductile deformation, but the final volumetric strain remained negative. Two specimens were tested under a confining pressure of 2000 psi. Their maximum negative volumetric strains occurred slightly before the peak principal stress differences were reached, and thereafter they exhibited a great tendency toward volume increase. At their rupture, positive volumetric strains of 0.38% and 1.1% were observed for these two specimens.

Results of undrained triaxial compression tests are presented in Figures 3.39 to 3.41 in which principal stress difference, shear induced pore water pressure, effective principal stress ratio, and $\bar{A}$-coefficient are plotted versus axial strain. The results are also summarized in Table 3.7. Specimen SL No. 105, which was tested with an initial effective confining pressure of 400 psi, showed slightly peculiar behavior at the initial stage of loading, Figure 3.39. This might be due to the existence of a weak zone in the specimen or due to insufficient initial seating of the specimen. A corrected axis for axial strains is given in Figure 3.39 to adjust the behavior. The corrected axial strains are used in the following discussion. Salem limestone specimens exhibited maximum principal stress difference at axial strains of 0.64% to 0.92% in undrained tests. These

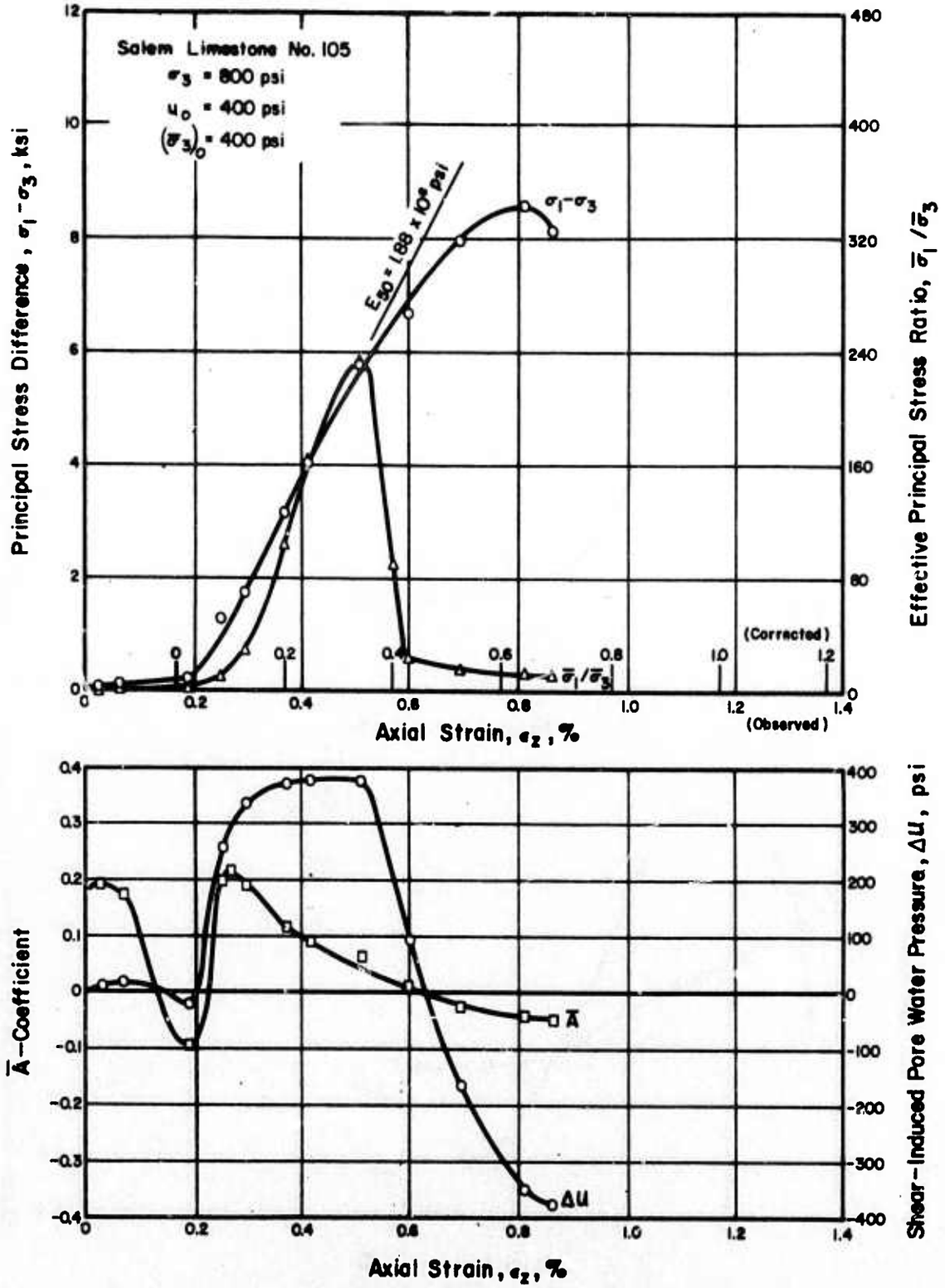

Fig. 3.39 Principal Stress Difference, Shear-Induced Pore Water Pressure, Effective Principal Stress Ratio, and $\bar{A}$-Coefficient Versus Axial Strain, Salem Limestone, No. 105

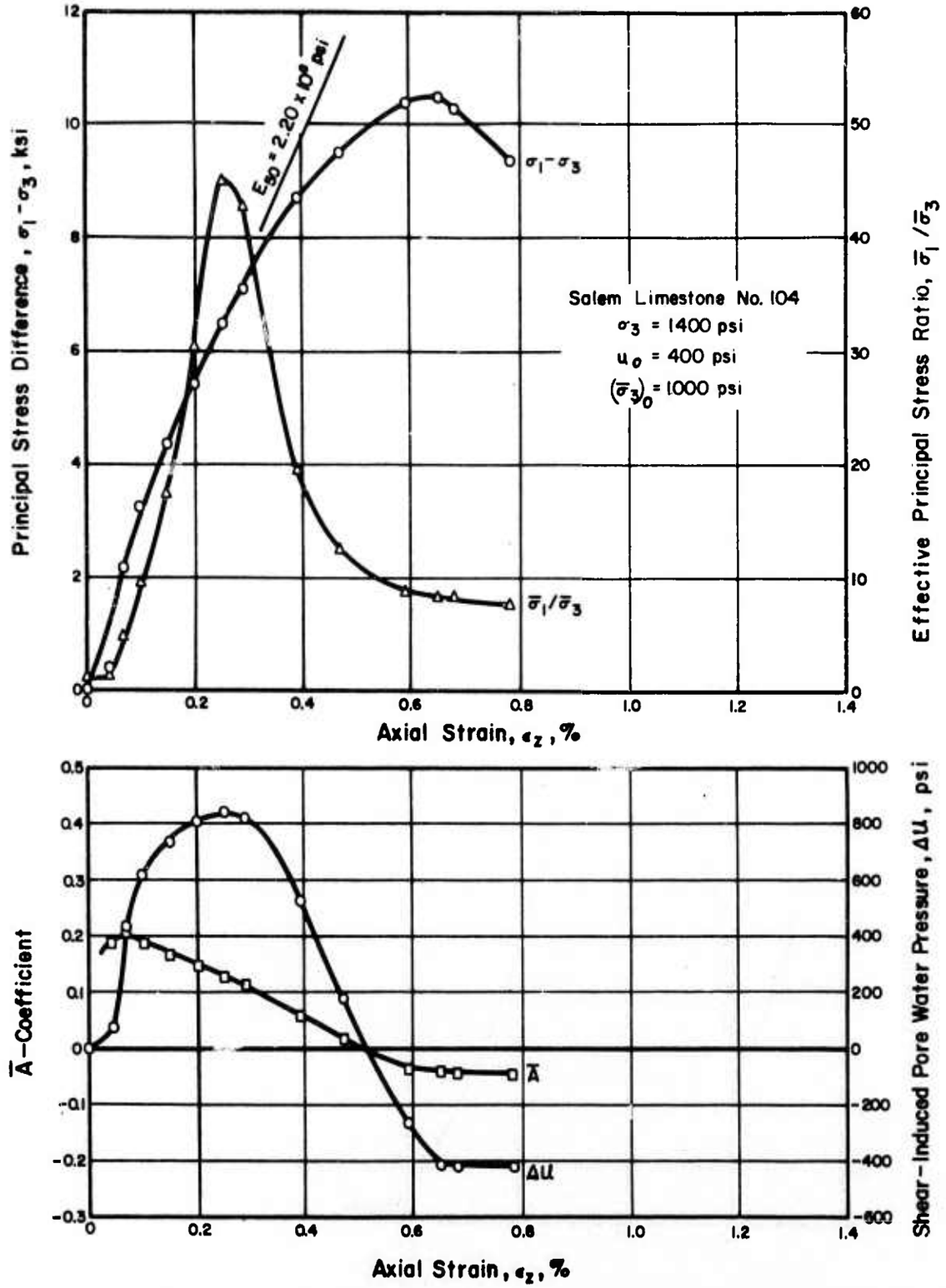

Fig. 3.40 Principal Stress Difference, Shear-Induced Pore Water Pressure, Effective Principal Stress Ratio, and $\bar{A}$-Coefficient Versus Axial Strain, Salem Limestone, No. 104

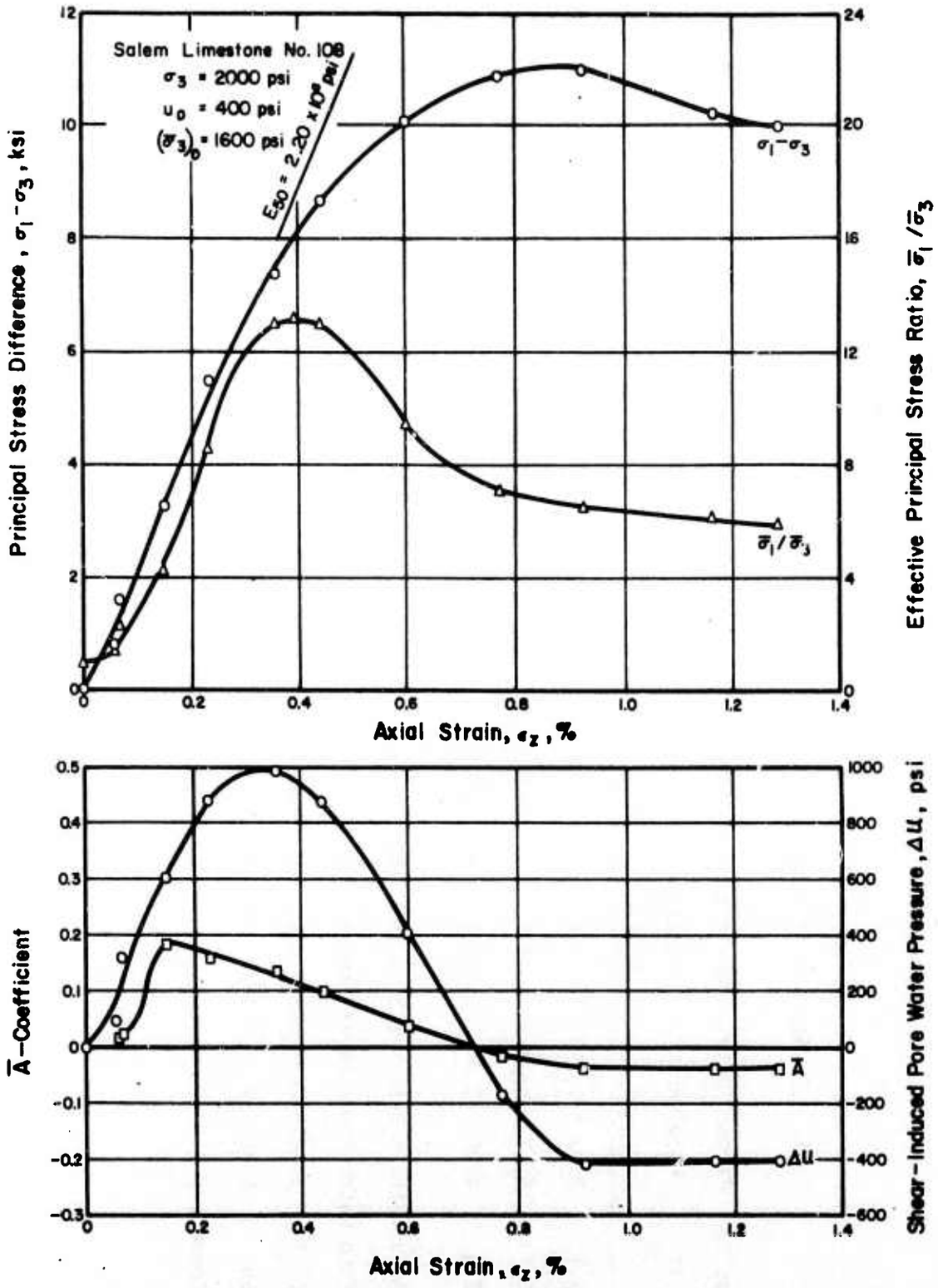

Fig. 3.41 Principal Stress Difference, Shear-Induced Pore Water Pressure, Effective Principal Stress Ratio, and $\bar{A}$-Coefficient Versus Axial Strain, Salem Limestone, No. 108

Table 3.7 Summary of Undrained Triaxial Compression Tests, Salem Limestone

Sample No.	Porosity n(%)	Permeability k(cm/sec) x 10^{-7}	Degree of Saturation S_r(%)	Confining Pressure σ_3 (psi)	$(\bar{\sigma}_3)_o$ (3) (psi)	At $(\sigma_1-\sigma_3)_{max}$			Maximum Value of		
						ε_Z (%)	$\sigma_1-\sigma_3$ (psi)	Δu (4) (psi)	Δu (4) (psi)	$\bar{A}$	$\bar{\sigma}_1/\bar{\sigma}_3$
105	12.1	1.78 ~ 1.18	100	800	400	0.64 (5)	8,620	- 350	377	0.217	235.0
104	12.7	4.47 ~ 2.11	100	1400	1000	0.65	10,480	- 415	844	0.205	42.5
108	12.6	4.06 ~ 3.03	100	2000	1600	0.92	11,010	- 417	987	0.195	13.2

Notes: (1) Axial Strain Rate = 2.35 x 10^{-4} in/in/min

(2) Pore Water Pressure at the Beginning of Tests = 400 psi

(3) $(\bar{\sigma}_3)_o$: Initial Effective Confining Pressure

(4) Δu : Shear-Induced Pore Water Pressure

(5) Corrected

strains at $(\sigma_1 - \sigma_3)_{max}$ are almost the same as or slightly higher than the corresponding strains in drained tests. Positive shear-induced pore water pressures were observed at the initial stage of loading for all of the specimens. As the loading continued, the pore pressures began to decrease and became negative. The $\overline{A}$- coefficient maximized at axial strains of about 0.1% and then decreased continuously until it became negative at or near rupture. The maximum observed $\overline{A}$- coefficient was about 0.2 for all of the tests. The effective principal stress ratio, $\overline{\sigma}_1/\overline{\sigma}_3$, maximized at the strain corresponding to the maximum shear-induced pore water pressure. The axial stress at this strain was equal to 50% to 60% of the maximum principal stress difference. The maximum effective principal stress ratio decreased with increasing initial effective confining pressure.

The stress conditions corresponding to the $(\sigma_1 - \sigma_3)_{max}$ for drained and undrained tests on Salem limestone are shown in a Mohr-Coulomb diagram in terms of effective stresses in Figure 3.42. A modified Mohr-Coulomb diagram is also plotted in Figure 3.42. In the modified Mohr-Coulomb diagram, the results plot almost as a straight line except for the tests performed under the highest confining pressures. The straight line can be represented by the following equation:

$$q_f = \overline{d} + \overline{p}_f \cdot \tan \overline{\psi}$$

where

$\overline{d}$ = 1.5 ksi and $\overline{\psi}$ = 30°.

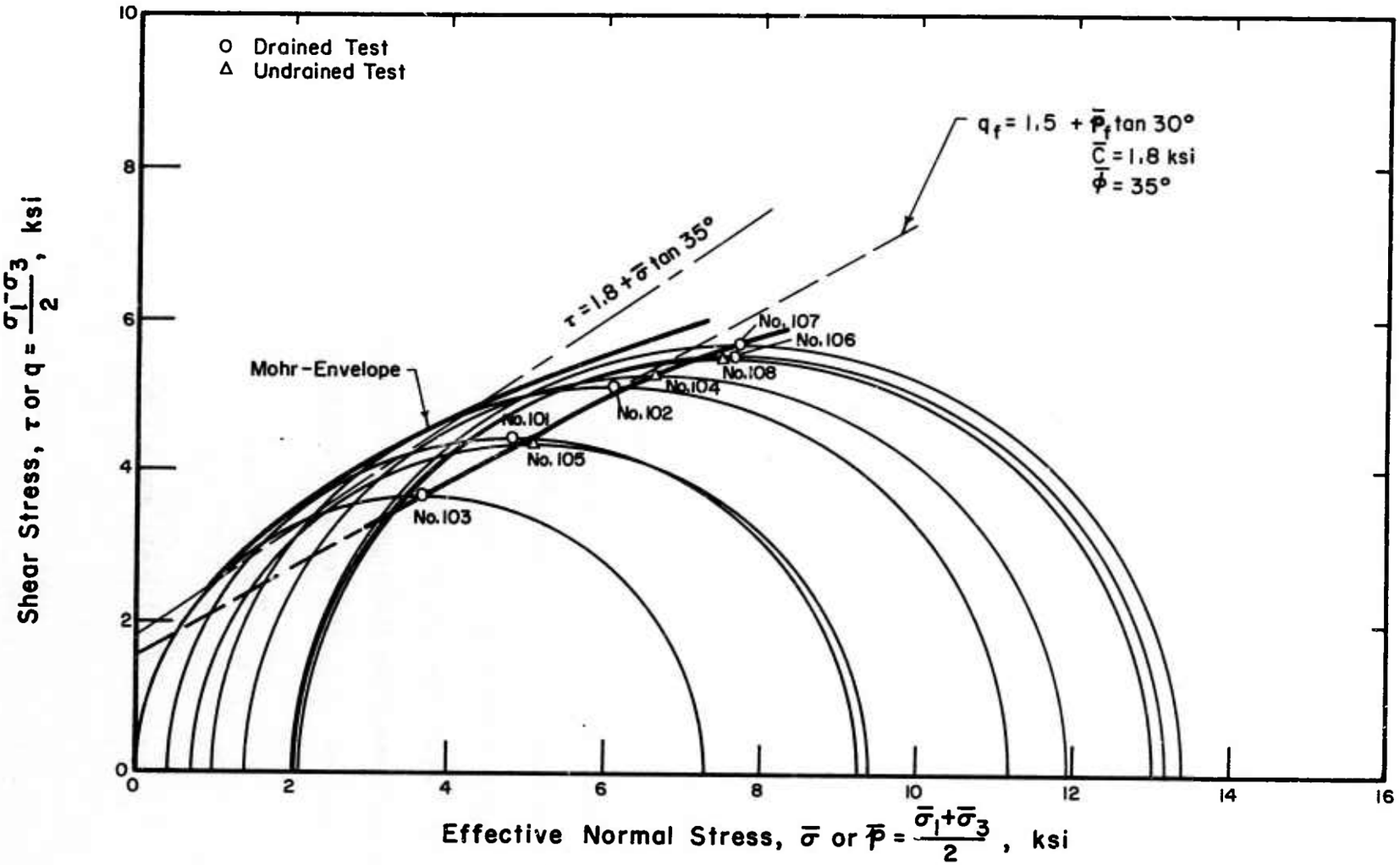

Fig. 3.42 Mohr-Coulomb Diagram, Salem Limestone

From $\bar{d}$ and $\bar{\psi}$, $\bar{c}$ and $\bar{\phi}$ for Salem limestone are calculated to be 1.8 ksi and 35°, respectively.

Relations between principal stress difference and axial strain for drained and undrained tests are summarized in Figures 3.43 and 3.44, respectively. The tangent moduli at 50% of maximum strength are shown in Table 3.8. An increase in confining pressure resulted in a higher Young's modulus under both drained and undrained conditions.

3.3.4 Test Results on Vermont Marble

The results of drained triaxial compression tests on Vermont marble are shown in Figures 3.45 to 3.47. Pore pressure measurements in some control tests indicated that tests on Vermont marble were only partially drained. The results are also summarized in Table 3.9. Vermont marble specimens exhibited maximum principal stress difference at axial strains of 0.42% to 0.91%. The axtial strain corresponding to maximum principal stress difference increased significantly as confining pressure increased. All of the specimens exhibited volume decreases and reached their maximum negative volumetric strains of 0.016% to 0.037% at axial strains of about 0.4%. Whereas all of the specimen exhibited considerable ductile deformation after the maximum principal stress difference was reached, volumetric strains remained negative throughout the tests. The maximum observed negative volumetric strain was 0.037% for the test with a confining pressure of 400 psi. The maximum value decreased with increasing confining pressure.

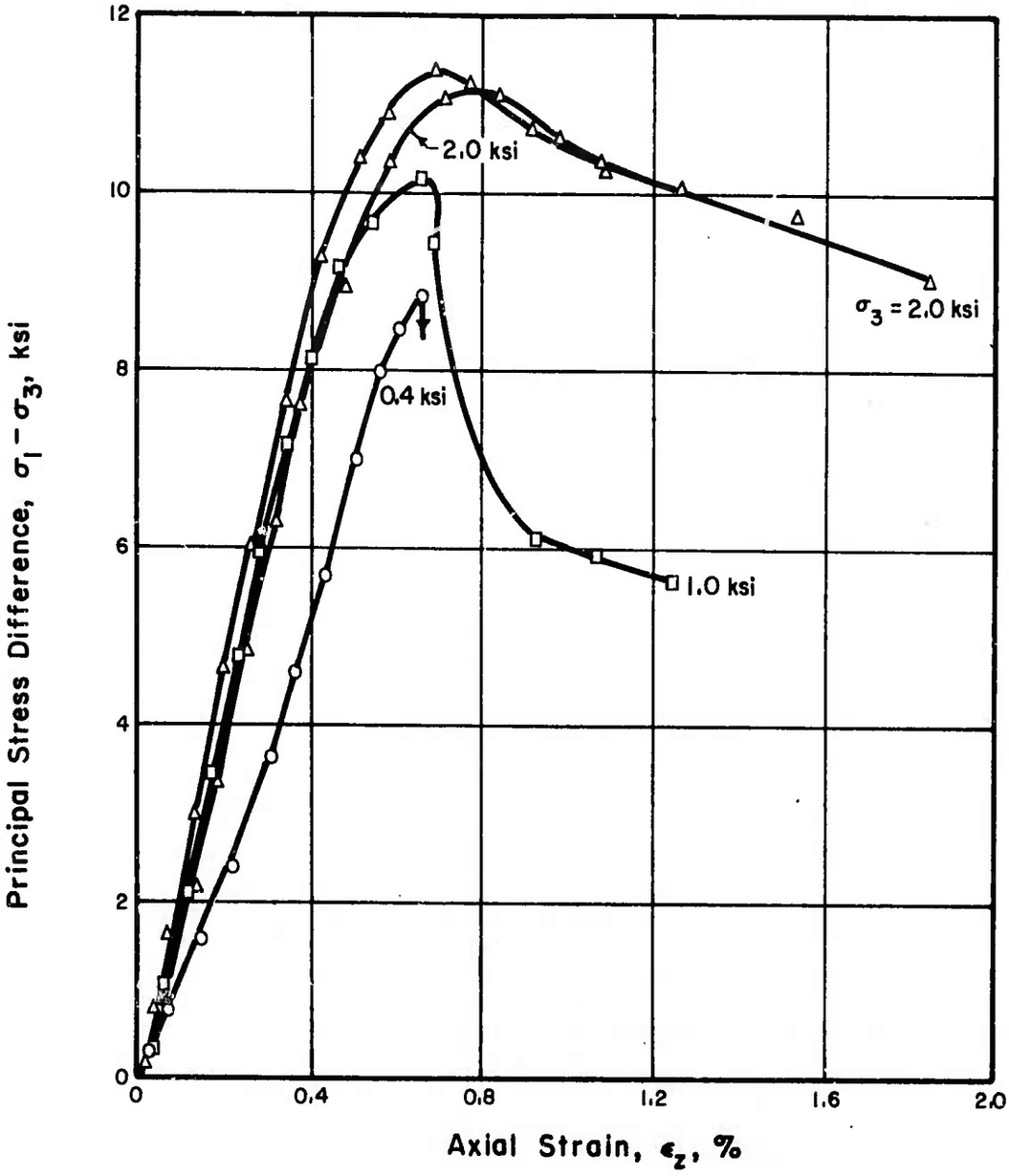

Fig. 3.43 Principal Stress Difference Versus Axial Strain, Drained Tests, Salem Limestone

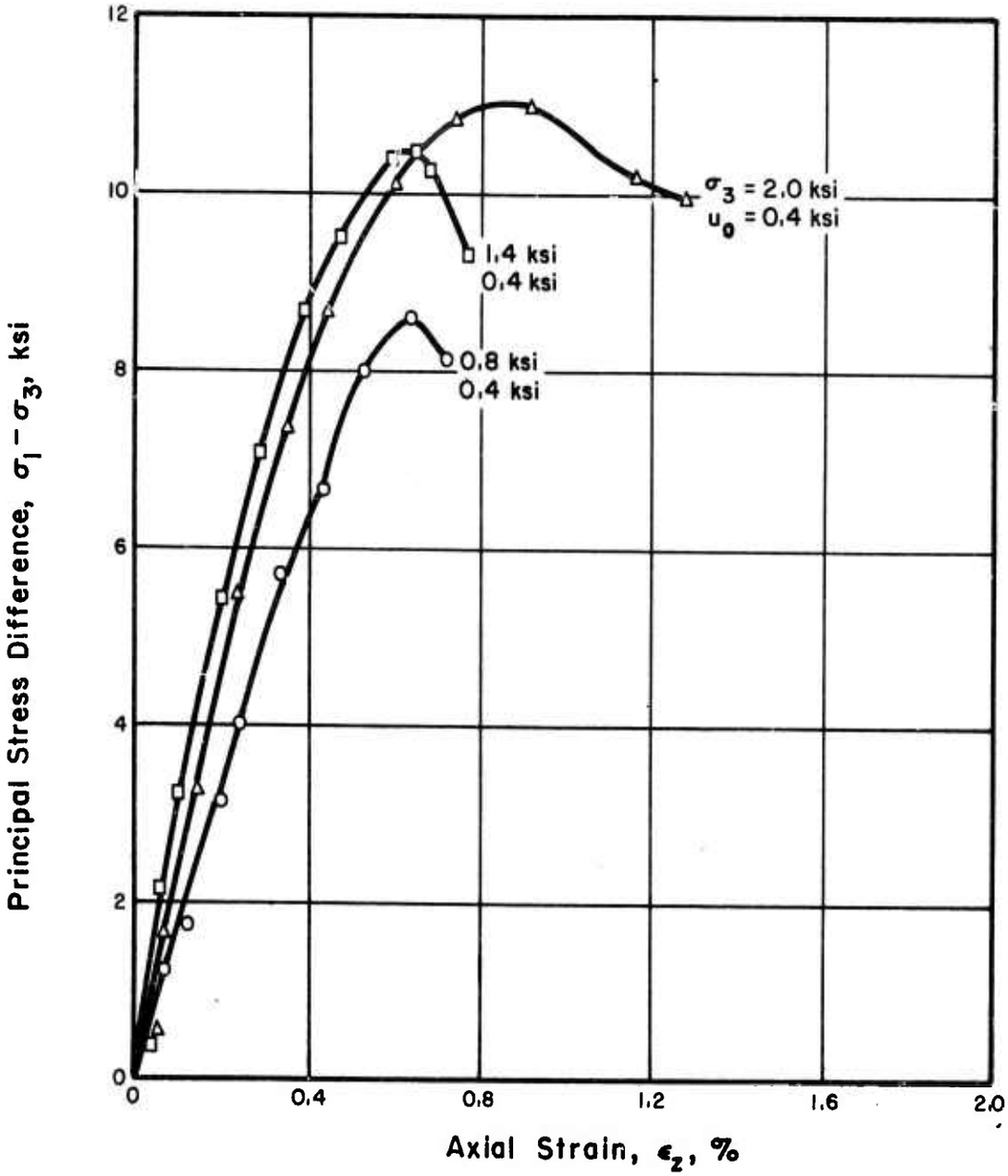

Fig. 3.44 Principal Stress Difference Versus Axial Strain, Undrained Tests, Salem Limestone

Table 3.8 Tangent Modulus at 50% of Maximum Strength, Salem Limestone

	Initial Effective Confining Pressure $(\bar{\sigma}_3)_o$ (psi)	Tangent Modulus at 50% of Maximum Strength E_{50} (psi)
Drained Tests	400	1.72×10^6
	1000	2.24×10^6
	2000	2.30×10^6 2.34×10^6
Undrained Tests	400	1.88×10^6
	1000	2.20×10^6
	1600	2.20×10^6

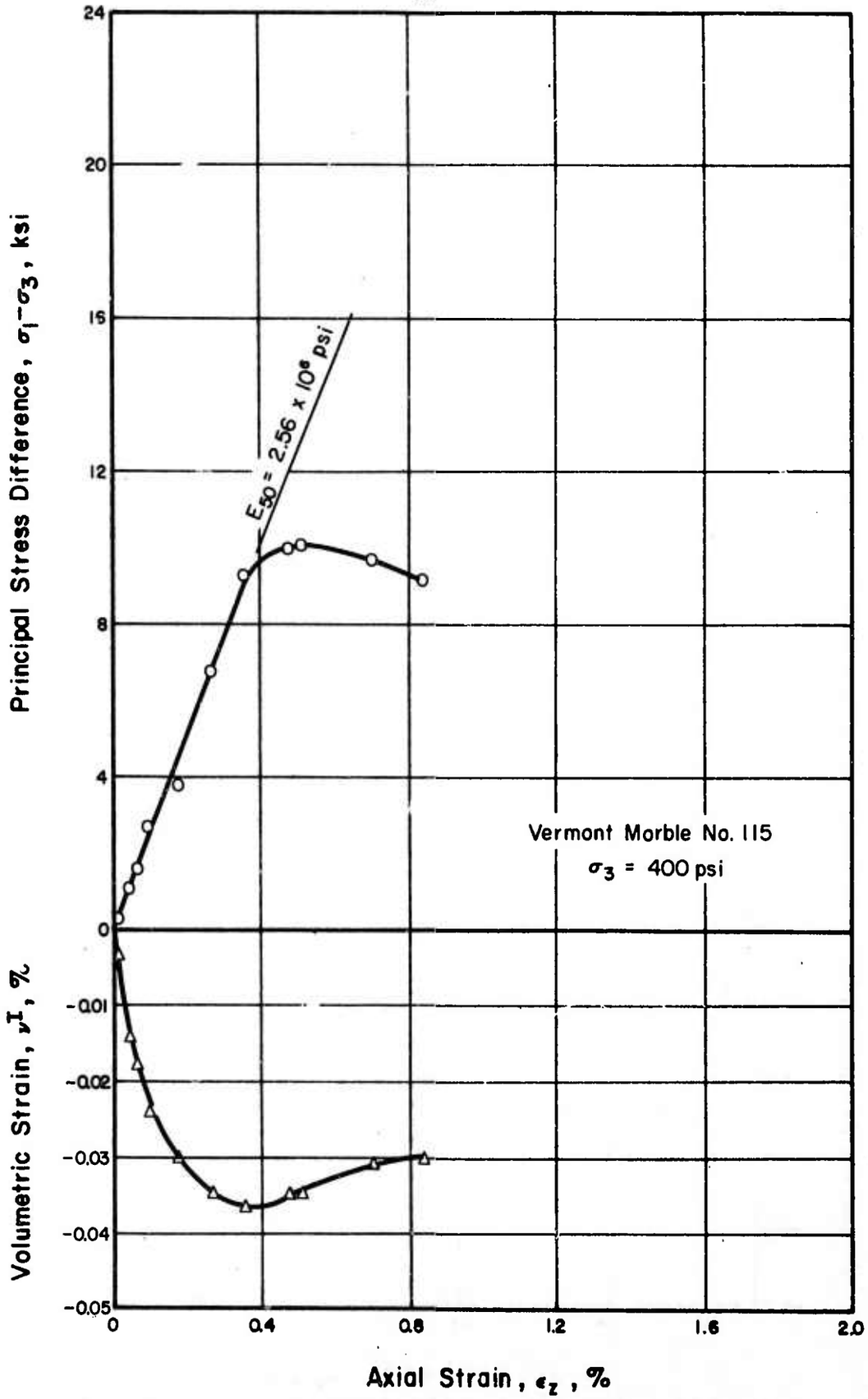

Fig. 3.45 Principal Stress Difference and Volumetric Strain Versus Axial Strain, Vermont Marble, No. 115

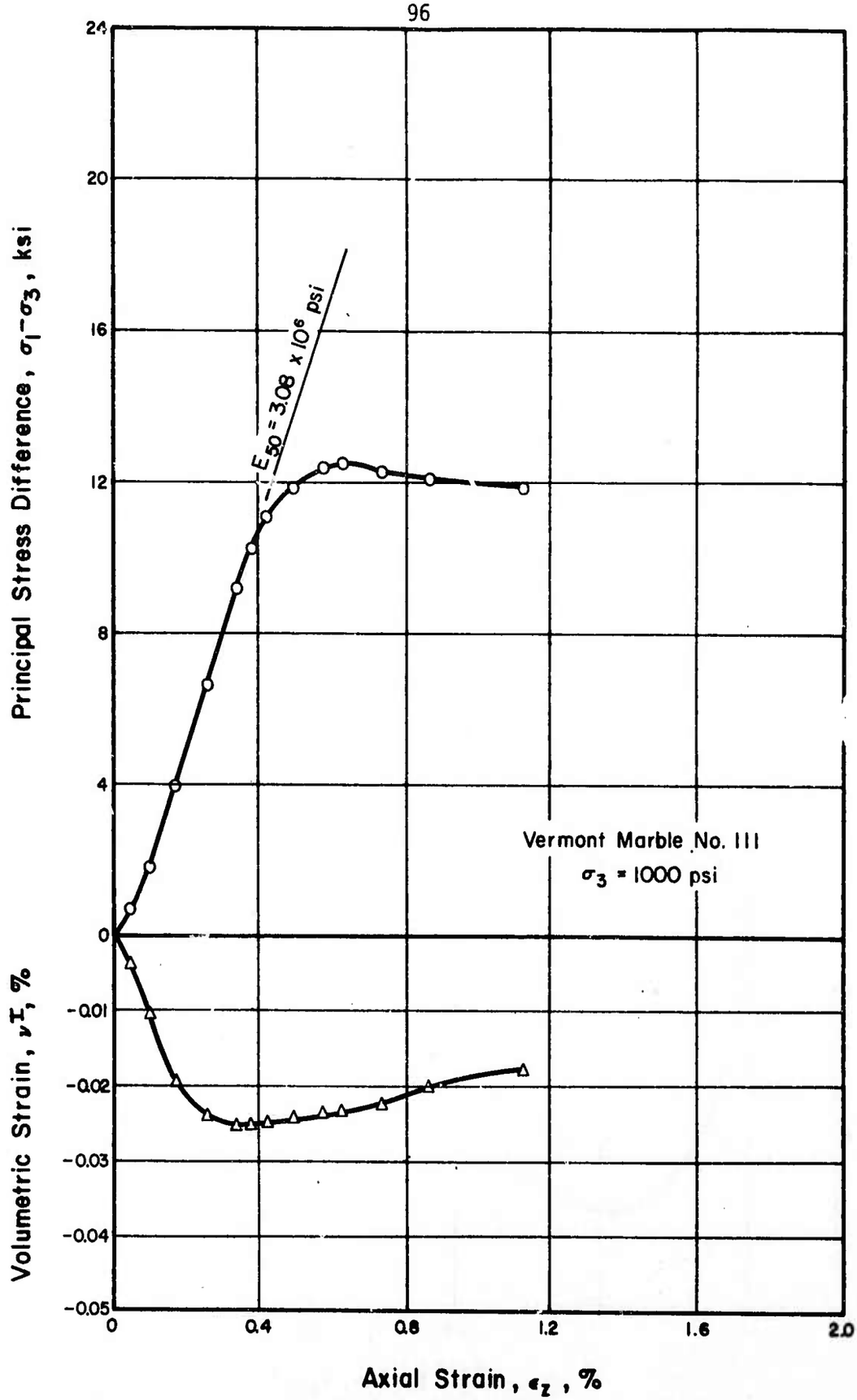

Fig. 3.46 Principal Stress Difference and Volumetric Strain Versus Axial Strain, Vermont Marble, No. 111

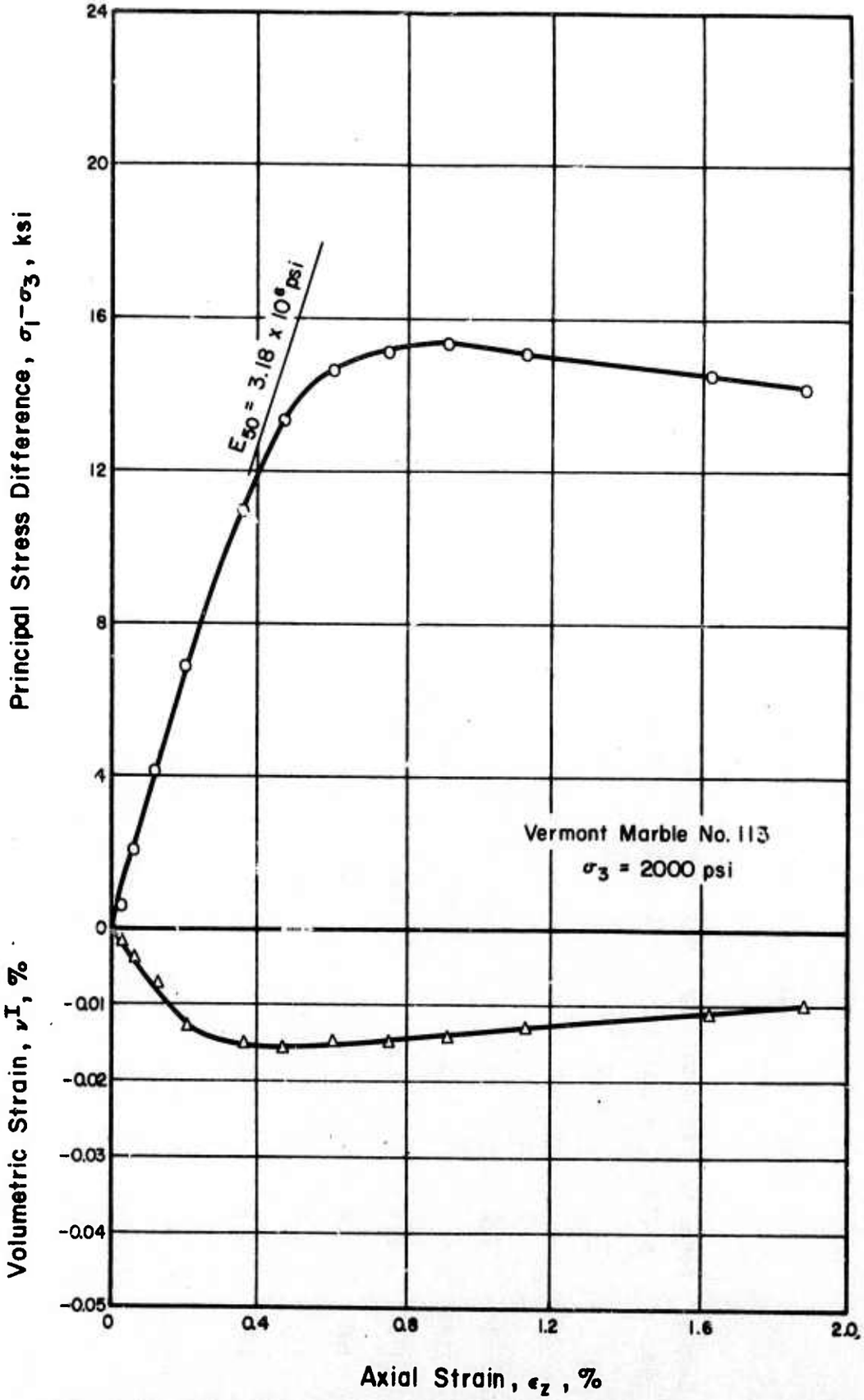

Fig. 3.47 Principal Stress Difference and Volumetric Strain Versus Axial Strain, Vermont Marble, No. 113

Table 3.9 Summary of Drained Triaxial Compression Tests, Vermont Marble

Sample No.	Porosity n (%)	Permeability k (cm/sec) x 10^{-10}	Degree of Saturation S_r (%)	Confining Pressure σ_3 (psi)	At $(\sigma_1 - \sigma_3)_{max}$			Max. Volumetric Strain v^I_{max} (%)
					Axial Strain ε_z (%)	$\sigma_1 - \sigma_3$ (psi)	Volumetric Strain v^I (%)	
2	1.9	--	39	0	0.445	7,090	--	--
110	2.1	--	93	0	0.423	8,370	--	--
115	2.1	9.3	100	400	0.510	10,480	-0.035	-0.037
105	1.9	7.8	100	500	0.691	11,910	(-0.080)(3)	(-0.090)(3)
111	2.1	2.9 ~ 1.1	92	1000	0.615	12,510	-0.024	-0.026
113	1.9	2.9	99	2000	0.911	15,400	-0.014	-0.016

Notes: (1) No. 105 ~ 115: Triaxial Tests, Strain Rate = 2.35 x 10^{-4} in/in/min

(2) No. 2: Uniaxial Tests, Strain Rate = 1.4 x 10^{-4} in/in/min

(3) Might be affected by a small amount of cell fluid leakage.

Results of undrained triaxial compression tests are presented in Figures 3.48 to 3.50 for each specimen tested. The undrained test results are also summarized in Table 3.10. Vermont marble specimens exhibited maximum principal stress difference at axial strains of 0.66% to 0.96% in undrained tests. The strains at $(\sigma_1 - \sigma_3)_{max}$ are higher than the corresponding strains in drained tests. Axial strain at maximum principal stress difference increased with increasing confining pressure. Positive shear-induced pore water pressures were observed at the initial stage of loading for all of the specimens. As the loading continued, the pore pressures began to decrease and became negative. The $\bar{A}$- coefficient maximized at the early stage of loading (at axial strains of 0.05% to 0.1%) and then decreased continuously until it became negative. The maximum observed $\bar{A}$- coefficients were 0.31 to 0.38. The effective principal stress ratio maximized at the strain corresponding to the maximum shear-induced pore water pressure. The axial stress at this strain was equal to 40% to 50% of the maximum principal stress difference. The value of the maximum effective principal stress ratio decreased with increasing initial effective confining pressure. A Mohr-Coulomb diagram and a modified Mohr-Coulomb diagram for Vermont marble are shown in Figure 3.51. Whereas the Mohr failure envelope is slightly concave to the normal stress axis, the modified Mohr-Coulomb diagram plots almost as a straight line according to the following equation:

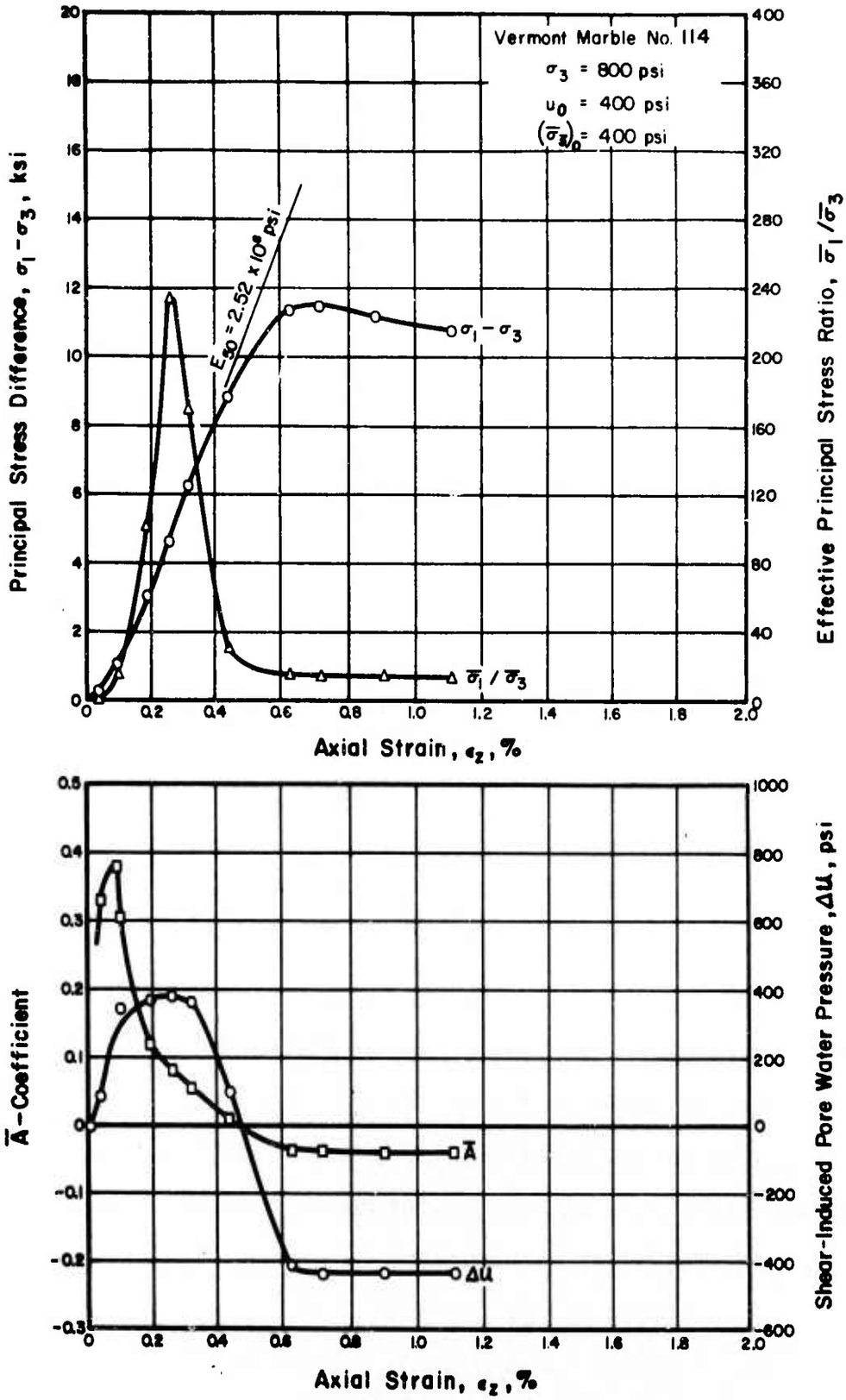

Fig. 3.48 Principal Stress Difference, Shear-Induced Pore Water Pressure, Effective Principal Stress Ratio, and $\bar{A}$-Coefficient Versus Axial Strain, Vermont Marble, No. 114

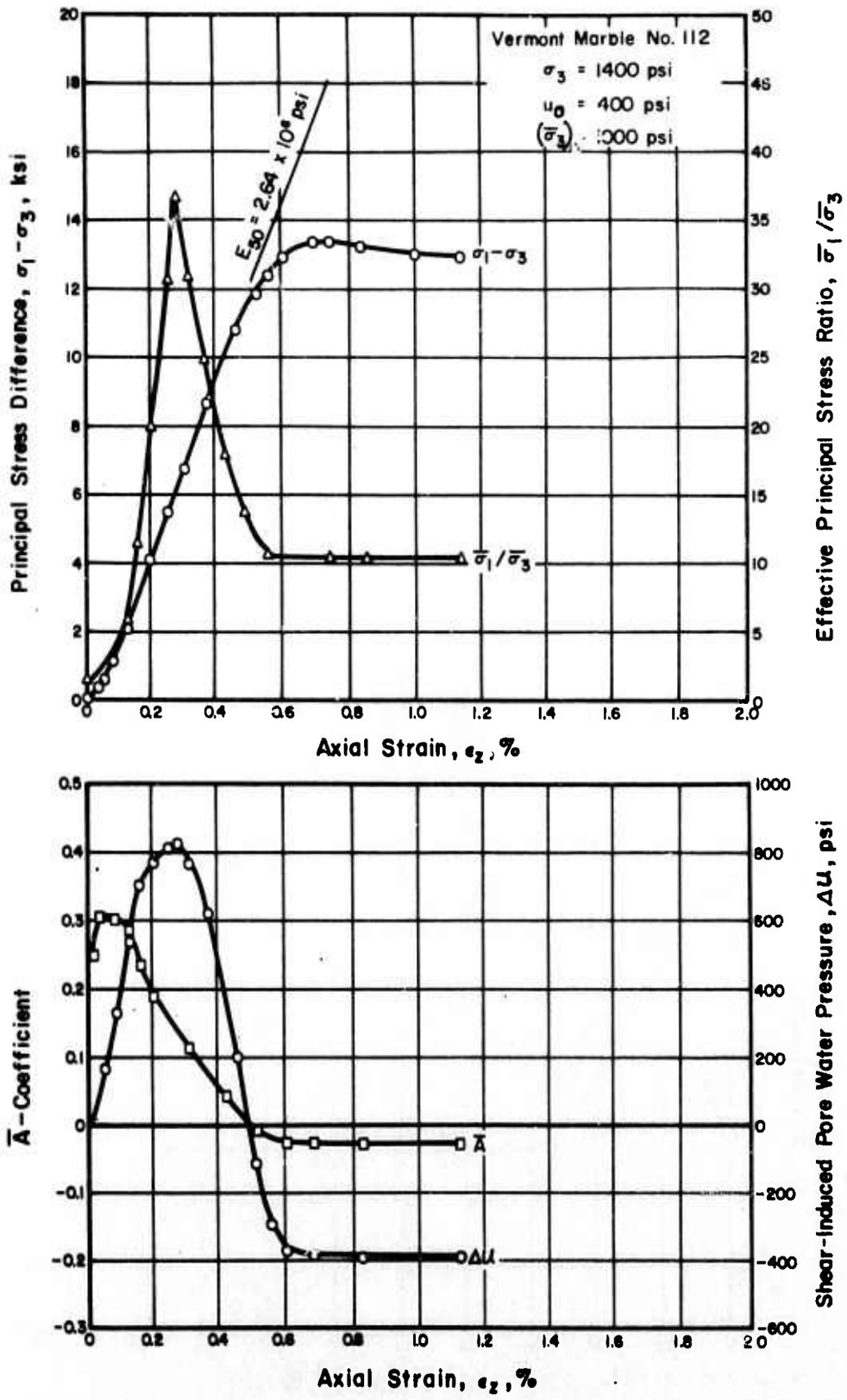

Fig. 3.49 Principal Stress Difference, Shear-Induced Pore Water Pressure, Effective Principal Stress Ratio, and $\bar{A}$-Coefficient Versus Axial Strain, Vermont Marble, No. 112

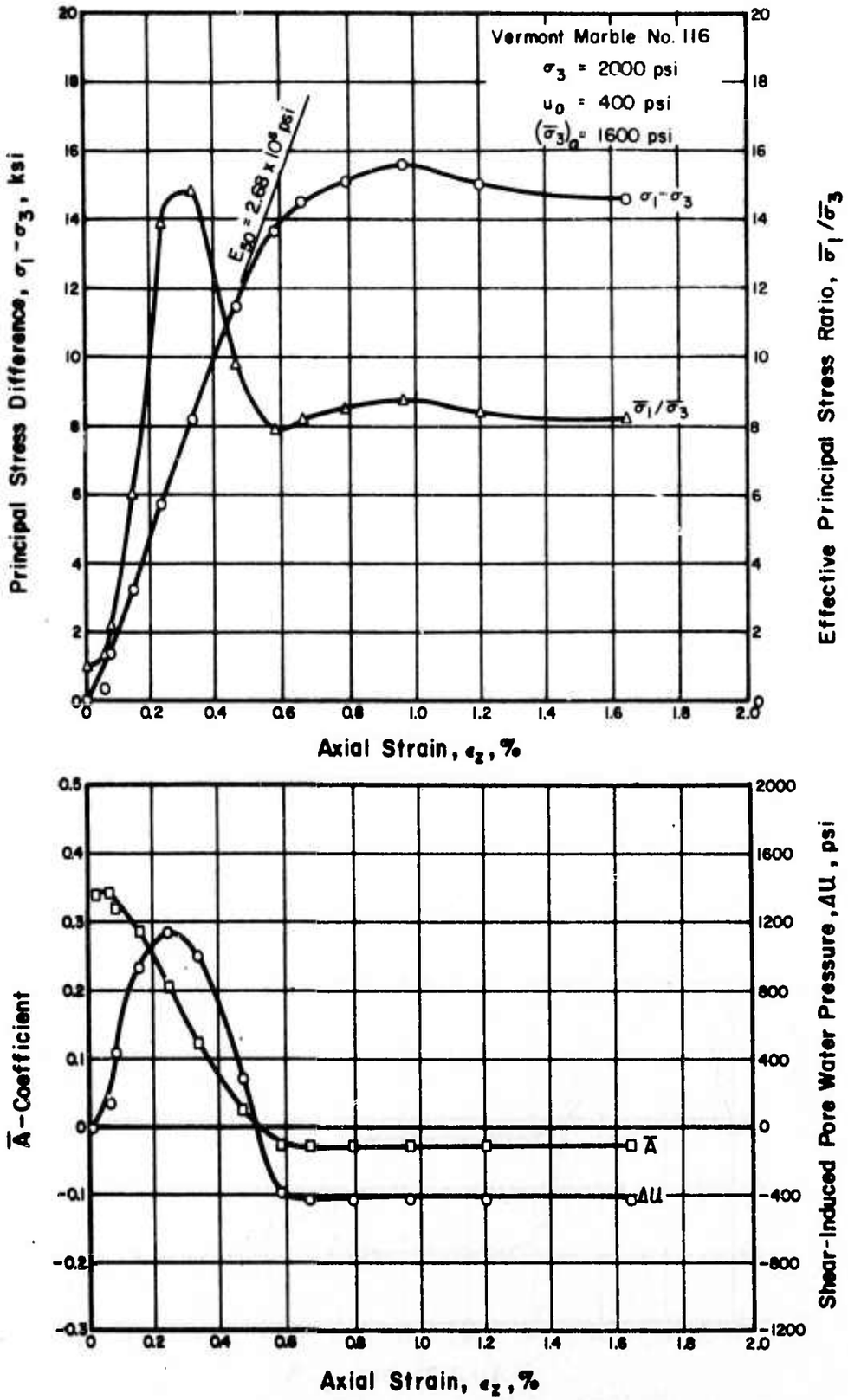

Fig. 3.50 Principal Stress Difference, Shear-Induced Pore Water Pressure, Effective Principal Stress Ratio, and $\overline{A}$-Coefficient Versus Axial Strain, Vermont Marble, No. 116

Table 3.10 Summary of Undrained Triaxial Compression Tests, Vermont Marble

Sample No.	Porosity n(%)	Permeability k(cm/sec) x 10^{-10}	Degree of Saturation S_r(%)	Confining Pressure σ_3 (psi)	$(\bar{\sigma}_3)_o^{(3)}$ (psi)	At $(\sigma_1-\sigma_3)_{max}$			Maximum Value of		
						ε_z (%)	$\sigma_1-\sigma_3$ (psi)	$\Delta u^{(4)}$ (psi)	$\Delta u^{(4)}$ (psi)	$\bar{A}$	$\bar{\sigma}_1/\bar{\sigma}_3$
114	2.2	6.1	100	800	400	0.658	11,600	- 420	380	0.380	234.0
112	2.4	8.8 ~ 2.3	88	1400	1000	0.739	13,520	- 400	834	0.308	37.0
116	2.1	6.0	95	2000	1600	0.960	15,600	- 422	1152	0.340	14.8

Note: (1) Axial Strain Rate = 2.35 x 10^{-4} in/in/min

(2) Pore Water Pressure at the Beginning of Tests = 400 psi

(3) $(\bar{\sigma}_3)_o$: Initial Effective Confining Pressure

(4) Δu : Shear-Induced Pore Water Pressure

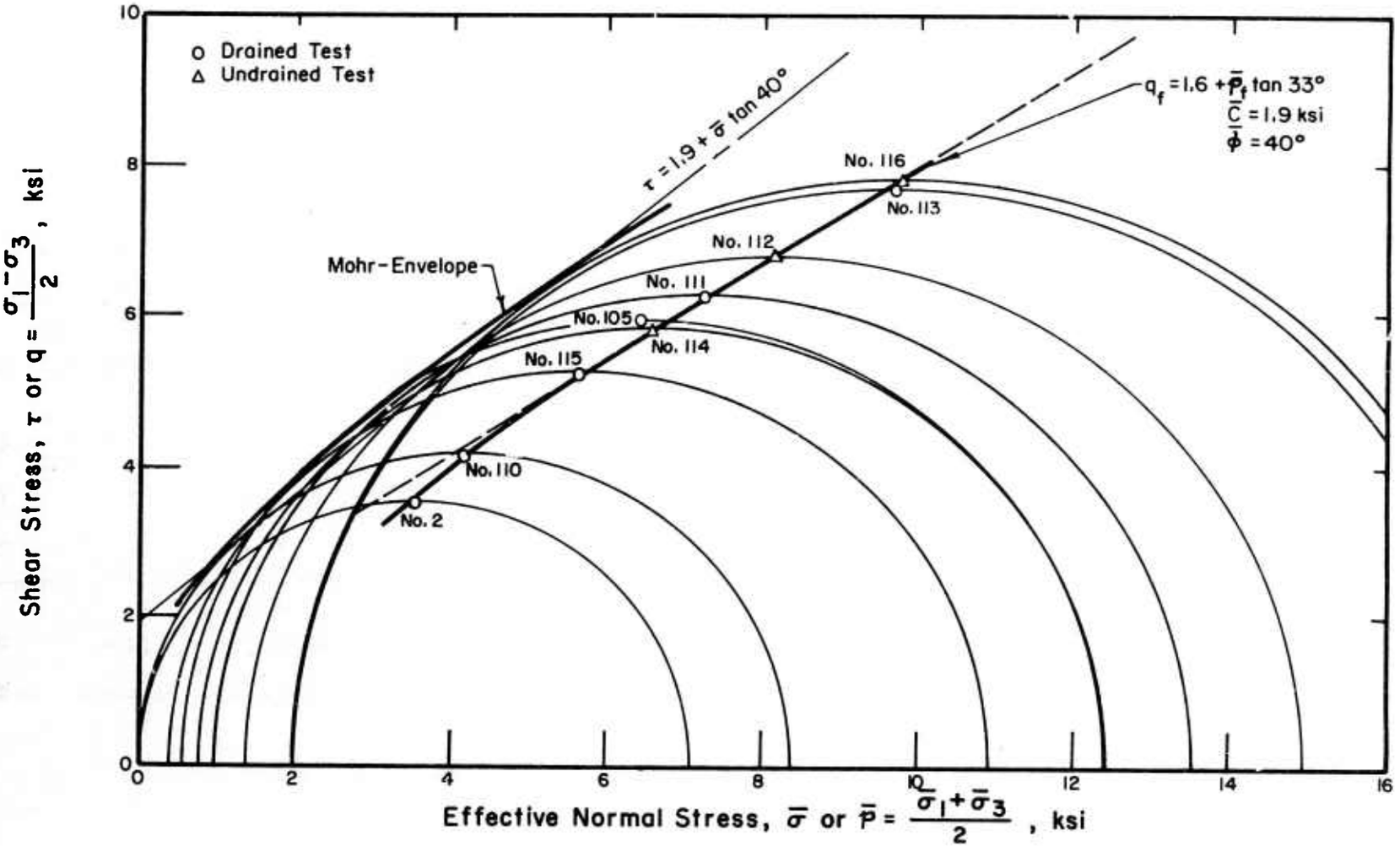

Fig. 3.51 Mohr-Coulomb Diagram, Vermont Marble

$$q_f = \bar{d} + \bar{p}_f \cdot \tan \bar{\psi}$$

where

$$\bar{d} = 1.6 \text{ ksi and } \bar{\psi} = 33°.$$

From $\bar{d}$ and $\bar{\psi}$, $\bar{c}$ and $\bar{\phi}$ for Vermont marble are calculated to be 1.9 ksi and 40°, respectively.

Relations between principal stress difference and axial strain for drained and undrained tests are summarized in Figures 3.52 and 3.53. The tangent moduli at 50% of maximum strength are shown in Table 3.11. An increase in confining pressure resulted in a higher Young's modulus under both drained and undrained conditions. Also for specimens with the same initial effective confining pressure, drained tests gave higher moduli values than undrained tests.

3.3.5 Test Results on Barre Granite

The results of drained triaxial compression tests on Barre granite are shown in Figures 3.54 to 3.56. Pore pressure measurements in several control tests indicated that these tests were only partially drained. The results are also summarized in Table 3.12. Barre granite specimens exhibited maximum principal stress difference at axial strains of 0.32% to 1.42%. The axial strain corresponding to maximum principal stress difference increased as confining pressure increased. All of the specimens exhibited volume decreases and reached their maximum negative volumetric strains of 0.057% to 0.084% at axial strains of 0.6% to 0.8%.

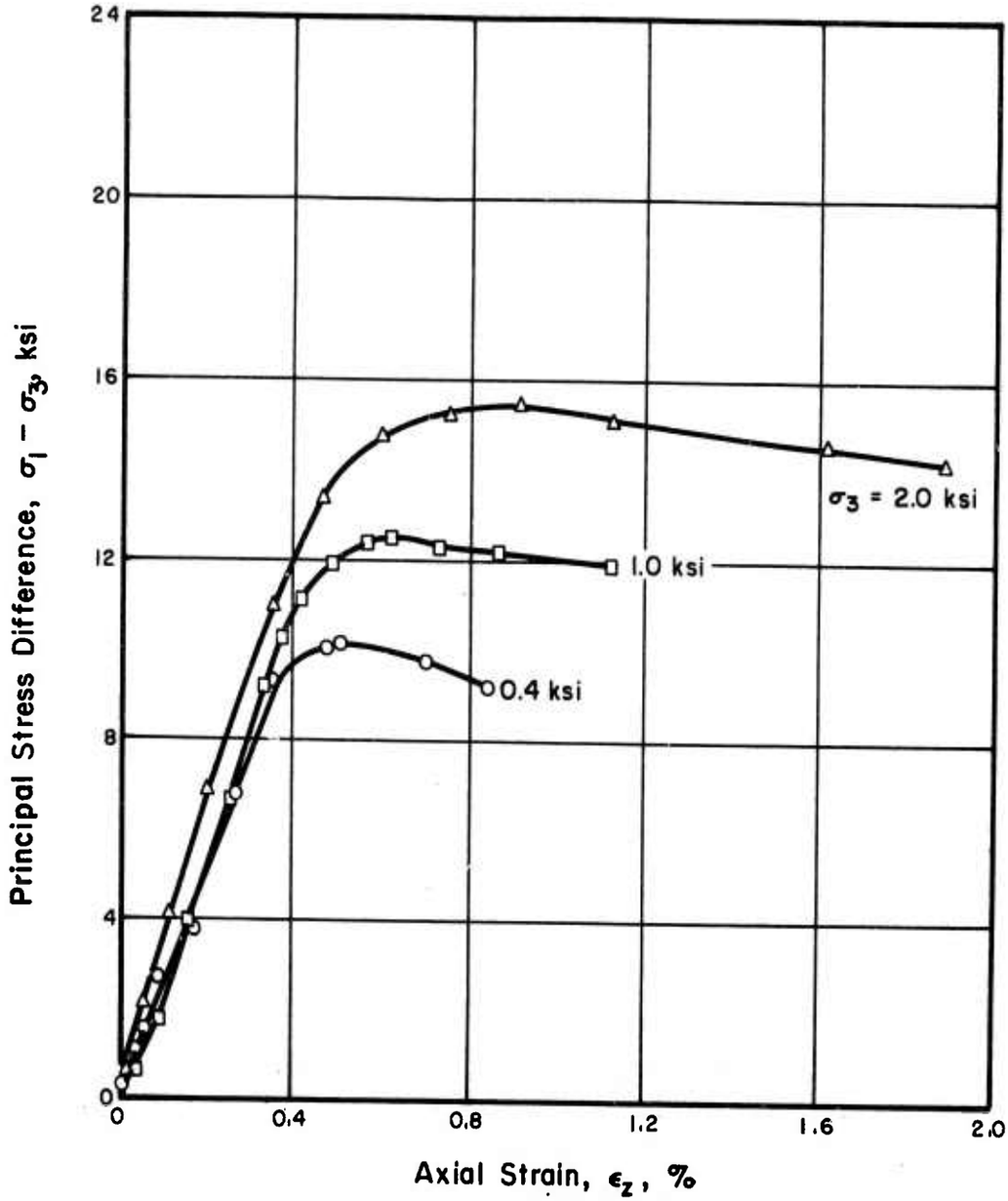

Fig. 3.52 Principal Stress Difference Versus Axial Strain, Drained Tests, Vermont Marble

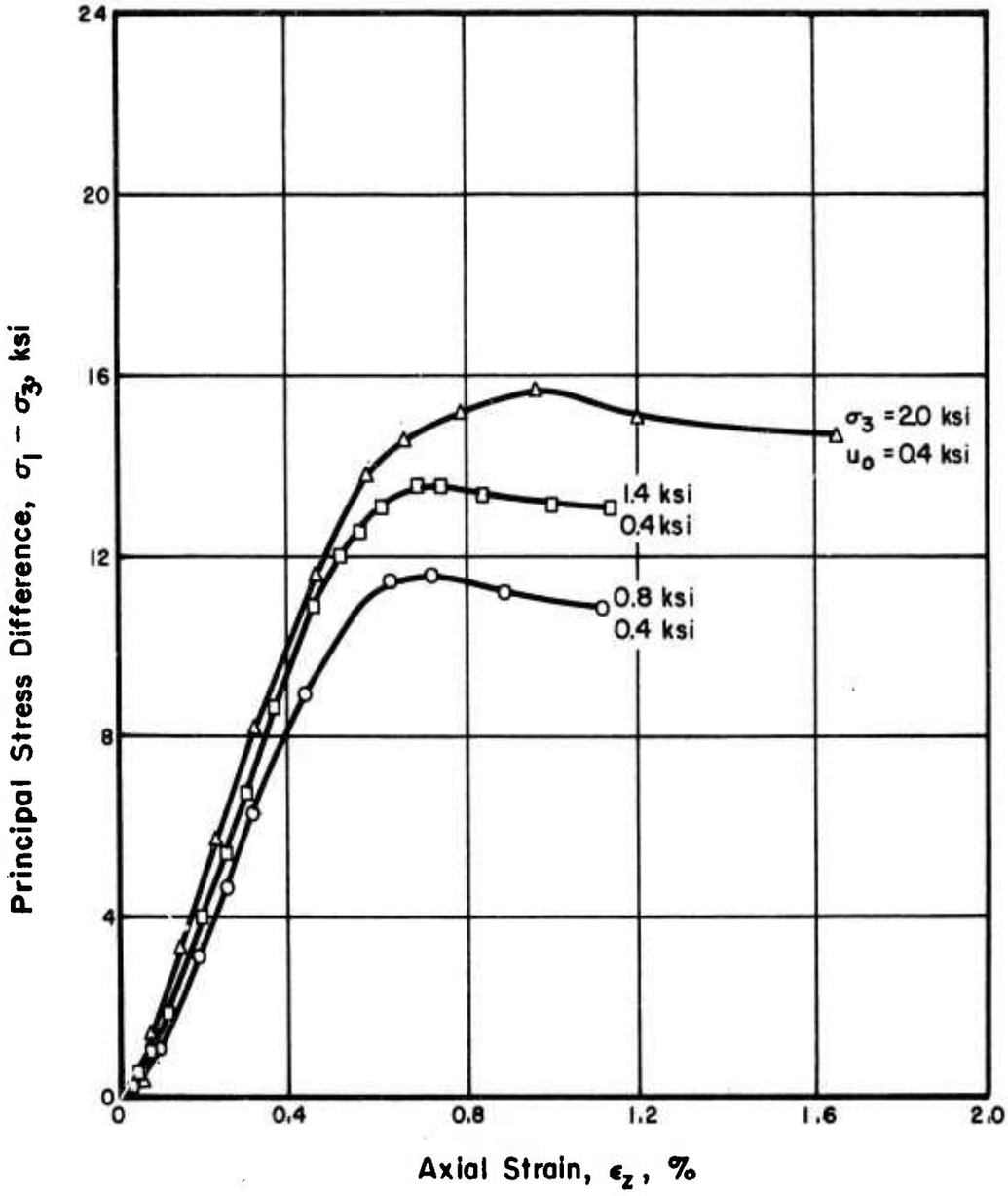

Fig. 3.53 Principal Stress Difference Versus Axial Strain, Undrained Tests, Vermont Marble

Table 3.11 Tangent Modulus at 50% of Maximum Strength, Vermont Marble

	Initial Effective Confining Pressure ($\bar{\sigma}_3$)$_o$ (psi)	Tangent Modulus at 50% of Maximum Strength E_{50} (psi)
Drained Tests	400	2.56×10^6
	1000	3.08×10^6
	2000	3.18×10^6
Undrained Tests	400	2.52×10^6
	1000	2.64×10^6
	1600	2.68×10^6

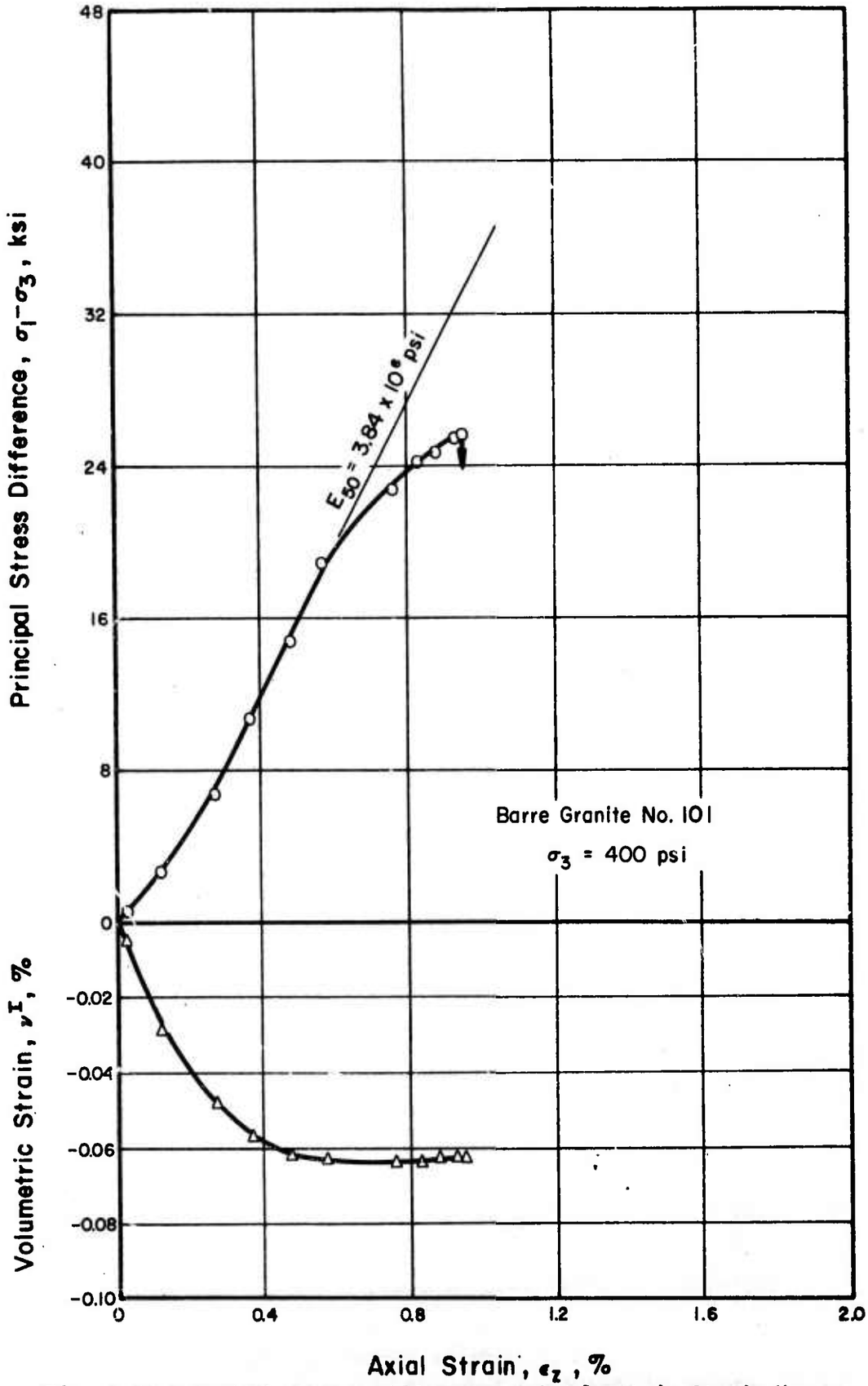

Fig. 3.54 Principal Stress Difference and Volumetric Strain Versus Axial Strain, Barre Granite, No. 101

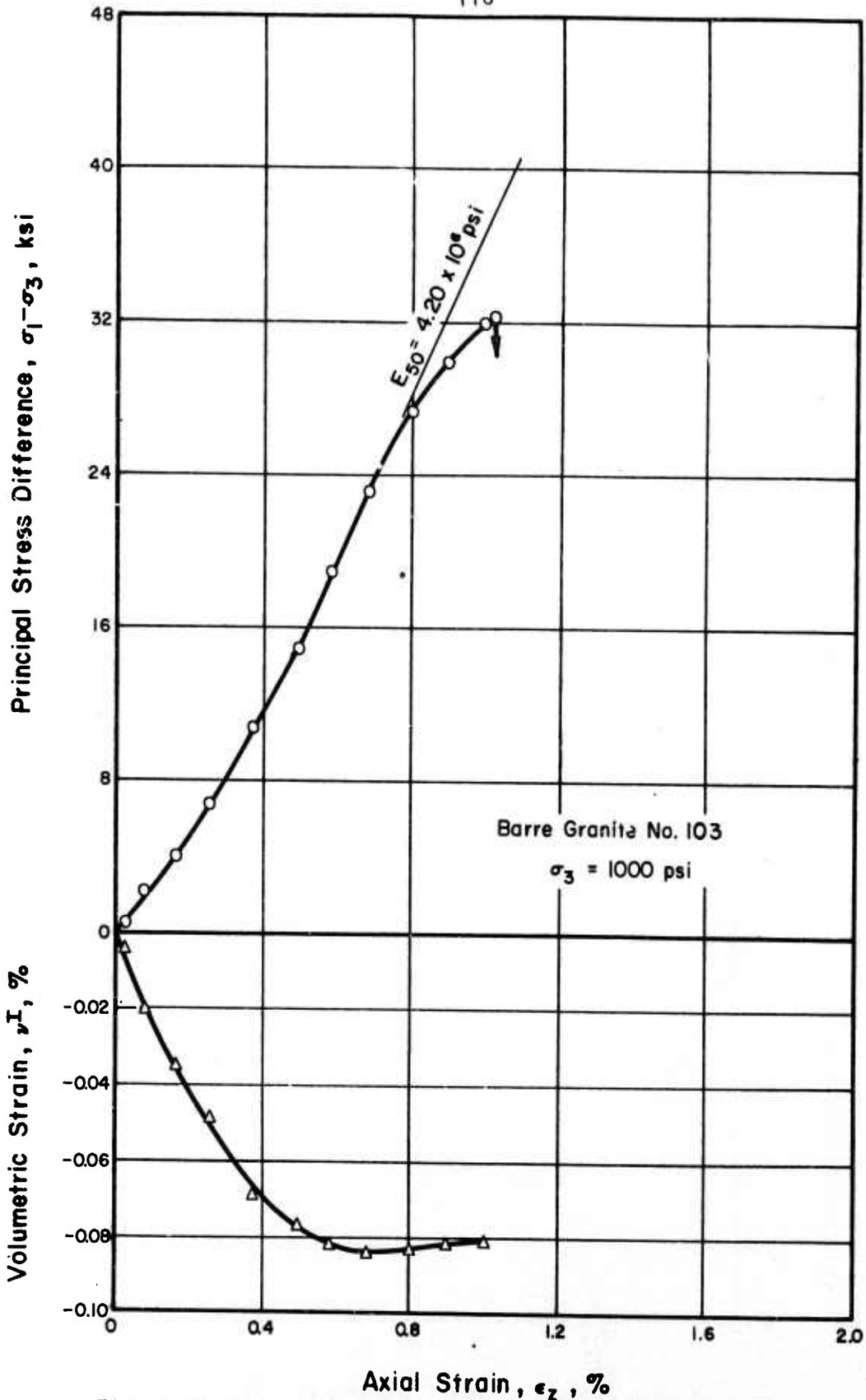

Fig. 3.56 Principal Stress Difference and Volumetric Strain Versus Axial Strain, Barre Granite, No. 103

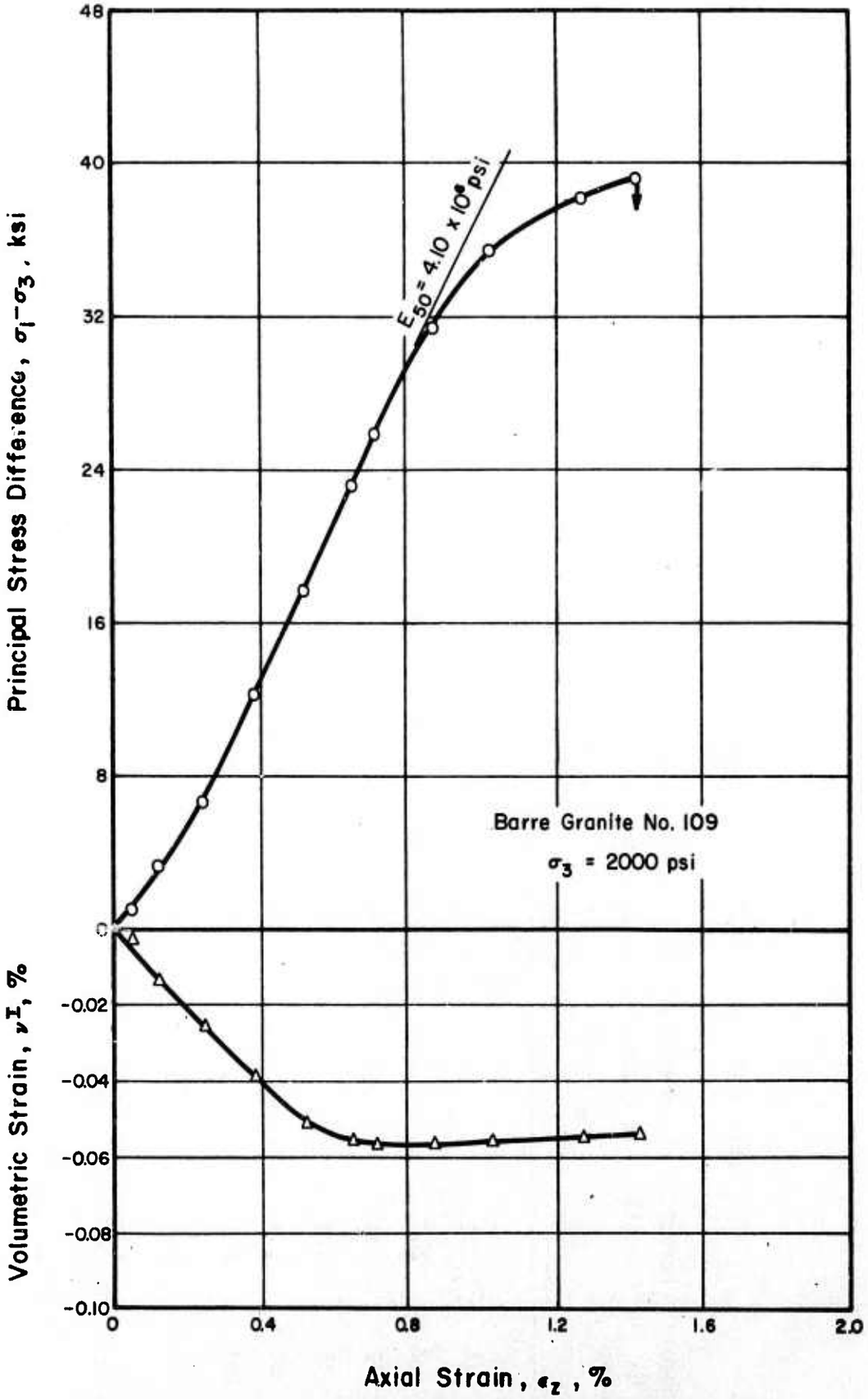

Fig. 3.56 Principal Stress Difference and Volumetric Strain Versus Axial Strain, Barre Granite, No. 109

Table 3.12 Summary of Drained Triaxial Compression Tests, Barre Granite

Sample No.	Porosity n (%)	Permeability k (cm/sec) x 10^{-10}	Degree of Saturation S_r (%)	Confining Pressure σ_3 (psi)	At $(\sigma_1 - \sigma_3)_{max}$			Max. Volumetric Strain ν^I_{max} (%)
					Axial Strain ε_z (%)	$\sigma_1 - \sigma_3$ (psi)	Volumetric Strain ν^I (%)	
1	2.1	--	56	0	0.432	16,300	--	--
2	2.2	--	51	0	0.433	21,200	--	--
12	2.1	--	73	0	0.327	18,000	--	--
15	2.3	--	59	0	0.319	17,000	--	--
101	2.9	11.4 ~ 6.9	100	400	0.950	25,700	-0.063	-0.064
103	2.6	5.5	100	1000	1.000	32,250	-0.081	-0.084
109	2.4	8.4	95	2000	1.424	39,300	-0.054	-0.057

Notes: No. 101, 103, 109: Triaxial Tests, Strain Rate = 2.35×10^{-4} in/in/min

No. 1, 2, 12, 15 : Uniaxial Tests, Strain Rate = 1.4×10^{-4} in/in/min

Upon reaching the maximum negative volumetric strains, the volumetric strains remained practically constant until the specimens ruptured. This might be partly due to the low permeability of the specimens (not sufficient time allowed for volume changes). The loading rates and degree of drainage will be discussed in Section 4.

Results of undrained triaxial compression tests are presented in Figures 3.57 to 3.59 for each specimen tested. The results are also summarized in Table 3.13. Barre granite specimens exhibited maximum principal stress difference at axial strains of 0.9% to 1.8% in undrained tests. These strains at $(\sigma_1 - \sigma_3)_{max}$ in undrained tests are higher than the corresponding strains in drained tests. The magnitude of the axial strain at $(\sigma_1 - \sigma_3)_{max}$ increased with increasing confining pressure. Although all of the specimens ruptured suddenly when maximum principal stress difference was reached, tangent moduli of the specimens decreased significantly while the specimens were approaching rupture in undrained tests. Positive shear-induced pore water pressures were observed at the initial stage of loading for all of the specimens. As the loading continued, the pore pressures began to decrease and became negative. The $\bar{A}$- coefficient maximized at the early stage of loading (at axial strains less than 0.1%) and then decreased continuously until it became negative. The maximum observed $\bar{A}$- coefficients were 0.25 to 0.27. The effective principal stress ratio maximized at the strain corresponding to or slightly exceeding the maximum shear-induced pore water pressure. The

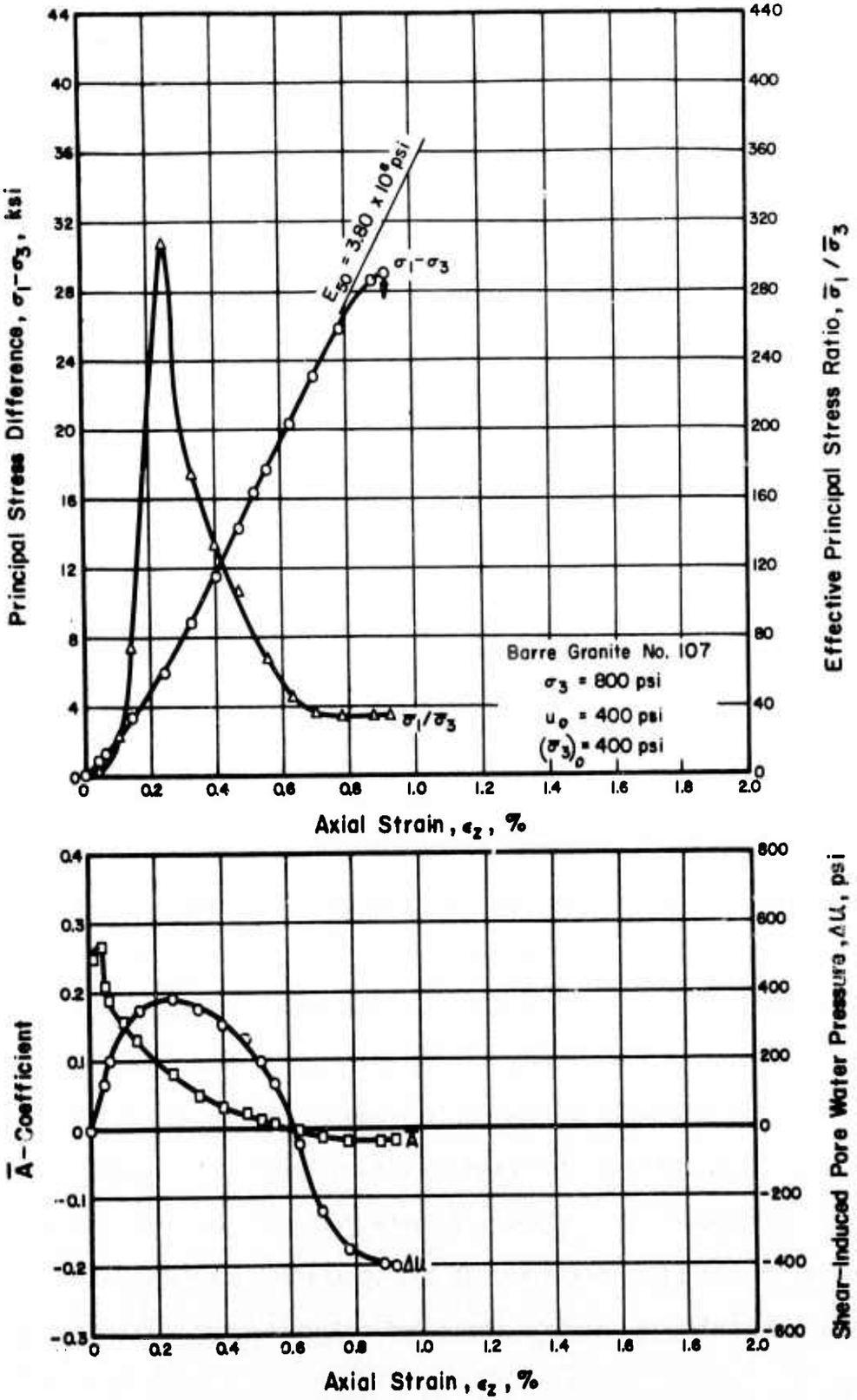

Fig. 3.57 Principal Stress Difference, Shear-Induced Pore Water Pressure, Effective Principal Stress Ratio, and $\bar{A}$-Coefficient Versus Axial Strain, Barre Granite, No. 107

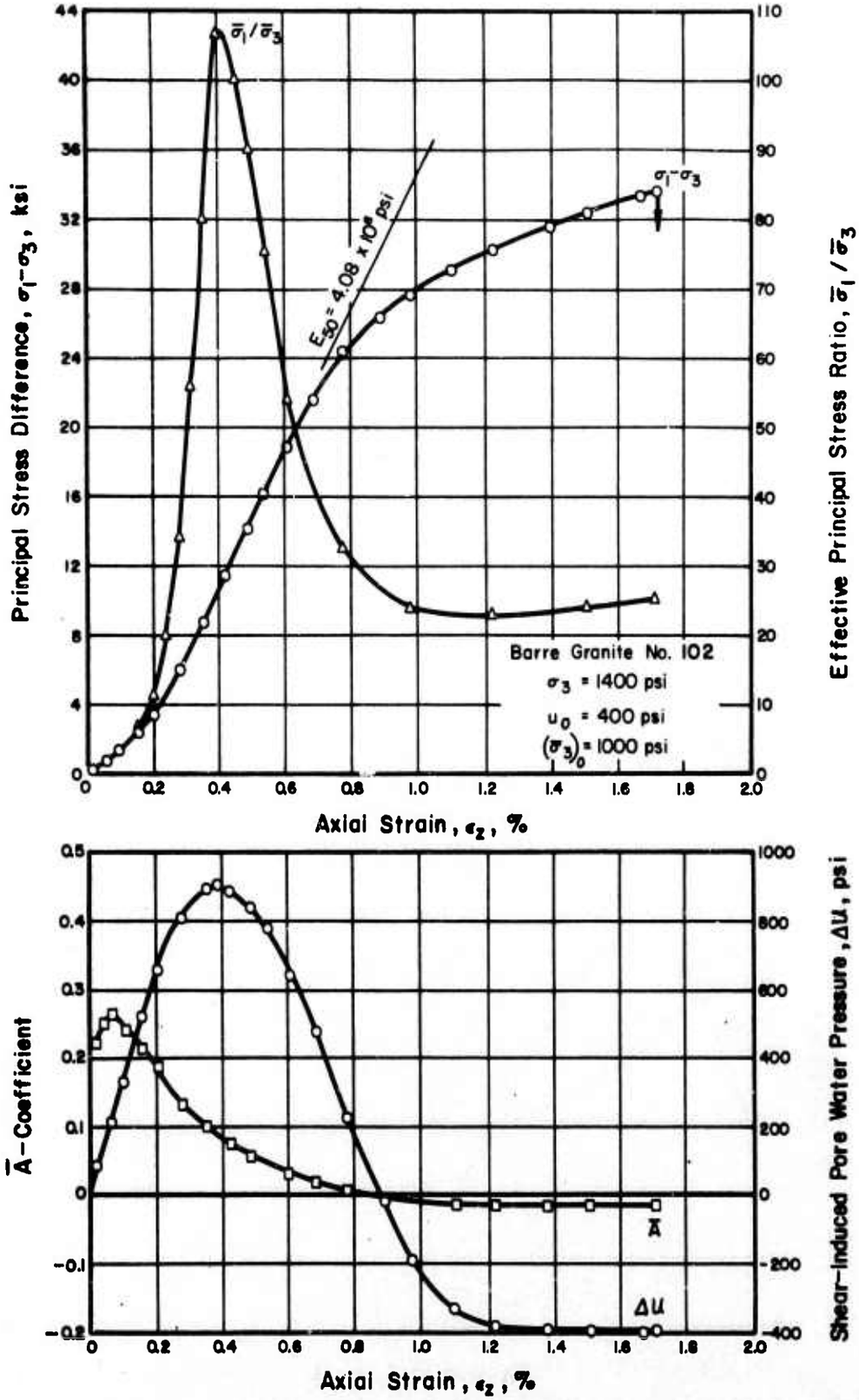

Fig. 3.58 Principal Stress Difference, Shear-Induced Pore Water Pressure, Effective Principal Stress Ratio, and $\bar{A}$-Coefficient Versus Axial Strain, Barre Granite, No. 102

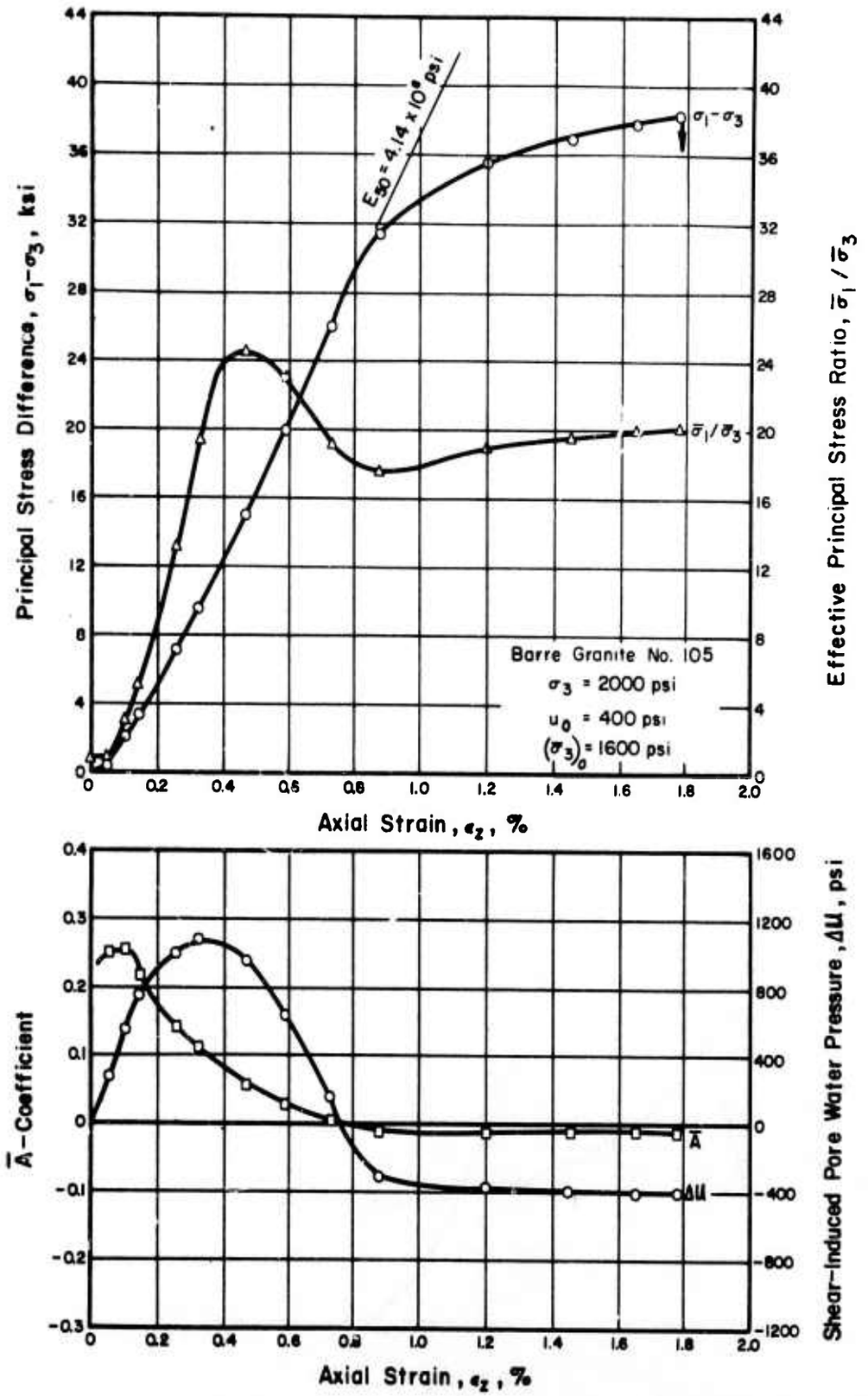

Fig. 3.59 Principal Stress Difference, Shear-Induced Pore Water Pressure, Effective Principal Stress Ratio, and $\bar{A}$-Coefficient Versus Axial Strain, Barre Granite, No. 105

Table 3.13 Summary of Undrained Triaxial Compression Tests, Barre Granite

Sample No.	Porosity n(%)	Permeability k(cm/sec) x 10^{-10}	Degree of Saturation S_r(%)	Confining Pressure σ_3 (psi)	$(\bar{\sigma}_3)^{(3)}$ (psi)	At $(\sigma_1-\sigma_3)_{max}$			Maximum Value of		
						ε_Z (%)	$\sigma_1-\sigma_3$ (psi)	$\Delta u^{(4)}$ (psi)	$\Delta u^{(4)}$ (psi)	$\bar{A}$	$\bar{\sigma}_1/\bar{\sigma}_3$
107	2.8	7.0 ~ 6.0	100	800	400	0.910	29,000	- 400	380	0.268	308
102	2.8	9.5 ~ 7.8	95	1400	1000	1.715	33,800	- 395	903	0.264	107
105	2.9	11.0 ~ 5.8	94	2000	1600	1.780	38,300	- 400	1083	0.253	24.6

Note: (1) Axial Strain Rate = 2.35 x 10^{-4} in/in/min

(2) Pore Water Pressure at the Beginning of Tests = 400 psi

(3) $(\bar{\sigma}_3)_o$: Initial Effective Confining Pressure

(4) Δu : Shear-Induced Pore Water Pressure

axial stress at this strain was equal to 30% to 40% of the maximum principal stress difference. The maximum effective principal stress ratio decreased with increasing initial effective confining pressure. A Mohr-Coulomb diagram and a modified Mohr-Coulomb diagram for Barre granite are shown in Figure 3.60. Whereas the Mohr failure envelope is concave to the normal stress axis, the results of the modified Mohr-Coulomb diagram plot approximately on a straight line according to the following equation:

$$q_f = \bar{d} + \bar{p}_f \cdot \tan \bar{\psi}$$

where

$$\bar{d} = 1.5 \text{ ksi and } \bar{\psi} = 40°.$$

From $\bar{d}$ and $\bar{\psi}$, $\bar{c}$ and $\bar{\phi}$ for Barre granite are calculated to be 2.0 ksi and 57°, respectively.

Relations between principal stress difference and axial strain for drained and undrained tests are summarized in Figures 3.61 and 3.62. The tangent moduli at 50% of maximum strength are shown in Table 3.14. These values are higher than the moduli for other types of rock which were tested and are in the range of 3.8×10^6 psi to 4.2×10^6 psi.

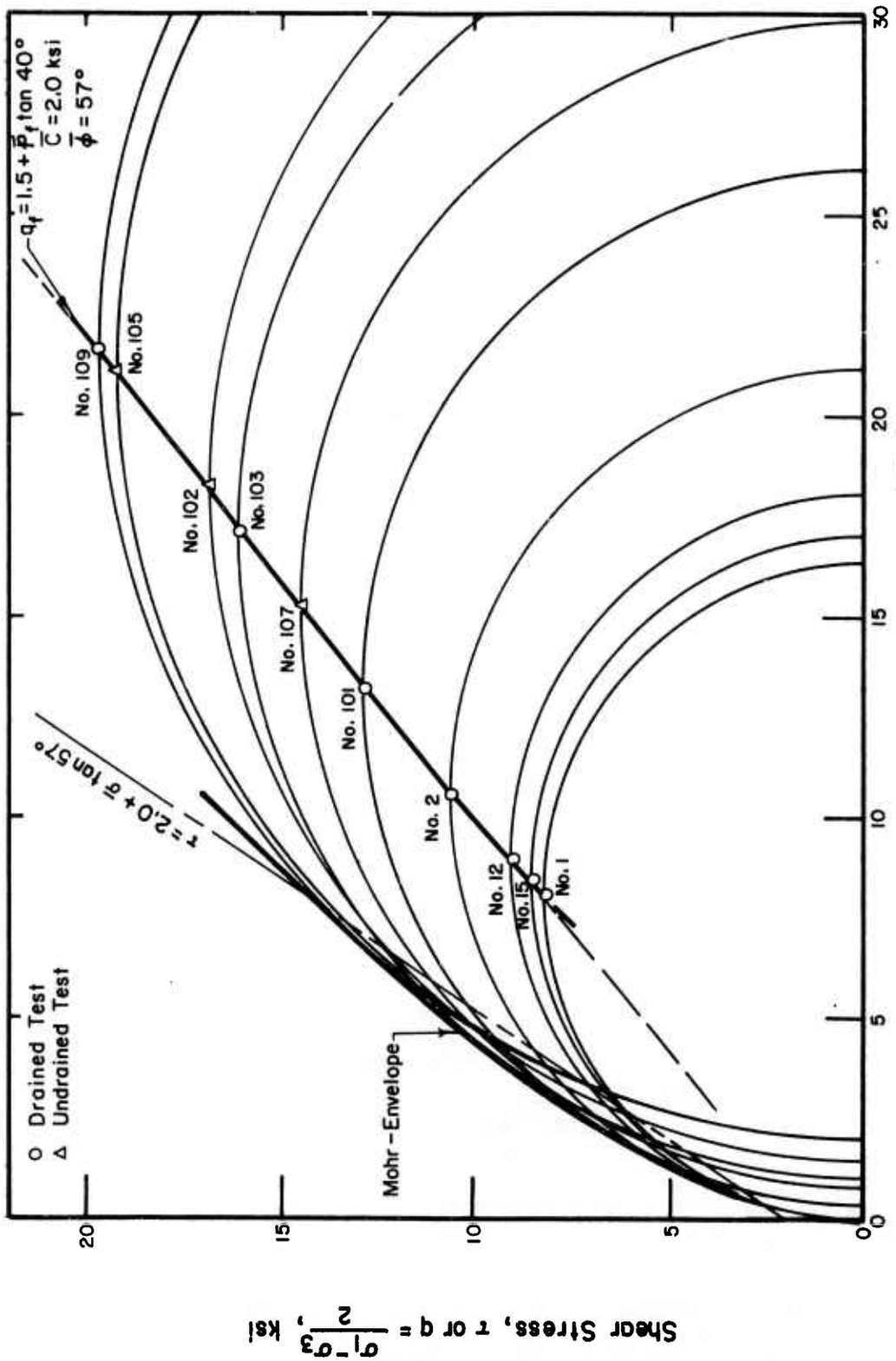

Fig. 3.60 Mohr-Coulomb Diagram, Barre Granite

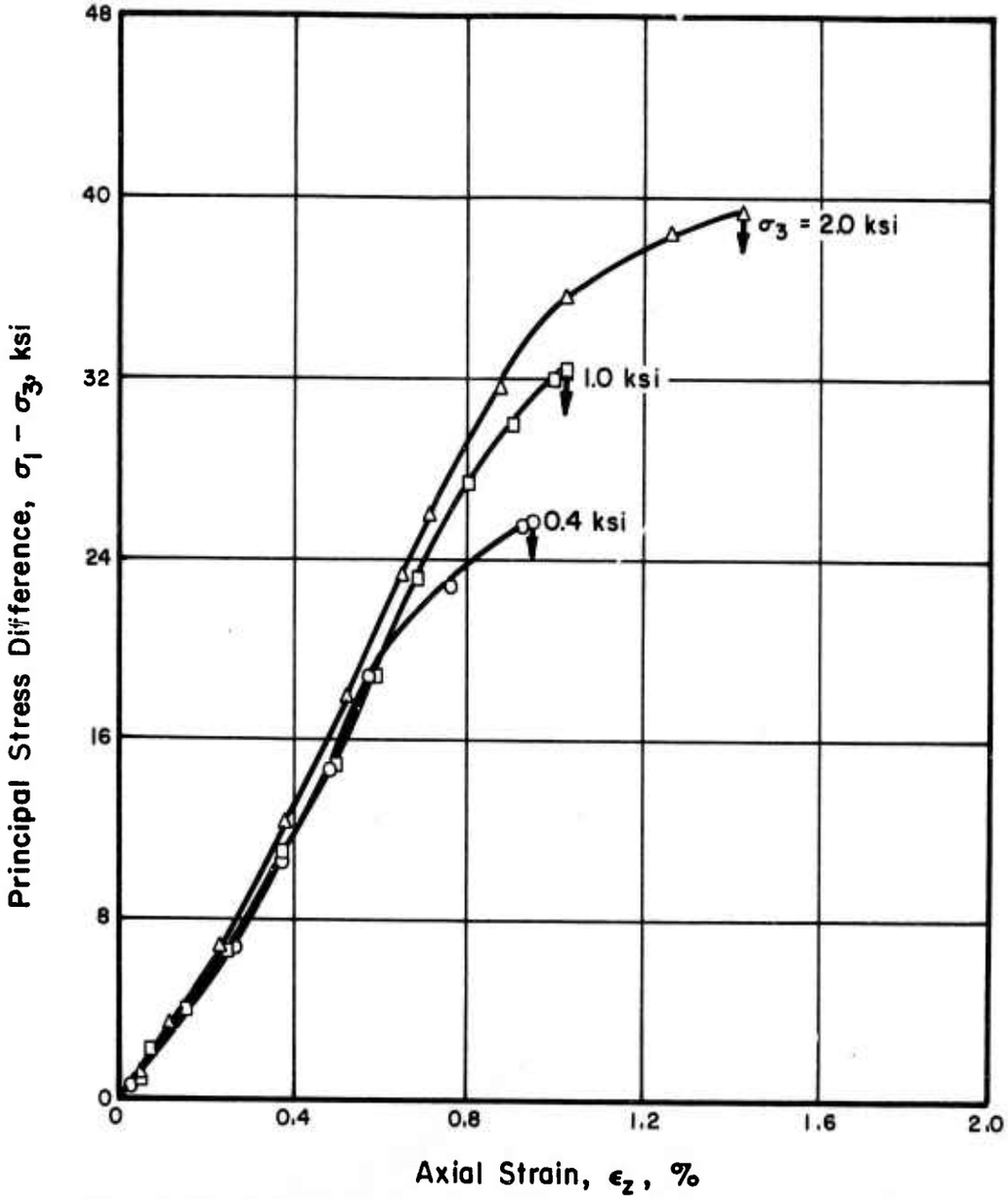

Fig. 3.61 Principal Stress Difference Versus Axial Strain, Drained Tests, Barre Granite

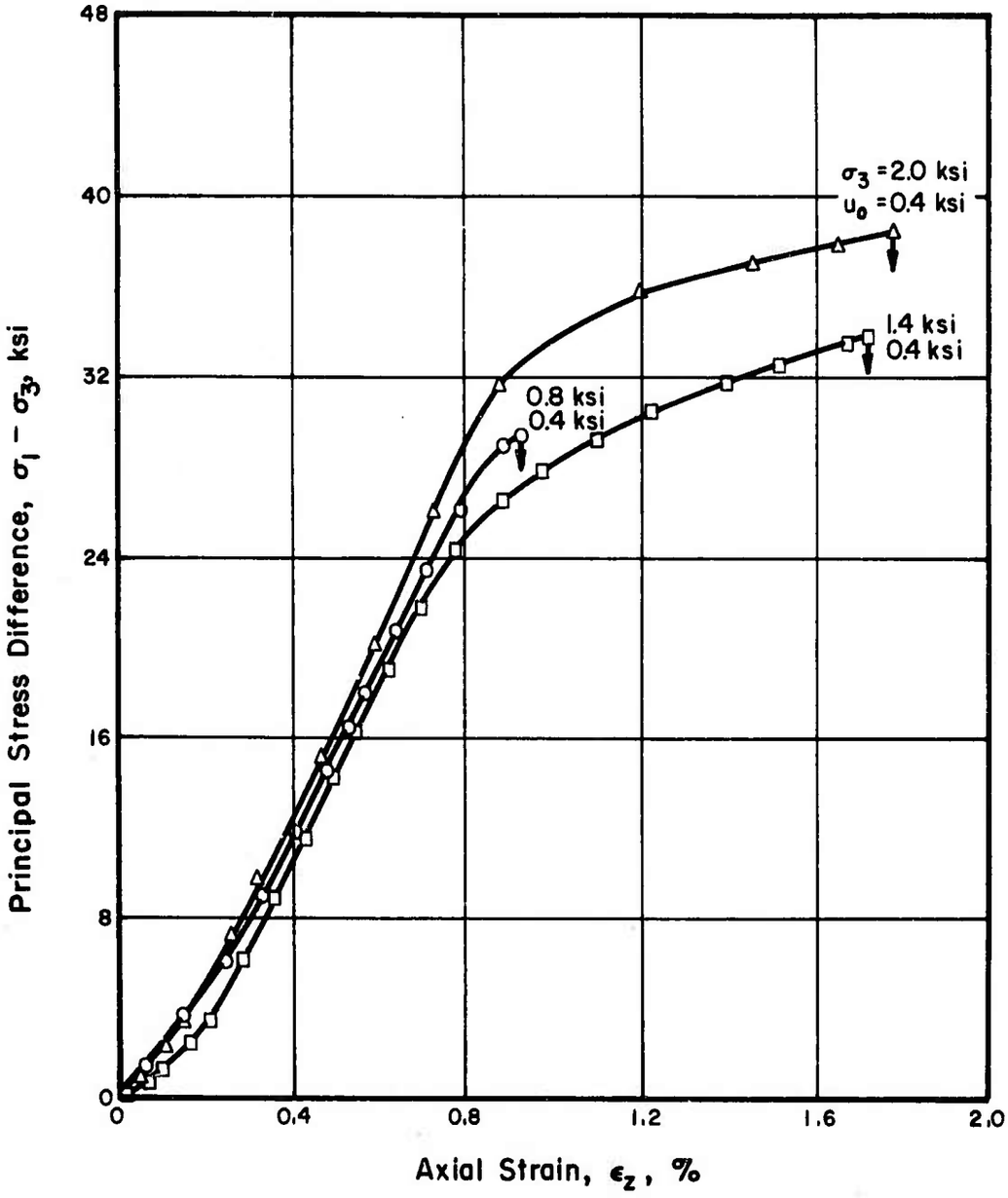

Fig. 3.62 Principal Stress Difference Versus Axial Strain, Undrained Tests, Barre Granite

Table 3.14 Tangent Modulus at 50% of Maximum Strength, Barre Granite

	Initial Effective Confining Pressure $(\bar{\sigma}_3)_o$ (psi)	Tangent Modulus at 50% of Maximum Strength E_{50} (psi)
Drained Tests	400	3.84×10^6
	1000	4.20×10^6
	2000	4.10×10^6
Undrained Tests	400	3.80×10^6
	1000	4.08×10^6
	1600	4.14×10^6

SECTION 4

DISCUSSION

4.1 Loading Rates

As mentioned in Section 3, all of the triaxial compression tests were performed using a rate of strain of 3.0×10^{-4} in/in/min. This rate was selected based on the strain rate study reported in Section 3.1. In this section, the significance of the strain rate study and the effects of strain rate on the results of triaxial compression tests, particularly with respect to drainage conditions and pore water pressure, will be considered and discussed.

In drained triaxial compression tests, a drainage line to the top of the rock specimen was connected to a pipette and volume changes of the specimen were measured, i.e., the specimen was drained from one end only. In order to check the degree of pore pressure dissipation during the drained tests, a pore water pressure transducer was connected to a drainage line leading to the bottom of the specimen. Figures 4.1 to 4.4 show the results of these pore water pressure measurements. For comparison the observed shear-induced pore water pressures in the corresponding undrained tests are also shown in the figures. In the drained tests on Berea sandstone and Salem limestone, the observed changes in the pore water pressure are very small and it could be concluded that the strain rate used for these tests was slow enough

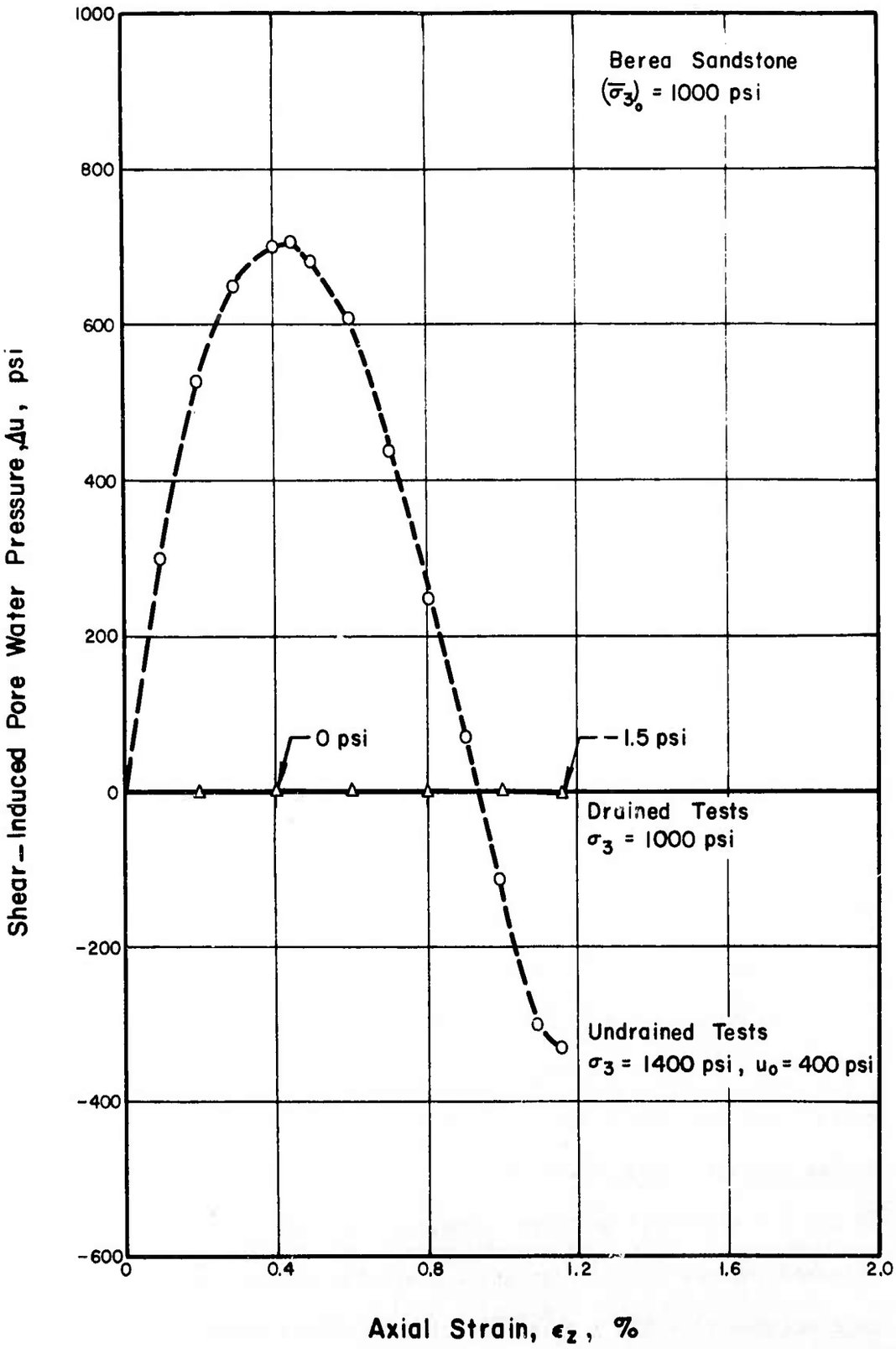

Fig. 4.1 Shear-Induced Pore Water Pressure in Drained and Undrained Tests, Berea Sandstone

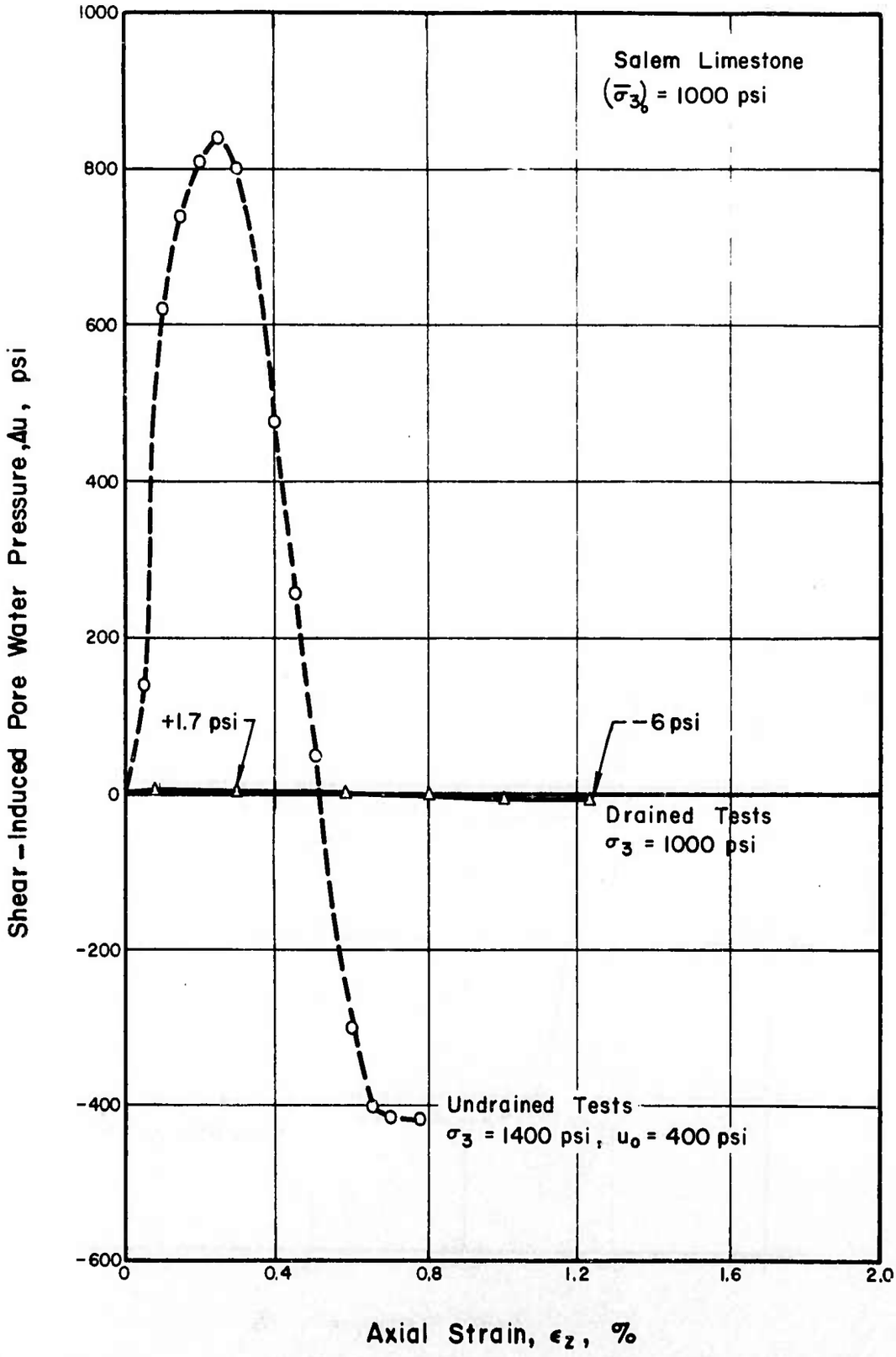

Fig. 4.2 Shear-Induced Pore Water Pressure in Drained and Undrained Tests, Salem Limestone

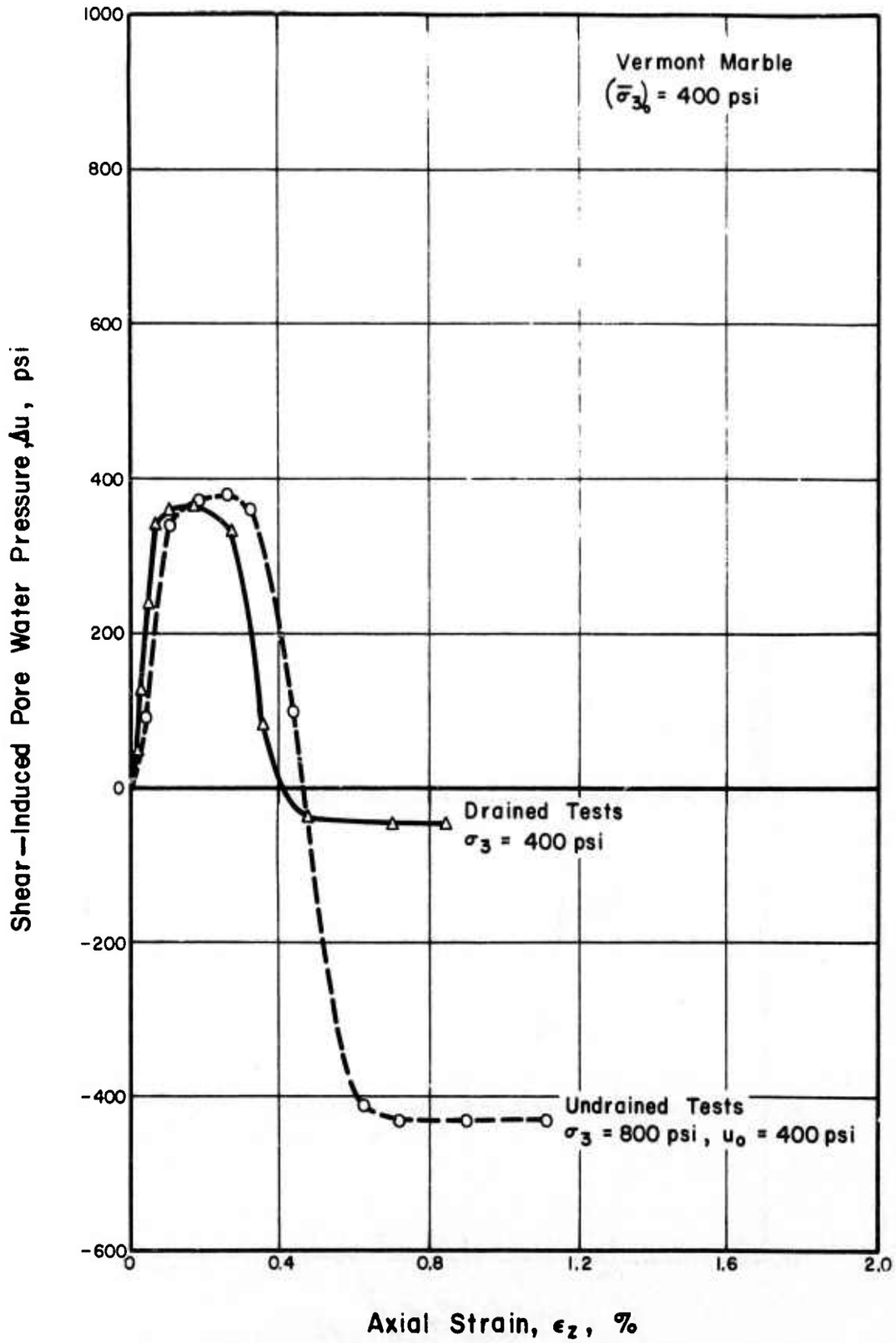

Fig. 4.3 Shear-Induced Pore Water Pressure in Drained and Undrained Tests, Vermont Marble

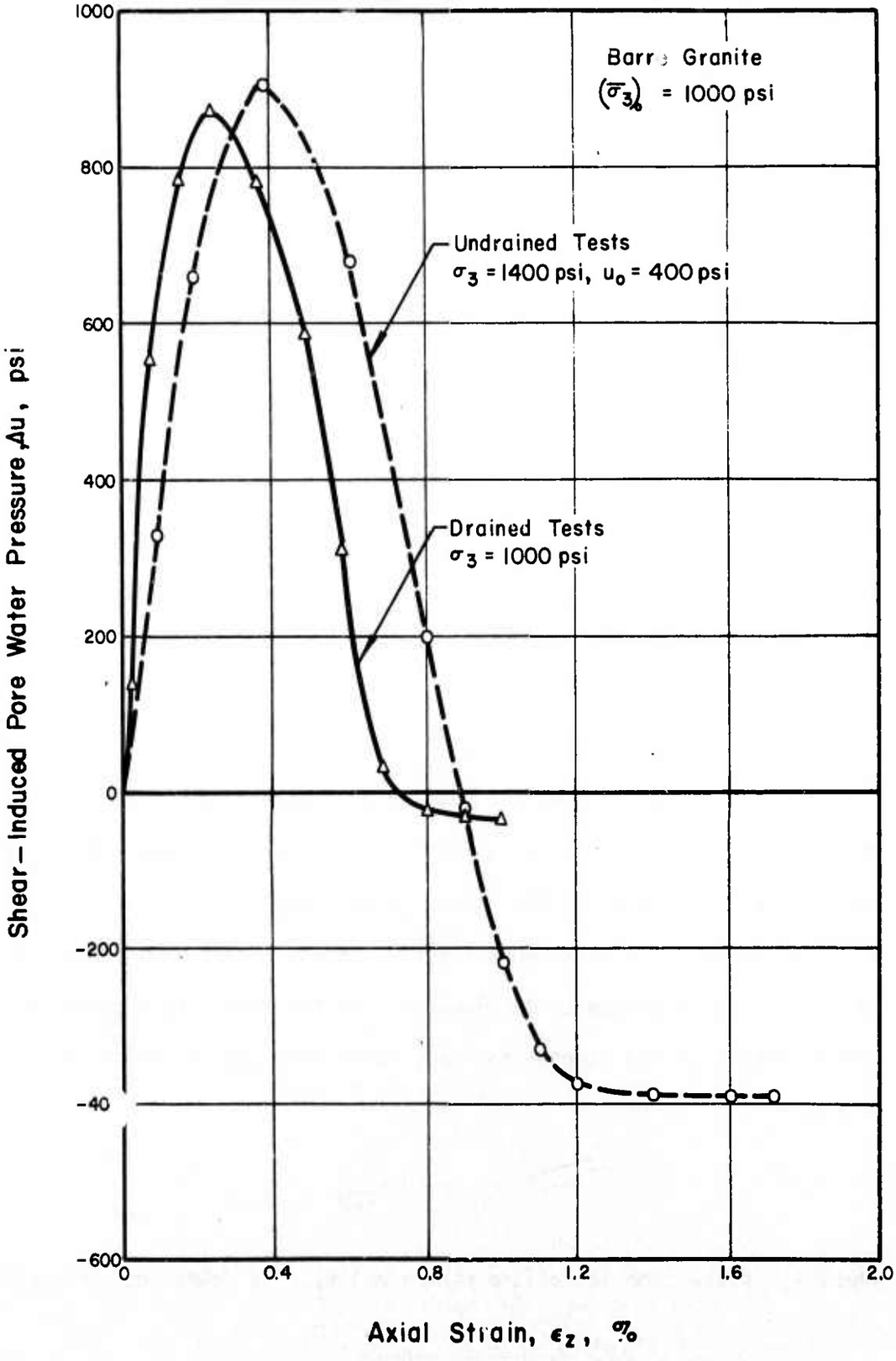

Fig. 4.4 Shear-Induced Pore Water Pressure in Drained and Undrained Tests, Barre Granite

to provide drained conditions for these rock types. On the other hand in "drained" tests on Vermont marble and Barre granite, the observed pore water pressures at the closed end of specimens are not small and compared to the undrained tests are rather significant. These measurements indicate that these rocks were tested under partially drained conditions.

At present (1973) there is no rigorous theoretical or empirical method available for estimating the rate of axial strain for drained triaxial tests on rock. The method of monitoring the pore water pressure at one end of the specimen while drainage is allowed from the other end appears to be the most practical method. This method is recommended for future studies.

Based on simplifying assumptions, analytical methods have been developed (Bishop and Henkel, 1962) for estimating the proper rates of loading for drained and undrained triaxial compression tests on normally consolidated, insensitive soils (with a tendency to decrease in volume during shear). These methods cannot be expected to apply to tests on rock; at least not without modification. However, they may be used to obtain a rough estimate of the loading rate for rock. As an example, for drained triaxial compression tests with drainage allowed from one end only:

$$t_f = 9\, t_{100}$$

where t_f is the time to failure strain and t_{100} is determined from the

rate of consolidation under the final effective confining pressure, Figure 4.5. For Vermont marble specimens t_{100} ranged from 500 minutes to 1000 minutes, thus giving a range of 3 to 6 days for t_f. Assuming a reasonable value for axial strain at failure a range of 0.8×10^{-6} to 1.5×10^{-6} in/in/min is obtained. Thus even a rough computation indicates that drained tests on Vermont marble and Barre granite were performed too rapidly.

For the following reasons (partly beyond the control of the investigator) in this study it was not possible to perform fully drained tests on Vermont marble and Barre granite.

1) The contract required the completion of all the triaxial tests reported herein in one year. Only one special triaxial cell was constructed for this study and only one pressure control and one loading system were available.
2) The slow rates of loading, which are required for some tests, are beyond the range of loading rates which can be obtained by the Tinius-Olsen testing machine.
3) For long-term tests some modifications would be required to further reduce the leakage through membrane and end seals. Under the present testing conditions the rate of leakage was 3.6×10^{-3} cc/hour under a fluid pressure difference of 2000 psi.

In regard to partially drained tests on Vermont marble and Barre granite the following observations can be made.

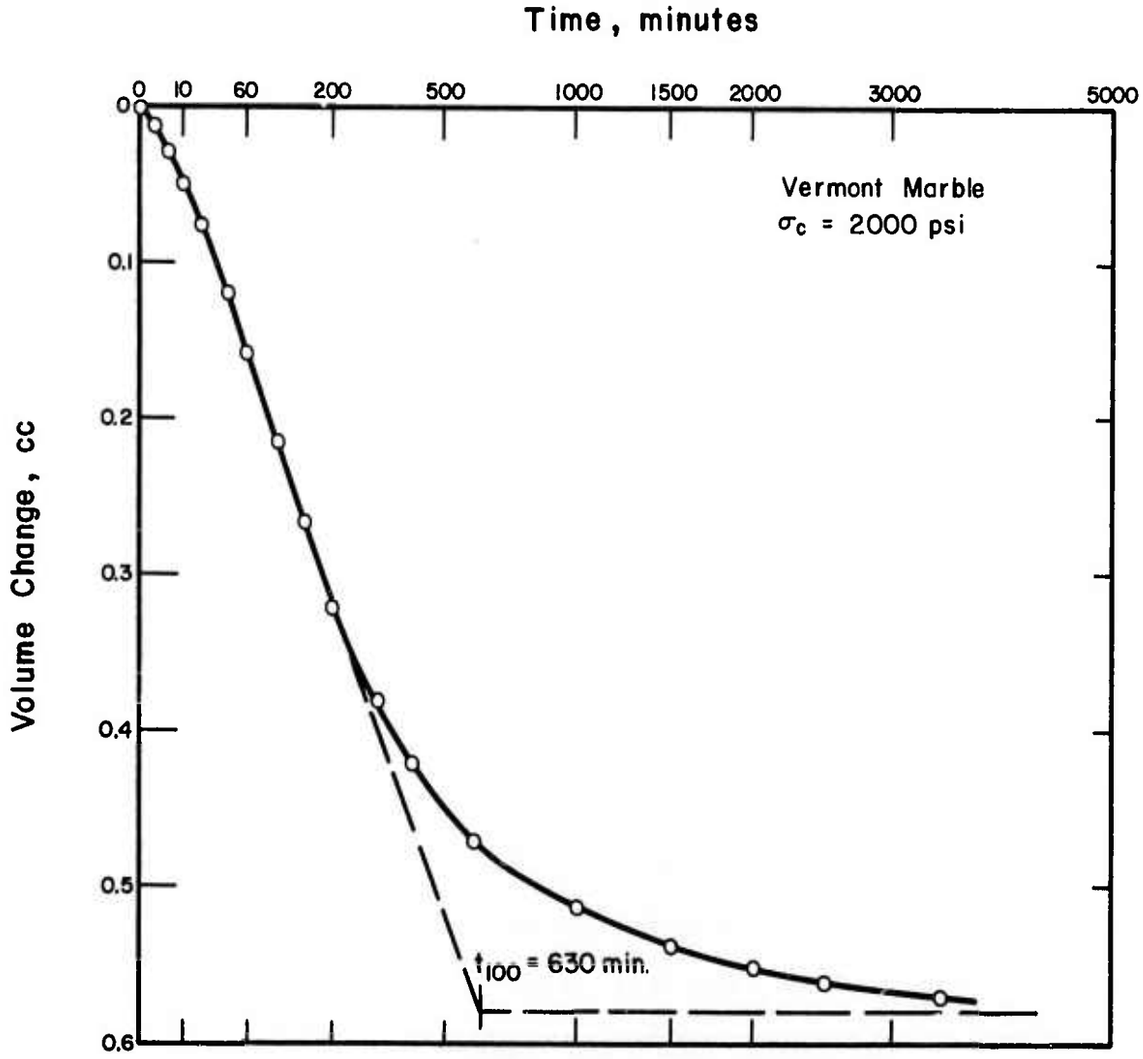

Fig. 4.5 Relationship between the Volume Change and Square Root Time under an All-Around Pressure of 2,000 psi, Vermont Marble

1) The magnitude of the computed volumetric strains based on the total volume of the sample would tend to underestimate the magnitude of volumetric strains for fully drained tests.
2) The effective stresses are not equal to the total stresses at all points of the rock except when the excess pore water pressure is equal to zero.

In undrained tests it was not possible to monitor excess pore pressures inside of the rock specimens. However it appears that the measured pore water pressures at the end of the specimens represent reasonably accurately the shear-induced pore water pressures.

Finally it should be pointed out that in determining a rate of strain for proper measurement of shear-induced pore water pressures in undrained tests and for full dissipation of excess pore water pressures in drained tests, the influence of strain rate on the deformation and strength of rock by mechanisms other than pore pressure effects should not be neglected.

4.2 Pore Pressure Coefficient B

4.2.1 Theoretical Evaluation of B-Coefficient

Skempton's B-coefficient, defined as the pore water pressure response to a change in spherical component of total stress, was originally applied to soils (Skempton, 1954). When the B-coefficient

is used for rock, it is a measure of the relative compressibility of the rock mass (rock skeleton), rock solids, and pore fluid. The measured pore pressure response also reflects the compressibility of the pore-pressure measuring system. This includes the compressibility of the drainage connections, the compressibility of the fluid in the measuring system, and the compressibility of the sensing device, e.g. the transducer. In the study of the B-coefficient response of relatively incompressible materials such as rocks, it is necessary to minimize the compressibility of the pore-pressure measuring system as much as possible. However, within practical limits it is not possible to eliminate completely the compressibility of the measuring system, and therefore an attempt should be made to estimate the effect of system compressibility on the measured pore water pressures.

The compressibility of rock mass (decrease in total volume) reflects intergranular contact resistance, interparticle interference, grain deformability, and grain strength. In addition to frictional resistance at the contacts, the contact resistance includes the effects of intergranular cement-bonds. The contact resistance will play a major role in deformation of rock when it is subjected to shear stresses, and it probably will be of the same order of magnitude for most rocks. The interference component will be the most important factor for spherical stress change. This interference will increase as porosity decreases. Individual mineral grains can also deform (at constant solid volume) without rotation and translation (flow into pores). In addition to

the porosity of the rock mass, the existence of microcracks and other factors also increase the compressibility of rock mass.

When the pores of rock are saturated with water (S_r = 100%), the compressibility of pore water probably is equal to the compressibility of free water. When there is air in addition to water (S_r < 100%) the compressibility of the pore fluid is less than the compressibility of free water.

The compressibility of rock-forming solids (minerals) probably reflects the repairing of some imperfect arrangement and bonding of crystal units and possibly to a lesser degree a decrease in spacing between these units.

Taking the aforementioned factors into account, the following equations can be derived for the B-coefficient of rock:

Equation I If it could be assumed that the compressibilities of rock solids (minerals) and the pore-pressure measuring system were small and negligible as compared to the compressibilities of the rock skeleton and pore fluid (Skempton, 1954) and all of the voids were filled with water, the B-coefficient could be expressed in terms of the porosity and the volume compressibilities of the pore fluid and rock mass (skeleton). When a rock specimen is subjected to an increment in spherical component of total stress, $\Delta\sigma_3$, the increase in effective stress, $\Delta\bar{\sigma}_3$, is:

$$\Delta\bar{\sigma}_3 = \Delta\sigma_3 - \Delta u$$

where Δu is the change in pore fluid pressure. The volume change of the rock specimen, ΔV_{sk}, is:

$$\Delta V_{sk} = C_{sk} V(\Delta\sigma_3 - \Delta u)$$

where C_{sk} is the volume (bulk) compressibility of the rock skeleton, i.e., the unit decrease in total volume, $\Delta V/V$, per unit increase in effective spherical stress, $\Delta\bar{\sigma}_3$, and V is the original volume of the rock specimen. The change in volume of the void space, ΔV_v, is:

$$\Delta V_v = C_w n V \Delta u$$

where C_w is the compressibility of the pore fluid, i.e., the unit decrease in volume of pore fluid per unit increase in pore fluid pressure, and n is the porosity of the rock skeleton. The decrease in volume of the rock mass, ΔV_{sk}, must be equal to the decrease in volume of the pore fluid. Hence,

$$C_{sk} V(\Delta\sigma_3 - \Delta u) = C_w n V \Delta u$$

and

$$B = \frac{\Delta u}{\Delta\sigma_3} = \frac{1}{1 + n \frac{C_w}{C_{sk}}} \qquad (4.1)$$

Equation II In the derivation of Equation I, the compressibility of rock solids was assumed to be zero. Table 4.1 shows that the compressibilities

Table 4.1(a) Compressibility of Rock-Forming Minerals
(After Smithsonian Physical Tables, 1933)

	per kg/cm^2	per psi
Quartz*	2.66×10^{-6}	0.187×10^{-6}
Gypsum**	2.57	0.181
Orthoclase*	2.09	0.147
Aragonite**	1.56	0.110
Calcite*	1.35	0.095
Dolomite**	1.23	0.087

* at 30°C
** at 0°C

Table 4.1(b) Volume Compressibility of Rock Solids
(After Zisman, 1933, Unjacketed Tests)

	per kg/cm^2	per psi
Quartzitic Sandstone	2.7×10^{-6}	0.19×10^{-6}
Quincy Granite	1.9	0.13
Vermont Marble	1.4	0.10
Limestone	2.5	0.18

of rock-forming minerals are in the range of $1 \sim 3 \times 10^{-6}$ per kg/cm^2 or $0.07 \sim 0.02 \times 10^{-6}$ per psi. The rock-solid compressibilities are comparable to the observed compressibilities of rock skeleton (see Figure 3.18) at confining pressures equal to and exceeding 1000 psi. Equation II will be derived taking into account the compressibility of rock solids, using the method of Bruhn (1972). Again, the compressibility of the pore-pressure measuring system is neglected and all of the void spaces are assumed to be filled with water. Furthermore it is assumed that void spaces are interconnected and Terzaghi's effective stress principle is valid. When a rock specimen is subjected to an increment of total spherical stress, $\Delta\sigma_3$, the sum of the components of volume change of rock skeleton in undrained condition must be equal to the sum of the changes in volume of each of the rock constituents.

The volume change of rock skeleton under an increment of total spherical stress, $\Delta\sigma_3$, in undrained condition is composed of two components: (a) the volume change of the rock skeleton caused by the change in effective stress, and (b) the volume change of the rock skeleton caused by the change in volume of rock solids constituting the rock skeleton. The change in volume of rock solids is caused by the change in pore fluid pressure and intergranular stress. The first component, ΔV_{sk_1}, the volume change of the rock skeleton caused by the changes in effective stress, has been already expressed in the derivation of Equation I and is:

$$\Delta V_{sk_1} = C_{sk} V(\Delta\sigma_3 - \Delta u)$$

The expression for the second component, ΔV_{sk_2}, the volume change of the rock skeleton caused by the change in pore fluid pressure, was originally proposed by Skempton (1961). Each mineral particle constituting the rock skeleton undergoes compression and the rock skeleton decreases in volume by an amount:

$$V_{sk_2} = C_{min} V \Delta u$$

where C_{min} is the volume compressibility of mineral particles constituting the rock, i.e., the unit decrease in volume of mineral particles per unit increase in all-around fluid pressure. Thus, the volume change of rock skeleton under an increment of total spherical stress in undrained condition, ΔV_{sk}, is:

$$\Delta V_{sk} = \Delta V_{sk_1} + \Delta V_{sk_2} = C_{sk} V(\Delta\sigma_3 - \Delta u) + C_{min} V \Delta u$$

The sum of the changes in volume of each of the rock constituents under an increment of total spherical stress in undrained condition is composed of the following three terms: (a) the volume change of the pore fluid (void space) due to the change in pore fluid pressure, (b) the volume change of mineral particles constituting the rock specimen due to the change in pore fluid pressure, and (c) the volume change of mineral particles constituting the rock specimen due to the change in intergranular stresses. The volume change of the pore fluid is expressed in terms of the compressibility of the pore fluid, C_w, and thus:

$$\Delta V_v = C_w \, nV \, \Delta u$$

The volume change of mineral particles is expressed in terms of the volume compressibility of mineral particles, C_{min}, as follows:

$$\Delta V_{min} = C_{min} \, (1-n) \, V \, \Delta u$$

The third term, the volume change of mineral particles due to the change in intergranular stresses, can be further subdivided into two components: (a) elastic changes in volume of mineral particles under changes in intergranular contact stresses, and (b) inelastic volume changes of mineral particles caused by the change in intergranular contact stresses. The inelastic volume changes most likely take place at intergranular contact zones and are caused by crushing of grains, plastic slips at contact points, breakdown of cementing bonds, etc. The first component, i.e. elastic changes in volume of mineral particles under changes in contact stresses, may be estimated by assuming that mineral particles behave by and large elastically under the change in stress conditions. Volume changes of this nature are expressed by the following equation:

$$\frac{\Delta V}{V} = \frac{1}{E} (1 - 2\nu)(\Delta\sigma_x + \Delta\sigma_y + \Delta\sigma_z)$$

where E and ν are the Young's modulus and Poisson's ratio of mineral particles, respectively, and $\Delta\sigma_x$, $\Delta\sigma_y$ and $\Delta\sigma_z$ represent stress changes

in the grains due to intergranular stresses. In order to get an idea about the order of magnitude of this component, consider an element of mineral subjected to stress changes such that:

$$\Delta\sigma_x = (\Delta\sigma_3 - \Delta u), \text{ and } \Delta\sigma_y = \Delta\sigma_z = 0$$

Let $E = 1.0 \times 10^{-7}$ psi and $\nu = 0.3$ for the mineral element, then $\frac{\Delta V}{V} = 0.08 \times 10^{-6}$ per psi.

The inelastic volume changes of mineral particles due to the change in intergranular contact stresses cannot be readily expressed in simple terms. However, in order to complete the derivation of Equation II, the following simplifying assumption may be made. The volume change of mineral particles due to the change in intergranular stress is considered a linear function of the changes in effective stresses, where the constant of proportionality is expressed by $\overline{C}_{min}$. Therefore the third term is:

$$\overline{C}_{min} (1-n) V (\Delta\sigma_3 - \Delta u)$$

Bruhn (1972) experimentally studied the significance of the compressibility of solids due to the changes in intergranular stresses for Berea sandstone. Based on the assumption that all of the components of rock compressibility were measured accurately, he back calculated the solid compression by contact stresses. Bruhn concluded that the compressibility of rock solids due to the changes in intergranular stresses could represent 30 to 40 percent of the total compressibility

of rock. However, Bruhn's measurements of rock skeleton compressibility using strain gages do not agree favorably with the results of the present study, and he did not consider the influence of the compressibility of the pore-water-pressure measuring system in his computations.

By equating the sum of the components of volume change of rock skeleton and the sum of the changes in volume of each of the rock constituents, we obtain:

$$C_{sk}\, V(\Delta\sigma_3 - \Delta u) + C_{min}\, V\, \Delta u$$

$$= C_w\, n\, V\, \Delta u + C_{min}\, (1-n)\, V\, \Delta u + \overline{C}_{min}\, (1-n)\, V\, (\Delta\sigma_3 - \Delta u)$$

This equation can be solved for $\frac{\Delta u}{\Delta\sigma_3}$, and

$$B = \frac{\Delta u}{\Delta\sigma_3} = \frac{1}{1 + n\left[\dfrac{C_w - C_{min}}{C_{sk} - (1-n)\,\overline{C}_{min}}\right]}$$

However the procedure which is used to measure the compressibility of the rock skeleton in the present study gives the value of $[C_{sk} - (1-n)\cdot \overline{C}_{min}]$ directly. Therefore the equation for the B-coefficient becomes

$$B = \frac{\Delta u}{\Delta\sigma_3} = \frac{1}{1 + n\left(\dfrac{C_w - C_{min}}{C'_{sk}}\right)} \qquad (4.2)$$

where $C'_{sk} = [C_{sk} - (1-n)\,\overline{C}_{min}]$

Equation III As previously pointed out, the measured pore pressure response also reflects the compressibility of the pore-pressure measuring system. This includes the compressibility of the drainage connections and sensing device and the compressibility of the fluid in the measuring system. Wissa (1969) derived an expression for the measured B-coefficient which takes into account the compressibility of the measuring system as described below. He assumed that soil (or rock) solids are incompressible.

The rock specimen and pore-pressure measuring system are considered as a unit. The volume change of the unit (rock skeleton and measuring system) in undrained condition is equal to the sum of the changes in volume of component materials contained in the unit. Therefore the volume change of the unit is expressed by the sum of the volume change of rock skeleton, $C_{sk}\ V\ (\Delta\sigma_3 - \Delta u)$, and the volume change of measuring system caused by the change in pore fluid pressure, $-(C_L + C_M)\Delta u$, where C_L is the compressibility of pore water lines and is equal to the change in internal volume of the lines per unit change in pressure, and C_M is the compressibility of the pore-pressure measuring device and is equal to the change in volume of the device per unit change in pressure. The minus sign is used to indicate volume increase. As the mineral particles are considered to be incompressible, the change in volume of materials contained in the unit is the sum of (a) the change in volume of pore fluid in the rock specimen, $C_w\ n\ V\ \Delta u$, and (b) the change in volume of pore fluid in the measuring system,

$C'_w V_L \Delta u$, where C'_w and V_L are the compressibility and the volume of fluid in the measuring system, respectively. By equating the volume change of the unit to the volume change of materials contained in the unit, the following equation is obtained:

$$C_{sk} V (\Delta\sigma_3 - \Delta u) - (C_L + C_M)\Delta u = C_w n V \Delta u + C'_w V_L \Delta u$$

This equation can be solved for $\frac{\Delta}{\Delta\sigma_3}$, and thus:

$$B = \frac{\Delta u}{\Delta\sigma_3} = \frac{1}{1 + n\frac{C_w}{C_{sk}} + (\frac{C'_w}{C_{sk}})(\frac{V_L}{V}) + \frac{C_L + C_M}{C_{sk} V}} \qquad (4.3)$$

4.2.2 Comparison of Theoretical and Observed B-Coefficient

In order to calculate theoretical values of the B-coefficient by means of the equations derived in 4.2.1, it is necessary to obtain appropriate values for the parameters involved in those equations. The parameters are:

1) compressibility of the pore water; C_w,
2) volume (bulk) compressibility of the rock skeleton, C_{sk} or C'_{sk},
3) volume compressibility of mineral particles due to the changes in spherical component of total stress, C_{min},
4) volume compressibility of mineral particles due to the changes in intergranular stress, $\bar{C}_{min}$,
5) porosity of the rock skeleton, n,

6) compressibility of drainage lines, C_L,

7) compressibility of pore-pressure measuring device, C_M,

8) volume of water in the measuring system, V_L.

The compressibility of ordinary water is primarily a function of temperature and pressure. The influence of temperature on the compressibility of water at a pressure of one atmosphere is shown in Figure 4.6. As a function of pressure, the compressibility of water decreases rapidly at first and then slowly as pressure increases. Table 4.2 shows the influence of pressure on the compressibility of water at various temperature levels.

The B-coefficient measurements were performed under a constant room temperature of 26°C $\pm$ 0.5°C, and the values of the pore water pressure ranged from 50 psi to 2000 psi. Under these conditions, the compressibility of water, C_w, can be taken approximately as a constant and equal to 44 x 10^{-6} per kg/cm^2 (45 x 10^{-6} per atm or 3.1 x 10^{-6} per psi). This is the compressibility of deaired, pure water. The pore water in the rock specimen might not have been completely deaired (although distilled, deaired water was used in the saturation operations) or the pore spaces might not have been perfectly saturated. These possibilities probably increased the compressibility of pore water in the rock specimen during the B- or A- coefficient measurements.

The bulk compressibility of the rock skeleton, C'_{sk}, was measured for all rock types tested and is reported in Section 3 (see

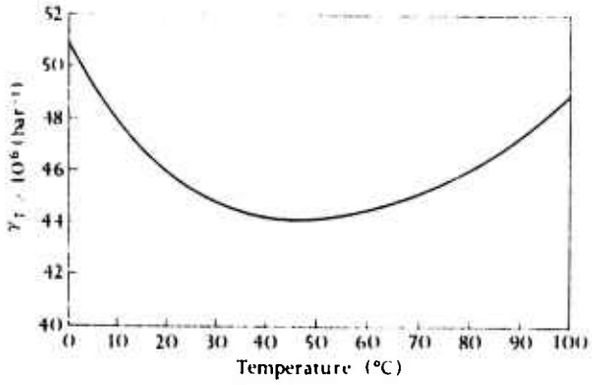

Fig. 4.6 Isothermal Compressibility of Water, γ_T, Versus Temperature. Data from Kell (1967). (After Eisenberg and Kauzman, 1969)

Table 4.2 Isothermal Compressibility of Ordinary Water (after Dorsey, 1940)

Unit of $P = 1$ atm; of $\beta_m = 10^{-6}$ per atm. 1 atm = 1.03323 kg/cm²

$t \rightarrow$ / P_1	0	10	20	30	40	50	60	80	100	Ref.
					β_m					
					$P_2 = P_1 + 25$					
1	52.5	50.0	49.1							A
	45.7	45.3	44.9	44.8	44.9	45.2	45.7	47.4	49.9	SK
25	51.6	49.2	47.6							A
	45.3	44.8	44.5	44.4	44.5	44.9	45.4	47.0	48.0	SK
75	50.2	47.0	45.3							A
	44.5	44.0	43.6	43.6	43.7	44.0	44.6	46.1	48.6	SK
125	49.1	46.3	44.6							A
	43.6	43.1	42.9	42.8	42.9	43.3	43.8	45.3	47.7	SK
175	48.8	46.0	43.8							A
	42.8	42.3	42.1	42.0	42.2	42.5	43.0	44.6	46.9	SK
					$P_2 = P_1 + 100$					
0	51.1	48.3	46.8	46.0	44.9	44.9	45.5		47.8	A
	44.6	44.1	43.8	43.7	43.8	44.1	44.6		48.7	SK
			45.8							RS
100	49.2	46.1	44.2	43.6	42.9	42.5	42.7		46.8	A
	43.3	42.8	42.6	42.6	42.7	43.0	43.5	45.1	47.4	SK
			44.8							RS
200	48.0	45.3	43.4	42.4	41.4	41.6	41.5	43.6	45.9	A
	41.7	41.3	41.1	41.1	41.2	41.6	42.0	43.5	45.7	SK
			42.4							RS
400	45.5	43.0	41.5	40.6	40.4	39.9	39.4	40.8	43.4	A
			39.9							RS
600	42.9	40.5	39.4	38.7	38.2	37.7	38.3	38.7	40.7	A
800	40.6	38.9	37.3	37.4	36.2	36.2	36.3	36.3	38.2	A
900			36.5	36.0	35.3	35.3	36.0	35.7	37.1	A

References:

A E. H. Amagat. Values have been selected from his more extended table.

RS T. W. Richards and W. N. Stull.

SK L. B. Smith and F. G. Keyes. Values derived directly from their table of specific volumes.

Figure 3.18). As the confining pressure increases, the compressibility decreases rapidly at first and then slowly at high confining pressures. Regarding the procedure which was used to measure the compressibility of the rock skeleton in the present study, the following remarks should be made:

1) The measured C'_{sk} values reported in Section 3 include the compressibility of mineral particles due to the change in intergranular stresses. Thus the measured volumetric strains are expected to be somewhat less than the volumetric strains measured by external strain gages.
2) Intrusion of the rubber membrane into the surface voids and top and bottom contact spaces of the specimen is expected to increase the observed volumetric strains by a small but unknown amount.
3) Influence of the leakage of cell fluid into the rock specimen on the measured volumetric strains is calculated on the basis of the observed rate of leakage and is estimated to be no more than 0.3% of the measured volumetric strains.

The volume compressibility of rock skeleton was measured by Zisman (1933) on several types of rock using a lever piezometer. His study included measurements on Vermont marble, Quincy granite, and Rockport granite (note that granites used in his study are different from

the granite used in the present study). Figure 4.7(a) shows a comparison of Zisman's results and the results of the present measurements. For Vermont marble at low confining pressures, the C'_{sk} values of the present study are about 30 percent higher than Zisman's C_{sk} values. However, in general the agreement between the two measurements is fairly reasonable.

King (1969) and Bruhn (1972) measured the volume compressibility of the rock skeleton of Berea sandstone specimens using foil strain gages. Figure 4.7(b) shows a comparison of their results and the results of the present study on Berea sandstone. Although the C'_{sk} values of the present study are a little higher than their results, generally the agreement between the measurements is again reasonable. C'_{sk} is actually expected to be lower than C_{sk}. However, the above comparison shows that the C'_{sk} values of the present study are actually slightly higher than the values of C_{sk} obtained by King and Bruhn. This implies either the effect of the term $(1-n)\overline{C}_{min}$ is very small or the influence of rubber-membrane intrusion exceeds the effect of the term $(1-n)\overline{C}_{min}$.

The compressibility of some rock-forming minerals and rock solids compressibility for several rocks (from unjacketed tests) are given in Table 4.1 (a) and (b) (see Section 4.2.2). It is seen that the compressibilities of rock solids are of the same order of magnitude as the compressibility of minerals constituting the rocks. The

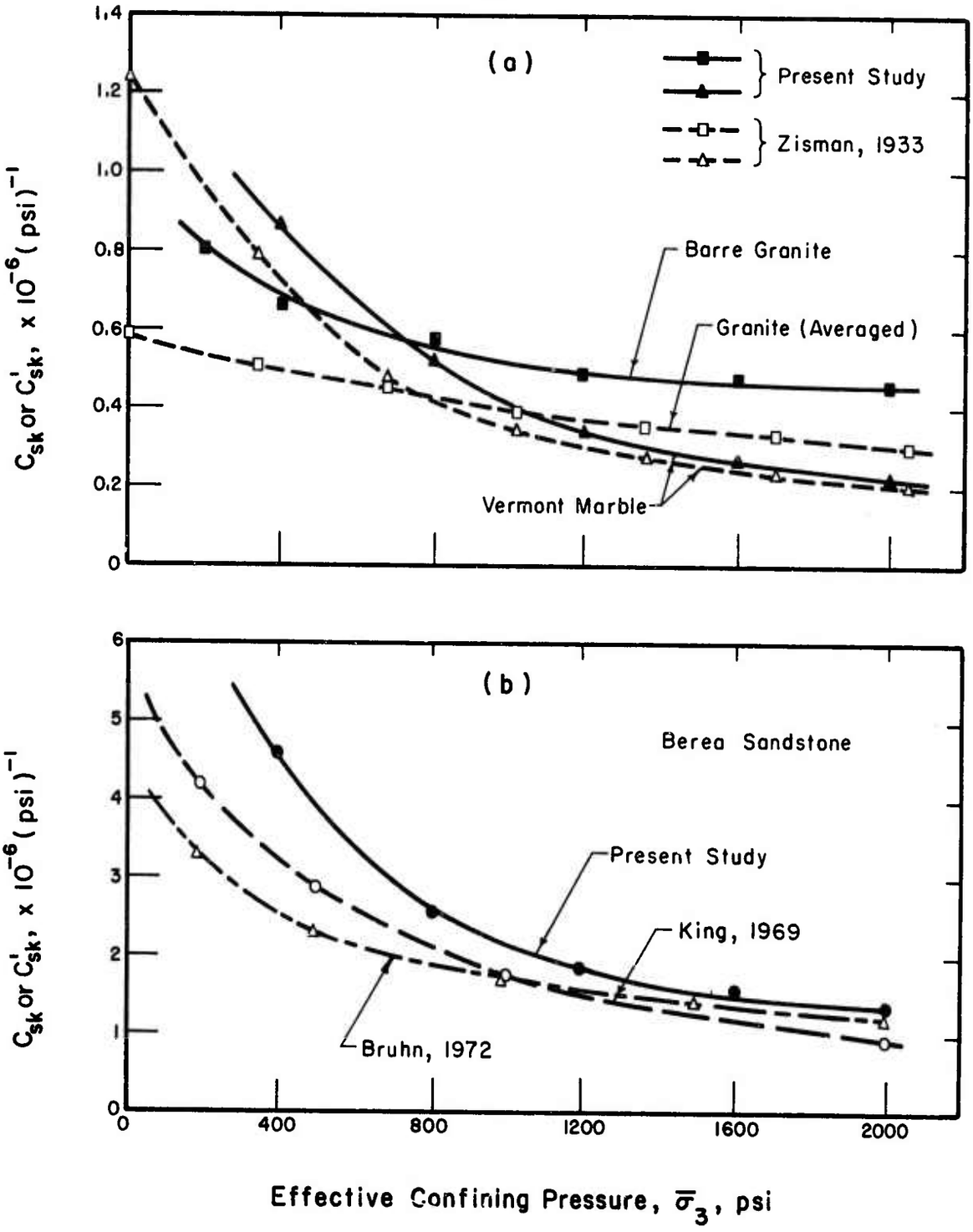

Fig. 4.7 Comparison of the Volume Compressibility of Rock Skeleton

following values are estimated to represent the compressibilities of mineral particles, C_{min}, for each type of rock tested herein.

Table 4.3 Estimated Volume Compressibility of Mineral Particles, C_{min}

Rock Type	C_{min} $(psi)^{-1} \times 10^{-6}$
Berea Sandstone	0.19
Salem Limestone	0.18
Vermont Marble	0.10
Barre Granite	0.13

The compressibility of drainage lines, C_L, is calculated with the known dimensions of the lines and using the Young's modulus of stainless steel. These calculations gave the value of C_L of 2×10^{-8} $in.^3$ per psi, or a value of C_L/V of 1.3×10^{-9} per psi which is less than 0.5% of C_{sk}. The compressibility of the Dynisco, Model PT25 electric pressure transducer with a range of 0 to 1000 psi is 3×10^{-8} $in.^3$ per psi ($C_M/V = 1.9 \times 10^{-9}$ per psi, which is less than 0.9% of C_{sk}). The compressibility of the Statham, Model PG 856-5M transducer with a range of 0 to 5000 psi is less than the compressibility of the Dynisco transducer. As the value of C_{sk} is in the range of 3.5×10^{-6} to 5×10^{-4} $in.^3$ per psi, the value of the term $(C_L + C_M)/C_{sk}V$ is in the range of 1×10^{-4} to 1.4×10^{-2}. Thus, the effect of this term on the measured B-coefficients is very small and can be neglected.

The volume of water in the measuring system, V_L, is 0.27 in.^{3} Therefore the value of the term $(C'_w/C_{sk})(V_L/V)$ is in the range of 0.0017 to 0.24, indicating that this term does influence the measured values of the B-coefficient.

Theoretical evaluations of the B-coefficient by Equations 4.1, 4.2, and 4.3 are made on each type of rock. The results are shown in Figures 4.8 to 4.11 together with the experimentally observed B-coefficients. Equations 4.1 and 4.2 gave almost identical values of the B-coefficient for all rock types. The results indicate that the influence of the compressibility of rock solids on the B-coefficient is not significant at least for the rock types tested and within the pressure ranges used in the present study. Equation 4.3 predicts lower values than Equations 4.1 and 4.2, especially on low porosity rocks such as Vermont marble and Barre granite. Although the triaxial cell and the pore-water-pressure measuring system used in the present study were carefully designed and constructed, the system compressibility still influences the measured B-values of low porosity rocks. The most important factor in the present study is the compressibility of water in the measuring system. It would be practically impossible to further reduce the volume of water in the measuring system and completely eliminate the influence of the compressibility of the measuring system. Therefore it is important to be aware that the experimentally measured B-coefficients on low porosity rocks will be usually lower than the actual values. The observed results should be

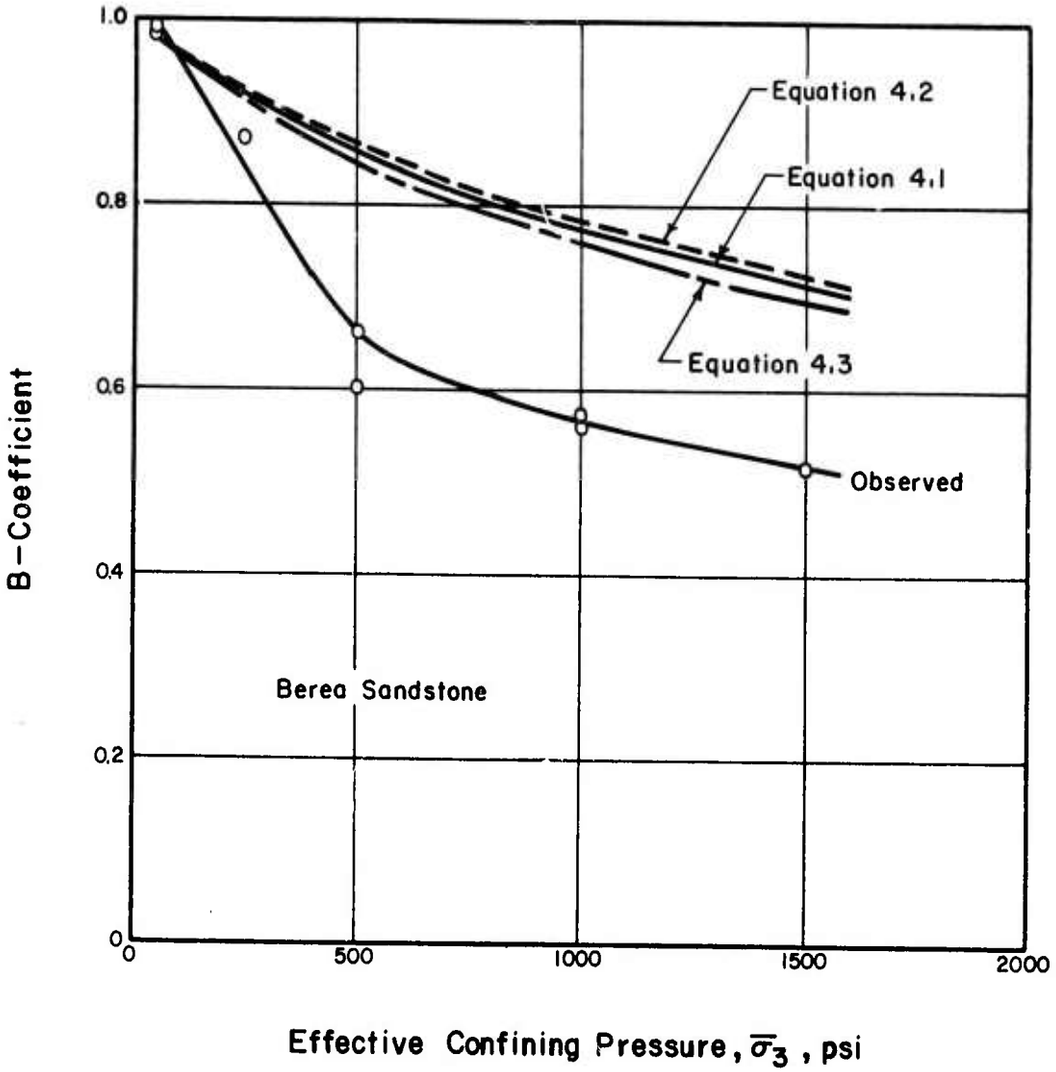

Fig. 4.8 Theoretical Evaluation of B-Coefficients, Berea Sandstone

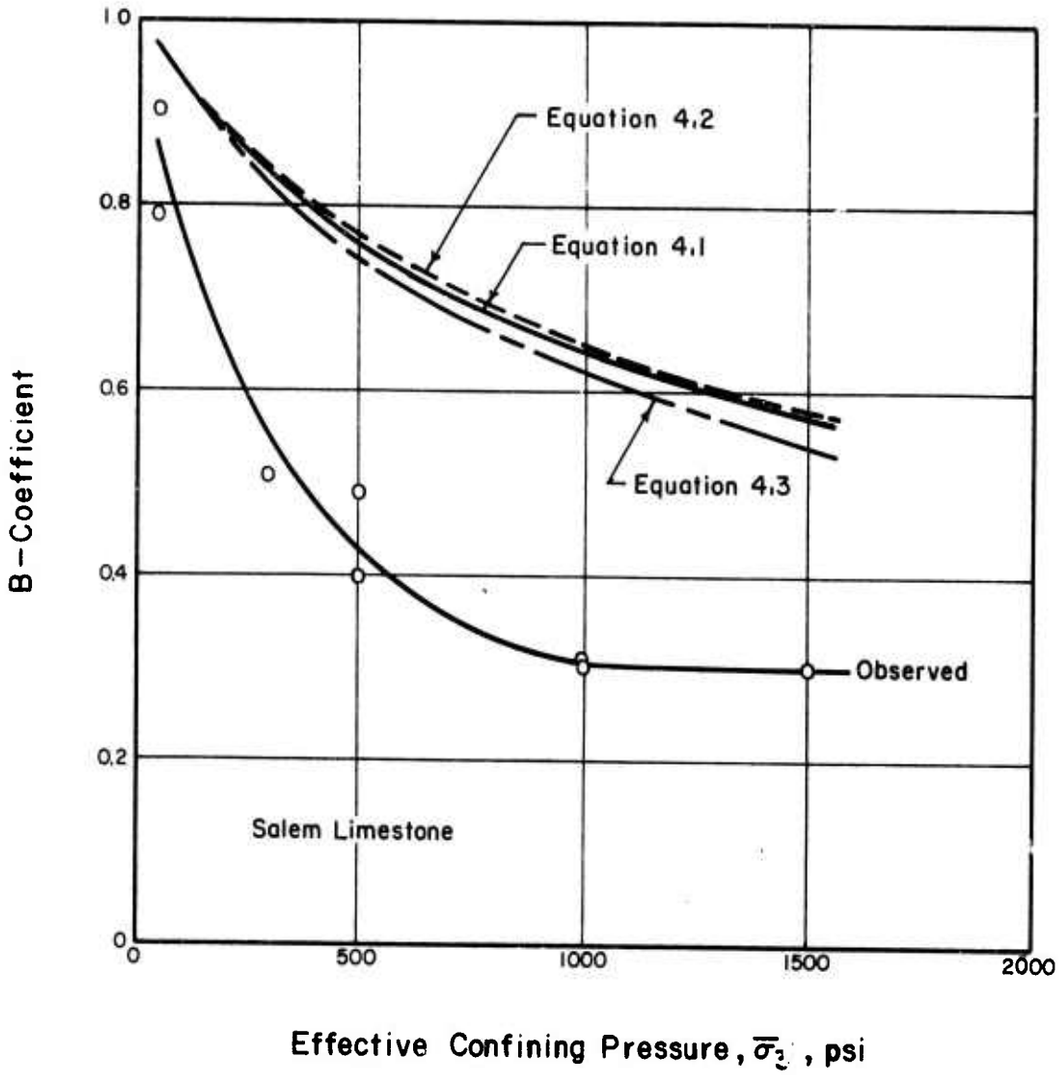

Fig. 4.9 Theoretical Evaluation of B-Coefficients, Salem Limestone

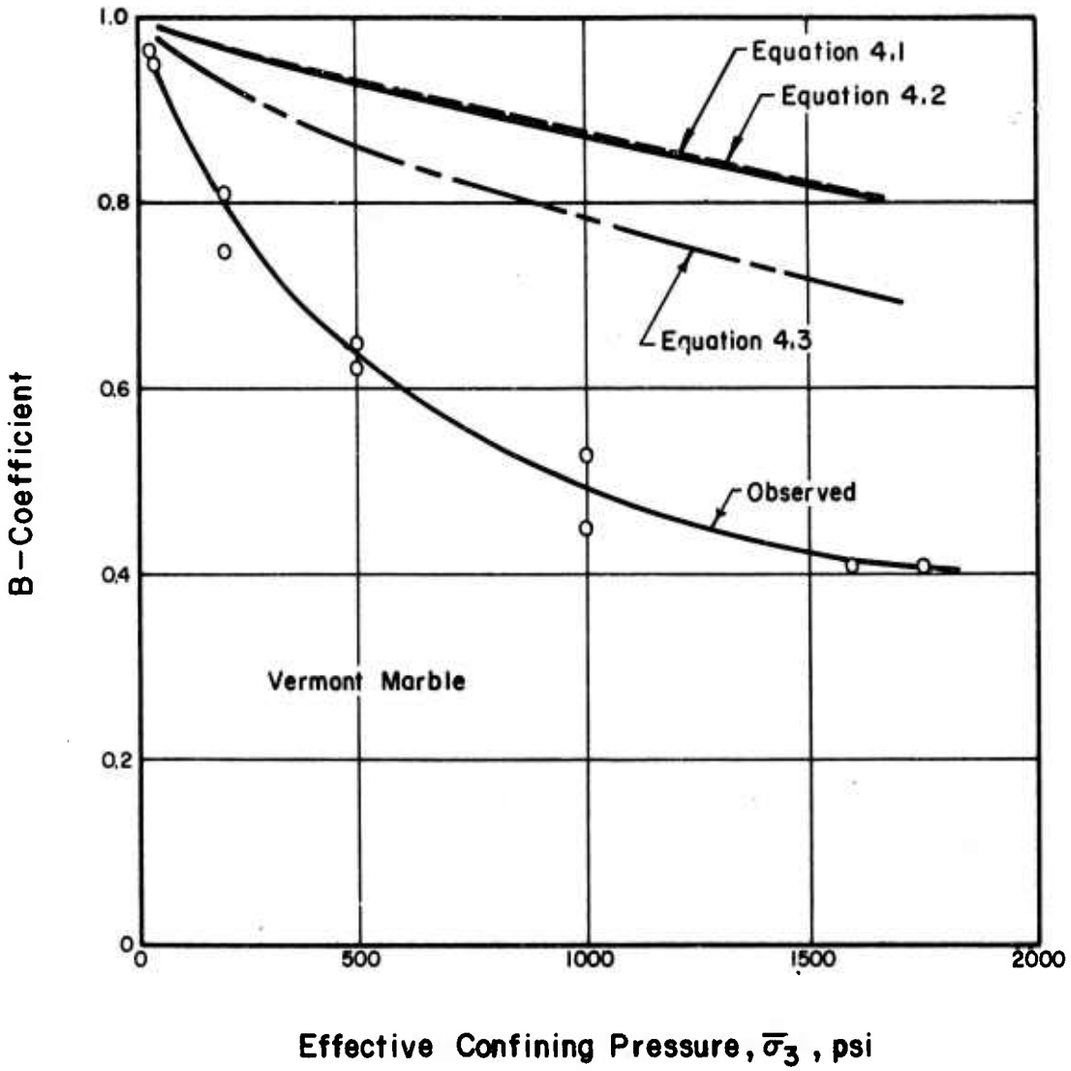

Fig. 4.10 Theoretical Evaluation of B-Coefficients, Vermont Marble

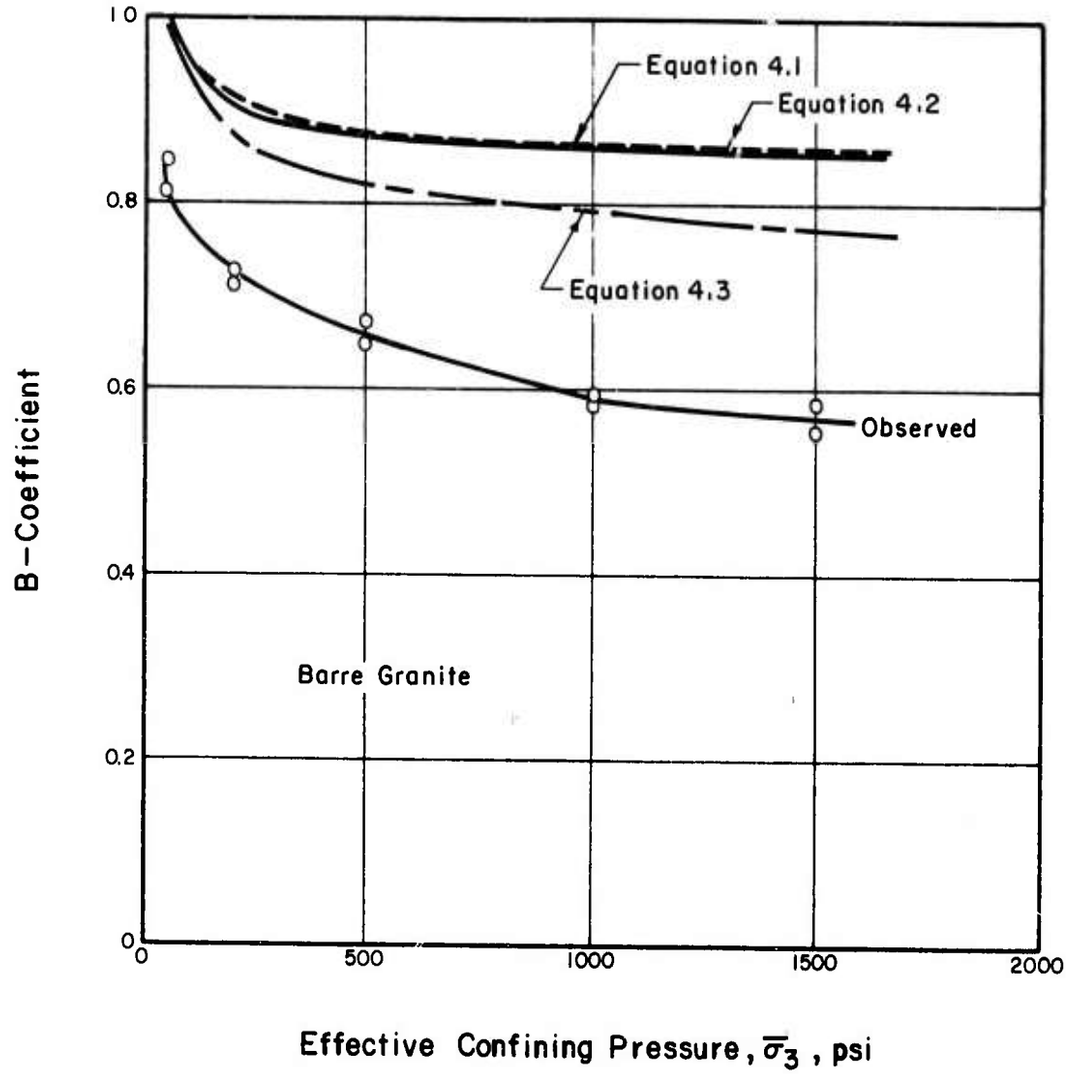

Fig. 4.11 Theoretical Evaluation of B-Coefficients, Barre Granite

modified by the amount equal to the difference which is indicated by Equations 4.1 and 4.3, in order to exclude the influence of system compressibility.

The most significant results shown in Figures 4.8 to 4.11 are that the theoretically calculated B-coefficients are in all cases higher than the experimental results (by 0 to 20% at lower effective confining pressures and by 40 to 100% at higher effective confining pressures). Figure 4.12 is a comparison of the theoretical and experimental B-values reported by Bruhn (1972) on Berea sandstone, showing a similar discrepancy between experimental and theoretical results. As it has already been pointed out, the most likely source of the discrepancy is the difference in the compressibility of pure water and the compressibility of pore water in rock. It might be difficult if not impossible to remove all of the air bubbles trapped in poorly connected voids in the rock specimen. Dissolved air in the pore water during pressure saturation operation also could increase the compressibility of pore water. These possibilities can be experimentally studied by using more sophisticated equipment and different kinds of pore fluids but are left for future studies.

4.2.3 Concluding Remarks

On the basis of measurements reported herein and the discussion, and the previous work which has been reviewed, the following

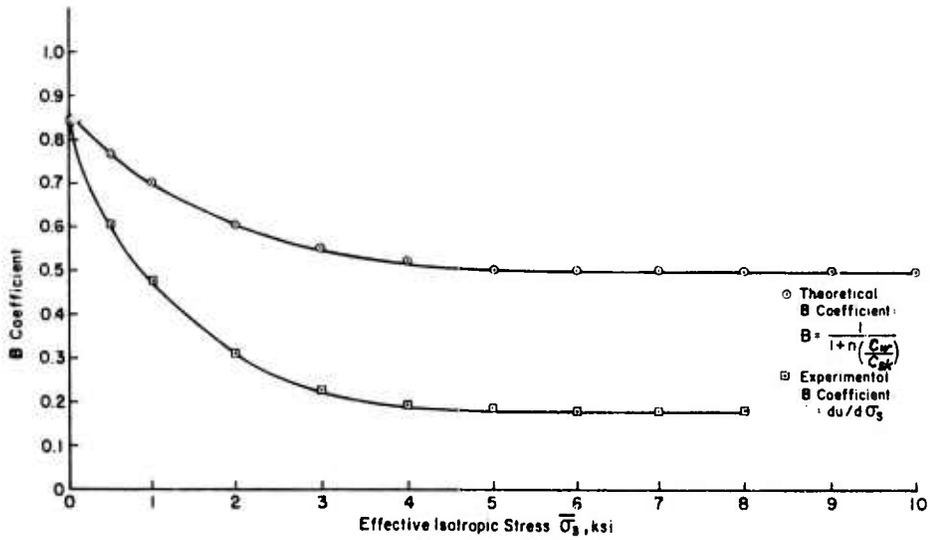

Fig. 4.12 Theoretical and Experimental B-Coefficients, Berea Sandstone (After Bruhn, 1972)

concluding remarks are made on the B-coefficient of intact rock.

1) B-coefficient of intact rock is not generally equal to unity, nor is it a constant. It is a function of the effective confining pressure, and decreases with the increasing effective confining pressure. The observed values of B-coefficient for the rocks tested herein range between 0.3 and 1.0.

2) To check for complete saturation of soils, it is a common procedure to obtain a B-coefficient of unity. For intact rocks a saturation criterion first proposed by Wissa (1969) for stiff soils has been found satisfactory in the present study. The saturation criterion is "Check for complete saturation by measuring the pore-pressure response at several back pressures keeping the effective confining pressure constant. The pore-pressure response (B-coefficient) should be constant and independent of the magnitude of the back pressure."

3) The main factors influencing the value of B-coefficient for intact rock are:

   a) degree of saturation, S_r,

   b) compressibility of pore water, C_w,

   c) bulk compressibility of the rock skeleton, C_{sk} or C'_{sk},

   d) porosity of rock skeleton, n.

The influence of the compressibility of the pore-water-pressure measuring system on the measured B-values could be significant, depending

on the type of rock and the pore-water-pressure measuring system being used. In the present study, the compressiblity of water in the measuring system lowered the experimentally observed B-values, by 0 to 4% on high porosity rocks and by 1 to 12% on low porosity rocks.

4.3 Pore Pressure Coefficients A and $\bar{A}$

4.3.1 Summary of Experimental Results

The A- and $\bar{A}$-coefficients are defined by Skempton (1954) using the following equations:

$$\Delta u = B[\Delta\sigma_3 + A(\Delta\sigma_1 - \Delta\sigma_3)] \tag{4.4}$$

$$\Delta u = B\,\Delta\sigma_3 + \bar{A}(\Delta\sigma_1 - \Delta\sigma_3) \tag{4.5}$$

where Δu is the change in pore water pressure, B is the B-coefficient, $\Delta\sigma_1$ is the change in major principal stress, and $\Delta\sigma_3$ is the change in minor principal stress. In case of undrained triaxial compression tests in which the confining pressure, σ_3, is kept constant during shearing stage ($\Delta\sigma_3 = 0$), the $\bar{A}$-coefficient at any axial strain is the ratio of the change in pore water pressure to the change in axial stress, i.e., $\bar{A} = \Delta u/\Delta\sigma_1$. In the present study the shear-induced pore water pressure was divided by the axial stress increase at the corresponding axial strain in order to obtain the $\bar{A}$-value.

Before presenting a summary of the pore pressure and volume change data from the triaxial compression tests, the following experimental problem should be noted. In undrained triaxial compression

tests with pore water pressure measurements, the following conditions, among others, must be met in order to obtain proper measurement of shear-induced pore pressures. The magnitude of the positive shear-induced pore pressure cannot exceed the difference between cell pressure and back pressure, i.e., when $\Delta u > 0$, $|\Delta u| \leq (\bar{\sigma}_3)_o = (\sigma_3)_o - u_o$. Also the magnitude of the negative shear-induced pore pressure cannot be less than the value of back pressure, i.e., when $\Delta u < 0$, $|\Delta u| \leq u_o$. This simply means that the total pore water pressure during the shearing stage must be greater than zero and less than the cell pressure. When total pore pressure exceeds the cell pressure, the confining rubber membrane will expand and separate from the sample and the test can no longer be considered as undrained, i.e. $\Delta V_v \neq 0$. When total pore water pressure approaches zero and tends to become negative, the system will cavitate at relatively small negative water pressures. In the present study the first condition was satisfied in almost all tests (with the possible exception of tests at 400 psi effective confining pressure). However it appears that in a number of tests the latter condition was not satisfied and therefore it was not possible to measure the negative shear-induced pore water pressures less than the back pressure of 400 psi which was used throughout the study. This problem could not be avoided since higher back pressures would mean lower initial effective confining pressures (the triaxial cell has a capacity of 2000 psi).

In Figure 4.13 shear-induced pore water pressure, Δu; the $\bar{A}$-coefficient in undrained tests, and volumetric strain, v^I, in drained tests versus axial strain are summarized for the tests on Berea sandstone. Positive shear-induced pore water pressures were observed at the initial stage of loading for all of the specimens. The pore pressures peak at about one third of the axial strain corresponding to the maximum principal stress difference. Note that the negative volumetric strain and the positive pore water pressure maximize at approximately the same axial strain, in drained and undrained tests with equal initial effective confining pressures. As the loading is continued, the pore pressures begin to decrease and become negative for all specimens in undrained tests. In the drained tests the initial volume decrease is followed by a volume increase. The magnitude of the maximum shear-induced pore water pressure increases with increasing initial effective confining pressure. The $\bar{A}$-coefficients maximize at the early stage of loading and then decrease continuously until they become negative at or near rupture. Note that the magnitude of the maximum $\bar{A}$-coefficient decreased with increasing initial effective confining pressure.

The shear-induced pore water pressures, $\bar{A}$-coefficients, and volumetric strain data for Salem limestone, Vermont marble and Barre granite are summarized in Figures 4.14 to 4.16.

In general, the behavior of these rocks is similar to that of the Berea sandstone. However, the volumetric strain measurements

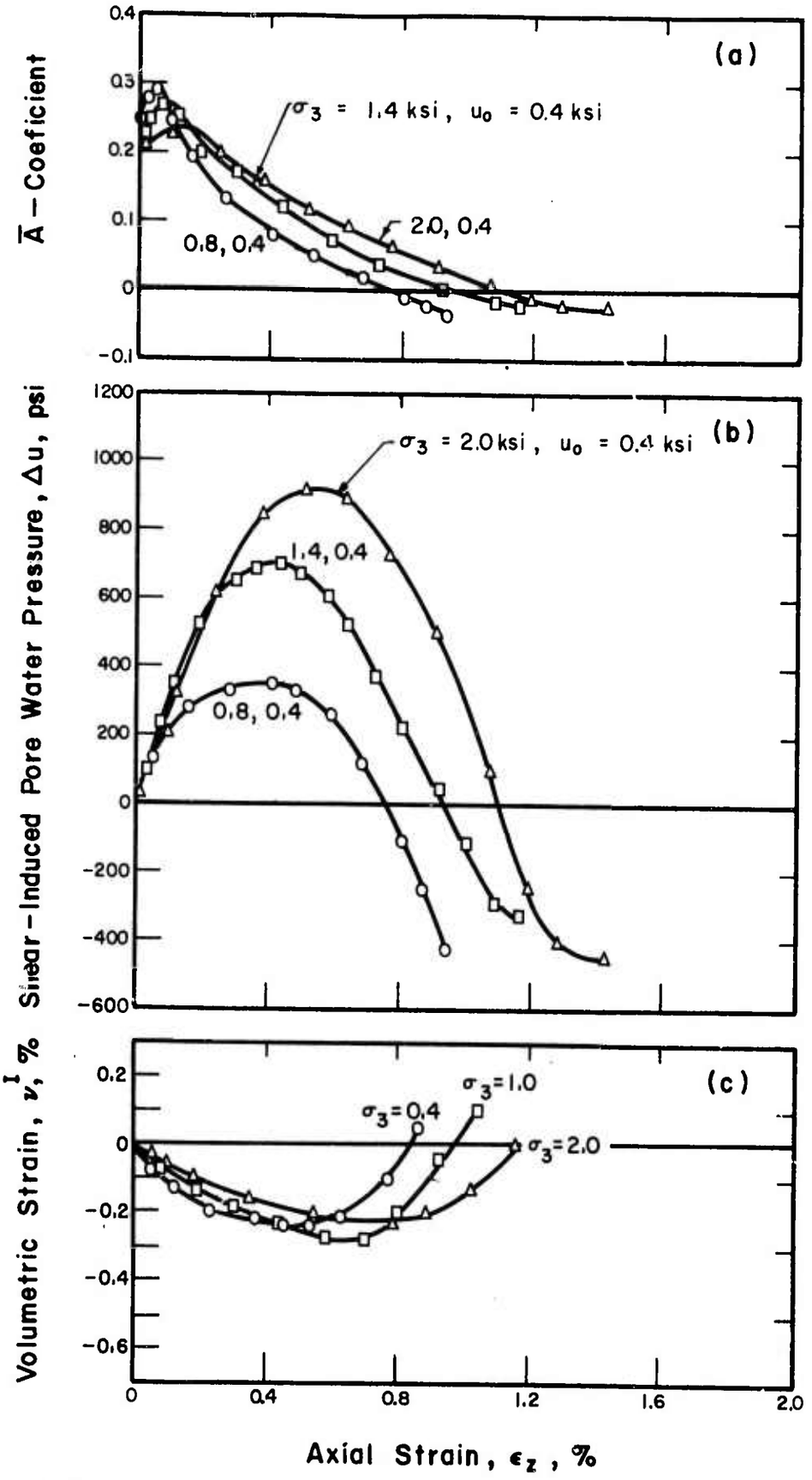

Fig. 4.13 Shear-Induced Pore Water Pressure, $\bar{A}$-Coefficient, and Volumetric Strain Versus Axial Strain, Berea Sandstone

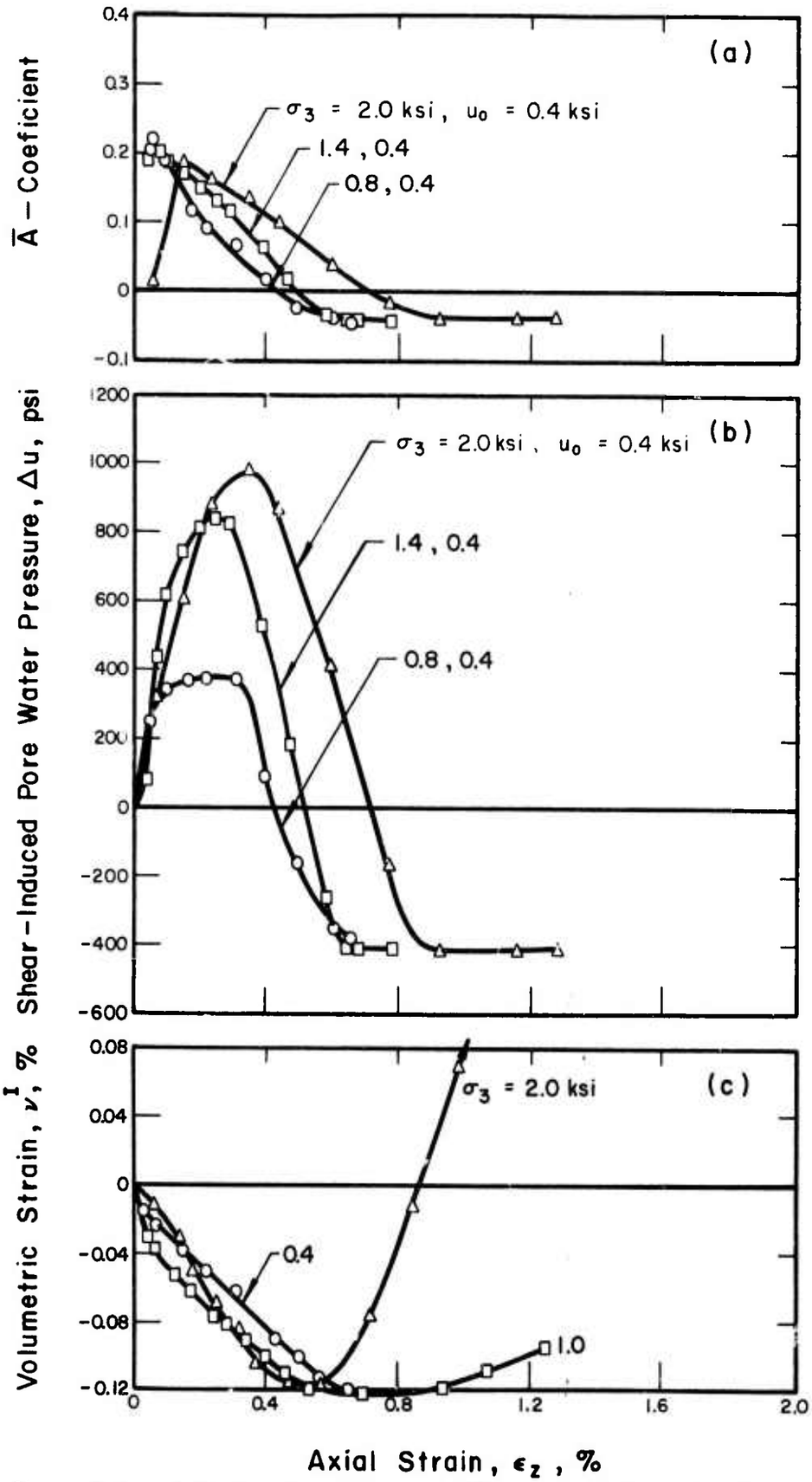

Fig. 4.14 Shear-Induced Pore Water Pressure, $\bar{A}$-Coefficient, and Volumetric Strain Versus Axial Strain, Salem Limestone

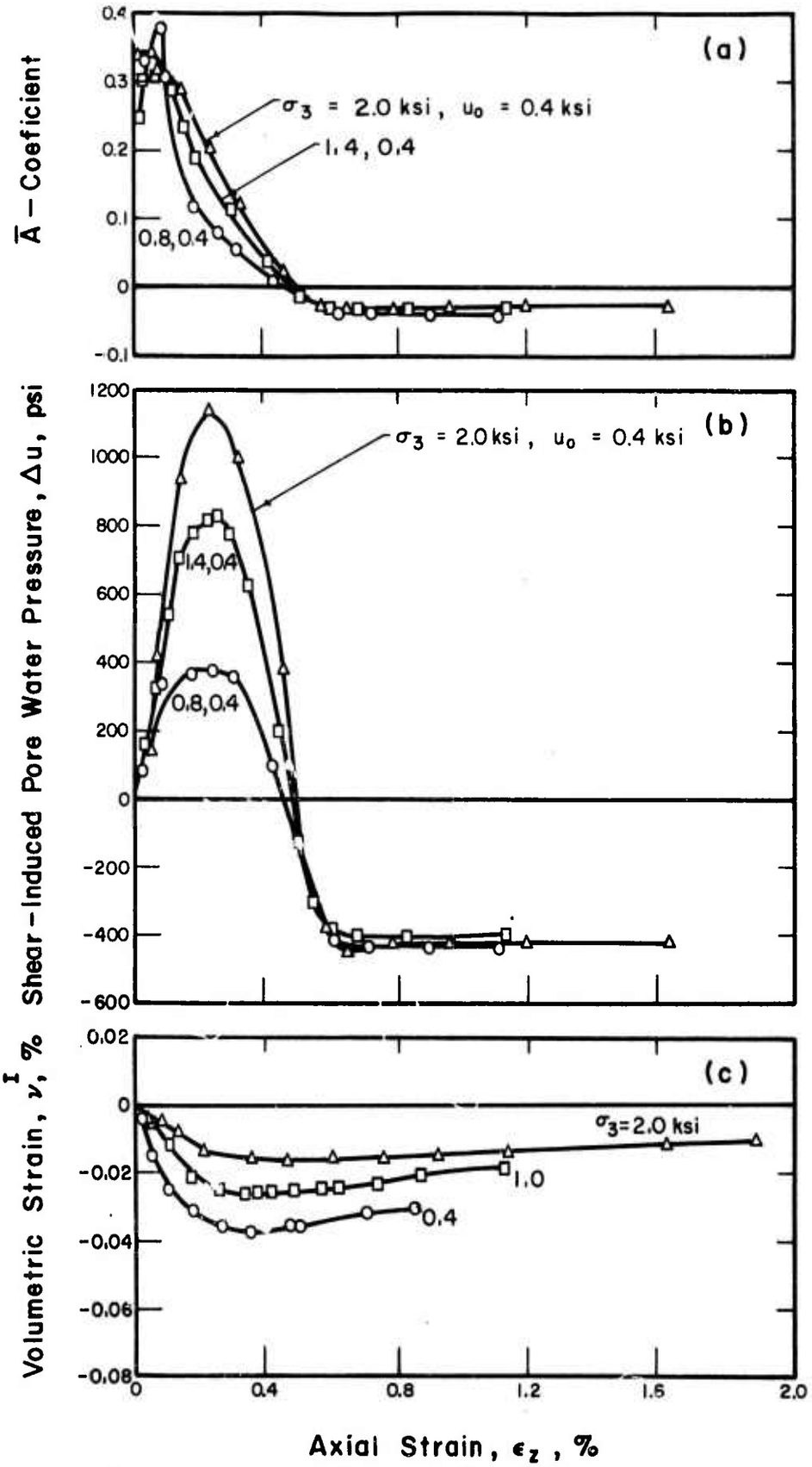

Fig. 4.15 Shear-Induced Pore Water Pressure, $\bar{A}$-Coefficient, and Volumetric Strain Versus Axial Strain, Vermont Marble

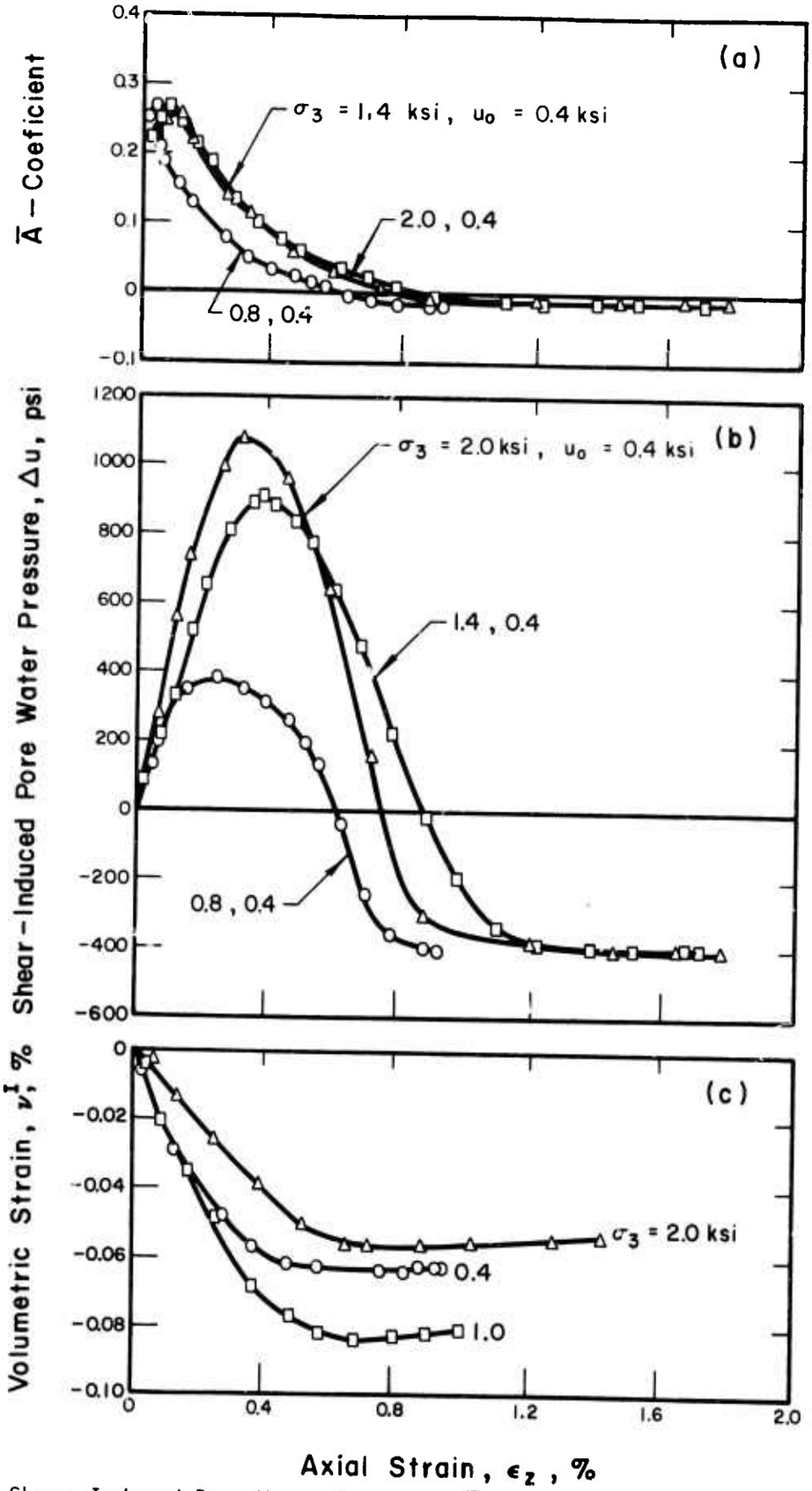

Fig. 4.16 Shear-Induced Pore Water Pressure, $\bar{A}$-Coefficient, and Volumetric Strain Versus Axial Strain, Barre Granite

beyond the axial strain corresponding to the maximum negative values on Vermont marble and Barre granite are not consistent with the tendency which is inferred from the observed shear-induced pore water pressures (shear-induced pore water pressures in undrained tests became very negative while volumetric strains in drained tests remained contractive). This discrepancy is probably related to the rate of loading which was too rapid in drained tests on Vermont marble and Barre granite.

Figure 4.17 shows the relation between observed maximum shear induced pore water pressure, $(\Delta u)_{max}$, and the initial effective confining pressure, $(\bar{\sigma}_3)_o$. At low initial effective confining pressures $(\Delta u)_{max}$ is almost equal to $(\bar{\sigma}_3)_o$, but as $(\bar{\sigma}_3)_o$ increases $(\Delta u)_{max}$ becomes less than $(\bar{\sigma}_3)_o$. It should be noted that the less porous rocks such as Vermont marble and Barre granite showed higher shear-induced pore water pressures than rocks with higher porosities. Berea sandstone, which has the highest porosity among the rocks tested, showed the lowest $(\Delta u)_{max}$. Table 4.4 and Figure 4.18 show the maximum values of the $\bar{A}$-coefficient in undrained triaxial compression tests for all rock types. There is a slight decrease in the maximum $\bar{A}$-values with increasing initial effective confining pressure for all rock types. Note that $\bar{A} = B \cdot A$. It should be recalled that B-coefficients decreased with increasing effective confining pressure. This could be partly responsible for the observed $\bar{A}$ behavior.

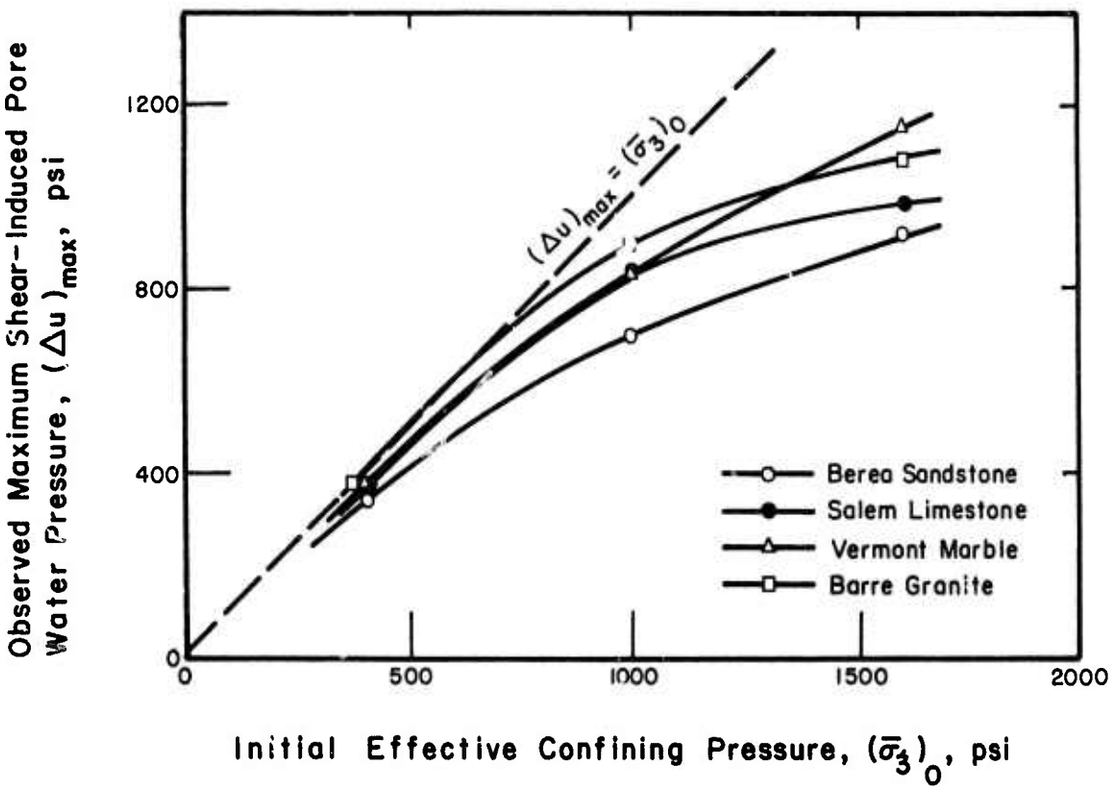

Fig. 4.17 Observed Maximum Shear-Induced Pore Water Pressure Versus Initial Effective Confining Pressure

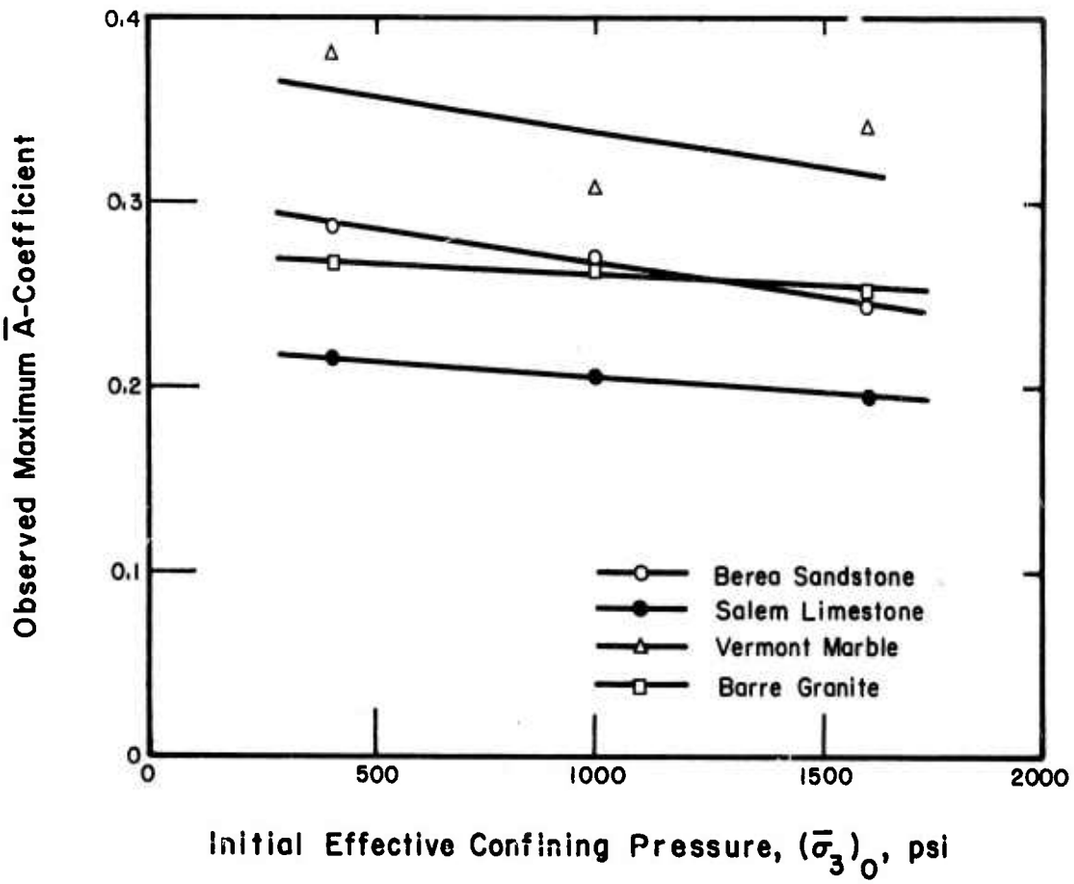

Fig. 4.18 Observed Maximum $\bar{A}$-Coefficient Versus Initial Effective Confining Pressure

Table 4.4 Observed Maximum Values of $\bar{A}$-Coefficient

Rock Type	Initial Effective Confining Pressure $(\bar{\sigma}_3)_o$ (psi) 400	1000	1600
Berea Sandstone	0.288	0.270	0.244
Salem Limestone	0.217	0.205	0.195
Vermont Marble	0.380	0.304	0.340
Barre Granite	0.268	0.264	0.253

4.3.2 Theoretical Evaluation of A- and $\bar{A}$-Coefficient

When the A-coefficient is used for rock, it is a measure of the tendency of the rock structure to compress or expand (densify or loosen) when it is subjected to shear stresses. It appears that the energy required for compression or expansion will be a function of the coefficient of compressibility or expansibility of the rock skeleton under shear stresses.

Skempton (1954) derived an equation for the A-coefficient under the following assumptions: (1) void spaces are interconnected and Terzaghi's effective stress principle is valid, (2) compressibilities of minerals constituting soil or rock and the pore-pressure measuring system are small and negligible as compared to the compressibilities of soil or rock skeleton and pore fluid. By the increment of principal stress difference, $\Delta\sigma_1 - \Delta\sigma_3$, the pore pressure is increased

by Δu_d and the corresponding changes in the effective principal stresses are:

$$\Delta\bar{\sigma}_1 = (\Delta\sigma_1 - \Delta\sigma_3) - \Delta u_d$$

and

$$\Delta\bar{\sigma}_3 = - \Delta u_d$$

Furthermore, it is assumed that the soil or rock skeleton behaves elastically, and the bulk modulus, K, is given by

$$K = \frac{E}{3(1-2\nu)}$$

where E and ν are Young's modulus and Poisson's ratio of the soil or rock skeleton, respectively. The volume change (volume decrease is taken as positive) of the specimen under the increment of principal stress difference is:

$$\Delta V = (\frac{1}{K})\ V\ (\frac{\Delta\bar{\sigma}_1 + \Delta\bar{\sigma}_2 + \Delta\bar{\sigma}_3}{3})$$

As $\Delta\bar{\sigma}_2$ is equal to $\Delta\bar{\sigma}_3$ for a cylindrical specimen in triaxial tests,

$$\Delta V = (\frac{1}{K})\ V\ \frac{1}{3}(\Delta\bar{\sigma}_1 + 2\Delta\bar{\sigma}_3)$$

or

$$\Delta V = (\frac{1}{K})\ V\ \frac{1}{3}[(\Delta\sigma_1 - \Delta\sigma_3) - 3\Delta u_d]$$

The change in volume of the void space, ΔV_v, is:

$$\Delta V_v = C_w \, n \, V \, \Delta u_d$$

where C_w is the compressibility of the pore fluid. But these two volume changes must be identical, and hence,

$$(\frac{1}{K}) \, V \, \frac{1}{3}[(\Delta\sigma_1 - \Delta\sigma_3) - 3\Delta u] = C_w \, n \, V \, \Delta u_d$$

and

$$\Delta u_d = \frac{1}{n \, C_w} \cdot \frac{1}{3}(\Delta\sigma_1 - \Delta\sigma_3)$$
$$1 + \frac{}{(1/K)}$$

Since 1/K is equal to C_{sk}, the above equation is rewritten as:

$$\Delta u = B \cdot \frac{1}{3}(\Delta\sigma_1 - \Delta\sigma_3)$$

where B is the B-coefficient. In general, however, soils or rocks are not elastic and the above expression must be written in the form:

$$\Delta u_d = B \cdot A(\Delta\sigma_1 - \Delta\sigma_3)$$

where A is a coefficient to be determined experimentally. Therefore, the present derivation implies that A = 1/3 for elastic materials.

Combining the expressions for the pore pressure response due to the increments of all-around stress, $\Delta\sigma_3$, and principal stress

difference, $\Delta\sigma_1 - \Delta\sigma_3$, we have:

$$\Delta u = B[\Delta\sigma_3 + A(\Delta\sigma_1 - \Delta\sigma_3)] \tag{4.4}$$

Equation 4.4 can be rewritten in the form:

$$\Delta u = B[\tfrac{1}{3}(\Delta\sigma_1 + 2\Delta\sigma_3) + \frac{3A-1}{3}(\Delta\sigma_1 - \Delta\sigma_3)] \tag{4.6}$$

Equation 4.6 shows that, for an elastic material, i.e., A = 1/3, the pore pressure is controlled by changes in the mean principal stress, whereas in case of A ≠ 1/3 the shear stress has a marked influence on the pore pressures.

Scott (1963) formulated a similar equation for the pore water pressure response of a soil element in undrained condition as follows:

$$\Delta u = \frac{1}{1 + n\frac{C_w}{C_{sk}}}\left[\Delta\sigma_{oct} + \frac{D}{C_{sk}} \cdot \Delta\tau_{oct}\right] \tag{4.7}$$

where $\Delta\sigma_{oct} = \frac{1}{3}(\Delta\sigma_1 + \Delta\sigma_2 + \Delta\sigma_3)$,

$$\Delta\tau_{oct} = \frac{1}{3}\sqrt{(\Delta\sigma_1 - \Delta\sigma_2)^2 + (\Delta\sigma_2 - \Delta\sigma_3)^2 + (\Delta\sigma_3 - \Delta\sigma_1)^2} \ ,$$

and D is an arbitrary coefficient which is positive or negative depending upon the tendency of the soil to contract or expand on shear. In terms of principal stress increments we can rewrite Equation 4.7 as

$$\Delta u = \frac{1}{1 + n \frac{C_w}{C_{sk}}} \left[\Delta\sigma_3 + \left(\frac{\sqrt{2}D}{3C_{sk}} + \frac{1}{3}\right)(\Delta\sigma_1 - \Delta\sigma_3)\right]$$

or

$$A = \frac{\sqrt{2}D}{3C_{sk}} + \frac{1}{3} \qquad (4.8)$$

Bjerrum (1954) derived an equation for the shear-induced pore water pressures in undrained triaxial compression tests on saturated soils in terms of the compressibility parameters under different stress conditions, i.e., C_c^I, C_s^{II}, and C_c^{III}, Fig. 4.19. C_c^I represents the coefficient of compressibility of a cylindrical specimen, measured in a drained triaxial compression test with constant lateral stress. C_s^{II} corresponds to the coefficient of compressibility of a cylindrical specimen, measured in a drained triaxial lateral extension test with constant axial stress. C_c^{III} is a coefficient of compressibility measured under an all-around stress increase in drained condition (i.e. $C_c^{III} = C_{sk}$). Bjerrum assumed the pore water to be incompressible as compared to the soil structure.

When a saturated element of soil is loaded under undrained condition by an axial stress $\Delta\sigma_1$, a pore water pressure Δu will develop (assume Δu positive), and we have:

$$\Delta\bar{\sigma}_1 = \Delta\sigma_1 - \Delta u$$

$$\Delta\bar{\sigma}_2 = \Delta\bar{\sigma}_3 = -\Delta u$$

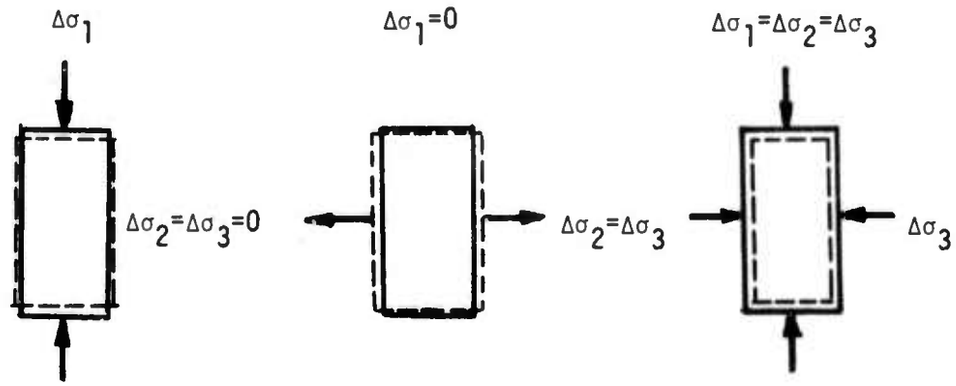

$$C_c^I = \frac{\Delta V}{V} \cdot \frac{1}{\Delta\sigma_1} \qquad C_s^{II} = \frac{\Delta V}{V} \cdot \frac{1}{\Delta\sigma_3} \qquad C_c^{III} = \frac{\Delta V}{V} \cdot \frac{1}{\Delta\sigma_3}$$

$(\Delta V<0,\ \Delta\sigma_3<0)$

(Note that decrease in volume is taken as positive)

Fig. 4.19 Compressibility Parameters C_c^I, C_s^{II}, and C_c^{III}

By definition, volume of the sample remains constant. If a drained triaxial compression test is performed on the same specimen by applying the axial load slowly and at the same time decreasing the all-around confining pressure such that the volume of the specimen remains constant, the effective stress in both tests should be the same and the decrease in cell pressure in the drained test should be equal to the increase in pore pressure in the undrained test. Therefore we can analyze the drained test in terms of effective stresses and compressibility parameters instead of the undrained test. The drained test can be considered as the superposition of two separate drained tests. In one test, the axial stress is increased by $\Delta\sigma_1 - \Delta\sigma_3$ while lateral stress is kept constant, thus:

$$\frac{\Delta V}{V} = C_c^I (\Delta\sigma_1 - \Delta\sigma_3)$$

In the second test, the lateral stress is decreased by $\Delta\sigma_3$ while the axial stress remains constant, therefore

$$-\frac{\Delta V}{V} = C_s^{II} \Delta\sigma_3$$

However, in the superimposed drained test the net volume change is equal to zero and therefore:

$$C_c^I (\Delta\sigma_1 - \Delta\sigma_3) = C_s^{II} \Delta\sigma_3$$

but as $\Delta\sigma_3 = \Delta u$, we have:

$$C_c^I (\Delta\sigma_1 - \Delta u) = C_s^{II} \Delta u$$

or

$$\Delta u/\Delta\sigma_1 = \bar{A} = \frac{1}{1 + \frac{C_s^{II}}{C_c^I}} \tag{4.9}$$

Lambe and Whitman (1969 pp. 396-398) derived an equation for $\bar{A}$ using an approach similar to that of Bjerrum, except that they include the compressibility of pore fluid in the volume changes. Their equation is:

$$\bar{A} = \frac{1}{1 + \frac{C_s^{II}}{C_c^I} + n\frac{C_w}{C_c^I}}$$

When $C_s^{II} = 2C_c^I$ (elastic material), the equation reduces to

$$\bar{A} = \frac{1}{3 + n\frac{C_w}{C_c^I}} \tag{4.10}$$

An equation for $\bar{A}$ is derived herein based on the following consideration. For an increment, $\Delta\sigma_1$, of axial load in an undrained triaxial compression test, a pore water pressure of Δu_1 is developed. For the present, assume $\Delta u_1 > 0$; therefore

$$\Delta\bar{\sigma}_1 = \Delta\sigma_1 - \Delta u$$

$$\Delta\bar{\sigma}_2 = - \Delta u$$

and

$$\Delta\bar{\sigma}_3 = - \Delta u$$

The two components of $\Delta\bar{\sigma}_1$ may be considered separately such that:

$$(\Delta\bar{\sigma}_1)_a = \Delta\sigma_1$$

and

$$(\Delta\bar{\sigma}_1)_b = - \Delta u$$

Therefore we may replace the undrained triaxial compression test with two separate tests. In one test, a drained triaxial compression test is performed such that an axial load of $\Delta\sigma_1$ is applied and volume changes are measured in order to calculate ν^I. In a second drained test (with an initial back pressure) the pore water pressure is increased by Δu and again volume changes are measured and ν^{III} is computed. From the drained tests we have:

$$\Delta V/V = \nu^I = C_c^I \Delta\sigma_1$$

and

$$\Delta V/V = \nu^{III} = -C_s^{III} \Delta u$$

Also the volume decrease of rock constituents (ignore compressibility of solids, etc.) is:

$$n\ V\ C_w\ \Delta u$$

Therefore

$$VC_c^I\ \Delta\sigma_1 - VC_s^{III}\ \Delta u = nVC_w\Delta u$$

and we have:

$$\bar{A} = \frac{\Delta u}{\Delta\sigma_1} = \frac{1}{n\frac{C_w}{C_c^I} + \frac{C_s^{III}}{C_c^I}} \qquad (4.11)$$

Note that all of the compressibility and expansibility parameters involved in Equation 4.11 can be measured by means of conventional triaxial tests. Thus, shear-induced pore water pressures in undrained triaxial compression tests can be estimated with the parameters obtained from drained tests.

4.3.3 Comparison of Experimental and Theoretical $\bar{A}$-Coefficient

Equations 4.10 and 4.11 are in terms of the compressibility parameters which can be computed from the results of drained all-around compression and triaxial compression tests. C_c^I can be calculated from the drained triaxial compression tests, at any axial strain as:

$$C^{I} = \frac{\nu^{I}}{\Delta\bar{\sigma}_1}$$

where ν^{I} is volumetric strain corresponding to the particular axial strain and axial stress increase of $\Delta\bar{\sigma}_1$. C_s^{III} is defined in the similar way for the all-around drained compression test as:

$$C_s^{III} = \frac{\nu^{III}}{\Delta\bar{\sigma}_3}$$

The values of ν^{III} are obtained from ν^{III} versus $\bar{\sigma}_3$ relations (Fig. 3.17) (these curves were obtained for effective stress increase but are applicable for effective stress decrease; elastic behavior in confined compression is assumed). Total volumetric strains (negative or positive) are taken for effective stress changes from $(\bar{\sigma}_3)_o$ to $[(\bar{\sigma}_3)_o - \Delta u]$, i.e., $\Delta\bar{\sigma}_3 = \Delta u$. In summary C_c^I and C_s^{III} are secants measured from the pre-shear condition of the test. Figure 4.20 shows the procedure which is used to compute $\bar{A}$ from the results of the drained tests. The computations have been made for a drained test on Berea sandstone, $(\bar{\sigma}_3)_o$ = 400 psi. The shear-induced pore pressures from an undrained test with $(\bar{\sigma}_3)_o$ = 400 psi are used in conjunction with Figure 3.17, to obtain C_s^{III} or C_c^{III} values. The agreement between the values of $\bar{A} = \Delta u/\Delta\sigma_1$ from the undrained tests and $\bar{A}$-values from Equation 4.11 is surprisingly good. Similar results and comparisons for Berea sandstone under different initial effective

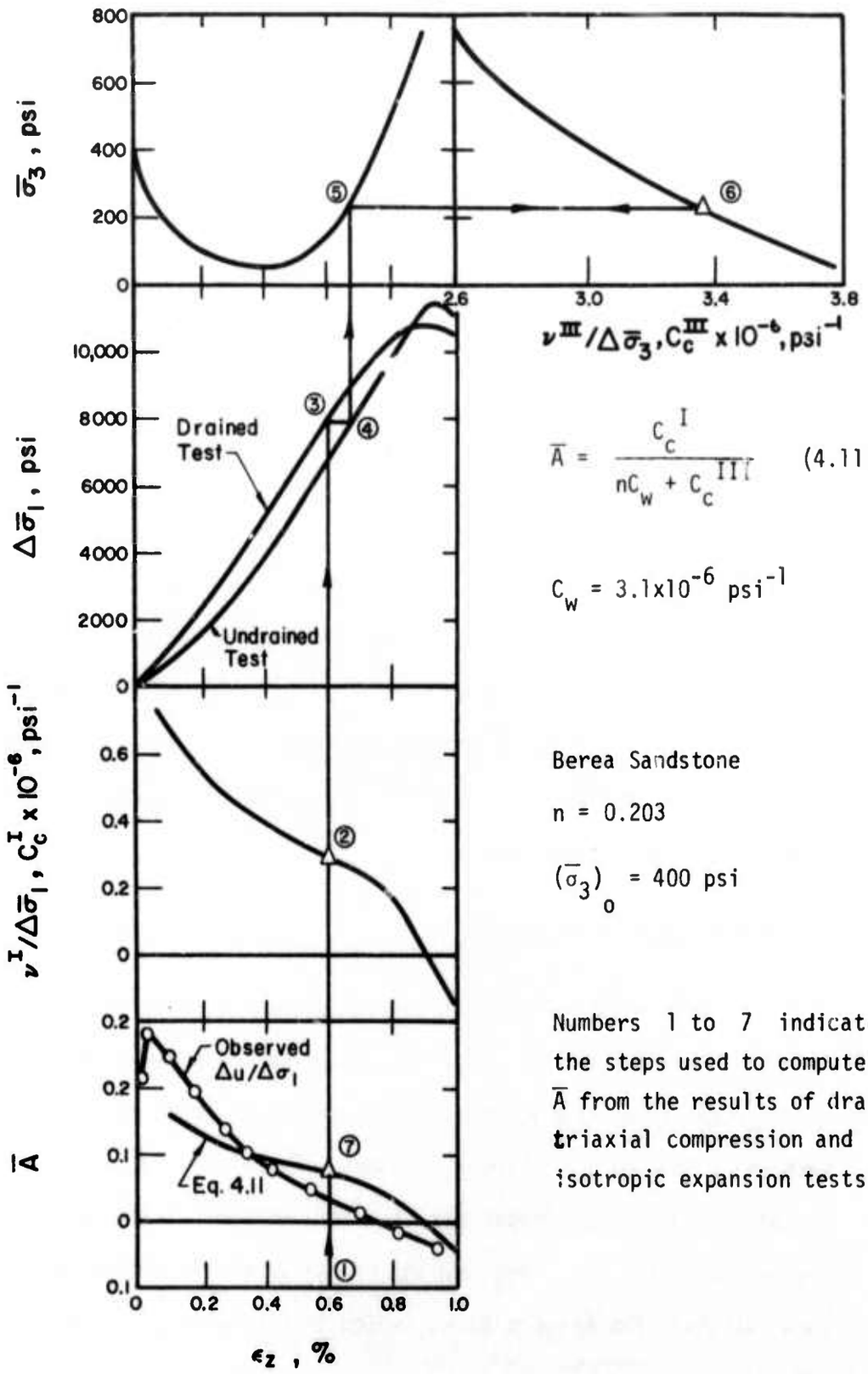

$$\bar{A} = \frac{C_c^{I}}{nC_w + C_c^{III}} \qquad (4.11)$$

$C_w = 3.1 \times 10^{-6}$ psi^{-1}

Berea Sandstone

n = 0.203

$(\bar{\sigma}_3)_o$ = 400 psi

Numbers 1 to 7 indicate the steps used to compute $\bar{A}$ from the results of drained triaxial compression and isotropic expansion tests

Fig. 4.20 Procedure to Compute $\bar{A}$-Coefficient from the Results of Drained Triaxial Compression and Isotropic Expansion Tests

confining pressures are shown in Figure 4.21. Also values of $\bar{A}$ computed by means of Equation 4.10 are shown. It appears that Equation 4.10 which is based on the assumption of elastic behavior predicts the value of $\bar{A}$ at small axial strains reasonably well. However, for a range in axial strain from 0.1% to 1% Equation 4.11 agrees better with the observed values. Typical comparisons of the observed values of $\bar{A}$ and values from Equations 4.10 and 4.11 are shown in Figures 4.22 to 4.24. The agreement is particularly poor in case of impervious rocks such as Barre granite and Vermont marble. As was previously pointed out, "drained" tests on these rocks were not fully drained, and complete pore pressure dissipation did not take place. This problem is probably one of the sources of discrepancy. Figure 4.25 shows the difference between observed volumetric strains and volumetric strains which would give complete agreement between Equation 4.11 and $\Delta u/\Delta\sigma_1$ values.

4.3.4 Concluding Remarks

When a saturated soil or rock element is subjected to an increment of shear stress, $\Delta\sigma_1$, the shear-induced pore water pressure, Δu, represents the change in effective confining pressure required to keep the volume of the element constant. Therefore the magnitude of the shear-induced pore water pressure is a measure of the tendency of the rock skeleton to undergo volume change under the influence of shear stress. The $\bar{A}$-coefficient (which is the ratio of Δu to $\Delta\sigma_1$)

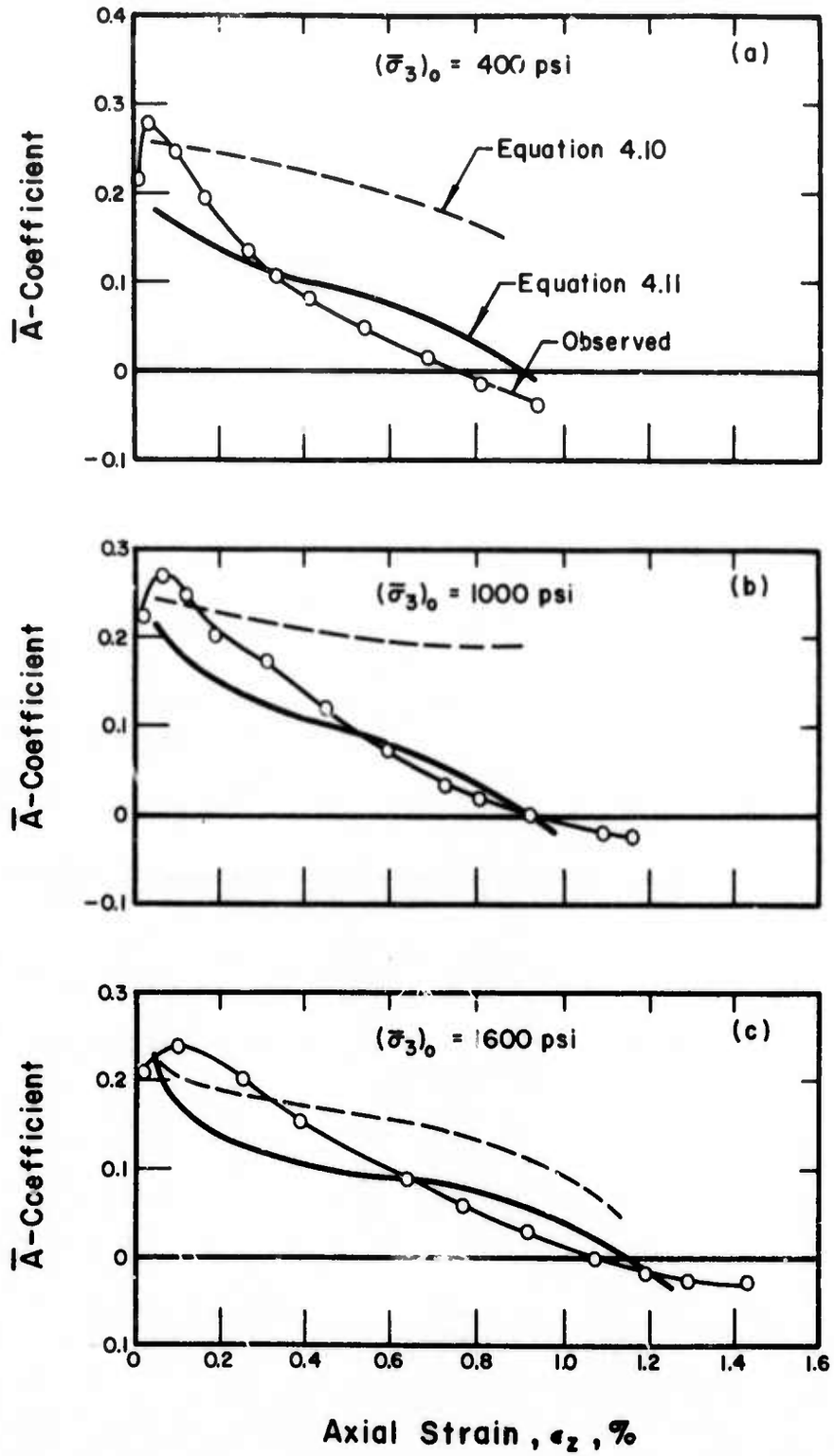

Fig. 4.21 Theoretical Evaluation of $\bar{A}$-Coefficients, Berea Sandstone

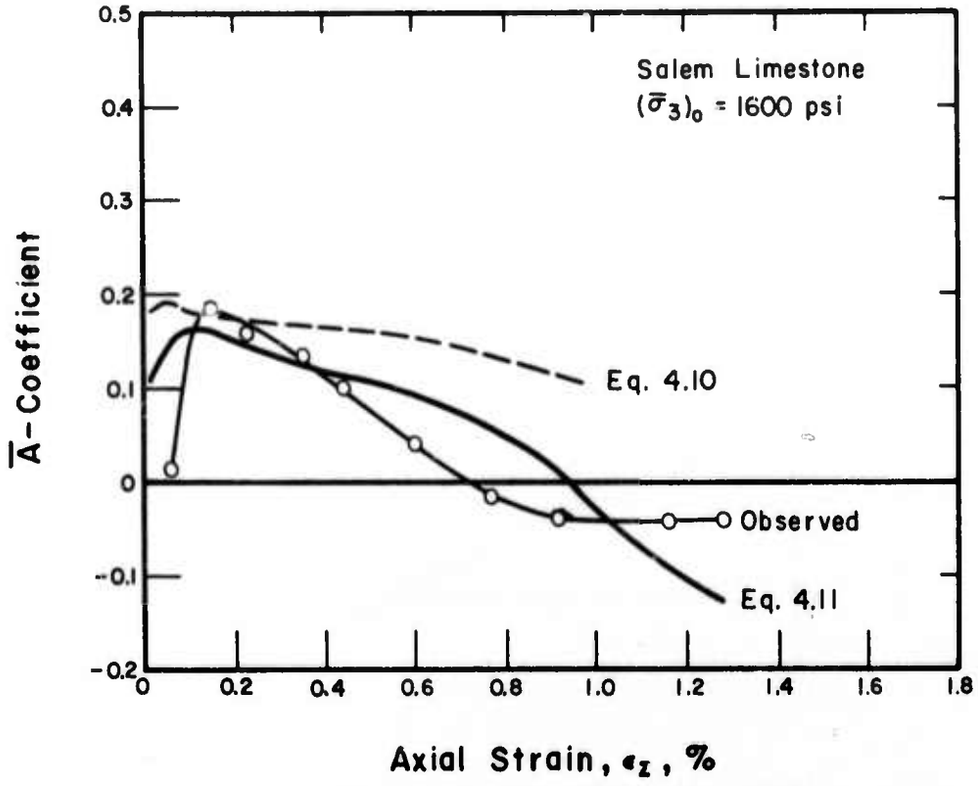

Fig. 4.22 Theoretical Evaluation of $\bar{A}$-Coefficients, Salem Limestone

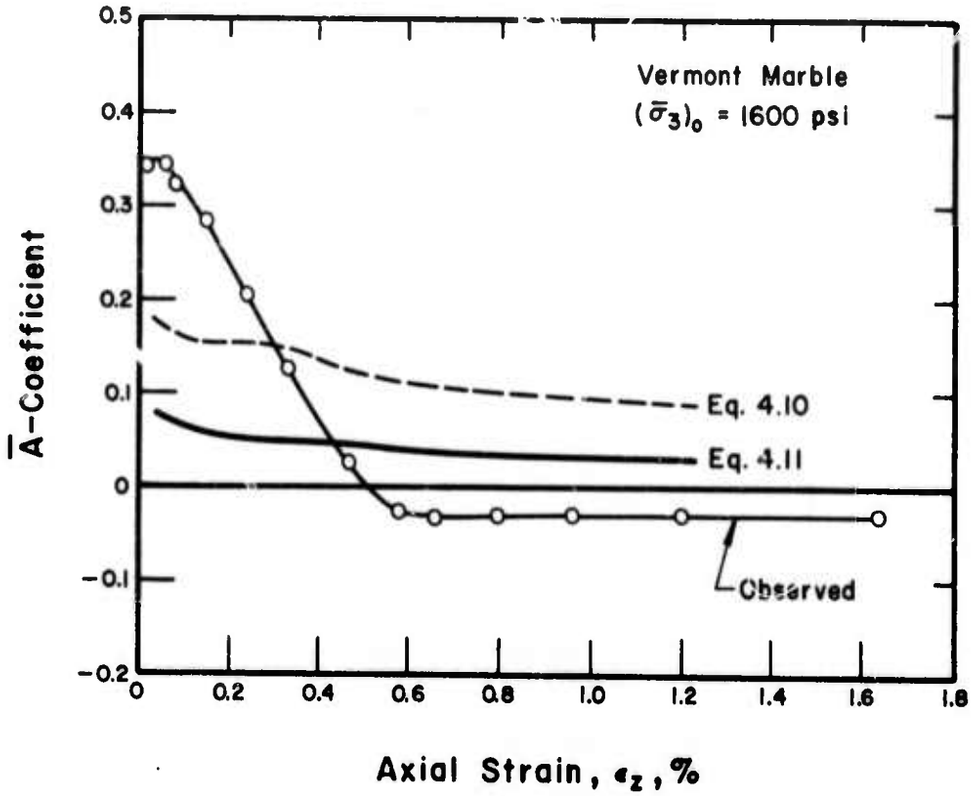

Fig. 4.23 Theoretical Evaluation of $\bar{A}$-Coefficients, Vermont Marble

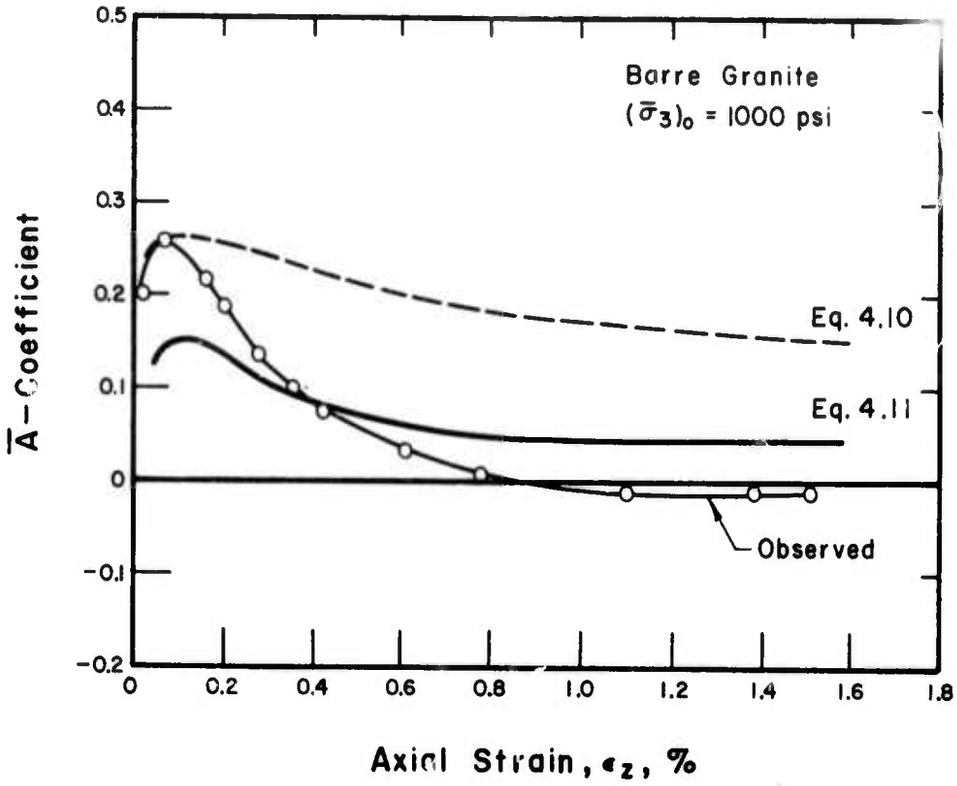

Fig. 4.24 Theoretical Evaluation of $\bar{A}$-Coefficients, Barre Granite

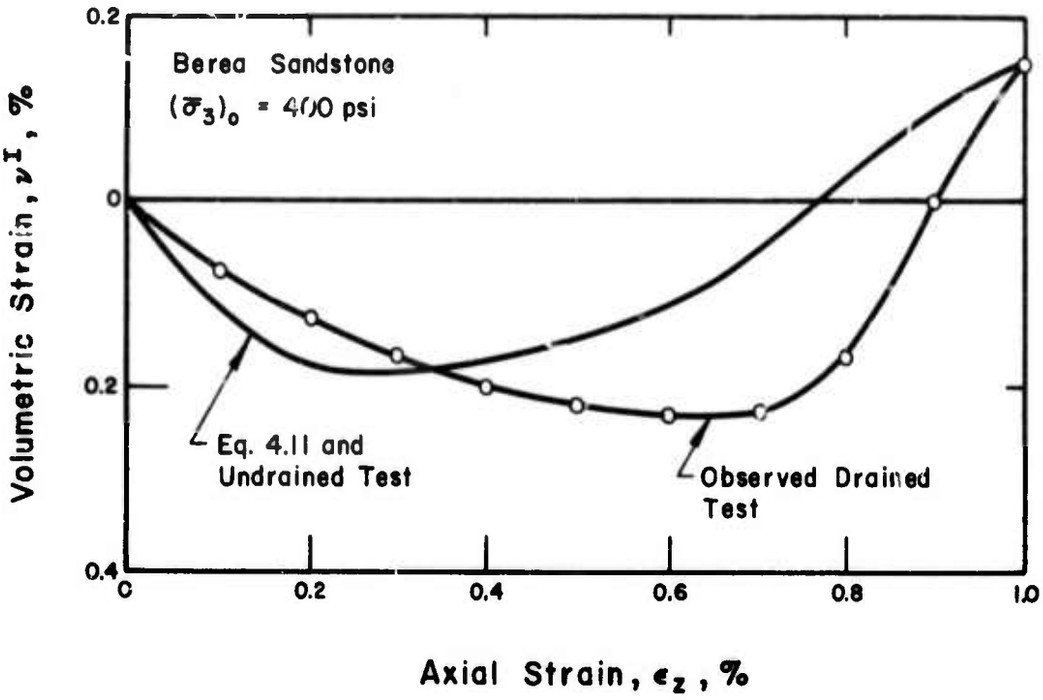

Fig. 4.25 Comparison of Observed Volumetric Strain and Volumetric Strain Calculated by Equation 4.11, Berea Sandstone

adjusts the measured response for the magnitude of shear stress and therefore it represents a property of the element. It is reasonable to expect the $\bar{A}$-coefficient to be a function of the characteristics of rock structure, particularly with respect to the pre-shear state of effective stress. These structural characteristics manifest themselves in terms of the compressibility and expansibility properties of rock under drained conditions. Therefore it is equally reasonable to expect large changes in pore water pressure as the intensity of the tendency to change volume, expressed in terms of parameters, C_c^I, C_s^{II}, C_s^{III} etc., increases. In general a tendency to contract will produce increases in pore water pressure (reduction in effective confining pressure) and the tendency to expand will decrease pore water pressure. For a normally consolidated material (this excludes practically all rocks, except in rare cases when certain rock types are subjected to very high effective confining pressures) volume decrease takes place on the compression curve and volume increase takes place in the rebound curve. In general, the coefficients of compressibility (on compression curve) will be greater than the coefficients of expansibility (on rebound curve). However, when a material is on the rebound or reloading curve, the coefficients of volume change corresponding to a volume increase can be greater than the coefficients of compressibility.

In all four rocks tested in this study and under all effective confining pressures, positive shear-induced pore water pressures

developed in undrained tests and rock skeletons compressed in drained tests at the early stage of loading. The $\bar{A}$-coefficients corresponding to the maximum positive shear-induced pore pressures range from 0.2 to 0.4. This is reasonable and corresponds to an elastic behavior (see for example Skempton's equation for A-coefficient, Section 4.3.2) of rock structure at small axial strains (or shear stresses). The positive pore pressures indicate that at this stage the overall tendency of rock structure is to compress. As soon as the applied shear stresses are sufficient to overcome shearing resistance at grain contacts, some of the cohesive bonds are destroyed and the tendency of the dense rock skeleton is to expand (internal "contact" or short-range stresses exceed the external effective confining pressure). In undrained tests pore water pressure decreases, and in drained tests the rock expands. In case of rocks which are rather brittle, particularly under relatively low initial effective confining pressures, it will not always be possible to measure the maximum potential for dilatancy, since a brittle fracture will terminate the test. However, the results of the present study show that in all cases shear-induced pore water pressures become negative after the initial stage of contraction.

The $\bar{A}$-coefficients maximized at axial strains less than or equal to 0.1% and then continuously decreased and became negative before rupture. Vermont marble showed the highest values of $\bar{A}_{max}$, Barre granite and Berea sandstone were intermediate and Salem limestone exhibited the lowest values.

4.4 Dependence of Deformation and Strength of Rock on Effective Stress

The stress-strain, volume change, shear-induced pore water pressure and strength data indicate that the principle of effective stress holds for the rocks tested in this investigation. That is to say that the changes in effective normal stress, defined as total normal stress minus the pore water pressure, control deformation and strength of these rocks. It should be emphasized that the conclusions of the present study are based on only a limited range of variation in effective stress. However, this range of effective stress corresponds to the range of effective stress which is of interest to engineering practice. Also the triaxial cell, particularly in combination with relatively low confining pressures, cannot be used to study the behavior of most rocks at all levels of stress and strain since a brittle fracture generally terminates the test at relatively low strain levels. Therefore the present conclusions are applicable only to pre-peak shear stress condition.

4.4.1 Dependence of Deformation on Effective Stress

Figures 4.26 and 4.27 show the values of tangent modulus, E_{50}, at the stress level corresponding to 50% of peak principal stress difference versus initial effective confining pressure, $(\bar{\sigma}_3)_o$, for drained and undrained triaxial compression tests. For all rock types and in drained and undrained tests, E_{50} increases with increasing $(\bar{\sigma}_3)_o$. Similar trends have been previously reported (Serdengecti and

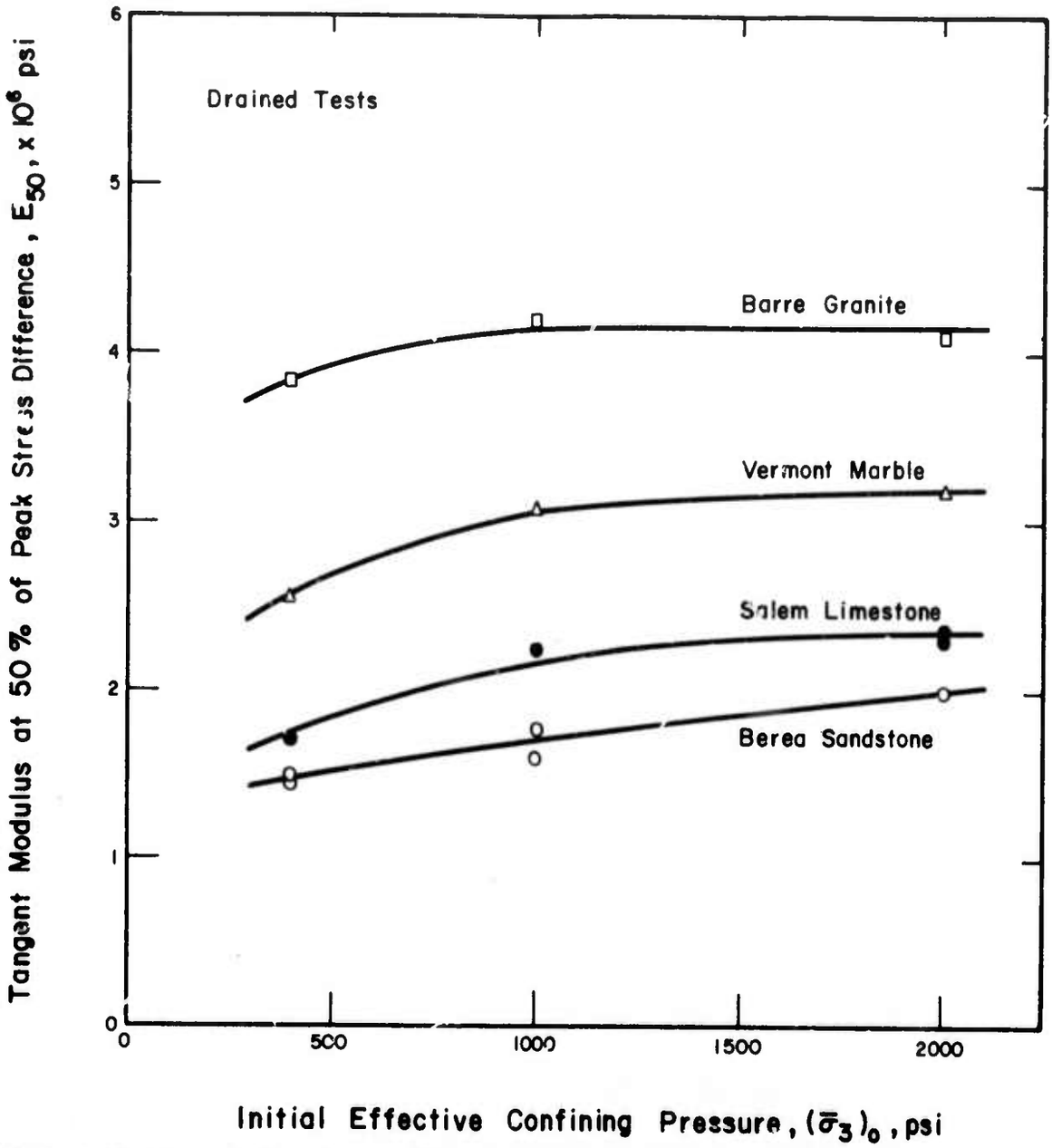

Fig. 4.26 Tangent Modulus at 50% of Peak Principal Stress Difference Versus Initial Effective Confining Pressure, Drained Tests

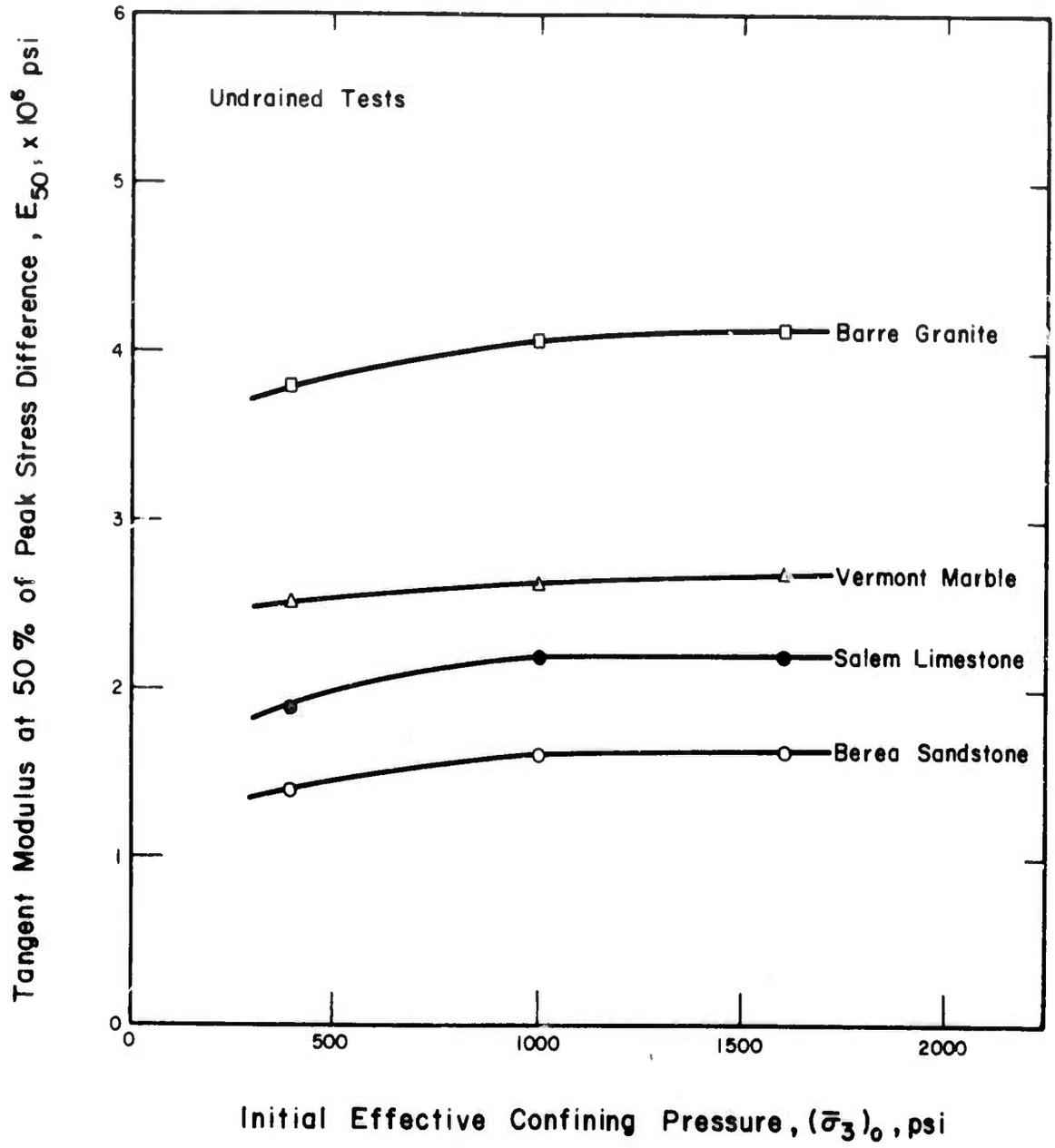

Fig. 4.27 Tangent Modulus at 50% of Peak Principal Stress Difference Versus Initial Effective Confining Pressure, Undrained Tests

Boozer, 1961; King, 1969; Bruhn, 1972). However, in all cases the rate of increase in E_{50} with $(\bar{\sigma}_3)_o$ decreases rapidly and appears to level off. This is a reasonable behavior since an increase in E_{50} at relatively small effective stress levels is primarily associated with the closure of microcracks. It appears that for each rock type, an additional increment of effective confining pressure beyond a certain pressure has little influence on the porosity and structure of the rock and therefore has little influence on deformability. This behavior is consistent with the nature of volume changes and Skempton's B-coefficients that were measured under increasing effective confining pressure, Figures 3.13 to 3.17.

In all tests, in the range of axial strain at which E_{50} is computed, the rocks had a tendency to decrease in volume; i.e. drained tests experienced volumetric compression and in undrained tests positive shear-induced pore water pressures developed. Consistent with the pore pressure and volume change data, a comparison of Figures 4.26 and 4.27 show that the values of E_{50} from drained tests are slightly higher than the corresponding values from undrained tests. However, when the E_{50} values from drained and undrained tests are compared in terms of the effective confining pressure, $\bar{\sigma}_3$, at the stress level at which E_{50} is computed, the drained and undrained tests indicate a single relationship between E_{50} and $\bar{\sigma}_3$, Figure 4.28.

Figures 4.29 and 4.30 show that, when drained and undrained tests are compared at a given initial effective confining pressure,

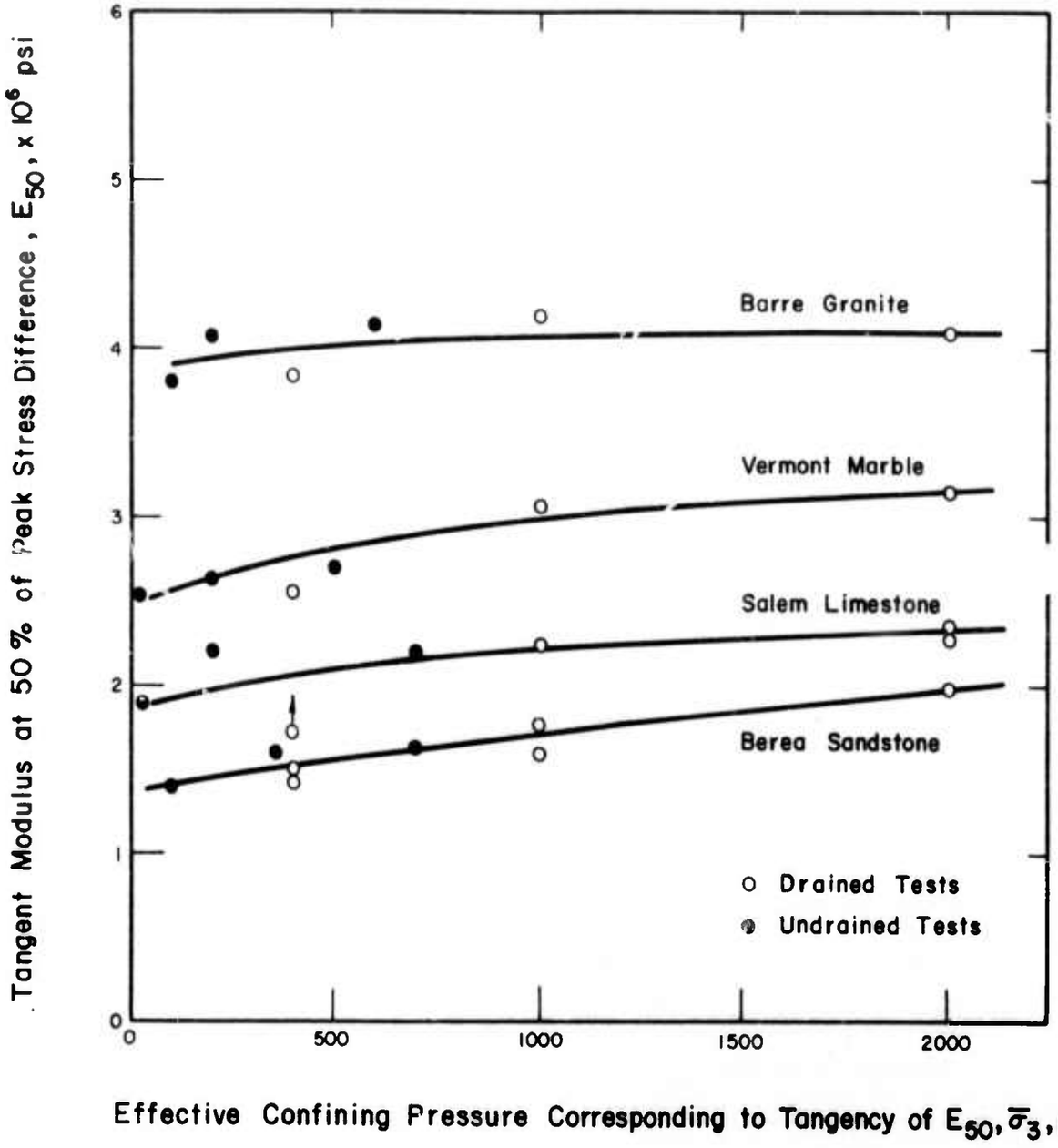

Fig. 4.28 Tangent Modulus at 50% of Peak Principal Stress Difference Versus Effective Confining Pressure Corresponding to Tangency

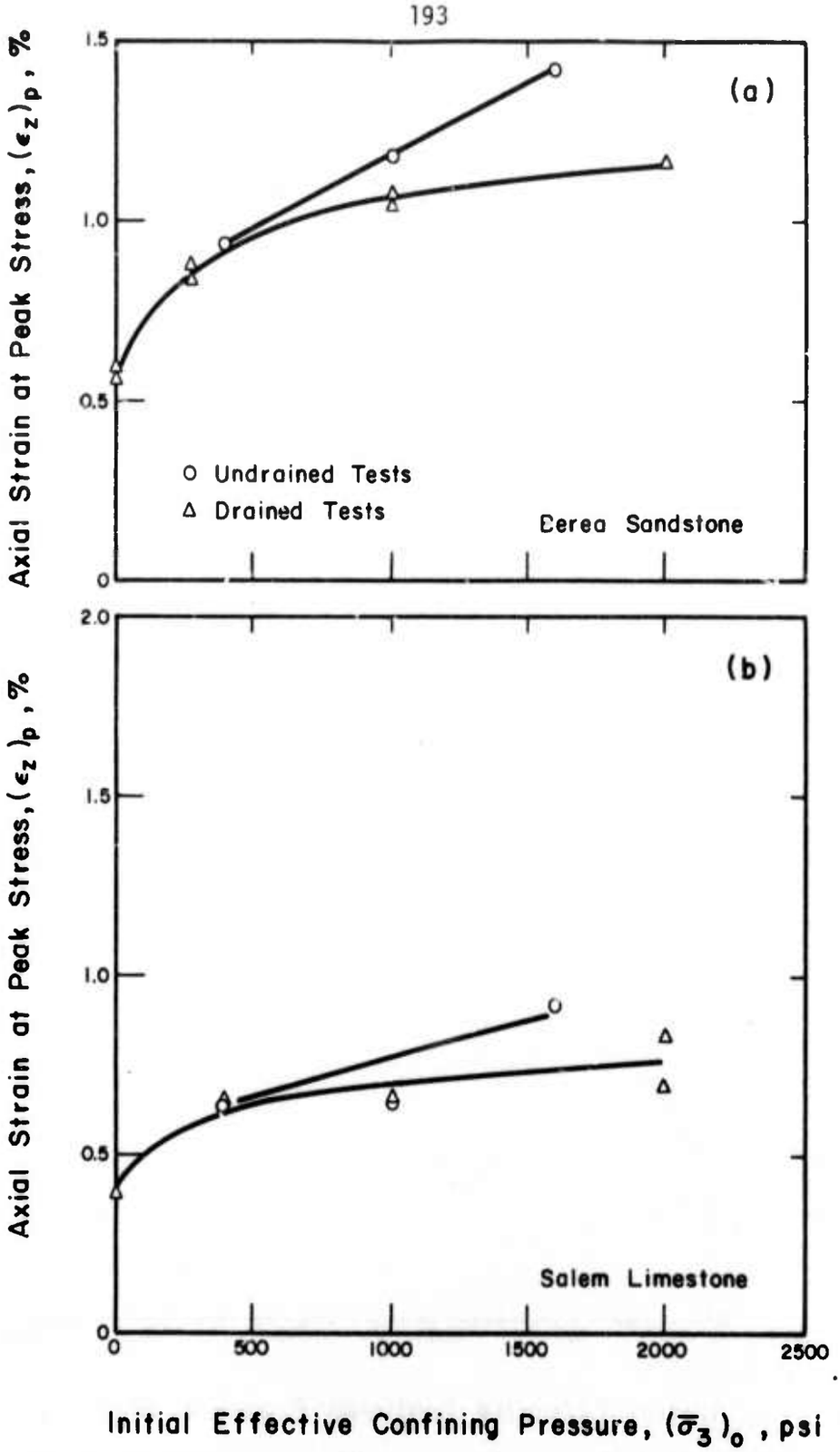

Fig. 4.29 Axial Strain at Peak Stress Versus Initial Effective Confining Pressure, Berea Sandstone and Salem Limestone

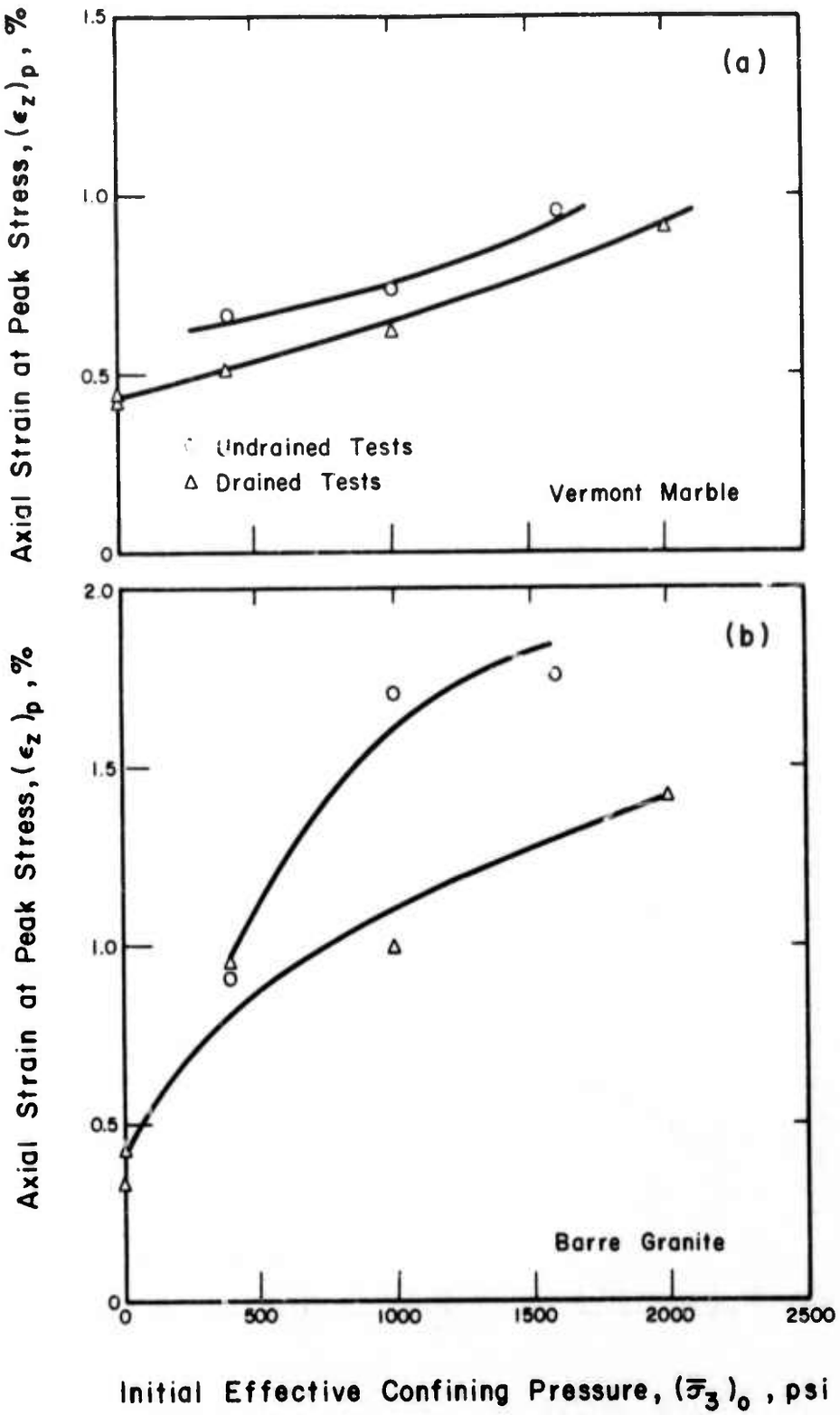

Fig. 4.30 Axial Strain at Peak Stress Versus Initial Effective Confining Pressure, Vermont Marble and Barre Granite

the drained tests reached peak axial stress at smaller axial strain than the undrained tests. Similar results have been reported by Bruhn (1972) for Berea sandstone. As can be seen from stress path curves in Figures 4.31 to 4.34, all rocks were in a state of dilation at failure.

4.4.2 Failure Criteria in Terms of Effective Stress

The Mohr-Coulomb failure diagrams in terms of effective stress have been given for all rock types in Section 3, Figures 3.32, 3.42, 3.51 and 3.60. The Mohr-Coulomb failure criterion in terms of the effective normal and shear stress on the failure plane is defined as:

$$\tau_f = \bar{c} + \bar{\sigma}_f \tan \bar{\phi}$$

where

τ_f is shear stress on failure plane

σ_f is effective normal stress on failure plane

$\bar{c}$ is cohesion intercept

$\bar{\phi}$ is angle of internal friction,

Figures 3.32, 3.42, 3.51 and 3.60 show that the drained and undrained tests result in a single failure envelope for each type of rock. In all cases the failure envelope is concave to the normal stress axis. This observation is consistent with the B-coefficient and spherical compression data. That is, initially the shear strength increases rapidly as effective normal stress increases. This apparently corresponds to the closure of microcracks. However, beyond a certain effective stress level the increasing effective normal stress does not

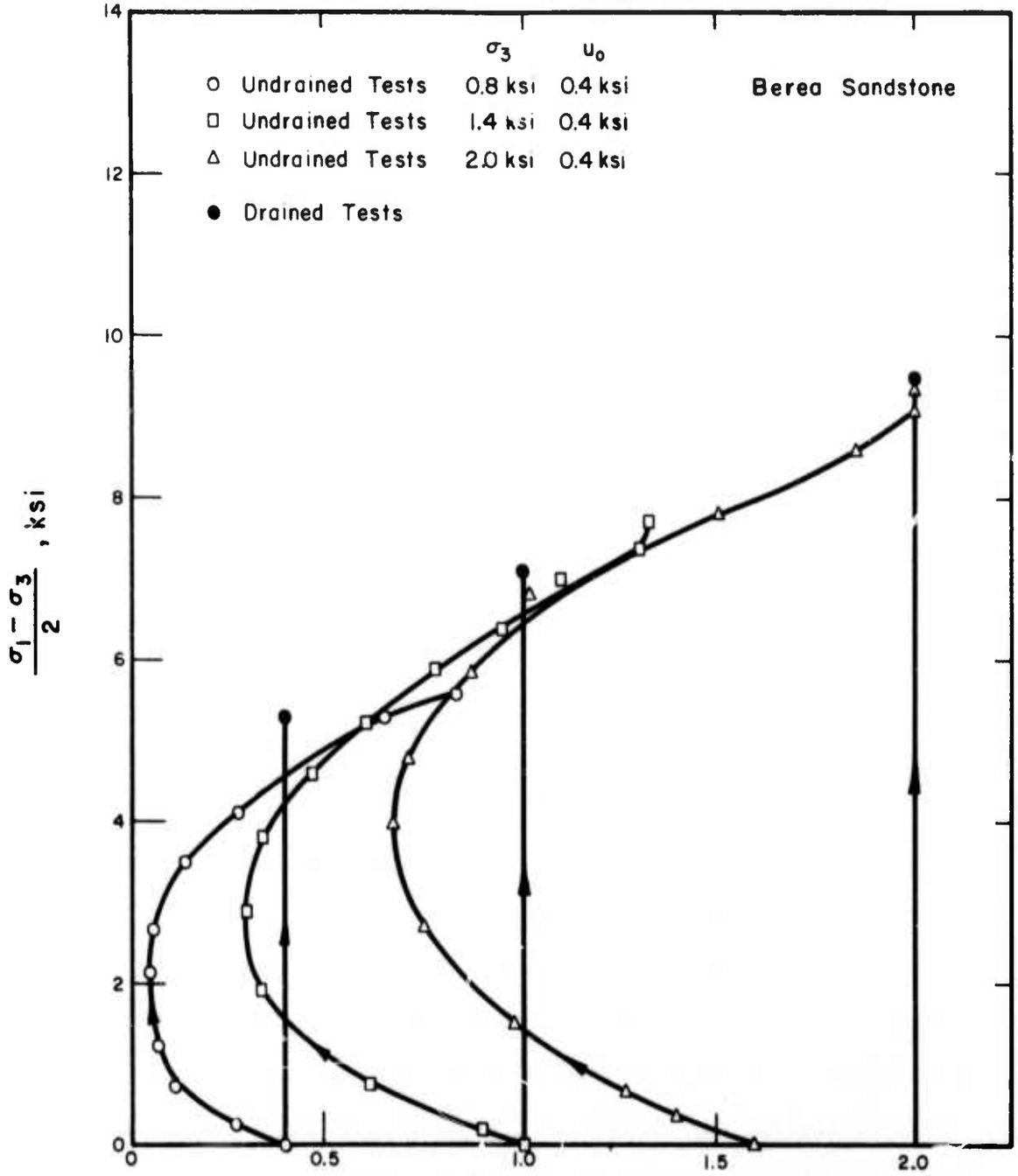

Fig. 4.31 Stress Path, Berea Sandstone

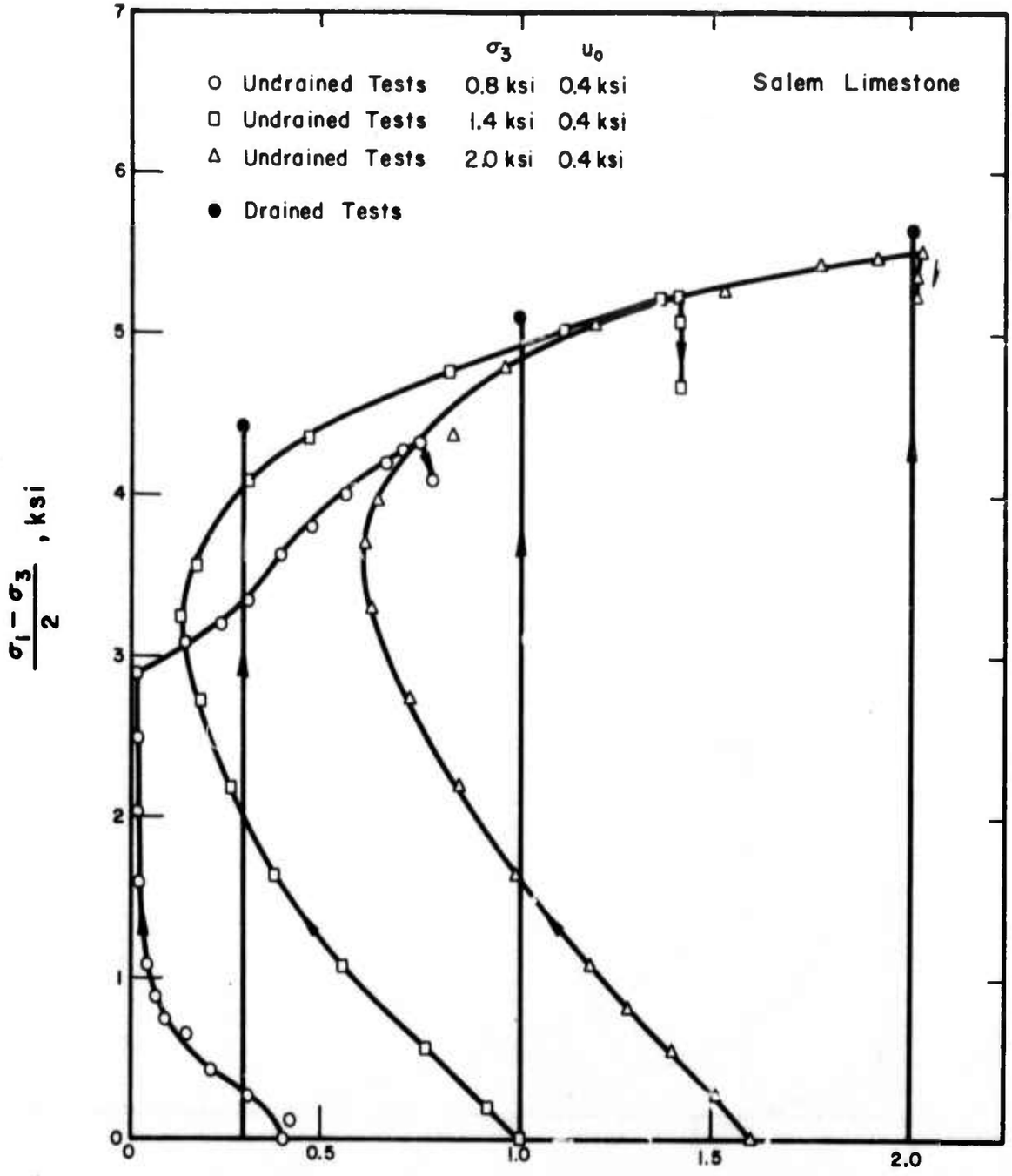

Fig. 4.32 Stress Path, Salem Limestone

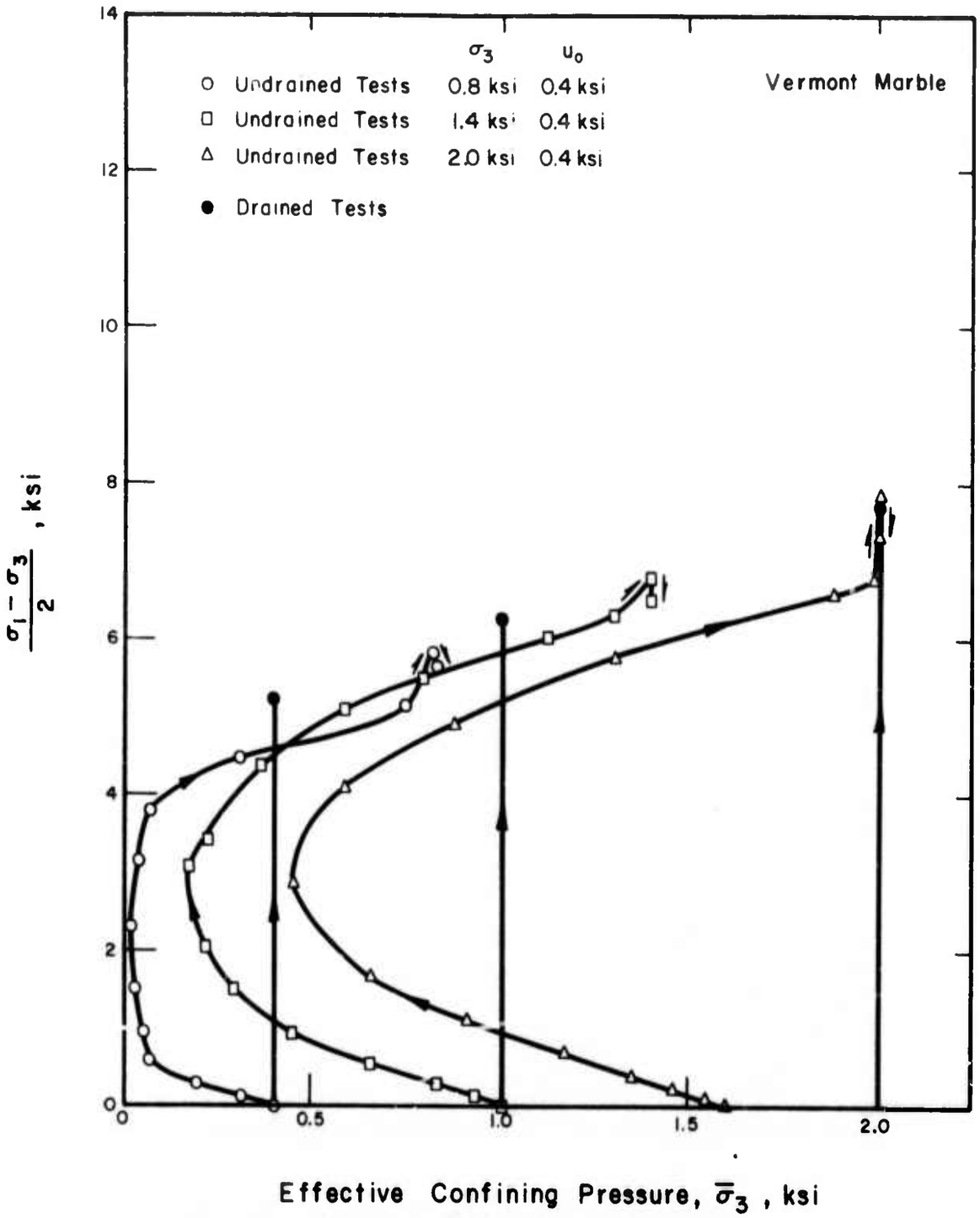

Fig. 4.33 Stress Path, Vermont Marble

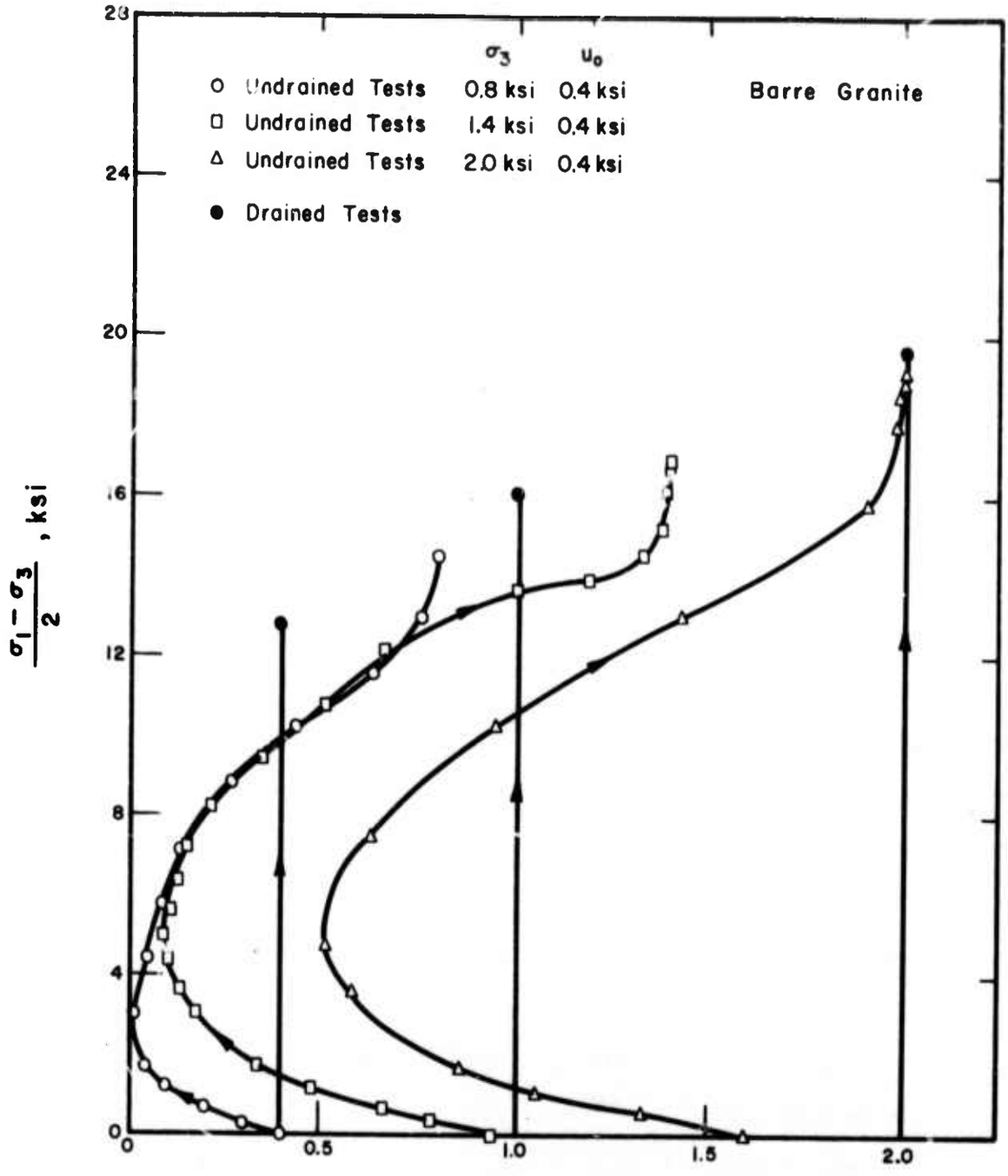

Fig. 4.34 Stress Path, Barre Granite

substantially influence rock porosity and structure, and the rate of increase in shear strength decreases.

The modified Mohr-Coulomb failure envelopes (maximum shear stress, q, versus the corresponding effective normal stress, $\bar{p}$) for all rock types are almost straight lines, Figures 3.32, 3.42, 3.51, 3.60. The values of $\bar{c}$ and $\bar{\phi}$ computed from the slope, $\bar{\psi}$, and intercept, $\bar{d}$, of these lines using the relations

$$\sin \bar{\phi} = \tan \bar{\psi}$$

and

$$\bar{c} = \bar{d}/\cos \bar{\phi}$$

are given in Table 4.5. These values are in agreement with the results which have been reported previously by other investigators (Serdengecti and Boozer, 1961; Boozer et al, 1963; Hendron, 1968; Lane, 1969; Robinson and Holland, 1969; Bruhn, 1972).

Table 4.5 Parameters for Mohr-Coulomb Failure Criterion

	$\bar{\psi}$ (degrees)	$\bar{d}$ (ksi)	$\bar{\phi}$ (degrees)	$\bar{c}$ (ksi)
Berea Sandstone	37	0.9	49	1.5
Salem Limestone	30	1.5	35	1.8
Vermont Marble	33	1.6	40	1.9
Barre Granite	40	1.5	57	2.0

SECTION 5
SUMMARY AND CONCLUSIONS

The principal results of this study are as follows:

1) A 2000 psi-capacity triaxial compression cell was designed and constructed for this study. The special design provisions allowed saturation of low porosity rock specimens under pressure gradient and back pressure, and accurate control or measurement of volume changes and pore water pressures. The cell was used successfully to study the stress-strain, pore pressure, and volume change characteristics of cylindrical rock specimens (2 1/8-inch daimeter, 4 1/4-inch long) in response to increasing all-around pressure or increasing axial load under drained and undrained conditions.

2) Isotropic compression and triaxial compression tests under drained and undrained conditions were performed on Berea sandstone, Salem limestone, Vermont marble, and Barre granite.

3) The method of saturating intact rock specimens using a pressure gradient (800 psi pore pressure difference between bottom and top of specimen) and back pressuring technique, together, provided satisfactory degrees of saturation. Under a given effective confining pressure, a constant B-coefficient

response, independent of the magnitude of back pressure, indicated a satisfactory degree of saturation.

4) A series of drained triaxial compression tests were performed on Vermont marble in order to study strain rate effects. Six specimens were tested at an effective confining pressure of 500 psi and using rates of axial strain ranging from 9.5×10^{-6} in/in/min to 5.9×10^{-3} in/in/min. For rates of axial strain less than about 3×10^{-4} in/in/min , peak principal stress difference remained practically constant while at higher rates it decreased. Based on these results and consideration of the limitations of time and equipment, all of the triaxial compression tests were performed at a rate of strain of 3×10^{-4} in/in/min. Pore pressure measurements in drained tests indicated that the rate of strain was not sufficiently slow for complete dissipation of pore pressures in drained tests on Vermont marble and Barre granite.

5) Drained isotropic compression tests gave values of rock skeleton compressibility in the range of 0.3×10^{-5} to 1.5×10^{-5} psi^{-1} at an effective confining pressure of 100 psi; these values decreased to a range of 0.2×10^{-6} to 1.4×10^{-6} psi^{-1} at an effective confining pressure of 2000 psi. With increasing effective isotropic stress, the bulk compressibility of rock skeleton approached the compressibilities of mineral particles constituting the rock.

6) For all four rock types, the value of B-coefficient is a function of the effective confining pressure. At small effective pressures, the values of B-coefficient were in the range of 0.85 to 1.0; they decreased continuously as a function of effective confining pressure to a range of 0.3 to 0.6 at 1500 psi.

7) The B-coefficients were also computed using theoretical equations (Skempton, 1954; Wissa, 1969; Bruhn, 1972) in terms of the porosity and compressibility of rock skeleton and compressibility of pore water as well as the compressibilities of pore-pressure measuring system and mineral particles. The theoretical B-coefficients were higher than the experimental values for all rock types; by 5 to 20% at lower effective confining pressures and by 40 to 100% at higher pressures. All of the parameters used in the computations were either directly measured or could be estimated fairly accurately, with the exception of the compressibility of pore water. It is possible that the compressibility of <u>pore water</u> is different than the compressibility of <u>free, pure, deaired water</u>.

8) The drained triaxial compression tests were performed at confining pressures of 400 psi, 1000 psi, and 2000 psi. The undrained tests were performed using confining pressures of 800 psi, 1400 psi, and 2000 psi and an initial back pressure of 400 psi (initial effective confining pressures; 400 psi, 1000 psi and 1600 psi).

9) Berea sandstone and Barre granite exhibited pseudo-shear type failure mode, while Salem limestone and Vermont marble exhibited shear type failure (Terzaghi, 1945). Vermont marble and Salem limestone experienced ductile strains before complete rupture, especially under high effective confining pressures, while Berea sandstone and Barre granite exhibited brittle fracture by violent rupture.

10) All of tne rock specimens tested exhibited volume decreases in drained tests and developed positive shear-induced pore water pressures in undrained tests at the initial stage of loading. The volume decreases and pore pressure increases leveled off at about one third of the axial strain corresponding to the maximum principal stress difference. Upon further loading the specimens started to dilate, leading to volumetric expansions in drained tests and pore pressure decreases in undrained tests. High negative shear-induced pore water pressures developed toward failure and in some tests the back pressure of 400 psi was not sufficient for the proper measurement of shear-induced pore pressures.

11) The $\bar{A}$-coefficient maximized at the early stage of loading (at axial strains of less than 0.1%) and then decreased continuously, becoming negative at or near rupture for all rock types. The maximum $\bar{A}$-coefficient for the rocks tested

in the present study ranged between 0.2 and 0.4. A slight decrease in the maximum $\bar{A}$-values with increasing initial effective confining pressure was observed for all rock types.

12) The equations for A- or $\bar{A}$-coefficient were summarized (Skempton, 1954; Bjerrum, 1954; Scott, 1963; Lambe and Whitman, 1969). A new equation for the $\bar{A}$-coefficient was proposed in terms of the compressibility coefficients from drained isotropic compression tests (effective stress decrease) and drained triaxial compression tests. The new equation and the equation proposed by Lambe and Whitman (1969) were compared with $\bar{A}$-values from undrained tests. The proposed equation agreed with reasonable accuracy (better than Lambe and Whitman's equation) with the directly measured $\bar{A}$-values for Berea sandstone and Salem limestone. However the $\bar{A}$-measurements on Vermont marble and Barre granite did not agree with the values given by the equations. It is suggested that drained tests on these rocks were performed at too fast a loading rate.

13) The stress-strain, volume change, shear-induced pore water pressure and strength data indicate that the principle of effective stress holds for the rocks tested in this investigation. That is, the changes in effective normal stress, defined as total normal stress minus the pore water pressure,

control deformation and strength of these rocks (within the range of variation in effective stress used in the present study).

14) Tangent modulus at the stress level corresponding to 50% of peak principal stress difference, E_{50}, increased with increasing initial effective confining pressure for all rock types. The values of E_{50} from drained tests were slightly higher than the corresponding values from undrained tests. However, when E_{50} values from drained and undrained tests were compared in terms of the effective confining pressure, $\bar{\sigma}_3$, at the stress level at which E_{50} was computed, the drained and undrained tests indicated a single relationship between E_{50} and $\bar{\sigma}_3$.

15) At a given initial effective confining pressure, the drained test reached the peak axial stress at a smaller axial strain than the undrained test.

16) The drained and undrained tests resulted in a single Mohr-Coulomb failure envelope in terms of effective stress for each rock type. In all cases the failure envelope was concave to the normal stress axis. The modified Mohr-Coulomb failure envelope plotted almost as a straight line for each rock type.

REFERENCES

Bieniawski, Z. T. (1967), "Mechanism of Brittle Fracture of Rocks," International Journal of Rock Mechanics and Mining Sciences, Parts 1 and 2, October.

Bishop, A. W. and D. J. Henkel (1962), "The Measurement of Soil Properties in the Triaxial Test," 2nd Ed., London, Edward Arnold, pp. 123-127.

Bjerrum, L. (1954), "Theoretical and Experimental Investigations on the Shear Strength of Soils," Norwegian Geotechnical Institute, Publication Nr. 5, pp. 1-113.

Boozer, G. D., K. H. Hiller, and S. Serdengecti (1963), "Effects of Pore Fluids on the Deformation Behavior of Rocks Subjected to Triaxial Compression," Rock Mechanics, Pergammon Press, pp. 579-625.

Brace, W. F. (1968), "The Mechanical Effects of Pore Pressure on Fracturing of Rocks," Proceedings, Conference on Research in Tectonics, Geological Survey of Canada, Paper 68-52.

Brace, W. F. and J. D. Byerlee (1966), "Recent Experimental Studies of Brittle Fracture of Rocks," 8th Symposium of Rock Mechanics, Minnesota, pp. 58-81.

Brace, W. F. and R. J. Martin, III (1968), "A Test of the Law of Effective Stress for Crystalline Rocks of Low Porosity," International Journal of Rock Mechanics & Mining Sciences, Vol. 5, p. 415.

Bredthauer, R. O. (1957), "Strength Characteristics of Rock Samples Under Hydrostatic Pressure," Trans. American Soc. of Mechanical Engineers 79, pp. 695-708.

Bruhn, R. W. (1972), "A Study of the Effects of Pore Pressure on the Strength and Deformability of Berea Sandstone in Triaxial Compression," U. S. Army Corps of Engineers, Missouri River Division Laboratory, Omaha, Nebraska, Third Interim Report, MRD Laboratory No. 64/493.

Colback, P. S. B. and B. L. Wiid (1965), "The Influence of Moisture Content on the Compressive Strength of Rocks," Proceedings of Rock Mechanics Symposium, Dept. of Mines, Ottawa.

Deere, D. U. and R. P. Miller (1966), "Engineering Classification and Index Properties for Intact Rock," Air Force Weapons Laboratory Technical Report NO. AFWL-TR-65-116.

Donath, F. A. and L. S. Fruth (1971), "Dependence of Strain-Rate Effects on Deformation Mechanism and Rock Type," Journal of Geology, Vol. 79, No. 3, pp. 347-371.

Dorsey, N. W. (1940), "Properties of Ordinary Water-Substance," New York, Reinhold Publishing Corporation, pp. 245-246.

Eisenberg, D. and W. Kauzman (1969), "The Structure and Properties of Water," Oxford University Press, New York and Oxford.

Griggs, D. T. (1936), "Deformation of Rocks Under High Confining Pressures," Journal of Geology, Vol. XLIV, pp. 541-577.

Handin, J. R., V. Hager, Jr., M. Friedman and J. N. Feather (1963), "Experimental Deformation of Sedimentary Rocks Under Confining Pressure: Pore Pressure Tests," Bulletin of the American Association of Petroleum Geologists, Vol. 47, No. 5.

Heard, H. C. (1960), "Transition from Brittle Fracture to Ductile Flow in Solenhofen Limestone as a Function of Temperature, Confining Pressure and Interstitial Fluid Pressure," Fluid Pressures in Rock Deformation, Geological Socl. of America Memoir 79, pp. 193-226.

Hendron, A. J. Jr., (1968), "Mechanical Properties of Rock," Rock Mechanics in Engineering Practice, Ed., K. G. Stagg and O. C. Zienkiewicz, John Wiley and Sons, pp. 21-53.

Horn, H. M. and D. U. Deere (1962), "Frictional Characteristics of Minerals," Geotechnique, Vol. 12, pp. 319-335.

King, M. S. (1969), "Static and Dynamic Elastic Moduli of Rocks Under Pressure," Rock Mechanics-Theory and Practice, 11th Symposium on Rock Mechanics, Berkeley, pp. 329-351.

Kjaernsli, B. and A. Sande (1966), "Compressibility of Some Coarse Grained Material," Norwegian Geotechnical Institute, pp. 245-251.

Kowalski, W. C. (1966), "The Interdependence between the Strength and Void Ratio of Limestones and Marls in Connection With Their Water Saturating and Anisotropy," 1st International Conference on Rock Mechanics, Lisbon, pp. 143-144.

Krech, W. (1973), Personal communication, Information taken from "A Standard Rock Suite for Rapid Excavation Research," by W. W. Krech, F. A. Henderson, and K. E. Hjelmstad, proposed BuMines IC.

Lambe, T. W. and R. V. Whitman (1969), "Soil Mechanics," John Wiley and Sons, Inc., pp. 396-398.

Lane, K. S. (1969), "Engineering Problems Due to Fluid Pressure in Rock," 11th Symposium of Rock Mechanics, pp. 501-537.

Lee, K. L., R. A. Morrison and S. C. Haley (1969), "A Note on the Pore Pressure Parameter B," Seventh International Conference on Soil Mechanics and Foundation Engineering, Vol. 1, pp. 231-238.

Mesri, G., R. A. Jones, and K. Adachi (1972), "Influence of Pore Water Pressure on the Engineering Properties of Rock," Annual Report Submitted to ARPA and Bureau of Mines, University of Illinois at Urbana-Champaign, 102 pp.

Mesri, G. and K. Adachi (1972), "Influence of Pore Water Pressure on the Engineering Properties of Rock," Semiannual Technical Report Submitted to ARPA and Bureau of Mines, University of Illinois at Urbana-Champaign, 41 pp.

Murrel, S. A. F. (1963), "A Criterion for Brittle Fracture of Rocks and Concrete Under Triaxial Stress, and the Effect of Pore Pressure on the Criterion," Rock Mechanics, Ed., C. Fairhurst, Pergammon Press, pp. 563-577.

Neff, T. L. (1966), "Equipment for Measuring Pore Pressure in Rock Specimens Under Triaxial Load," Special Technical Publication 402, American Society for Testing and Materials.

Ohnishi, Y. (1973), "Laboratory Measurement of Induced Water Pressures in Jointed Rocks," Ph.D. Thesis, University of California, Berkeley.

Rebinder, P. A. and V. Likhtman (1957), Proc. Second International Congress Surface Activity, Vol. III, pp. 503-580, Academic Press, New York.

Richart, F. E., Brandtzaeg and R. L. Brown (1928), "A Study of the Failure of Concrete Under Combined Compressive Stresses," Publication of the Engineering Experiment Station, University of Illinois, Bulletin No. 185.

Robinson, L. H. (1959), "Effects of Pore and Confining Pressure on Failure Characteristics of Sedimentary Rocks," Quarterly Colorado School of Mines, Vol. 54, No. 3, (Incorporated in 1959 Rock Mechanics Symposium).

Robinson, L. H. and W. E. Holland (1969), "Some Interpretations of Pore Fluid Effects in Rock Failure," Rock Mechanics-Theory and Practice, 11th Symposium on Rock Mechanics.

Ros, M. and A. Eichinger (1928), "Versuche zur Klarung der Frage der Bruchgefahr. II. Nichtmetcallische Stoffe," Zurich, Eidgenossische Materialprofungsanstalt an der Eidgenossischen Technischen Hochscule, June, p. 57. (Diskussionsbericht Nr. 28).

Schwartz, A. E. (1964), "Failure of Rock in Triaxial Shear Test," 6th Symposium on Rock Mechanics, Rolla, pp. 109-131.

Scott, R. F. (1963), "Principles of Soil Mechanics," Addison-Wesley, Reading, Mass., pp. 270-275.

Serdengecti, S. and G. D. Boozer (1961), "The Effects of Strain Rate and Temperature on the Behavior of Rock Subjected to Triaxial Compression," 4th Symposium on Rock Mechanics, pp. 83-97.

Skempton, A. W. (1954), "The Pore Pressure Coefficients A and B," Geotechnique, December, pp. 143-152.

Skempton, A. W. (1961), "Effective Stress in Soils, Concrete and Rocks," Proceedings, Conference on Pore Pressure and Suction in Soils, Butterworth, London, pp. 4-16.

Smithsonian Physical Tables (1933), 8th Ed. Prepared by F. E. Foule, Smithsonian Institution, p. 157.

Terzaghi, K. (1923), Die Berechnung der Durchlassikeitsziffer des Tones aus dem Verlauf der Hydrodynamischen Spannungserscheinungen: Sitz. Akad. Wiss. Wien, V. 132, pp. 105-124.

Terzaghi, K. (1934),"Die Wirksame Flachen porositat des Betons," Zietschrift Osters. Ing. u. Arch.-ver., Heft 2.

Terzaghi, K. (1945), "Stress Conditions for the Failure of Saturated Concrete and Rock," reproduced in From Theory to Practice in Soil Mechanics, pp. 181-197.

Trollope, D. H. and E. T. Brown (1966), "Effective Stress Criteria of Failure of Rock Masses," 1st International Congress on Rock Mechanics, Lisbon, Vol. 1, pp, 515-519.

Walsh, J. B. and W. F. Brace (1966), "Cracks and Pores in Rocks," 1st International Conference on Rock Mechanics, Lisbon, pp. 643-646.

Wissa, A. E. (1969), "Pore Pressure Measurement in Saturated Stiff Soils," Journal of Soil Mechanics and Foundations Div., ASCE, July, pp. 1063-1073.

Zisman, W. A. (1933), "Compressibility and Anistropy of Rocks at and Near the Earth's Surface," Proc. N.A.S., Geology, Vol. 19.

APPENDIX A

DETAILED DESIGN DRAWINGS OF HIGH CAPACITY TRIAXIAL CELL TOP

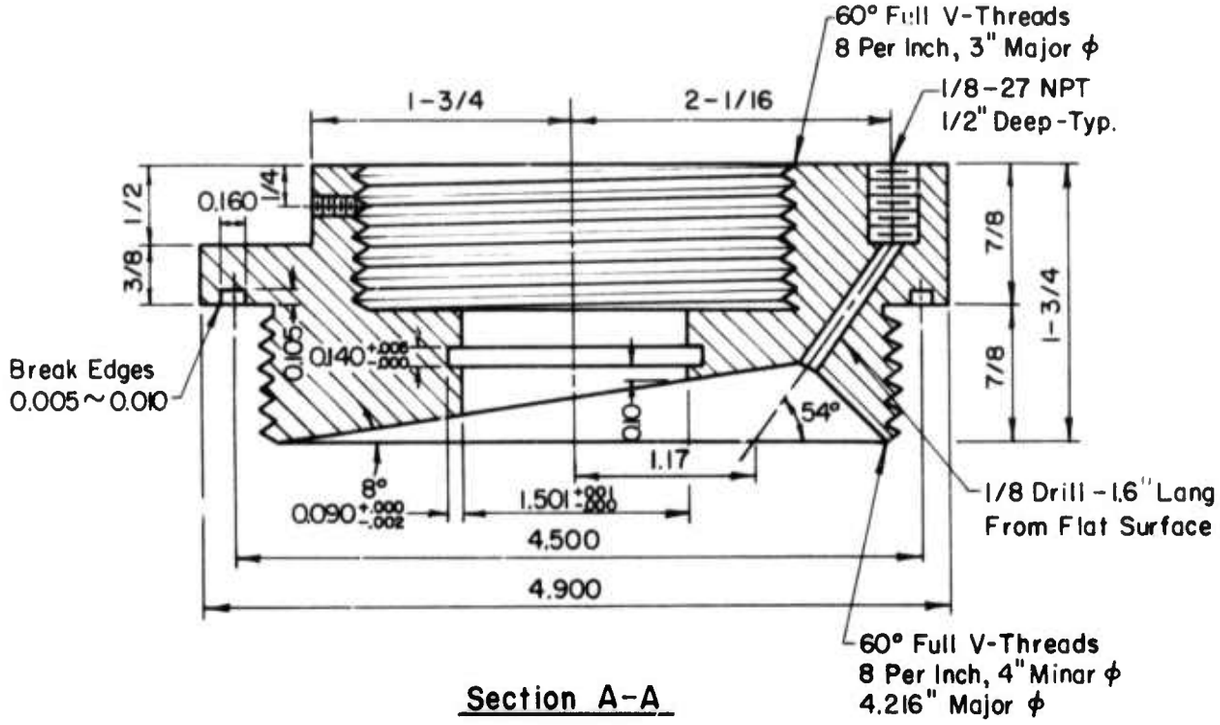

Section A-A

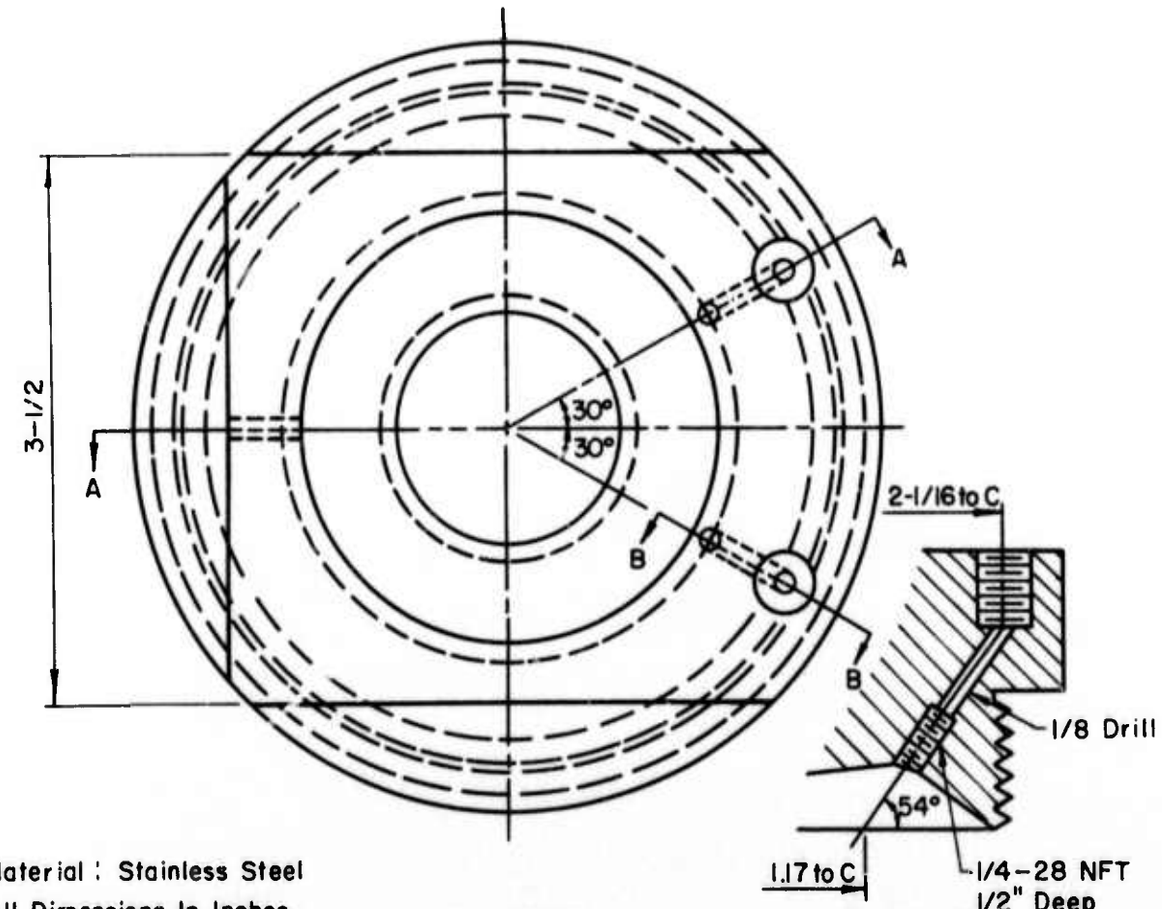

Material : Stainless Steel
All Dimensions In Inches

Top View

Section B-B

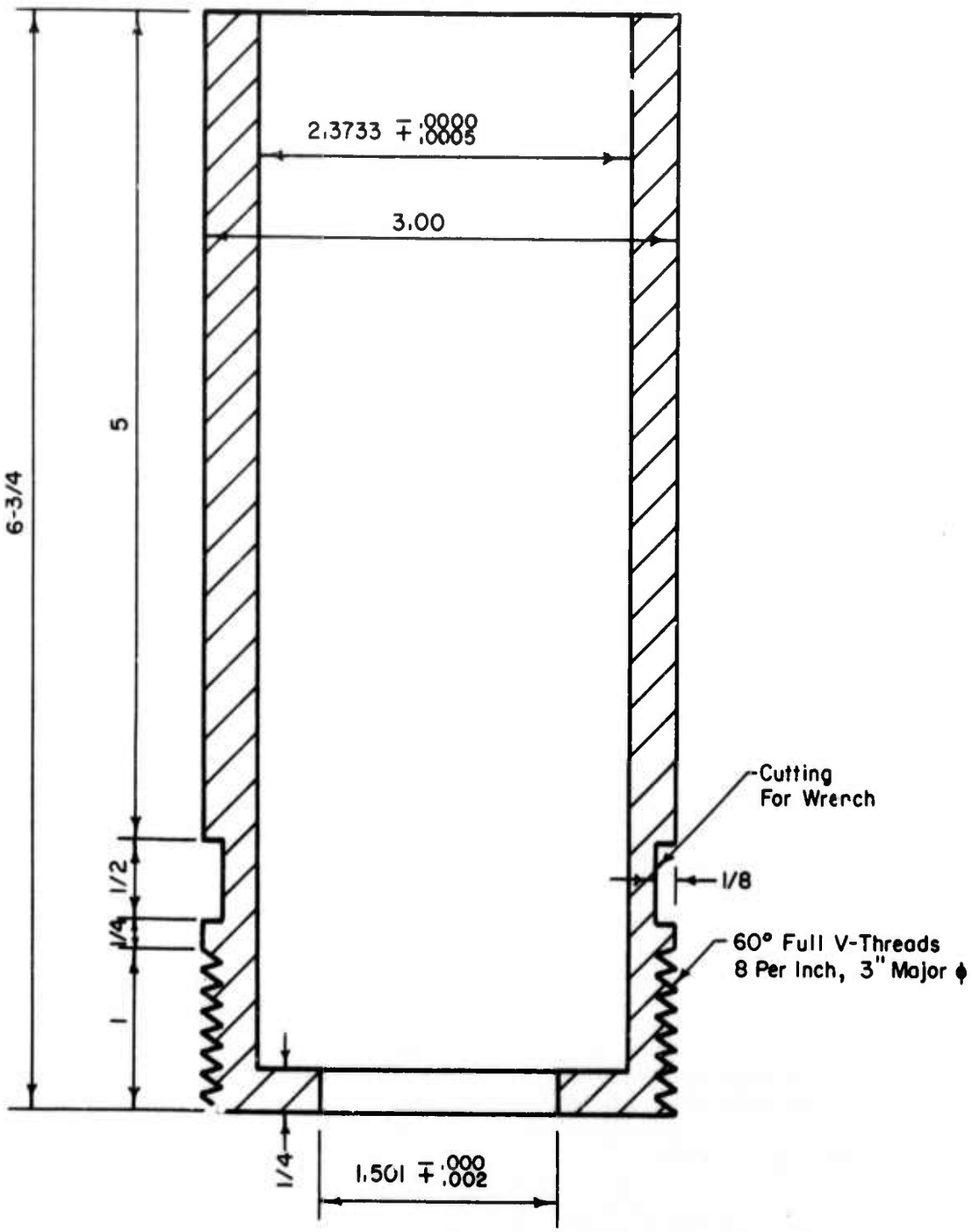

Material: Stainless Steel

All Dimensions In Inches

Piston Stopper

(Stainless Steel)

Section A-A

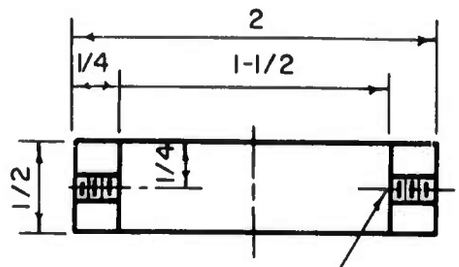

Top View

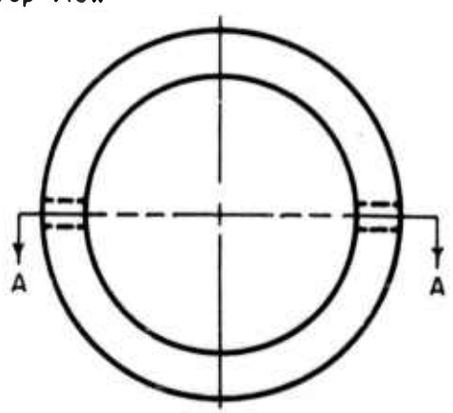

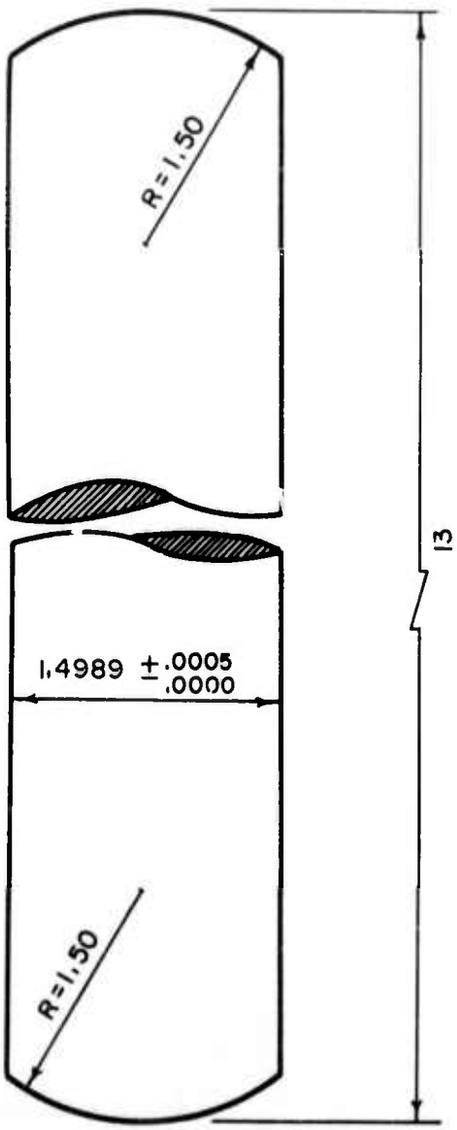

Material: Thomson Stainless Steel, Hardened Shaft 1.5" Diam.

All Dimensions In Inches

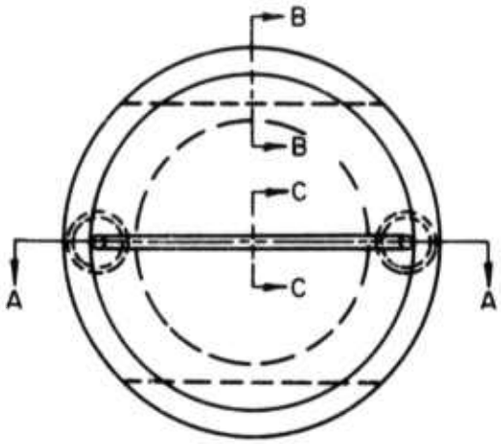

Bottom View

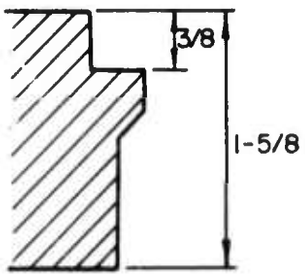

Section B-B

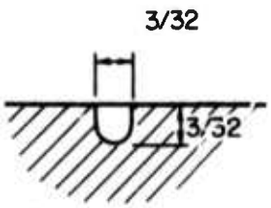

Section C-C

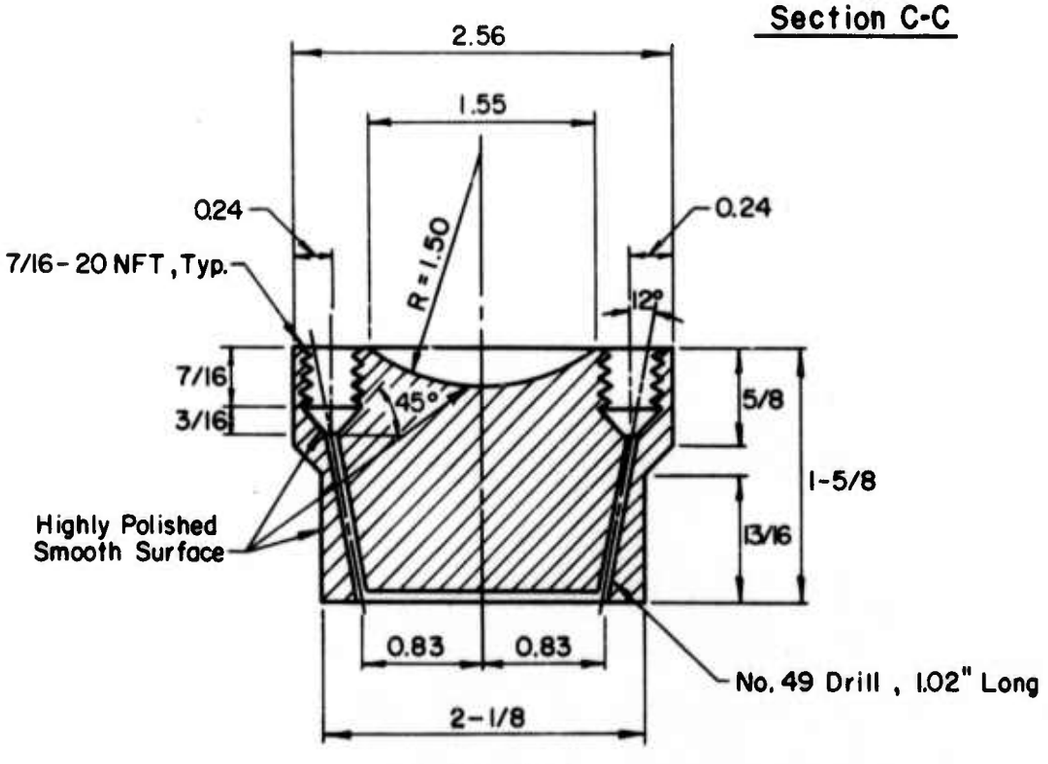

Section A-A

Material: Stainless Steel Round

All Dimensions In Inches

APPENDIX B

DESCRIPTION OF PORE PRESSURE TRANSDUCERS

MODEL PG856

Thin Film Strain Gage Pressure Transducer

DESCRIPTION

This transducer represents the culmination of several years of extensive research and development in thin film strain gage techniques. The sensing element of the Model PG856 Transducer utilizes a vacuum-deposited, fully active strain gage bridge.

The unit employs a beam-diaphragm sensing assembly. A ceramic film is deposited onto the beam to provide electrical insulation for the bridge elements. Four strain gages are vacuum-deposited onto the insulator and are connected electrically into a bridge circuit. The specially developed strain gage material exhibits the excellent stability, gage factor, and resistance characteristics required in a strain gage transducer.

The instrument's flush-diaphragm construction permits direct exposure to pressure media, and produces a system response flat (±5%) to one-fifth the transducer's natural frequency. The diaphragm materials used in the Model PG856 Transducer are Types 17-4 PH and 17-7 PH stainless steel. Either lightweight aluminum or corrosion-resistant steel adapters may be used to convert the Model PG856 to a cavity-type instrument. Adapters are available in a variety of pipe and tube fittings.

SPECIFICATIONS

1.1 Model Designation, Typical Pressure Ranges, Maximum psig, Natural Frequency, and Static Acceleration Response (The acceleration response quoted represents the output of the transducer due to stimulus applied in the sensitive axis, including vibration at frequencies up to approximately 20% of the natural frequency. Above this frequency, the response will increase in accordance with the behavior of an undamped single-degree-of-freedom system.)

Model Designation	Range (psig)	Maximum (psig)	Approximate Natural Frequency (Hz)	Static Response (% FS/g)
PG856-15	0-15	30	3,500	0.06
PG856-25	0-25	50	4,500	0.04
PG856-50	0-50	100	6,000	0.02
PG856-100	0-100	200	9,000	0.015
PG856-150	0-150	300	10,000	0.01
PG856-250	0-250	375	11,000	0.01
PG856-500	0-500	750	13,000	0.01
PG856-1M	0-1,000	1,500	17,500	0.01
PG856-2M	0-2,000	3,000	24,000	0.01
PG856-5M	0-5,000	7,500	34,000	0.01

SPECIFICATION NUMBER 17596

Product Bulletin TF0009
March, 1970 10M

ATHAM INSTRUMENTS, INC., Measurement Systems Division • 2230 Statham Boulevard • Oxnard, California 93030 • (805) 487-8511 • Telex 6-5923

MODEL PG856

Thin Film Strain Gage Pressure Transducer

1.2	Pressure media	Fluids compatible with Types 17-4 PH and 17-7 PH stainless steel
1.3	Transduction	Resistive, balanced, fully active strain gage bridge
1.4	Nominal bridge resistance	350Ω
1.5	Excitation	10V DC or AC (rms) through carrier frequencies
1.6	Full-scale output (open circuit)	3 mV/V nominal
1.7	Resolution	Infinitesimal
1.8	Non-linearity and hysteresis	Less than 0.5% FS (terminal)
1.9	Compensated temperature range	-65 to +250°F
1.10	Thermal sensitivity shift	Less than 0.01%/°F
1.11	Thermal zero shift	Less than 0.01% FS/°F
1.12	Pressure connection	Flush diaphragm; adapters are available for conversion to chamber-type pickup.
1.13	Electrical connection	Four numbered terminal pins; electrical disconnect assemblies Model DC12 and Model DC13 are available.
1.14	Weight	Approximately 0.6 oz
1.15	Identification	The model designation, serial number, range, maximum excitation, and manufacturer are marked on each unit.
1.16	Dimensions	Outline Drawing No. 52221 applies.
1.17	Calibration	Statham pressure transducers are calibrated individually by qualified technicians using specialized equipment of laboratory accuracy. Pertinent data are furnished at time of shipment.

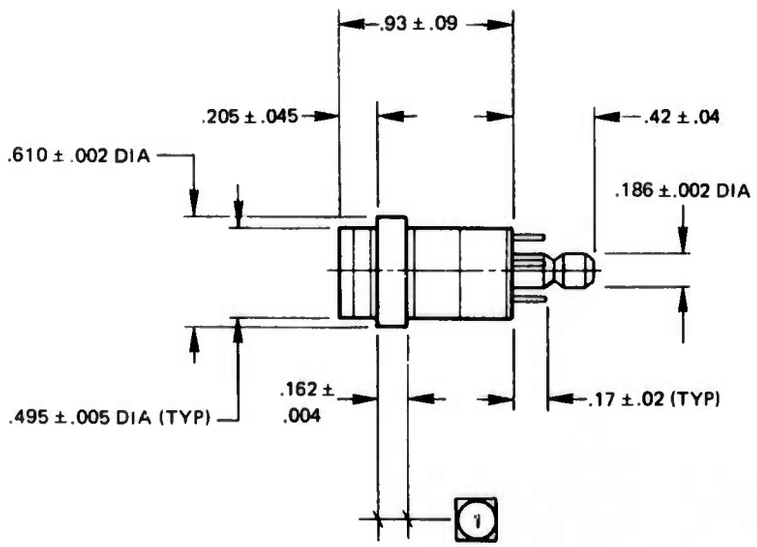

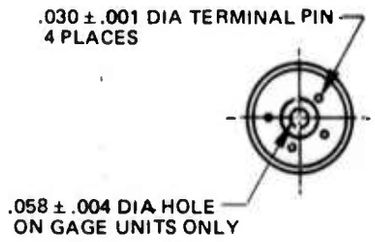

NOTES: (1) CLAMP ON THESE SURFACES ONLY.

OUTLINE DRAWING 52221

For special ranges, higher accuracies, or other modifications to parameters, please contact the factory or our sales office in your area.

All correspondence relating to the equipment described herein must reference this Specification Number 17596.

Printed by Statham, Oxnard, California, USA

TEMPERATURE COMPENSATED PRESSURE TRANSDUCER
DATA SHEET

DATE:	7-12-72
CUSTOMER:	UNIVERSITY OF ILLINOIS
CUSTOMER'S ORDER NO.	303910
OUR PRODUCTION NO.	50033
OUR SPECIFICATION NO.	17596

This report has been prepared by our Standards Laboratory. The following data are important to the operation of the pressure transducer:

PRESSURE TRANSDUCER MODEL NO.	PG856-5M
SERIAL NO.	2640
PRESSURE RANGE:	0 to 5000 psig
COMPENSATED TEMPERATURE INTERVAL:	-65 °F TO +250 °F
INPUT TERMINALS: 1 and 4	*(Green and Red)*
OUTPUT TERMINALS: 2 and 3	*(Black and White)*
EXCITATION — E:	10 volts
INPUT RESISTANCE — R_{in}:	340 ohms
OUTPUT RESISTANCE — R:	321 ohms
CALIBRATION FACTOR — F:	.7505 microvolts (open circuit) per volt per psi

The strain sensitive resistance wire elements of the transducer are arranged in the form of a Wheatstone bridge. Either *ALTERNATING* or *DIRECT* current may be used to excite the pressure transducer, depending upon the requirements of the indicating or recording instrument.

paw